NACA TN 3072

NATIONAL ADVISORY COMMITTEE FOR AERONAUTICS

TECHNICAL NOTE 3072

A THEORETICAL INVESTIGATION OF THE AERODYNAMICS OF WING-TAIL COMBINATIONS PERFORMING TIME-DEPENDENT MOTIONS AT SUPERSONIC SPEEDS

By John C. Martin, Margaret S. Diederich,
and Percy J. Bobbitt

Langley Aeronautical Laboratory
Langley Field, Va.

Washington
May 1954

LE

NATIONAL ADVISORY COMMITTEE FOR AERONAUTICS

TECHNICAL NOTE 3072

A THEORETICAL INVESTIGATION OF THE AERODYNAMICS OF WING-TAIL COMBINATIONS PERFORMING TIME-DEPENDENT MOTIONS AT SUPERSONIC SPEEDS

By John C. Martin, Margaret S. Diederich,
and Percy J. Bobbitt

SUMMARY

A theoretical investigation is presented of the contribution of horizontal tails to the lift and pitching moment due to angle of attack, a constant rate of pitch, and a constant vertical acceleration. Numerical values of the aerodynamic coefficients associated with these motions are presented for a number of two-dimensional wing-tail combinations, a triangular wing-tail combination, and a number of rectangular-wing—triangular-tail combinations.

Methods for calculating the flow fields behind wings with constant vertical acceleration are developed. Calculated results are presented for the upwash behind two-dimensional wings and for certain regions behind triangular and rectangular wings for a constant rate of pitch and for constant vertical accelerations. A method of treating unsteady aerodynamics based on an infinite series of stability derivatives of successively higher order is also presented.

INTRODUCTION

The development of the linearized theory of supersonic flow has permitted a first-order evaluation of a number of stability derivatives for a wide variety of isolated wings. (For example, see refs. 1 to 9.) The linearized theory may also be used in the calculation of the aerodynamic derivatives of the wing-tail combinations. Considerations of the effects of the horizontal tails located behind wings of necessity entail a knowledge of the upwash induced by the wing. The upwash from wings performing steady motions can be calculated by use of the various methods presented in references 10 to 15. A method of calculating the upwash in the region of the viscous wake behind wings with a constant vertical acceleration at supersonic speeds is presented in reference 16. Except for the methods and results presented in references 16 to 19, little consideration has been given to the theoretical calculation of the contribution of the horizontal tail to the aerodynamic derivatives.

The primary object of the present paper is a theoretical investigation of the contribution of the horizontal tail to the pitching moment due to a constant vertical acceleration. An investigation of this pitching moment entails a knowledge of a number of other factors which in themselves are useful in other supersonic flow problems. Inasmuch as a knowledge of these other factors is required in the primary investigation, the present paper has a number of secondary objectives such as: (1) the establishment of a method of treating unsteady aerodynamics of aircraft by the use of an infinite series of stability derivatives of successively higher order, (2) the development of theoretical methods for the calculations of sidewash and upwash behind wings which have local angle-of-attack distributions which vary linearly with time, (3) an investigation of exact and approximate methods for the calculation of sidewash and upwash behind wings with constant vertical acceleration, and (4) an investigation of exact and approximate methods for the calculations of the lift and pitching moment due to a constant angle of attack and a constant rate of pitch.

The upwash behind two-dimensional wings with a constant vertical acceleration is determined and calculated results are presented. The upwash along the center line of the wake behind triangular wings with subsonic leading edges is determined for a constant rate of pitch and for a constant vertical acceleration; calculated results are presented for a number of triangular wings and Mach numbers. The upwash in the wake in the plane of the wing behind rectangular wings is determined for a constant vertical acceleration; calculated results are presented for a number of rectangular wings and Mach numbers.

Exact linearized results are presented for the lift and pitching moment resulting from angle of attack, steady pitching, and a constant vertical acceleration for a number of two-dimensional wing-tail combinations, a triangular wing-tail combination, and a number of rectangular-wing—triangular-tail combinations. Some of these exact results are compared with results calculated from a number of simple approximate relations which are often used in calculations for subsonic wing-tail combinations.

SYMBOLS

A	aspect ratio
a	velocity of sound in free stream
$B = \sqrt{M^2 - 1}$	
b	wing span

C_L lift coefficient, $\dfrac{\text{Lift}}{\frac{1}{2}\rho V^2 S_W}$

$$C_{L_{\alpha}} = \left.\frac{\partial C_L}{\partial \alpha}\right|_{\alpha \to 0}$$

$$C_{L_{\dot{\alpha}}} = \left.\frac{\partial C_L}{\partial \frac{\dot{\alpha}\bar{c}}{2V}}\right|_{\dot{\alpha} \to 0}$$

$$C_{L_{\ddot{\alpha}}} = \left.\frac{\partial C_L}{\partial \frac{\ddot{\alpha}\bar{c}^2}{4V^2}}\right|_{\ddot{\alpha} \to 0}$$

$\Delta C_{L_{\alpha}}$ horizontal-tail contribution to $C_{L_{\alpha}}$

$\Delta C_{L_{\dot{\alpha}}}$ horizontal-tail contribution to $C_{L_{\dot{\alpha}}}$

$$C_{L_q} = \left.\frac{\partial C_L}{\partial \frac{q\bar{c}}{2V}}\right|_{q \to 0}$$

$$C_{L_{\dot{q}}} = \left.\frac{\partial C_L}{\partial \frac{\dot{q}\bar{c}^2}{4V^2}}\right|_{\dot{q} \to 0}$$

$$C_{L_{\ddot{q}}} = \left.\frac{\partial C_L}{\partial \frac{\ddot{q}\bar{c}^3}{8V^3}}\right|_{\ddot{q} \to 0}$$

ΔC_{L_q} horizontal-tail contribution to C_{L_q}

C_m pitching-moment coefficient, $\dfrac{\text{Moment}}{\frac{1}{2}\rho V^2 S_W \bar{c}_W}$

$$C_{m_{\alpha}} = \left.\frac{\partial C_m}{\partial \alpha}\right|_{\alpha \to 0}$$

$$C_{m_{\dot{\alpha}}} = \left.\frac{\partial C_m}{\partial \frac{\dot{\alpha}\bar{c}}{2V}}\right|_{\dot{\alpha}\to 0}$$

$$C_{m_{\ddot{\alpha}}} = \left.\frac{\partial C_m}{\partial \frac{\ddot{\alpha}\bar{c}^2}{4V^2}}\right|_{\ddot{\alpha}\to 0}$$

ΔC_{m_α}	horizontal-tail contribution to C_{m_α}
$\Delta C_{m_{\dot{\alpha}}}$	horizontal-tail contribution to $C_{m_{\dot{\alpha}}}$

$$C_{m_q} = \left.\frac{\partial C_m}{\partial \frac{q\bar{c}}{2V}}\right|_{q\to 0}$$

$$C_{m_{\dot{q}}} = \left.\frac{\partial C_m}{\partial \frac{\dot{q}\bar{c}^2}{4V^2}}\right|_{\dot{q}\to 0}$$

$$C_{m_{\ddot{q}}} = \left.\frac{\partial C_m}{\partial \frac{\ddot{q}\bar{c}^3}{8V^3}}\right|_{\ddot{q}\to 0}$$

ΔC_{m_q}	horizontal-tail contribution to C_{m_q}
C_p	pressure coefficient, $\frac{\text{Pressure}}{\frac{1}{2}\rho V^2}$
c	root chord
$\bar{c}$	mean aerodynamic chord
d	arbitrary distance along x-axis associated with a shift in center-of-gravity location (see table I)
d_o	distance from apex of a triangular wing to axis of pitch
ds	differential area

E	complete elliptic integral of second kind with modulus k, $\int_0^1 \sqrt{\frac{1 - k^2\lambda}{1 - \lambda^2}}\,d\lambda$
E'	complete elliptic integral of second kind with modulus k'
F	force
F_0^α	$\frac{1}{\alpha}$ times force associated with first term of equation (1)
F_1^α	$\frac{2V}{\dot{\alpha}\bar{c}}$ times force associated with second term of equation (1)
F_2^α	$\frac{4V^2}{\ddot{\alpha}\bar{c}^2}$ times force associated with third term of equation (1)
F_0^q	$\frac{2V}{q\bar{c}}$ times force associated with first term of equation (2)
F_1^q	$\frac{4V^2}{\dot{q}\bar{c}^2}$ times force associated with second term of equation (2)
F_2^q	$\frac{8V^3}{\ddot{q}\bar{c}^3}$ times force associated with third term of equation (2)
f	arbitrary function associated with local angle-of-attack distribution on a wing (see eq. (14a))
$f\!\!\int$	finite part of an integral
G	function associated with Mach surface formed by envelope of after Mach cones springing from trailing edge of wing
h	arbitrary function associated with local angle of attack of an airfoil (see eq. (D1))
h_1, h_2	limits of integration (see eq. (21))
J	function associated with equation of trailing edge of wing (see eq. (20))

K complete elliptic integral of first kind with modulus k,

$$\int_0^1 \frac{d\lambda}{\sqrt{(1 - \lambda^2)(1 - k^2\lambda^2)}}$$

$$K_q = \frac{q}{\pi\left[\frac{1 - 2B^2m^2}{1 - B^2m^2} E'(Bm) + \frac{B^2m^2}{1 - B^2m^2} K'(Bm)\right]}$$

K' complete elliptic integral of first kind with modulus k'

k variable of integration

$$k_1 = \frac{Bmx_1}{x - x_1}$$

$$k_2 = \frac{x - x_1}{Bmx_1}$$

$$k_3 = \frac{x - c}{Bmc}$$

$$k_4 = \frac{Bmc}{x - c}$$

$$k' = \sqrt{1 - k^2}$$

l distance from center of gravity to centroid of area of tail

M free-stream Mach number, $\frac{V}{a}$

M_s surface formed by envelope of after Mach cones springing from trailing edge of wing

$\overline{M}$ moment

$\overline{M}_0^{\alpha}$ $\frac{1}{\alpha}$ times moment associated with first term of equation (1)

$\overline{M}_1^{\alpha}$ $\frac{2V}{\dot{\alpha}c}$ times moment associated with second term of equation (1)

$\overline{M}_2^{\alpha}$	$\frac{4V^2}{\ddot{\alpha}\bar{c}^2}$ times moment associated with third term of equation (1)
$\overline{M}_0^{q}$	$\frac{2V}{q\bar{c}}$ times moment associated with first term of equation (2)
$\overline{M}_1^{q}$	$\frac{4V^2}{\dot{q}\bar{c}^2}$ times moment associated with second term of equation (2)
$\overline{M}_2^{q}$	$\frac{8V^3}{\ddot{q}\bar{c}^3}$ times moment associated with third term of equation (2)
m	tangent of semivertex angle of triangular wing
m_t	cotangent of trailing-edge sweep angle of wing
P	local static pressure minus free-stream static pressure
q	rate of pitch

$\dot{q} = \frac{\partial q}{\partial t}$

$\ddot{q} = \frac{\partial^2 q}{\partial t^2}$

$R = \sqrt{X^2 - B^2\left(Y^2 + Z^2\right)}$

S	area of airfoil surface
t	time
t_o	arbitrary instant of time
Δu_r	discontinuity in $\frac{\partial\theta_2}{\partial x}$ which is induced within plan-form boundaries by discontinuity in θ_2 across region of wake
V	free-stream velocity
w	velocity of vertical translation

$X = x - x_1$	
$Y = y - y_1$	
x, y, z	rectangular coordinates
x_1, y_1	auxiliary rectangular coordinates
$\bar{x}$	distance from leading edge of wing to center of gravity measured in streamwise direction
$\bar{z}$	distance between plane of wing and plane of tail
α	angle of attack, angle between body axes and free-stream direction at the center of gravity (see fig. 25(b))
$\dot{\alpha} = \frac{\partial \alpha}{\partial t}$;	the motion of center of gravity associated with this term corresponds to a constant vertical acceleration and is sometimes referred to as a plunging motion
$\ddot{\alpha} = \frac{\partial^2 \alpha}{\partial t^2}$	
Γ	spanwise circulation for an airfoil which has a spanwise circulation equal to $\Omega(x,y)$ at wing trailing edge
θ	component of potential function resulting from constant vertical acceleration
θ_1, θ_2	components of θ
θ_q	potential function due to constant rate of pitch
θ_q'	potential function due to constant rate of pitch about the axis $x = \frac{B^2 V t_o}{M^2}$
$\overline{\frac{\partial}{\partial z} \frac{\theta_q}{q c_w}}$	average value of $\frac{\partial}{\partial z} \frac{\theta_q}{q c_w}$ at horizontal-tail location
λ	variable of integration
ξ	variable of integration

ρ	mass density of air
σ	local angle-of-attack distribution
$\dot{\sigma} = \frac{\partial \sigma}{\partial t}$	
σ_1, σ_2	components of effective angle of attack on a tail which are associated with constant vertical acceleration
$\bar{\sigma}_2$	average value of σ_2 at horizontal-tail location
ϕ	potential function
ϕ_0^α	potential function associated with first term of equation (1)
ϕ_1^α	potential function associated with second term of equation (1)
ϕ_2^α	potential function associated with third term of equation (1)
ϕ_0^q	potential function associated with first term of equation (2)
ϕ_1^q	potential function associated with second term of equation (2)
ϕ_2^q	potential function associated with third term of equation (2)
ψ,Ω	components of potential function resulting from constant vertical acceleration (see eq. (9))
Ω_p	part of function Ω associated with induced effect on wing
Ω_w	part of function Ω associated with wake
Ω_α	potential function associated with constant angle of attack
$\overline{\frac{\partial}{\partial z} \frac{\Omega_\alpha}{\alpha V}}$	average value of $\frac{\partial}{\partial z} \frac{\Omega_\alpha}{\alpha V}$ at horizontal-tail location

Subscripts:

LE	leading edge of airfoil
t	tail

TE	trailing edge of airfoil
w	wing

Expressions such as $C_{L_\alpha}\big|_t$ and $C_{m_q}\big|_t$ refer to the stability derivatives of a tail surface considered as an isolated wing. Such expressions as $\Omega(0^+)$ mean that the value of Ω is obtained by approaching zero from a positive direction.

STATEMENT OF THE PROBLEM

This paper contains an investigation of the contribution of the horizontal tail to the lift and pitching moment produced by a constant angle of attack, a constant rate of pitch, and a constant vertical acceleration. Unfortunately, the need for finding the force and moment associated with a constant vertical acceleration is not always recognized. In order to clarify the reasons for investigating this force and moment, an approach to the more general problem of calculating the effect of unsteady motions on the forces and moments on an aircraft undergoing a certain type of longitudinal motion is presented.

Throughout the text the vertical velocity produced behind wings with a constant vertical acceleration at an angle of attack or in a pitching motion will be referred to as upwash. Negative upwash is, of course, commonly referred to as downwash.

Consider the problem of finding the force and moment acting on the wing and horizontal tail of an aircraft undergoing longitudinal motions in which the forward velocity is constant. The force and moment are determined not only by the instantaneous velocities but also by their past values. The approach to the problem of calculating the effect of unsteady longitudinal motions presented in this paper takes into account the time history of the velocities as well as their instantaneous values.

For many stability studies, the aircraft can be considered a rigid body and if the changes in the forward velocity are neglected, its longitudinal motion can be broken down into two components: (1) the vertical translation of the center of gravity and (2) the rotation of the center of gravity.

The velocity of the vertical translation w and the velocity of rotation q of the center of gravity may be expressed as a power series in time about some arbitrary instant of time t_o. These two power series are

$$\frac{w}{V} = \alpha(t) = \alpha\Big|_{t=t_o} + (t - t_o)\dot{\alpha}\Big|_{t=t_o} + \frac{(t - t_o)^2}{2!}\ddot{\alpha}\Big|_{t=t_o} + \ldots \tag{1}$$

and

$$q(t) = q\Big|_{t=t_o} + (t - t_o)\dot{q}\Big|_{t=t_o} + \frac{(t - t_o)^2}{2!}\ddot{q}\Big|_{t=t_o} + \ldots \tag{2}$$

If it is assumed that the forces and moments can be calculated with sufficient accuracy by the linearized theory of supersonic flow, the following partial differential equation must be satisfied in the flow field:

$$B^2\phi_{xx} - \phi_{yy} - \phi_{zz} + \frac{2V}{a^2}\phi_{xt} + \frac{1}{a^2}\phi_{tt} = 0 \tag{3}$$

Since the preceding differential equation is linear, the flow associated with each term of equations (1) and (2) can be considered separately, and the total force and moment may then be found by summing the results from the individual terms.

The boundary conditions associated with each of the first three terms of equations (1) and (2) are: The potential function associated with each term is zero upstream of the wing disturbance. On the wing and tail surfaces, the flow must be tangent to the surfaces; thus,

$$\frac{\partial\phi_0^\alpha}{\partial z} = -\alpha V \qquad \frac{\partial\phi_0^q}{\partial z} = -qx$$

$$\frac{\partial\phi_1^\alpha}{\partial z} = -\dot{\alpha}V(t - t_o) \qquad \frac{\partial\phi_1^q}{\partial z} = -\dot{q}x(t - t_o)$$

$$\frac{\partial\phi_2^\alpha}{\partial z} = -\frac{\ddot{\alpha}V}{2!}(t - t_o)^2 \qquad \frac{\partial\phi_2^q}{\partial z} = -\frac{\ddot{q}x}{2!}(t - t_o)^2$$

In the region of the wake of the wing upstream of any disturbance from the tail surface, the pressure must be zero; thus, in the region of the wake

$$\frac{\partial\phi_0^\alpha}{\partial x} + \frac{1}{V}\frac{\partial\phi_0^\alpha}{\partial t} = 0 \qquad \frac{\partial\phi_0^q}{\partial x} + \frac{1}{V}\frac{\partial\phi_0^q}{\partial t} = 0$$

$$\frac{\partial\phi_1^\alpha}{\partial x} + \frac{1}{V}\frac{\partial\phi_1^\alpha}{\partial t} = 0 \qquad \frac{\partial\phi_1^q}{\partial x} + \frac{1}{V}\frac{\partial\phi_1^q}{\partial t} = 0$$

$$\frac{\partial\phi_2^\alpha}{\partial x} + \frac{1}{V}\frac{\partial\phi_2^\alpha}{\partial t} = 0 \qquad \frac{\partial\phi_2^q}{\partial x} + \frac{1}{V}\frac{\partial\phi_2^q}{\partial t} = 0$$

Solutions of equation (3) which satisfy the boundary conditions set forth in the preceding paragraph allow the calculation of the force and moment associated with each term of equations (1) and (2). The total force and moment can be written as

$$F = \alpha\Big|_{t=t_o} F_0^\alpha + \dot{\alpha}\Big|_{t=t_o} \frac{\bar{c}}{2V} F_1^\alpha(t) + \ddot{\alpha}\Big|_{t=t_o}\left(\frac{\bar{c}}{2V}\right)^2 F_2^\alpha(t) + \ . \ . \ . \ +$$

$$q\Big|_{t=t_o} \frac{\bar{c}}{2V} F_0^q + \dot{q}\Big|_{t=t_o}\left(\frac{\bar{c}}{2V}\right)^2 F_1^q(t) + \ddot{q}\Big|_{t=t_o}\left(\frac{\bar{c}}{2V}\right)^3 F_2^q(t) + \ . \ . \ .$$

$$\bar{M} = \alpha\Big|_{t=t_o}\bar{M}_0^\alpha + \dot{\alpha}\Big|_{t=t_o} \frac{\bar{c}}{2V} \bar{M}_1^\alpha(t) + \ddot{\alpha}\Big|_{t=t_o}\left(\frac{\bar{c}}{2V}\right)^2 \bar{M}_2^\alpha + \ . \ . \ . \ +$$

$$q\Big|_{t=t_o}\left(\frac{\bar{c}}{2V}\right)\bar{M}_0^q + \dot{q}\Big|_{t=t_o}\left(\frac{\bar{c}}{2V}\right)^2 \bar{M}_1^q(t) + \ddot{q}\Big|_{t=t_o}\left(\frac{\bar{c}}{2V}\right)^3 \bar{M}_2^q(t) + \ . \ . \ .$$

The F and $\bar{M}$ expressions in the preceding equations are functions of time and are not zero when $t = t_o$. The force and moment at $t = t_o$ can be written in coefficient form as

$$\begin{aligned} C_L = {} & \alpha\Big|_{t=t_o} C_{L_\alpha} + \dot{\alpha}\Big|_{t=t_o} \frac{\bar{c}}{2V} C_{L_{\dot{\alpha}}} + \ddot{\alpha}\Big|_{t=t_o}\left(\frac{\bar{c}}{2V}\right)^2 C_{L_{\ddot{\alpha}}} + \cdot \cdot \cdot + \\ & q\Big|_{t=t_o} \frac{\bar{c}}{2V} C_{L_q} + \dot{q}\Big|_{t=t_o}\left(\frac{\bar{c}}{2V}\right)^2 C_{L_{\dot{q}}} + \ddot{q}\Big|_{t=t_o}\left(\frac{\bar{c}}{2V}\right)^3 C_{L_{\ddot{q}}} + \cdot \cdot \cdot \end{aligned} \qquad (4)$$

$$\begin{aligned} C_m = {} & \alpha\Big|_{t=t_o} C_{m_\alpha} + \dot{\alpha}\Big|_{t=t_o} \frac{\bar{c}}{2V} C_{m_{\dot{\alpha}}} + \ddot{\alpha}\Big|_{t=t_o}\left(\frac{\bar{c}}{2V}\right)^2 C_{m_{\ddot{\alpha}}} + \cdot \cdot \cdot + \\ & q\Big|_{t=t_o} \frac{\bar{c}}{2V} C_{m_q} + \dot{q}\Big|_{t=t_o}\left(\frac{\bar{c}}{2V}\right)^2 C_{m_{\dot{q}}} + \ddot{q}\Big|_{t=t_o}\left(\frac{\bar{c}}{2V}\right)^3 C_{m_{\ddot{q}}} + \cdot \cdot \cdot \end{aligned} \qquad (5)$$

The coefficients C_{L_α}, $C_{L_{\dot{\alpha}}}$, C_{m_α}, $C_{m_{\dot{\alpha}}}$, C_{L_q}, and C_{m_q} are the standard stability derivatives. The remaining quantities can be considered as stability derivatives which take into account the unsteady-flow effects other than the $\dot{\alpha}$ effect.

The series given by equations (4) and (5) are assumed to converge; however, in subsonic flow there is some evidence that the series may not converge for two-dimensional airfoils. In supersonic flow, the force and moment (calculated on the basis of linearized flow theory) depend only on the flow field between the leading edge of the wing and the trailing edge of the tail. Since only a small portion of the flow field is involved for supersonic flows, it is expected that these series will converge.

In the present paper, it is assumed that the force and moment can be approximated sufficiently accurately by

$$C_L = \alpha C_{L_\alpha} + \frac{\dot{\alpha}\bar{c}}{2V} C_{L_{\dot{\alpha}}} + \frac{q\bar{c}}{2V} C_{L_q} \qquad (6)$$

and

$$C_m = \alpha C_{m_\alpha} + \frac{\dot{\alpha}\bar{c}}{2V} C_{m_{\dot{\alpha}}} + \frac{q\bar{c}}{2V} C_{m_q} \tag{7}$$

The problem to be considered is the evaluation of the contribution of the horizontal tail to the derivatives contained in equations (6) and (7).

CALCULATION OF FLOW FIELDS OF AIRFOILS HAVING LINEAR ANGLE-OF-ATTACK VARIATIONS WITH TIME

Basic Theory

In the preceding section the aerodynamic lifting force and pitching moment were expressed as an infinite series of stability derivatives. The first stability derivatives of the series which are associated with unsteady flows were shown to be associated with the lift and moment resulting from a constant vertical acceleration. In this section methods are presented for the calculation of the flow fields produced by wings with a constant vertical acceleration and the potential function on the surface of tails which are located behind these wings.

In order to calculate the flow field produced by a wing which has a constant vertical acceleration and the potential function on a horizontal tail behind the wing, the solution of two unsteady-flow problems will be utilized. The first problem is the calculation of the upwash induced by the wing at a constant vertical acceleration, and the second is the calculation of the pressure on an airfoil which has a local angle-of-attack distribution which varies linearly with time. These two problems are special cases of the more general problem of calculating the flow induced by an airfoil which has an arbitrary angle-of-attack distribution which varies linearly with time. This general problem is formulated and the solutions to the other problems are taken from it. The effects of the rolling up of the wake and other distortions are neglected and the wake is assumed to remain in the plane of the wing.

The linearized partial differential equation (eq. (3)) for unsteady supersonic flow is

$$B^2\phi_{xx} - \phi_{yy} - \phi_{zz} + \frac{2V}{a^2}\phi_{xt} + \frac{1}{a^2}\phi_{tt} = 0$$

where the x-axis lies along the free-stream direction. The potential for a zero-thickness lifting airfoil is antisymmetric with respect to the plane of the wing ($z = 0$ plane). It is therefore necessary only to determine the potential above the plane for $z = 0$. This potential can be determined by specifying the boundary conditions in the plane of the wing and the potential upstream of the airfoil disturbance. The boundary and initial conditions for the potential for the region above an airfoil which has a local angle of attack varying linearly with time may be given as

$$\phi = 0 \tag{8a}$$

upstream of the wing disturbance,

$$\phi_z = -\dot{\sigma}Vf(x,y)(t - t_o) \tag{8b}$$

on the plan form, and

$$P = -\rho(V\phi_x + \phi_t) = 0 \tag{8c}$$

for $z = 0$ (the plane of the wing) off the plan form. The condition given by equation (8c) is necessary to insure that there is no pressure discontinuity across the wake.

From the preceding boundary condition, it follows that

$$V\phi_x(x,y,0,t) + \phi_t(x,y,0,t) = 0$$

off the plan form. The general integral of this partial differential equation is any arbitrary function of y and $x - Vt$. The potential is assumed to be continuous in the stream direction, and the potential has been taken to be zero upstream of the wing disturbance; thus, the function must be zero for points not on the plan form or in the region of the wake. The boundary conditions can now be written as

$$\phi(x,y,z,t) = 0$$

upstream of the wing disturbance,

$$\phi(x,y,0,t) = 0$$

for $z = 0$ for points not on the plan form nor in the region of the wake,

$$\phi_z(x,y,0,t) = -\dot{\sigma}Vf(x,y)(t - t_o)$$

for $z = 0$ for points on the plan form, and

$$V\phi_x + \phi_t = 0$$

for $z = 0$ for points in the region of the wake.

A solution of equation (3) can be found by assuming a function of the form

$$\phi = \theta(x,y,z) + x\psi(x,y,z) + t\Omega(x,y,z) \tag{9}$$

This assumption appears reasonable since the boundary conditions are linear functions of time and equation (3) has the same form if x and t are interchanged.

Substituting equation (9) into equation (3) and equating powers of t yields

$$B^2\Omega_{xx} - \Omega_{yy} - \Omega_{zz} = 0 \tag{10a}$$

$$B^2\theta_{xx} + 2B^2\psi_x + B^2x\psi_{xx} - \theta_{yy} - x\psi_{yy} - \theta_{zz} - x\psi_{zz} + \frac{2V}{a^2}\Omega_x = 0 \tag{10b}$$

If ψ is set equal to $-\frac{V}{B^2a^2}\Omega$, equation (10b) reduces to

$$B^2\theta_{xx} - \theta_{yy} - \theta_{zz} - \frac{xV}{B^2a^2}\left(B^2\Omega_{xx} - \Omega_{yy} - \Omega_{zz}\right) = 0 \tag{11}$$

Substituting equation (10a) into equation (11) yields

$$B^2\theta_{xx} - \theta_{yy} - \theta_{zz} = 0 \tag{12}$$

Thus, under the assumption that

$$\psi = -\frac{V}{B^2a^2}\Omega$$

equation (9) may be written as

$$\phi = \theta(x,y,z) + \left(t - \frac{xM}{B^2a}\right)\Omega(x,y,z) \tag{13}$$

where θ and Ω are solutions of the partial differential equation for steady supersonic flow. Note that Ω does not have the dimensions of a potential of steady flow. Equation (13) was found by Clifford S. Gardner of New York University in an unpublished analysis using another approach and was used by Ribner in reference 16.

The boundary conditions require that

$$\phi_z = \theta_z + \left(t - \frac{xM}{B^2 a}\right)\Omega_z = -\dot{\sigma}Vf(x,y)(t - t_o)$$

on the plan form or, if the powers of t are equated,

$$\Omega_z = -\dot{\sigma}Vf(x,y) \tag{14a}$$

and

$$\theta_z - \frac{xM}{B^2 a}\Omega_z = \dot{\sigma}Vt_o f(x,y) \tag{14b}$$

Substituting equation (14a) into equation (14b) yields

$$\theta_z = \left(Vt_o - \frac{xM^2}{B^2}\right)\dot{\sigma}f(x,y) \tag{14c}$$

The boundary conditions also require that

$$\theta = 0 \tag{15a}$$

$$\Omega = 0 \tag{15b}$$

for all points either upstream of the wing disturbance or in the plane $z = 0$ which are not on the plan form or in the region of the wake and that

$$V\theta_x + \left(Vt - \frac{xM^2}{B^2}\right)\Omega_x - \frac{\Omega}{B^2} = 0 \tag{16}$$

for points in the region of the wake. When the powers of t are equated, equation (16) yields

$$\Omega_x = 0 \tag{17a}$$

$$V\theta_x - \frac{\Omega}{B^2} = 0 \tag{17b}$$

Equations (14a), (15b), and (17a) are the boundary conditions for a potential Ω for an airfoil which has a local angle of attack equal to $\dot{\sigma} f(x,y)$ in steady flow. Thus, since Ω satisfies the linearized partial differential equation for steady flow, it can be determined by the methods commonly used for obtaining steady-state solutions in supersonic flow.

Similarly, equations (14c) and (15a) are the boundary conditions for the potential θ for an airfoil which has a local angle of attack equal to $-\left(Vt_0 - \frac{xM^2}{B^2}\right)\frac{\dot{\sigma} f(x,y)}{V}$. Also, because θ satisfies the linearized partial differential equation for steady flow, in the region unaffected by the wake it can be found by the methods used in steady-flow calculations. However, inasmuch as the boundary condition of equation (17b) replaces the condition that in the region of the wake $\theta_x = 0$, which is implied in these methods, another approach must be used to obtain solutions in the region affected by the wake.

A convenient approach is to divide θ into two parts: $\theta = \theta_1 + \theta_2$ where θ_1 is the steady-flow solution for the given airfoil in the ordinary sense, that is, subject to the condition that $\frac{\partial \theta_1}{\partial x} = 0$ in the region of the wake. It follows that θ_2 must satisfy the following boundary conditions:

$$\theta_2(x,y,z) = 0 \tag{18a}$$

upstream of the wake influence,

$$\frac{\partial \theta_2(x,y,z)}{\partial z} = 0 \tag{18b}$$

on the wing plan form,

$$\theta_2(x,y,0) = 0 \tag{18c}$$

for points not on the wing plan form nor in the region of the wake, and

$$\frac{\partial\theta_2(x,y,0)}{\partial x} = \frac{1}{B^2V}\,\Omega(x,y,0) \tag{18d}$$

for points in the region of the wake.

The solution for $\theta_2(x,y,z)$ can be obtained in several ways. Two approaches are presented here. Both methods require that $\frac{\partial\theta_2}{\partial x}$ be known in the plane of the airfoil. The discontinuity in $\frac{\partial\theta_2}{\partial x}$ is zero everywhere except in the region of the viscous wake, and except (for the case of wings with subsonic trailing edges) in the region of the wing affected by the wake, where a discontinuity in $\frac{\partial\theta_2}{\partial x}$ is induced by virtue of the conditions expressed in equations (18b), (18c), and (18d). The value of the discontinuity in $\frac{\partial\theta_2}{\partial x}$ for points in the region of the viscous wake can be determined from equation (18d). In many cases, the discontinuity in $\frac{\partial\theta_2}{\partial x}$ induced on the plan form can be found by using the method developed in reference (20) for the pressure cancellation for subsonic trailing edges.

The first of the methods to be presented deals directly with the discontinuity in $\frac{\partial\theta_2}{\partial x}$ in the $z = 0$ plane. If $\frac{\Delta\partial\theta_2}{\partial x}$ is assumed to be known in the plane of the wing, then θ_2 is given by (from eq. (6), ref. 15)

$$\theta_2(x,y,z) = \frac{z}{2\pi B^2V}\iint_{\text{Wake}} \frac{\Delta\Omega(x_1,y_1,0)X}{\left(Y^2 + z^2\right)R}\,dx_1\,dy_1 + \frac{1}{2\pi}\iint_{\text{Wing}} \frac{z\,\Delta u_r\,X}{\left(Y^2 + z^2\right)R}\,dx_1\,dy_1 \tag{19}$$

where Δu_r is the discontinuity of $\frac{\partial \theta_2}{\partial x}$ across the $z = 0$ plane induced within the plan-form boundaries by the discontinuity of θ_2 across the wake and where $\Delta\Omega$ is the known discontinuity in Ω across the plane $z = 0$. Note that for wings with supersonic trailing edges Δu_r is zero.

Since Ω is the potential for an airfoil in steady flow, and since the potential discontinuity in the region of the wake for an airfoil in steady flow is constant in the x-direction, it follows that $\Delta\Omega$ is constant in the x-direction. In other words, $\Delta\Omega(x,y,0)$ is a function of y only and may be written as $\Delta\Omega(y)$.

If the equation of the trailing edge is given by

$$x_1 = J(y_1) \tag{20}$$

equation (19) can be written as

$$\theta_2(x,y,z) = \frac{z}{2\pi B^2 V}\int_{h_1}^{h_2} \frac{\Delta\Omega(y_1)}{Y^2 + z^2}\,dy_1 \int_{J(y_1)}^{x-B\sqrt{Y^2+z^2}} \frac{X}{R}\,dx_1 + \frac{1}{2\pi}\iint_{\text{Wing}} \frac{z\,\Delta u_r\,X}{\left(Y^2 + z^2\right)R}\,dx_1\,dy_1 \tag{21}$$

The limits on the outer integral of the first term of the right-hand side of equation (21) are taken across the span of the wing or to the limits of the forward Mach cone from the point (x,y,z). The first term on the right-hand side of equation (21) can be integrated with respect to x_1. The result of this operation is

$$\theta_2(x,y,z) = \frac{z}{2\pi B^2 V}\int_{h_1}^{h_2} \frac{\Delta\Omega(y_1)}{Y^2 + z^2}\sqrt{(x - J)^2 - B^2\left(Y^2 + z^2\right)}\,dy_1 + \frac{1}{2\pi}\iint_{\text{Wing}} \frac{z\,\Delta u_r\,X}{\left(Y^2 + z^2\right)R}\,dx_1\,dy_1 \tag{22}$$

The second method of calculating θ_2 is similar to the approach used by Ribner in reference 16. By this method an expression for $\frac{\partial\theta_2}{\partial x}$ is given and θ_2 is then found by integration.

The boundary conditions for $\frac{\partial\theta_2(x,y,z)}{\partial x}$ for wings with supersonic trailing edges are

$$\frac{\partial\theta_2(x,y,z)}{\partial x} = 0$$

upstream of the wake influence,

$$\frac{\partial\theta_2(x,y,0)}{\partial x} = 0$$

for points not in the region of the wake, and

$$\frac{\partial\theta_2(x,y,0)}{\partial x} = \frac{1}{B^2V}\,\Omega(x,y,0)$$

for points in the region of the wake. These boundary conditions are the same as the boundary conditions for the potential of a lifting line located at the trailing edge of the airfoil. The strength of this lifting line is $\frac{1}{B^2V}\Gamma$ where Γ is the spanwise circulation for an airfoil which has a spanwise circulation equal to the value of $\Omega(x,y,z)$ at the wing trailing edge. Thus,

$$\frac{\partial\theta_2(x,y,z)}{\partial x} = \frac{1}{B^2V}\,\Omega_w(x,y,z)$$

where $\Omega_w(x,y,z)$ is the part of $\Omega(x,y,z)$ which results from the discontinuity of $\Omega(x,y,z)$ through the region of the wake. The function $\Omega_w(x,y,z)$ is also the potential resulting from a lifting line which has a circulation of the amount Γ and is located at the trailing edge. It follows that

$$\theta_2(x,y,z) = \frac{1}{B^2V}\int_{M_s}^{x} \Omega_w(\lambda,y,z)\,d\lambda \tag{23}$$

where the lower limit is taken from the trailing-edge Mach surface M_s. (The expression "trailing-edge Mach surface" refers to the surface formed by the envelope of the after Mach cones springing from the trailing edge.)

The solution for $\theta_2(x,y,z)$ associated with wings which have subsonic trailing edges must include the effect of the potential induced on the plan-form area because of the condition that

$$\frac{\partial \theta_2(x,y,0)}{\partial z} = 0$$

on the wing plan form. Thus, if Ω_p denotes the effect of this induced potential for wings with subsonic trailing edges,

$$\theta_2(x,y,z) = \frac{1}{B^2V}\int_{M_s}^{x}\left[\Omega_p(\lambda,y,z) + \Omega_w(\lambda,y,z)\right]d\lambda \tag{24}$$

Two methods of finding the function $\theta_2(x,y,z)$ have been presented, the expressions for θ_2 being given by equation (22) and equation (24). The function $\theta_2(x,y,z)$ can also be obtained by other approaches, one of which will be utilized in an example which is presented at the end of this section.

In appendix A, equation (22) is differentiated and the following equations are obtained:

$$\frac{\partial \theta_2(x,y,z)}{\partial y} = \frac{z}{2\pi B^2V}\int_{h_1}^{h_2}\frac{\Delta\Omega(y_1)\left[-\frac{2(x - J)^2}{Y^2 + z^2} + B^2\right]Y}{\left(Y^2 + z^2\right)\sqrt{(x - J)^2 - B^2\left(Y^2 + z^2\right)}}\,dy_1 +$$

$$\frac{z}{2\pi}\frac{\partial}{\partial y}\iint_{\text{Wing}}\frac{X\,\Delta u_r}{\left(Y^2 + z^2\right)R}\,dx_1\,dy_1 \tag{25}$$

$$\frac{\partial\theta_2(x,y,z)}{\partial z} = \frac{1}{2\pi B^2 V}\int_{h_1}^{h_2} \frac{\Delta\Omega(y_1)}{\left(Y^2 + z^2\right)^2}\left[Y^2\sqrt{(x - J)^2 - B^2\left(Y^2 + z^2\right)} - \frac{z^2(x - J)^2}{\sqrt{(x - J)^2 - B^2\left(Y^2 + z^2\right)}}\right]dy_1 + \frac{z}{2\pi}\frac{\partial}{\partial z}\iint_{\text{Wing}} \frac{X\,\Delta u_r}{\left(Y^2 + z^2\right)_R}\,dx_1\,dy_1 \tag{26}$$

The differentiation of the double integrals of Δu_r was indicated only in the preceding equations, the reason being that the expressions resulting from the differentiation under the integral sign appear to be of little value in numerical calculations. For wings with supersonic trailing edges, Δu_r is zero. Thus, the double integrals vanish. For most problems where the wing has subsonic trailing edges, the sidewash and upwash contributed by the double integrals in the usual tail location could be approximated by the sidewash and upwash from a lifting line in the vicinity of the trailing edge. This lifting line should have a strength equal to $\frac{1}{B^2V}\,(\Delta\phi_2)_{TE}$ where $(\Delta\phi_2)_{TE}$ is the potential induced at the trailing edge by the discontinuity in θ_2 in the region of the wake.

In appendix A the following expressions are developed for $\frac{\partial\theta_2}{\partial y}$ and $\frac{\partial\theta_2}{\partial z}$ for wings with supersonic trailing edges:

$$\frac{\partial\theta_2(x,y,z)}{\partial y} = \frac{1}{B^2V}\int_{G(y,z)}^{x} \frac{\partial\Omega_w(\lambda,y,z)}{\partial y}\,d\lambda - \frac{1}{B^2V}\,\Omega_w(M_s)\,\frac{\partial G(y,z)}{\partial y} \tag{27}$$

$$\frac{\partial\theta_2(x,y,z)}{\partial z} = \frac{1}{B^2V}\int_{G(y,z)}^{x} \frac{\partial\Omega_w(\lambda,y,z)}{\partial z}\,d\lambda - \frac{1}{B^2V}\,\Omega_w(M_s)\,\frac{\partial G(y,z)}{\partial z} \tag{28}$$

where $\frac{\partial\Omega_w}{\partial y}$ and $\frac{\partial\Omega_w}{\partial z}$ are the sidewash and upwash from a lifting line with a strength equal to Γ and located at the trailing edge of the wing. For subsonic trailing edges,

$$\frac{\partial\theta_2(x,y,z)}{\partial y} = \frac{1}{B^2V}\int_{M_s}^{x}\frac{\partial\Omega_p(\lambda,y,z)}{\partial y}\,d\lambda + \frac{1}{B^2V}\int_{M_s}^{x}\frac{\partial\Omega_w(\lambda,y,z)}{\partial y}\,d\lambda \tag{29}$$

and

$$\frac{\partial\theta_2(x,y,z)}{\partial z} = \frac{1}{B^2V}\int_{M_s}^{x}\frac{\partial\Omega_p(\lambda,y,z)}{\partial z}\,d\lambda + \frac{1}{B^2V}\int_{M_s}^{x}\frac{\partial\Omega_w(\lambda,y,z)}{\partial z}\,d\lambda \tag{30}$$

where $\frac{\partial\Omega_p}{\partial y}$ and $\frac{\partial\Omega_p}{\partial z}$ are the sidewash and upwash resulting from the potential induced on the plan form by the discontinuity of Ω through the wake.

The total potential (from eq. (13)) in the region affected by the wake is, therefore,

$$\phi(x,y,z,t) = \theta_1(x,y,z) + \theta_2(x,y,z) + \dot{\sigma}\left(t - \frac{xM}{B^2a}\right)\frac{\Omega(x,y,z)}{\dot{\sigma}} \tag{31}$$

The sidewash and the upwash are therefore given by

$$\phi_y = \frac{\partial\theta_1}{\partial y} + \frac{\partial\theta_2}{\partial y} + \dot{\sigma}\left(t - \frac{xM}{B^2a}\right)\frac{\partial}{\partial y}\frac{\Omega}{\dot{\sigma}} \tag{32}$$

and

$$\phi_z = \frac{\partial\theta_1}{\partial z} + \frac{\partial\theta_2}{\partial z} + \dot{\sigma}\left(t - \frac{xM}{B^2a}\right)\frac{\partial}{\partial z}\frac{\Omega}{\dot{\sigma}} \tag{33}$$

The upwash on the plan form of a wing undergoing constant vertical acceleration is given by

$$\phi_z = -\dot{\alpha}V(t - t_o) \qquad (z = 0)$$

for axes attached to the wing. Therefore, for this motion,

$$f(x,y) = 1$$

and

$$\dot{\sigma} = \dot{\alpha}$$

The potential $\theta_1(x,y,z)$ is the steady-flow potential for an airfoil which has an angle-of-attack distribution equal to $-\frac{\dot{\sigma}}{V}\left(Vt_o - \frac{xM^2}{B^2}\right)f(x,y)$ or $-\frac{\dot{\alpha}}{V}\left(Vt_o - \frac{xM^2}{B^2}\right)$ and for which $\frac{\partial\theta_1}{\partial x} = 0$ in the wake. Since a wing having a constant rate of pitch about an axis located at $x = x_o$ has an angle-of-attack distribution equal to $\frac{q(x - x_o)}{V}$,

$$\theta_1(x,y,z) = \frac{M^2\dot{\alpha}}{qB^2}\theta_q'$$

where θ_q' is the steady-state potential due to a wing pitching about an axis located at $x = \frac{B^2Vt_o}{M^2}$.

The potential $\frac{\Omega(x,y,z)}{\dot{\sigma}}$ is the steady-flow potential resulting from a wing having an angle of attack equal to $f(x,y)$ or in this case unity. If Ω_α is the potential due to a wing having a constant angle of attack α,

$$\Omega(x,y,z) = \frac{\dot{\alpha}}{\alpha}\Omega_\alpha$$

The function θ_2 is given by equation (22) or equation (24).

Therefore, the sidewash and upwash are given by

$$\frac{\phi_y}{\dot{\alpha}c} = \frac{M^2}{B^2}\frac{\partial}{\partial y}\frac{\theta_q}{qc} + \left[\frac{V}{c}(t - t_o) - \frac{M^2x}{B^2c}\right]\frac{\partial}{\partial y}\frac{\Omega_\alpha}{\alpha V} + \frac{1}{\dot{\alpha}c}\frac{\partial\theta_2}{\partial y} \tag{34}$$

and

$$\frac{\phi_z}{\dot{\alpha}c} = \frac{M^2}{B^2}\frac{\partial}{\partial z}\frac{\theta_q}{qc} + \left[\frac{V}{c}(t - t_o) - \frac{M^2x}{B^2c}\right]\frac{\partial}{\partial z}\frac{\Omega_\alpha}{\alpha V} + \frac{1}{\dot{\alpha}c}\frac{\partial\theta_2}{\partial z} \tag{35}$$

where θ_q is the potential for the wing pitching about the axis $x = 0$. Equation (35) is used to calculate the upwash from a number of wings.

Upwash at the Trailing Edge

For wings with supersonic trailing edges, the upwash immediately behind the trailing edge is given by

$$\frac{\phi_z}{\dot{\alpha}c} = \frac{M^2}{B^2}\frac{\partial}{\partial z}\left(\frac{\theta_q}{qc}\right)_{TE} + \left[\frac{V}{c}(t - t_o) - \frac{M^2x}{B^2c}\right]\frac{\partial}{\partial z}\left(\frac{\Omega_\alpha}{\alpha V}\right)_{TE} + \frac{1}{\dot{\alpha}c}\left(\frac{\partial\theta_2}{\partial z}\right)_{TE} \tag{36}$$

The first two terms of this expression may be evaluated by the method of calculating the steady-flow upwash immediately behind the trailing edge (refs. 10, 11, and 15). The term $\left(\frac{\partial\theta_2}{\partial z}\right)_{TE}$ is (from appendix A) the expression $-\frac{1}{B^2V}\,\Omega_w(M_s)\,\frac{\partial G(y,z)}{\partial z}$ evaluated in the plane for $z = 0$ at the trailing edge of the wing.

Approximate Values of ϕ_y and ϕ_z

An approximation to the sidewash and upwash can be obtained by neglecting the terms which become constant for large values of x in equations (34) and (35). This approximation leads to the following expressions:

$$\frac{\phi_y}{\dot{\alpha}c} \approx \left[\frac{V}{c}(t - t_o) - \frac{x}{c}\right]\frac{\partial}{\partial y}\frac{\Omega_\alpha}{\alpha V} \tag{37a}$$

$$\frac{\phi_z}{\dot{\alpha}c} \approx \left[\frac{V}{c}(t - t_o) - \frac{x}{c}\right]\frac{\partial}{\partial z}\frac{\Omega_\alpha}{\alpha V} \tag{37b}$$

Equations (37) may also be obtained by assuming that the lift on the wing builds up instantaneously and that the upwash at a relatively large distance behind the wing is determined by steady-flow values of the lift distribution on the wing. It is not assumed, however, that the upwash at the tail location at a given instant corresponds to the lift distribution on the wing at the same instant. The assumption is made that there is a time lag between the lift distribution on the wing and the upwash induced by this lift distribution at the tail location. This time lag is the time required for a point moving with the free-stream velocity to travel from the wing location to the tail location. In the past it has been found that, by using the stability derivative $C_{m_{\dot{\alpha}}}$ calculated on the preceding assumptions, the airplane motions could generally be predicted with satisfactory accuracy (ref. 21). This accuracy seems to indicate that values of upwash from a wing having a constant vertical acceleration in subsonic flow, calculated on the basis of the preceding assumptions, are a good approximation to the exact values.

The question naturally arises as to whether the simple assumptions of instantaneous lift build-up and time-lag effect give a good approximation to the upwash from a wing which has a constant vertical acceleration at supersonic speeds. This question is investigated for a number of cases.

The values given by equations (37) are dependent upon the position of the origin of the x-axis. Since equations (37) represent a time-lag effect in the flow field, it seems logical that the origin of the x-axis should be located near the centroid of the wing area for wings with small amounts of sweep. For highly swept wings it seems logical to allow the origin of the x-axis to vary along the span so that the distance x in equations (37) represents the distance from the point under consideration to the center of the section of the wing which lies directly upstream of the point under consideration.

An approximate method of calculating the upwash behind wings with a constant acceleration which is more accurate than equation (37b) is as follows: Calculate the angle-of-attack and pitching components approximately by the use of lifting lines. (See refs. 13 and 15.) The component $\frac{\partial\theta_2}{\partial z}$ can be calculated exactly for wings with supersonic trailing edges and approximately for wings with subsonic trailing edges by neglecting the integral over the wing in equation (26). This method should yield results which are accurate to a fairly high degree except near the trailing edge or the Mach surface which springs from it since the main approximation is the calculation of the angle-of-attack and the pitching components by the use of lifting lines.

The Two-Dimensional Airfoil

One of the simplest time-dependent upwash problems is the two-dimensional airfoil which has a constant vertical acceleration.

For the region which is not affected by the wake, θ_2 is zero, and by inspection

$$\frac{\partial\theta_q}{\partial z} = -q(x - Bz)$$

The component $\frac{\partial\Omega_\alpha}{\partial z}$ is

$$\frac{\partial\Omega_\alpha}{\partial z} = -\alpha V$$

From equation (35), the upwash is given by

$$\frac{\phi_z}{\dot{\alpha}c} = \frac{M^2}{B}\frac{z}{c} - \frac{V}{c}(t - t_o) \tag{38}$$

From the region affected by the wake, $\frac{\partial\theta_q}{\partial z}$ and $\frac{\partial\Omega_\alpha}{\partial z}$ are zero and equation (35) yields

$$\frac{\phi_z}{\dot{\alpha}c} = \frac{1}{\dot{\alpha}c}\frac{\partial\theta_2}{\partial z} \tag{39}$$

From equation (28),

$$\frac{\partial\theta_2}{\partial z} = -\frac{1}{B^2V}\Omega_w(M_s)\frac{\partial G(y,z)}{\partial z} \tag{40}$$

When the y-axis is located along the leading edge of the wing (from eq. (A9) of appendix A),

$$G(y,z) = c + Bz \tag{41}$$

Since the potential function on the upper surface of a two-dimensional airfoil at a constant angle of attack is $\frac{\alpha Vx}{B}$ where x is measured from the leading edge, $\Omega_W(M_s)$ is given by

$$\Omega_W(M_s) = \frac{\dot{\alpha}Vc}{B} \tag{42}$$

Thus, the upwash in the region affected by the wake is found to be given by

$$\frac{\phi_z}{\dot{\alpha}c} = -\frac{1}{B^2} \tag{43}$$

Values of $\frac{\phi_z}{\dot{\alpha}c}$ at $t = t_o$ are plotted for various values of z in figure 1.

An examination of equation (37b) and figure 1 reveals that the approximation given by equation (37b) breaks down for the upwash behind a two-dimensional airfoil.

The Triangular Wing

The upwash along the center line of the wake is determined for a triangular wing with subsonic leading edges. Equation (35) indicates that the upwash induced by a wing with a constant vertical acceleration is made up of three components. One of these three components, $\frac{\partial}{\partial z}\frac{\Omega_\alpha}{\alpha V}$, is available in the published literature. (See refs. 11 and 12.) The two remaining components are derived in this paper.

The upwash along the center line of the wake of a triangular wing with a constant angle of attack is given in references 11 and 12. From either of these references the upwash along the center line of the wake can be written as

$$\frac{\partial}{\partial z}\frac{\Omega_\alpha}{\alpha V} = -\frac{2}{\pi E'(Bm)}\left\{k_4\left[E(k_3) - \left(1 - k_3^2\right)K(k_3)\right] + \int_0^1 \frac{K(k_1) - E(k_1)}{k_1 + Bm}\,dk_1 + \int_{k_3}^1 \frac{K(k_2) - E(k_2)}{k_2^2\left(1 + k_2 Bm\right)}\,dk_2\right\} \tag{44a}$$

for $c \leqq x \leqq (Bm + 1)c$, and

$$\frac{\partial}{\partial z}\frac{\Omega_\alpha}{\alpha V} = -\frac{2}{\pi E'(Bm)}\left[E(k_4) + \int_0^{k_4} \frac{K(k_1) - E(k_1)}{k_1 + Bm}\,dk_1\right] \tag{44b}$$

for $(Bm + 1)c \leqq x$. Figure 2 presents the variation of $\frac{\partial}{\partial z}\frac{\Omega_\alpha}{\alpha V}$ along the wake center line of a triangular wing for various values of Bm. These values were taken from references 11 and 12.

The upwash along the center line of the wake of a triangular wing with a constant rate of pitch is found in appendix B. From the results of this appendix the upwash along the wake center line can be expressed as follows:

$$\frac{\partial\theta_q(x,0,0)}{\partial z} = -2K_q c\left\{\frac{x}{c}\int_0^1 \frac{k_1\left[K(k_1) - E(k_1)\right]}{\left(Bm + k_1\right)^2}\,dk_1 - \frac{x}{c}\int_1^{k_3} \frac{K(k_2) - E(k_2)}{k_2^2\left(Bmk_2 + 1\right)^2}\,dk_2 - \frac{\left(1 - k_3^2\right)K(k_3) - E(k_3)}{k_3}\right\} \tag{45a}$$

for $c \leqq x \leqq (Bm + 1)c$, and

$$\frac{\partial\theta_q(x,0,0)}{\partial z} = -2K_q c\left(\frac{x}{c}\int_0^{k_4}\left\{\frac{\left[(B^2m^2 + 1)k_1 + Bm\right]K(k_1)}{(Bm + k_1)^2} - \frac{E(k_1)}{Bm + k_1}\right\}dk_1 + \left(2 - \frac{x}{c}\right)E(k_4) + \frac{Bm\left(1 - k_4^2\right)K(k_4)}{k_4}\right) \tag{45b}$$

for $(Bm + 1)c \leqq x$. Figure 3 presents the variation of $\frac{1}{qc}\frac{\partial\theta_q}{\partial z}$ along the center line of the wake for various values of the parameter Bm.

The upwash component $\frac{\partial\theta_2}{\partial z}$ along the wake center line is determined in appendix C. From the results of this appendix the upwash component $\frac{\partial\theta_2}{\partial z}$ along the center line of the wake is

$$\frac{\partial\theta_2}{\partial z} = -\frac{2\dot{\alpha}mc}{\pi BE'(Bm)}\left[2E(k_3) - \left(1 - k_3^2\right)K(k_3)\right] \tag{46a}$$

for $c \leqq x \leqq (Bm + 1)c$, and

$$\frac{\partial\theta_2}{\partial z} = -\frac{2\dot{\alpha}(x - c)}{\pi B^2E'(Bm)}\left[2E(k_4) - \left(1 - k_4^2\right)K(k_4)\right] \tag{46b}$$

for $(Bm + 1)c \leqq x$. Figure 4 presents the variation of $\frac{B^2}{\dot{\alpha}c}\frac{\partial\theta_2}{\partial z}$ along the wake center line for various values of the parameter Bm.

The three components of the time-dependent upwash along the wake center line were added to yield the upwash at $t = t_0$. Figure 5 presents the results of this addition. The contribution of each component is shown in figure 6 for a Mach number of 1.67 and an aspect ratio of 2.

Note that in this case no component is so small that it may be neglected. It can be seen from equation (35) that the upwash at any arbitrary time can be found from figures 2 and 5.

The results of exact and approximate calculations of the upwash behind triangular wings with a constant vertical acceleration are given in figures 7 and 8. Figure 7 presents values determined by the expression (eq. (35)) for exact linearized upwash values and values determined by the approximate relation (eq. (37b)) for various aspect ratios for a Mach number of 1.414. Figure 8 presents exact linearized values of the upwash and values determined by the approximate relation (eq. (37b)) for various Mach numbers for an aspect ratio of 2. The origin of the x-axis used in equation (37b) was located at the $\frac{2c}{3}$ point. Figures 7 and 8 indicate that equation (37b) yields results which are good approximations to the upwash along the center line of the wake of a delta wing with subsonic leading edges.

The Rectangular Wing

The upwash in the $z = 0$ plane behind a rectangular wing with a constant vertical acceleration is determined. From a knowledge of the upwash from the unswept wing of infinite span and the upwash from one tip of a semi-infinite rectangular wing, the upwash from a rectangular wing can be found as long as the Mach line from the leading edge of one tip section does not intersect the opposite tip. This was done for the wing at a constant angle of attack in reference 10 and for the wing pitching about its leading edge in reference 15.

The general upwash distribution behind a rectangular wing is not easily obtained in a convenient mathematical form. By use of equation (36) the upwash close to the wing trailing edge can, however, be expressed in a concise mathematical form. The upwash close to the trailing edge of one tip of a rectangular wing is given by

$$\frac{\phi_z}{\dot{\alpha}c} = -\frac{1}{\pi B^2}\cos^{-1}\left(\frac{2yB}{c} + 1\right) + \frac{2B}{\pi}\sqrt{-\frac{y}{c}\left(\frac{y}{c} + \frac{1}{B}\right)} - \frac{V(t - t_o)}{c}\left[1 - \frac{1}{\pi}\cos^{-1}\left(\frac{2yB}{c} + 1\right)\right] \tag{47}$$

where the coordinate axes are located at the leading edge of the tip section (see fig. 9). The spanwise upwash distribution close behind the trailing edge of a semi-infinite rectangular wing is obtained by putting negative values of y into equation (47).

The upwash distribution for the rectangular wing is presented in the form of curves. Unfortunately, the results for the time-dependent upwash from a wing with a certain aspect ratio at a given Mach number can not be transformed to the results for the upwash from a wing with a different aspect ratio and at a different Mach number as can be done for wings in steady flows. The upwash for the motions considered here, however, has been expressed in terms of steady-flow solutions. These steady-flow solutions can be transformed from one case to another. Each component of the upwash is given separately and then these components are combined for certain cases.

The upwash from a rectangular wing at a constant angle of attack was given in reference 10. Figure 10 presents the upwash from one tip of a rectangular wing at a constant angle of attack. In figure 11 the upwash distributions from both tips are combined for various values of the aspect ratio Mach number parameter AB.

The upwash from a rectangular pitching wing was presented in reference 15. Figure 12 shows the upwash distribution from one tip of a rectangular wing pitching about its leading edge. In figure 13 the upwash distributions from both tips are combined for various values of aspect ratio Mach number parameter AB for the axis of pitch located at the wing midchord point.

The upwash component $\frac{\partial \theta_2}{\partial z}$ was evaluated by using equation (28). Figure 14 shows the distribution of the upwash component $\frac{B^2}{\dot{\alpha} c} \frac{\partial \theta_2}{\partial z}$ behind one tip of a rectangular wing.

The three components of the time-dependent upwash for one tip of a rectangular wing were added to yield the time-dependent upwash behind one tip of a rectangular wing at $t = t_o$. Figure 15 presents the results of this addition for various Mach numbers. The contribution of each upwash component is shown in figure 16. This figure indicates that no one of the three components which make up the upwash at $t = t_o$ is so small that it may be neglected in upwash calculations. In figures 17 to 22 the upwash distributions from both tips are combined for various Mach numbers and aspect ratios. From equation (35) it can be easily seen that the upwash at any time can be determined from figures 11 and 17 to 22.

Figure 23 presents exact (linearized) and approximate values of upwash at $t = t_o$ for a wing with an aspect ratio of 1 for Mach numbers of 1.414 and 2.24 for x/c of 3 and 6. Figure 24 presents exact (linearized) and approximate values of upwash at $t = t_o$ for a wing with an aspect ratio of 3 for Mach numbers of 1.414 and 2.24 for x/c of 3 and 6. These two figures indicate that the approximate values are in fair agreement with the exact values for x/c of 6. As pointed out previously, the flow behind a rectangular airfoil may be considered as being made up of the effect of the tips and the effect of a two-dimensional airfoil. Since the approximation breaks down for the two-dimensional airfoil, the effect of the tips must be considerably larger than the effect of the two-dimensional airfoil in order that the approximation be valid. This explains the large discrepancy between the exact and approximate values shown in figure 24 for the region near the center of the wake.

It should be noted that the upwash distributions shown in figures 11, 13, and 17 to 24 have been plotted from the wing axis of symmetry out to the wing tip. In figures 10, 12, 14, 15, and 16, showing upwash distributions from one tip of a rectangular wing, the origin is located at the wing tip.

AERODYNAMIC COEFFICIENTS

In order to calculate the contribution of the horizontal tail to the aerodynamic coefficients a knowledge of the upwash produced by the wing is required. Exact (linearized) and approximate methods for the calculation of the upwash induced by a wing which has a constant vertical acceleration were presented in the preceding sections. It was found that the exact (linearized) upwash induced behind wings with a constant acceleration contains the upwash induced behind the same wing at a constant angle of attack and with a constant rate of pitch. In this section exact and approximate methods for the calculation of the aerodynamic coefficients on the horizontal tail are presented.

The calculation of the tail contribution to the derivatives considered in this paper can be accomplished by utilizing the concept of the "effective angle of attack." The effective angle of attack is defined in such a way that the local angle-of-attack distribution on the tail surface is changed in order to take into account the upwash induced by the wing. The tail surface is then considered as an isolated lifting surface on which the local angle-of-attack distribution is given by the effective angle of attack. Except for the two-dimensional wing-tail combination treated, the exact (linearized) values of the aerodynamic coefficients to be presented were obtained by numerical integrations.

The coordinate axes used in determining the aerodynamic coefficients are illustrated in figure 25(a). The origin is located at the center of gravity of the aircraft. The effect of changes in the center-of-gravity locations can be taken into account by the transformations presented in table I. The stability axes are illustrated in figure 25(b), and the transformations from body axes to stability axes are given in table I.

The Lift and Moment Due to Angle of Attack for Wing-Tail Combinations

<u>Equations for tail contribution</u>.- The effective angle of attack used in calculating the tail contribution to C_{L_α} and C_{m_α} is

$$\sigma = \alpha\left(1 + \frac{\partial}{\partial z}\frac{\Omega_\alpha}{\alpha V}\right) \tag{48}$$

The lifting pressure associated with equation (48) can be found by steady-flow methods.

The normal-force and moment coefficients resulting from the pressure difference through the tail surface can be expressed as

$$\Delta C_{L_\alpha} = \frac{2}{\alpha\rho V^2 S_t}\frac{S_t}{S_W}\iint_{Tail} \Delta P \, ds \tag{49}$$

$$\Delta C_{m_\alpha} = -\frac{2}{\alpha\rho V^2 S_t \bar{c}_t}\frac{S_t \bar{c}_t}{S_W \bar{c}_W}\iint_{Tail} x \, \Delta P \, ds \tag{50}$$

where x is measured from the axis about which the moment is taken.

An approximation of the contribution of the tail to the stability derivatives C_{L_α} and C_{m_α} can be found by making use of an arithmetic average of the upwash induced by the wing at the tail location. When this is done, ΔC_{L_α} and ΔC_{m_α} may be expressed as

$$\Delta C_{L_\alpha} = \frac{S_t}{S_W}\left(1 + \overline{\frac{\partial}{\partial z}\frac{\Omega_\alpha}{\alpha V}}\right)C_{L_\alpha}\Big|_t \tag{51}$$

$$\Delta C_{m_\alpha} = -\frac{S_t}{S_W}\left(1 + \overline{\frac{\partial}{\partial z}\frac{\Omega_\alpha}{\alpha V}}\right)\left(\frac{l}{\bar{c}_W} C_{L_\alpha}\Big|_t + \frac{\bar{c}_t}{\bar{c}_W} C_{m_\alpha}\Big|_t\right) \tag{52}$$

For most cases $\frac{l}{\bar{c}_w} C_{L_\alpha}\Big|_t$ is much greater than $\frac{\bar{c}_t}{\bar{c}_w} C_{m_\alpha}\Big|_t$ and therefore equation (52) can be approximated by

$$\Delta C_{m_\alpha} \approx -\frac{S_t}{S_w}\left(1 + \overline{\frac{\partial}{\partial z}\,\frac{\Omega_\alpha}{\alpha V}}\right)\frac{l}{\bar{c}_w}\, C_{L_\alpha}\Big|_t \tag{53}$$

<u>Two-dimensional wing-tail combinations</u>.- The C_{L_α} and the C_{m_α} for the two-dimensional wing-tail combination can be expressed in closed form. The sum of the wing and the tail contributions to these derivatives is as follows: For the case where the tail lies downstream of the Mach sheet from the trailing edge of the wing (see fig. 26(a)),

$$C_{L_\alpha} = \frac{4}{B}\left(1 + \frac{c_t}{c_w}\right) \tag{54}$$

and

$$C_{m_\alpha} = -\frac{2}{B}\left(1 - \frac{2\bar{x}}{c_w} + \frac{2c_t l}{{c_w}^2}\right) \tag{55}$$

For the case where the Mach sheet from the trailing edge of the wing intersects the tail surface (see fig. 26(b)),

$$C_{L_\alpha} = \frac{2}{B}\left(1 + \frac{\bar{x}}{c_w} + \frac{l}{c_w} + \frac{c_t}{2c_w} - \frac{B\bar{z}}{c_w}\right) \tag{56}$$

and

$$C_{m_\alpha} = -\frac{1}{B}\left[1 - \frac{2\bar{x}}{c_w} + \left(\frac{l}{c_w}\right)^2 + \left(\frac{c_t}{2c_w}\right)^2 - \left(\frac{\bar{x}}{c_w}\right)^2 - \left(\frac{B\bar{z}}{c_w}\right)^2 - \frac{2B\bar{z}}{c_w} + \frac{c_t l}{{c_w}^2} + \frac{2\bar{x}B\bar{z}}{{c_w}^2}\right] \tag{57}$$

For the case where the tail surface lies between the Mach sheet from the leading edge of the wing and the Mach sheet from the trailing edge of the wing (see fig. 26(c)),

$$C_{L_\alpha} = \frac{4}{B} \tag{58}$$

and

$$C_{m_\alpha} = -\frac{2}{B}\left(1 - 2\,\frac{\bar{x}}{c_W}\right) \tag{59}$$

Figure 27 presents a comparison of values of the C_{m_α} calculated by the preceding exact expressions with the values of the C_{m_α} where the tail contribution was calculated by the approximate relation given by equation (53). Equation (53) is a good approximation to the tail contribution to the C_{m_α} for the case considered in figure 27. The discontinuities in the curves in figure 27 correspond to points where the type of flow over the tail surface changes. (See fig. 26.)

A triangular wing-tail combination.- The C_{L_α} and C_{m_α} of a triangular wing-tail combination are considered. The wing has an aspect ratio of 2.31 and the aspect ratio of the tail is twice that of the wing. The wing and the tail are located in the same plane, and the root chord of the wing is four times the root chord of the tail. The Mach number is restricted to the range where the leading edge of the wing is subsonic and the leading edge of the tail is supersonic.

In reference 11 calculated values of upwash behind triangular wings with subsonic leading edges are presented. These values could be used to calculate the tail contribution to the C_{L_α} and C_{m_α} of the wing-tail combination which is being considered here. In order to be consistent with what follows, however, it is assumed that the spanwise variation of the upwash can be neglected and the upwash is determined by the values of the upwash along the center line of the wake. (An examination of the upwash values presented in reference 11 indicates that spanwise variation of the upwash is small in the region where the tail is located.)

Figure 28 presents the variation of C_{L_α} with l/c_W for three Mach numbers for the triangular wing-tail combination under consideration. Figure 29 presents the variation of C_{m_α} with l/c_W for two of the Mach numbers considered in figure 28. Figure 30 presents a comparison of the exact (linearized) values of the C_{m_α} with the values of C_{m_α} where the tail contribution was calculated by the approximate relation given by equation (53). Figure 30 indicates that equation (53) is a good approximation to the tail contribution to C_{m_α} for the cases being considered in this section.

Rectangular-wing—triangular-tail combinations.- The C_{L_α} and C_{m_α} of a number of rectangular-wing—triangular-tail combinations are considered. These wing-tail combinations are illustrated in figure 31 where the defining parameters are also presented. The center of gravity is located at the midchord point of the wing.

The variation of C_{L_α} with l/c_W of the rectangular-wing—triangular-tail combination for several Mach numbers is presented in figure 32 whereas the variation of C_{m_α} is given in figure 33. The decrease in C_{L_α} with increasing l/c_W is a result of the increase in the upwash with increasing l/c_W. In certain cases, the effect of the upwash from the wing on the tail is large enough to cause the total C_{m_α} to become destabilizing (fig. 33).

Figure 34 presents a comparison of the exact (linearized) values of C_{m_α} with the values of C_{m_α} where the tail contribution was calculated by the approximate relation given by equation (53). Figure 34 indicates that equation (53) is a good approximation to the tail contribution to C_{m_α} for the cases considered.

The Lift and Moment Due to Steady Pitching for Wing-Tail Combinations

General expressions for the aerodynamic coefficients.- The effective angle of attack of a tail surface in pitching motion is

$$\sigma = \frac{q\bar{c}_W}{V}\left(\frac{\bar{x}}{\bar{c}_W} + \frac{\partial}{\partial z}\frac{\theta_q}{q\bar{c}_W}\right) \tag{60}$$

where the origin of the x-axis is located at the axis of pitch. The lifting pressure associated with σ can be found by steady-flow methods.

The normal-force and moment coefficients resulting from the lifting pressure on the tail surface can be expressed as

$$\Delta C_{L_q} = \frac{1}{S_t}\frac{S_t}{S_w}\iint_{\text{Tail surface}} \frac{\Delta C_p}{\frac{q\bar{c}_w}{2V}}\,ds \tag{61}$$

$$\Delta C_{m_q} = -\frac{1}{S_t\bar{c}_t}\frac{S_t\bar{c}_t}{S_w\bar{c}_w}\iint_{\text{Tail surface}} \frac{x\,\Delta C_p}{\frac{q\bar{c}_w}{2V}}\,ds \tag{62}$$

where the moment axis is taken about the axis of pitch.

Approximations of the contribution of the tail to the stability derivatives C_{L_q} and C_{m_q} can be found by making use of an arithmetic average of the upwash induced by the wing at the tail location. When this is done, the C_{L_q} and C_{m_q} of the wing-tail combination may be expressed as

$$C_{L_q} = C_{L_q}\Big|_{\text{Wing}} + \frac{S_t}{S_w}\left(2\frac{l}{\bar{c}_w}C_{L_\alpha}\Big|_{\text{Tail}} + 2\overline{\frac{\partial}{\partial z}\frac{\theta_q}{q\bar{c}_w}}\,C_{L_\alpha}\Big|_{\text{Tail}} + \frac{\bar{c}_t}{\bar{c}_w}C_{L_q}\Big|_{\text{Tail}}\right) \tag{63}$$

$$\begin{aligned} C_{m_q} = C_{m_q}\Big|_{\text{Wing}} + \frac{S_t}{S_w}\Bigg[&-2\left(\frac{l}{\bar{c}_w}\right)^2 C_{L_\alpha}\Big|_{\text{Tail}} - \frac{l}{\bar{c}_w}\frac{\bar{c}_t}{\bar{c}_w}C_{L_q}\Big|_{\text{Tail}} - \\ &2\frac{l}{\bar{c}_w}\overline{\frac{\partial}{\partial z}\frac{\theta_q}{q\bar{c}_w}}\,C_{L_\alpha}\Big|_{\text{Tail}} + 2\frac{\bar{c}_t}{\bar{c}_w}\overline{\frac{\partial}{\partial z}\frac{\theta_q}{q\bar{c}_w}}\,C_{m_\alpha}\Big|_{\text{Tail}} + \\ &\left(\frac{\bar{c}_t}{\bar{c}_w}\right)^2 C_{m_q}\Big|_{\text{Tail}} + 2\frac{l}{\bar{c}_w}\frac{\bar{c}_t}{\bar{c}_w}C_{m_\alpha}\Big|_{\text{Tail}}\Bigg] \end{aligned} \tag{64}$$

where in this case l is the distance from the axis of pitch to the centroid of the tail area. (The axis of pitch and the moment axis for the stability derivatives of the isolated tail are located at the centroid of the tail area.)

Further approximations to C_{L_q} and C_{m_q} can be obtained by retaining only the highest powers of l/c_w in the preceding expressions. The following approximate relations are thereby obtained:

$$C_{L_q} \approx 2\,\frac{S_t}{S_w}\,\frac{l}{\bar{c}_w}\,C_{L_\alpha}\Big|_{\text{Tail}} \tag{65}$$

$$C_{m_q} \approx -2\,\frac{S_t}{S_w}\left(\frac{l}{\bar{c}_w}\right)^2 C_{L_\alpha}\Big|_{\text{Tail}} \tag{66}$$

Two-dimensional wing-tail combinations.- The equations for C_{L_q} and C_{m_q} for the two-dimensional wing-tail combinations can be expressed in closed form. The sum of the wing and the tail contributions to these derivatives are as follows: For the case where the tail lies downstream of the Mach sheet from the trailing edge of the wing (see fig. 26(a)),

$$C_{L_q} = \frac{4}{B}\left(1 - 2\,\frac{\bar{x}}{c_w} + 2\,\frac{lc_t}{c_w^2}\right) \tag{67}$$

and

$$C_{m_q} = -\frac{8}{B}\left[\frac{1}{3} - \frac{\bar{x}}{c_w} + \left(\frac{\bar{x}}{c_w}\right)^2 + \frac{1}{12}\left(\frac{c_t}{c_w}\right)^3 + \frac{c_t}{c_w}\left(\frac{l}{c_w}\right)^2\right] \tag{68}$$

For the case where the Mach sheet from the trailing edge of the wing intersects the tail surface (see fig. 26(b)),

$$C_{L_q} = \frac{2}{B}\left[\frac{3B\bar{z}c_t}{c_w^2} - \frac{2B\bar{z}l}{c_w^2} + 1 - \frac{2\bar{x}}{c_w} + \frac{lc_t}{c_w^2} + \left(\frac{B\bar{z}}{c_w}\right)^2 - \left(\frac{\bar{x}}{c_w}\right)^2 + \left(\frac{l}{c_w}\right)^2 + \left(\frac{c_t}{2c_w}\right)^2\right] \tag{69}$$

and

$$C_{m_q} = -\frac{2}{B}\left[\frac{2}{3} + \frac{2\bar{x}}{c_w}\left(\frac{1}{3}\,\frac{\bar{x}^2}{c_w^2} + \frac{\bar{x}}{c_w} - 1\right) + \frac{B\bar{z}}{c_w}\left(\frac{3lc_t}{c_w^2} + \frac{B^2\bar{z}^2}{3c_w^2} - \frac{l^2}{c_w^2} - 1 + \frac{2\bar{x}}{c_w} - \frac{c_t^2}{4c_w^2} - \frac{\bar{x}^2}{c_w^2}\right) + \frac{l}{c_w}\left(\frac{2}{3}\,\frac{l^2}{c_w^2} + \frac{lc_t}{c_w^2} + \frac{c_t^2}{2c_w^2}\right) + \frac{c_t^3}{12c_w^3}\right] \tag{70}$$

For the case where the tail surface lies between the Mach sheet from the leading edge of the wing and the Mach sheet from the trailing edge of the wing (see fig. 26(c)),

$$C_{L_q} = \frac{4}{B}\left(1 - \frac{2\bar{x}}{c_w} + \frac{2B\bar{z}c_t}{c_w^2}\right) \tag{71}$$

and

$$C_{m_q} = -\frac{8}{B}\left[\frac{1}{3} - \frac{\bar{x}}{c_w} + \left(\frac{\bar{x}}{c_w}\right)^2 + \frac{B\bar{z}lc_t}{c_w^3}\right] \tag{72}$$

Figure 35 presents a comparison between exact (linearized) values of the C_{L_q} calculated from equations (67), (69), and (71) and approximate values calculated by the use of equation (65). Figure 36 presents a comparison between exact (linearized) values of the C_{m_q} calculated from equations (68), (70), and (72) and approximate values calculated by the use of equation (66). Figures 35 and 36 indicate that the approximate relations given by equations (65) and (66) yield results which are in good agreement with the exact (linearized) values for l/c_w greater than 2 for the cases considered. The poor agreement between exact and approximate values of C_{L_q} for the values of l/c_w less than 1.75 (fig. 35) are a result of neglecting the effect of the upwash induced by the wing on the tail surface.

<u>A triangular wing-tail combination</u>.- The C_{L_q} and C_{m_q} of a triangular wing-tail combination are considered for the same configurations and Mach number range which were considered previously in the section on the lift and pitching moment due to angle of attack.

It is assumed that the spanwise variation of the upwash due to pitching can be neglected and that the upwash at the tail locations can be determined from the values of upwash along the center line of the wake. Under these assumptions the upwash at the tail location due to the wing pitching about its apex can be determined from figure 3. The upwash at any point on the center line of the wake due to the wing pitching about an axis at an arbitrary location can be found by the use of figures 2 and 3 and the relation

$$\frac{1}{qc}\frac{\partial\theta_q}{\partial z}\bigg|_{\substack{\text{Pitching about}\\ \text{arbitrary axis}}} = \frac{1}{qc}\frac{\partial\theta_q}{\partial z}\bigg|_{\substack{\text{Pitching}\\ \text{about apex}}} - \frac{d_o}{c}\frac{\partial}{\partial z}\frac{\Omega_\alpha}{\alpha V}$$

where d_o is the distance from the apex of the wing to the location of the arbitrary axis of pitch.

The variation of C_{L_q} and C_{m_q} with l/c_w for three Mach numbers is presented in figures 37 and 38, respectively.

A comparison between exact (linearized) values of C_{L_q} and the approximate values of C_{L_q} calculated from equation (65) is given in figure 39. The large discrepancy between the exact and approximate values for the lower Mach number is a result of neglecting the upwash from the wing due to pitching and C_{L_q} of the wing.

Figure 40 presents a comparison between exact (linearized) values of the C_{m_q} and approximate values of the C_{m_q} calculated from equation (66). This figure indicates that, for values of l/c_w greater than 2, equation (66) yields a good approximation to C_{m_q} for the two cases considered.

Plots of C_{L_q} and C_{m_q} for three different center-of-gravity locations at Mach number 1.44 are presented in figures 41 and 42, respectively; these plots indicate that the center-of-gravity location has a large effect on C_{L_q} and C_{m_q} for the cases considered.

Figure 43 presents a comparison between exact (linearized) values of C_{L_q} and values calculated from equation (65) for two different center-of-gravity locations. The poor agreement between exact and approximate values shown in figure 43 indicates that equation (65) should not be used when the center of gravity is not located near the centroid of the wing.

For two different center-of-gravity locations, a comparison between exact (linearized) values of C_{m_q} and values calculated from equation (66) is made in figure 44. Since the agreement for the lower values of l/c_w is poor, this comparison indicates that care should be exercised when equation (66) is used for cases where the center of gravity is not located near the centroid of the wing.

Rectangular-wing—triangular-tail combinations.- The C_{L_q} and C_{m_q} of a number of rectangular-wing—triangular-tail combinations are considered. These wing-tail combinations are illustrated in figure 31 where the defining parameters are also presented. These are the same configurations that were considered previously in the sections on the lift and pitching moment due to angle of attack.

The variation of C_{L_q} with l/c_w of the wing-tail combination for several Mach numbers is presented in figure 45 whereas the variation of C_{m_q} with l/c_w is presented in figure 46.

A comparison of the exact (linearized) values of C_{L_q} and approximate values calculated from equation (65) for two wing-tail configurations and two Mach numbers is presented in figure 47. There is good agreement between the exact and the approximate values for the cases considered.

Good agreement between the exact (linearized) values of C_{m_q} and the approximate values calculated from equation (66) for the cases considered is indicated in figure 48 which presents these values for two wing-tail configurations and two Mach numbers.

Figures 49 and 50 present C_{L_q} and C_{m_q}, respectively, for three different center-of-gravity locations at Mach number 1.414 for two different wing-tail combinations. These figures indicate that the center-of-gravity location has a large effect on C_{L_q} and C_{m_q} for the cases considered.

A comparison between exact (linearized) values of C_{L_q} and values calculated from equation (65) for two different center-of-gravity locations and two different configurations is presented in figure 51. The poor agreement between the exact and approximate values shown in figure 51 indicates that equation (65) should not be used when the center of gravity is not located near the centroid of the wing.

Figure 52 presents a comparison between exact (linearized) values of the C_{m_q} and values calculated from equation (66) for two different center-of-gravity locations and two different configurations. The poor agreement for the lower values of l/c_w shown in figure 52 indicates that results calculated from the approximate equation (66) are unreliable for center-of-gravity locations that are not near the centroid of the wing area.

The Lift and Moment Resulting From a Constant Vertical Acceleration for Wing-Tail Combinations

General expressions for aerodynamic coefficients.- The upwash on the horizontal-tail surface resulting from the constant vertical acceleration is given by

$$\phi_z = -\mathring{\alpha}V(t - t_o)$$

The upwash induced by the wing at the tail location is (from eq. (35))

$$\phi_z = \dot{\alpha}c \frac{M^2}{B^2} \frac{\partial}{\partial z} \frac{\theta_q}{qc} + \dot{\alpha}c\left[\frac{V}{c}(t - t_o) - \frac{M^2x}{B^2c}\right]\frac{\partial}{\partial z} \frac{\Omega_\alpha}{\alpha V} + \frac{\partial \theta_2}{\partial z}$$

The effective angle of attack of the tail is given by

$$\sigma = \dot{\alpha}(t - t_o)\left(1 + \frac{\partial}{\partial z} \frac{\Omega_\alpha}{\alpha V}\right) + \frac{\dot{\alpha}c}{V} \frac{M^2}{B^2} \frac{\partial}{\partial z} \frac{\theta_q}{qc} - \frac{\dot{\alpha}c}{V} \frac{M^2}{B^2} \frac{x}{c} \frac{\partial}{\partial z} \frac{\Omega_\alpha}{\alpha V} + \frac{1}{V} \frac{\partial \theta_2}{\partial z}$$

The preceding equation indicates that the effective angle of attack of the tail is made up of two components, one which varies linearly with time and one which is of a steady-state nature. It follows that, in order to determine the potential induced by the tail on its surface, it is necessary to solve two problems, one which has an angle-of-attack variation given by

$$\sigma_1 = \dot{\alpha}(t - t_o)\left(1 + \frac{\partial}{\partial z} \frac{\Omega_\alpha}{\alpha V}\right) \tag{73}$$

and one which has an angle-of-attack variation given by

$$\sigma_2 = \frac{\dot{\alpha}c}{V} \frac{M^2}{B^2} \frac{\partial}{\partial z} \frac{\theta_q}{qc} - \frac{\dot{\alpha}c}{V} \frac{M^2}{B^2} \frac{x}{c} \frac{\partial}{\partial z} \frac{\Omega_\alpha}{\alpha V} + \frac{1}{V} \frac{\partial \theta_2}{\partial z} \tag{74}$$

The potential corresponding to σ_1 can be found by the methods given in the theoretical development concerning upwash and the potential corresponding to σ_2 can be found by steady-flow methods.

After the potential is determined, the pressure can be found by making use of the relation

$$\Delta P = \rho(V \,\Delta\phi_x + \Delta\phi_t)$$

where $\Delta\phi$ represents the potential difference induced by the tail through its surface.

The normal force and moment resulting from the pressure difference through the tail surface can be expressed by

$$F_1^{\alpha} = \iint_{\text{Tail surface}} \Delta P \, ds$$

and

$$\bar{M}_1^{\alpha} = -\iint_{\text{Tail surface}} x \, \Delta P \, ds$$

The two quantities, F_1^{α} and $\bar{M}_1^{\alpha}$, can be expressed in coefficient form by

$$\frac{F_1^{\alpha}}{\frac{\rho}{2} V^2 S_w} = \frac{2}{\rho V^2 S_w} \iint_{\text{Tail surface}} \Delta P \, ds$$

and

$$\frac{\bar{M}_1^{\alpha}}{\frac{\rho}{2} V^2 S_w \bar{c}_w} = -\frac{2}{\rho V^2 S_w \bar{c}_w} \iint_{\text{Tail surface}} x \, \Delta P \, ds$$

The tail contribution to the stability derivatives $C_{L_{\dot{\alpha}}}$ and $C_{m_{\dot{\alpha}}}$ can be expressed as

$$\Delta C_{L_{\dot{\alpha}}} = \frac{4}{\dot{\alpha} \rho V S_t \bar{c}_t} \frac{S_t \bar{c}_t}{S_w \bar{c}_w} \iint_{\text{Tail surface}} \Delta P \, ds \qquad (75)$$

and

$$\Delta C_{m_{\dot{\alpha}}} = -\frac{4}{\dot{\alpha} \rho V S_t \bar{c}_t^{2}} \frac{S_t \bar{c}_t^{2}}{S_w \bar{c}_w^{2}} \iint_{\text{Tail surface}} x \, \Delta P \, ds \qquad (76)$$

The difficulties involved in calculating the exact values of the tail contribution to the stability derivatives $C_{L_{\dot{\alpha}}}$ and $C_{m_{\dot{\alpha}}}$ are in most cases too great for practical computations. The lift on tails with supersonic leading edges and trailing edges which are perpendicular to the free-stream direction can, however, be treated by the method presented in reference 22. Expressions for the moment on the tail are developed in appendix D for the case of an angle-of-attack distribution that increases linearly with time.

An approximation to the contribution of the tail to the stability derivatives $C_{L_{\dot{\alpha}}}$ and $C_{m_{\dot{\alpha}}}$ can be found (as was done in ref. 16) by making use of an arithmetic average value of the upwash induced by the wing at the tail location. When this is done, $\Delta C_{L_{\dot{\alpha}}}$ and $\Delta C_{m_{\dot{\alpha}}}$ may be expressed by

$$\Delta C_{L_{\dot{\alpha}}} = \frac{S_t \bar{c}_t}{S_w \bar{c}_w}\left[\left(1 + \overline{\frac{\partial}{\partial z}\,\frac{\Omega_\alpha}{\alpha V}}\right)C_{L_{\dot{\alpha}}}\Big|_{Tail} + \frac{2V}{\dot{\alpha}\bar{c}_t}\,\overline{\sigma_2}\,C_{L_\alpha}\Big|_{Tail}\right] \tag{77}$$

and

$$\Delta C_{m_{\dot{\alpha}}} = -\frac{S_t}{S_w}\left(\frac{\bar{c}_t}{\bar{c}_w}\right)^2\left[\frac{l}{\bar{c}_t}\left(1 + \overline{\frac{\partial}{\partial z}\,\frac{\Omega_\alpha}{\alpha V}}\right)C_{L_{\dot{\alpha}}}\Big|_{Tail} + \frac{2lV}{\dot{\alpha}\bar{c}_t^{\,2}}\,\overline{\sigma_2}\,C_{L_\alpha}\Big|_{Tail} + \right.$$

$$\left.\left(1 + \overline{\frac{\partial}{\partial z}\,\frac{\Omega_\alpha}{\alpha V}}\right)C_{m_{\dot{\alpha}}}\Big|_{Tail} + \frac{2V\overline{\sigma_2}}{\dot{\alpha}\bar{c}_t}\,C_{m_\alpha}\Big|_{Tail}\right] \tag{78}$$

where l is the distance from the center of gravity to the reference axis about which $C_{L_{\dot{\alpha}}}\big|_{Tail}$ and $C_{m_{\dot{\alpha}}}\big|_{Tail}$ are taken.

Further approximations to $C_{L_{\dot{\alpha}}}$ and $C_{m_{\dot{\alpha}}}$ can be obtained by retaining only the terms which are of the highest order in l in equations (77) and (78). When these terms are retained, the following approximate relations are obtained:

$$\Delta C_{L_{\dot{\alpha}}} \approx -2\,\frac{S_t}{S_w}\,\frac{l}{\bar{c}_w}\,\overline{\frac{\partial}{\partial z}\,\frac{\Omega_\alpha}{\alpha V}}\,C_{L_\alpha}\Big|_{Tail} \tag{79}$$

and

$$\Delta C_{m_{\dot{\alpha}}} \approx 2\,\frac{S_t}{S_w}\left(\frac{l}{\bar{c}_w}\right)^2\overline{\frac{\partial}{\partial z}\,\frac{\Omega_\alpha}{\alpha V}}\,C_{L_\alpha}\Big|_{Tail} \tag{80}$$

Equations (79) and (80) can also be obtained by assuming a time-lag effect in the downwash from the wing. Approximate expressions for wing-tail combinations are

$$C_{L_{\dot{\alpha}}} \approx C_{L_{\dot{\alpha}}}\Big|_{\text{Wing}} - 2\,\frac{S_t}{S_w}\,\frac{l}{\bar{c}_w}\,\overline{\frac{\partial}{\partial z}\,\frac{\Omega_\alpha}{\alpha V}}\,C_{L_\alpha}\Big|_{\text{Tail}} \tag{81}$$

and

$$C_{m_{\dot{\alpha}}} \approx 2\,\frac{S_t}{S_w}\left(\frac{l}{\bar{c}_w}\right)^2\,\overline{\frac{\partial}{\partial z}\,\frac{\Omega_\alpha}{\alpha V}}\,C_{L_\alpha}\Big|_{\text{Tail}} \tag{82}$$

The $C_{m_{\dot{\alpha}}}$ of the wing has been neglected in equation (82) because it is usually small.

Two-dimensional wing-tail combinations.- The equations for $C_{L_{\dot{\alpha}}}$ and $C_{m_{\dot{\alpha}}}$ for two-dimensional wing-tail combinations can be expressed in closed form. The sum of the wing and the tail contributions are as follows (these expressions were obtained by integrations of the pressure distribution resulting from a constant vertical acceleration over the wing and tail surfaces): For the case where the tail lies downstream of the Mach sheet from the trailing edge of the wing (see fig. 26(a)),

$$C_{L_{\dot{\alpha}}} = -\frac{4}{B^3}\left(1 + \frac{c_t}{c_w}\right)^2 \tag{83}$$

$$C_{m_{\dot{\alpha}}} = \frac{8}{B^3}\left[\frac{1}{3} - \frac{\bar{x}}{2c_w} + \frac{1}{12}\left(\frac{c_t}{c_w}\right)^3 + \frac{lc_t}{{c_w}^2}\left(1 + \frac{c_t}{2c_w}\right)\right] \tag{84}$$

For the case where the Mach sheet from the trailing edge of the wing intersects the tail surface (see fig. 26(b)),

$$\begin{aligned} C_{L_{\dot{\alpha}}} = -\frac{4}{B^3}\Bigg[1 &+ \frac{1}{2}\left(\frac{l}{c_w} - \frac{B\bar{z}}{c_w} + \frac{c_t}{2c_w} + \frac{\bar{x}}{c_w} - 1\right)\left(\frac{l}{c_w} - \frac{B\bar{z}}{c_w} + \right. \\ &\left. \frac{c_t}{2c_w} + \frac{\bar{x}}{c_w} + \frac{2M^2B\bar{z}}{c_w} + 1\right) - \frac{2M^2\bar{z}Bc_t}{{c_w}^2}\Bigg] \end{aligned} \tag{85}$$

$$C_{m_{\dot{\alpha}}} = -\frac{2M^2\bar{z}}{B^2c_w}\left(\frac{B^2\bar{z}^2}{c_w^2} + \frac{2B\bar{z}}{c_w} - \frac{2B\bar{z}\bar{x}}{c_w^2} - \frac{l^2}{c_w^2} + \frac{3lc_t}{c_w^2} - \frac{2\bar{x}}{c_w} - \frac{c_t^2}{4c_w^2} + \frac{\bar{x}^2}{c_w^2} + 1\right) +$$

$$\frac{2}{B^3}\left[\frac{B\bar{z}}{c_w}\left(\frac{B^2\bar{z}^2}{3c_w^2} - \frac{B\bar{z}\bar{x}}{c_w^2} - \frac{l^2}{c_w^2} - \frac{c_t l}{c_w^2} - \frac{c_t^2}{4c_w^2} + \frac{\bar{x}^2}{c_w^2} - 1\right) + \frac{\bar{x}}{c_w}\left(\frac{c_t^2}{4c_w^2} - \frac{\bar{x}^2}{3c_w^2} + \right.\right.$$

$$\left.\left.\frac{lc_t}{c_w^2} + \frac{l^2}{c_w^2} - 1\right) + \frac{l}{c_w}\left(\frac{2}{3}\frac{l^2}{c_w^2} + \frac{c_t^2}{2c_w^2} + \frac{lc_t}{c_w^2}\right) + \frac{2}{3} + \frac{c_t^3}{12c_w^3}\right] \tag{86}$$

For the case where the tail surface lies between the Mach sheet from the leading edge of the wing and the Mach sheet from the trailing edge of the wing (see fig. 26(c)),

$$C_{L_{\dot{\alpha}}} = -\frac{4}{B^3}\left(1 - 2\frac{M^2B\bar{z}c_t}{c_w^2}\right) \tag{87}$$

$$C_{m_{\dot{\alpha}}} = \frac{4}{3B^3}\left(2 - 3\frac{\bar{x}}{c_w} - 6\frac{M^2B\bar{z}lc_t}{c_w^3}\right) \tag{88}$$

A comparison between exact (linearized) values of the $C_{L_{\dot{\alpha}}}$ and values calculated from equation (81) is presented in figure 53 for two Mach numbers. The poor agreement between exact and approximate values shown in figure 53 is to be expected because the upwash behind the two-dimensional airfoil can not be approximated by a simple time-lag effect.

Figure 54 presents a comparison between exact (linearized) values of the $C_{m_{\dot{\alpha}}}$ and values calculated from equation (82) for two Mach numbers. This figure indicates that equation (82) can not be used for two-dimensional wing-tail combinations. The poor agreement between exact and approximate values shown in figure 54 is to be expected because the upwash behind the wing does not exhibit a time-lag effect.

A triangular wing-tail combination.- The $C_{L_{\dot{\alpha}}}$ and $C_{m_{\dot{\alpha}}}$ of a triangular wing-tail combination are considered for the same configuration with the same Mach number range which was considered previously in the sections on the lift and pitching moment due to angle of attack and in the sections on the lift and pitching moment due to pitching.

It is assumed that the spanwise variation of the upwash due to a constant vertical acceleration can be neglected and that the upwash at the tail location can be determined from the values of the upwash along the center line of the wake. Under these assumptions the upwash at the tail location due to a constant vertical acceleration at $t = t_o$ can be found from figure 5.

The variation of $C_{L_{\dot{\alpha}}}$ and $C_{m_{\dot{\alpha}}}$ with l/c_w for three Mach numbers is presented in figures 55 and 56, respectively.

A comparison between exact (neglecting spanwise variations in upwash) values of $C_{L_{\dot{\alpha}}}$ and approximate values calculated from equation (81) (fig. 57) shows good agreement between the exact and approximate values.

A similar comparison between exact (neglecting spanwise variations in upwash) values of $C_{m_{\dot{\alpha}}}$ and approximate values calculated from equation (82) (fig. 58) also shows good agreement between the exact and the approximate values.

Figure 59 presents the variation of $C_{m_{\dot{\alpha}}}$ for three different center-of-gravity locations for Mach number 1.44. This figure indicates that the center-of-gravity location has a large effect on $C_{m_{\dot{\alpha}}}$.

Exact (neglecting spanwise variations in upwash) values of $C_{m_{\dot{\alpha}}}$ and values calculated from equation (82) for two different center-of-gravity locations at Mach number 1.44 are compared in figure 60. The agreement between exact and approximate values is much poorer in these cases than for the cases shown in figure 58. This result indicates that equation (82) should not be used for cases where the center of gravity is not located near the centroid of the wing area.

Rectangular-wing—triangular-tail combinations.- The $C_{L_{\dot{\alpha}}}$ and $C_{m_{\dot{\alpha}}}$ of a number of rectangular-wing—triangular-tail combinations are considered. These wing-tail configurations are illustrated in figure 31 where the defining parameters are also presented. These are the same configurations that were considered previously in the sections on the lift and moment due to angle of attack and in the sections on the lift and moment due to pitching.

The variation of $C_{L_{\dot{\alpha}}}$ and $C_{m_{\dot{\alpha}}}$ with l/c_w for several Mach numbers is presented in figures 61 and 62, respectively.

Figure 63 presents a comparison between exact values of $C_{L_{\dot{\alpha}}}$ and values calculated from equation (81) for two different wing-tail combinations. Figure 63(a) shows good agreement between exact and approximate values for a wing with an aspect ratio of 1 whereas figure 63(b) shows poor agreement between the exact and approximate values for a wing with an aspect ratio of 4. This poor agreement is to be expected because the upwash behind the wing with an aspect ratio of 4 (fig. 63(b)) exhibits some of the two-dimensional characteristics.

A comparison between exact values of $C_{m_{\dot{\alpha}}}$ and the values calculated from equation (82) for two different wing-tail combinations is presented in figure 64. Figure 64(a) (aspect-ratio-1 wing) shows fairly good agreement between exact and approximate values, and figure 64(b) (aspect-ratio-4 wing) shows poor agreement which is caused by the two-dimensional character of the upwash behind the wing.

The variation of $C_{m_{\dot{\alpha}}}$ with l/c_w for three center-of-gravity locations for two configurations is given in figure 65. This figure indicates that the center-of-gravity location has a strong effect on $C_{m_{\dot{\alpha}}}$.

Figure 66 presents a comparison between exact values of $C_{m_{\dot{\alpha}}}$ and approximate values calculated from equation (82). Figure 66(a) indicates that equation (82) should not be used for cases where the center of gravity is not located near the centroid of the wing area for a wing of low aspect ratio whereas figure 66(b) indicates that equation (82) should not be used at all for wings of high aspect ratio.

The $C_{m_q} + C_{m_{\dot{\alpha}}}$ for a Number of Wing-Tail Combinations

The expression $C_{m_q} + C_{m_{\dot{\alpha}}}$ partly determines the damping of longitudinal oscillations of aircraft. For this reason, $C_{m_q} + C_{m_{\dot{\alpha}}}$ is given separate consideration in this section.

Figure 67 presents $C_{m_q} + C_{m_{\dot{\alpha}}}$ for a series of two-dimensional wing-tail combinations in which the center of gravity is located at the mid-chord point of the wing, l/c_w is equal to 2.25, the ratio c_t/c_w is $\frac{1}{2}$, and the height of the tail surface above the wing has various values. The discontinuities in slope of the curves in figure 67 correspond to points where the type of flow over the tail surface changes (see fig. 26). Figure 67 indicates that, when the tail lies between the Mach sheets from the leading and trailing edges of the wing (see fig. 26(c)), $C_{m_q} + C_{m_{\dot{\alpha}}}$ is decreased considerably from the values for the same combination where the wing and the tail lie in the same plane.

The variation of $C_{m_q} + C_{m_{\dot{\alpha}}}$ with l/c_w is presented in figure 68 for two Mach numbers for a two-dimensional wing-tail combination in which the center of gravity is located at the midchord point of the wing, the ratio c_t/c_w is $\frac{1}{2}$, and $\bar{z}/c_w$ is $\frac{1}{2}$. This figure indicates that $C_{m_q} + C_{m_{\dot{\alpha}}}$ is decreased by increasing l/c_w.

Figure 69 presents the variation of $C_{m_q} + C_{m_{\dot{\alpha}}}$ with Mach number for a two-dimensional wing-tail combination in which the center of gravity is located at the midchord point of the wing, the ratio l/c_w has various values, the ratio c_t/c_w is $\frac{1}{2}$, and the tail lies in the plane of the wing.

The relation between Mach number and center-of-gravity location which causes $C_{m_q} + C_{m_{\dot{\alpha}}}$ to be zero for five two-dimensional wing-tail combinations is shown in figure 70.

Figure 71 presents the variation of $C_{m_q} + C_{m_{\dot{\alpha}}}$ with l/c_w for three Mach numbers for the same triangular wing-tail combination as was considered previously. Figure 72 presents the variation of $C_{m_q} + C_{m_{\dot{\alpha}}}$ with l/c_w for various Mach numbers for the same rectangular-wing—triangular-tail combinations as were considered previously. These figures indicate that $C_{m_q} + C_{m_{\dot{\alpha}}}$ increases rapidly with l/c_w.

CONCLUDING REMARKS

The force and moment coefficients of an aircraft undergoing unsteady longitudinal motions at supersonic speeds can be expressed in terms of an infinite series of stability derivatives of successively higher orders. This representation of the aerodynamic forces and moments is felt to be useful in accounting for the unsteady influences in stability studies. In this paper attention is primarily devoted to the establishment of the more common stability derivatives. The stability derivatives resulting from unsteady motions that appear to be the most important are those associated with constant vertical acceleration. The calculation of the upwash by the linearized theory behind wings with constant vertical accelerations can be reduced to solving a number of steady-flow problems. One of these steady-flow problems is the determination of the upwash behind a wing at a constant angle of attack and another of these steady-flow problems is the determination of the flow behind a wing induced by a constant rate of pitch. The effects of the rolling up of the wake and other distortions are neglected and it is assumed that the wake remains in the plane of the wing.

For some plan forms the upwash at points which are not located near the Mach sheet from the trailing edge of the wing resulting from a constant vertical acceleration can be approximated very well by using the upwash due to a constant angle of attack and a time-lag effect. This approximation breaks down for the two-dimensional airfoil and yields poor results for high-aspect-ratio rectangular wings. The few calculated examples seem to indicate that in general a simple time-lag effect yields good approximations to the upwash due to a constant vertical acceleration behind unswept wings of low aspect ratio and yields a poor approximation to the upwash behind unswept wings of high aspect ratio. The effects of sweep were not investigated in any of the examples which were calculated.

For the wing-tail combinations investigated, the results indicate that the moment coefficient resulting from a steady pitching C_{m_q} can be approximated to a fairly high degree of accuracy by a simple expression. This approximation essentially involves accounting for the lift arising as a result of the geometric angle of attack at the tail associated with the pitching motion.

The results also indicate that the simple time-lag effect, which is sometimes used to calculate the moment resulting from a constant vertical acceleration $C_{m_{\dot{\alpha}}}$ for aircraft at subsonic speeds, is not reliable at supersonic speeds. A more reliable method of calculating $C_{m_{\dot{\alpha}}}$ would be to determine the upwash produced by a wing with a constant vertical acceleration. This can be accomplished by the methods developed herein or by calculating the components of the upwash by the use of lifting lines. The contribution of the horizontal tail to $C_{m_{\dot{\alpha}}}$ would then be found by the use of exact or approximate relations for the tail contribution to $C_{m_{\dot{\alpha}}}$ given herein.

The results for two-dimensional wing-tail combinations seem to indicate that the damping of longitudinal oscillations due to $C_{m_q} + C_{m_{\dot{\alpha}}}$ is increased considerably if the tail surface lies between the Mach sheet from the leading edge of the wing and the Mach sheet from the trailing edge of the wing. Calculated values of $C_{m_q} + C_{m_{\dot{\alpha}}}$ indicate that the damping contributed by this factor increases rapidly as the distance from the wing to the tail is increased.

Langley Aeronautical Laboratory,
National Advisory Committee for Aeronautics,
Langley Field, Va., December 11, 1953.

APPENDIX A

THE DIFFERENTIATION OF θ_2

The function θ_2 is given by equation (22) or equation (24). The expression for θ_2 as given by equation (22) is

$$\theta_2(x,y,z) = \frac{z}{2\pi B^2 V}\int_{h_1}^{h_2} \frac{\Delta\Omega(y_1)}{Y^2 + z^2}\sqrt{(x - J)^2 - B^2(Y^2 + z^2)}\,dy_1 + \frac{z}{2\pi}\iint_{\text{Wing}} \frac{X\,\Delta u_r}{(Y^2 + z^2)R}\,dx_1\,dy_1$$

By applying the rule for the differentiation of a definite integral with respect to a parameter to the first integral on the right-hand side of equation (22), $\frac{\partial\theta_2}{\partial y}$ and $\frac{\partial\theta_2}{\partial z}$ can be written as

$$\frac{\partial\theta_2(x,y,z)}{\partial y} = \frac{z}{2\pi B^2 V}\int_{h_1}^{h_2} \frac{\Delta\Omega(y_1)\left[\frac{-2(x - J)^2}{Y^2 + z^2} + B^2\right]Y}{(Y^2 + z^2)\sqrt{(x - J)^2 - B^2(Y^2 + z^2)}}\,dy_1 + \frac{z}{2\pi}\frac{\partial}{\partial y}\iint_{\text{Wing}} \frac{X\,\Delta u_r}{(Y^2 + z^2)R}\,dx_1\,dy_1 \qquad \text{(A1)}$$

$$\frac{\partial\theta_2(x,y,z)}{\partial z} = \frac{1}{2\pi B^2 V}\int_{h_1}^{h_2} \frac{\Delta\Omega(y_1)}{(Y^2 + z^2)^2}\left[Y^2\sqrt{(x - J)^2 - B^2(Y^2 + z^2)} - \frac{z^2(x - J)^2}{\sqrt{(x - J)^2 - B^2(Y^2 + z^2)}}\right]dy_1 + \frac{z}{2\pi}\frac{\partial}{\partial z}\iint_{\text{Wing}} \frac{X\,\Delta u_r}{(Y^2 + z^2)R}\,dx_1\,dy_1 \qquad \text{(A2)}$$

Equations (A1) and (A2) are valid when the limits of integration, h_1 and h_2, are either the Mach cone from the point x,y,z or the plan-form tips.

Equations (A1) and (A2) become indeterminate at the apex of the hyperbola as z approaches zero. The value of $\frac{\partial\theta_2(x,y,0)}{\partial y}$ can be found directly from $\theta_2(x,y,0)$ since this value is known. The value of $\frac{\partial\theta_2(x,y,0)}{\partial z}$ is given by (from eq. (17), ref. 15)

$$\frac{\partial\theta_2(x,y,0)}{\partial z} = -\frac{1}{2\pi}\iint_{\text{Wing+wake}} \frac{\frac{\partial^2\Delta\theta_2}{\partial x_1\,\partial y_1} R}{XY}\,dx_1\,dy_1 - \frac{1}{2\pi}\oint \frac{\frac{\partial\,\Delta\theta_2}{\partial x_1} R}{XY}\,dx_1 - \frac{B}{2}\Delta\frac{\partial\theta_2}{\partial x}$$

Separating the wing and wake integrals yields

$$\frac{\partial\theta_2(x,y,0)}{\partial z} = -\frac{1}{2\pi}\iint_{\text{Wing}} \frac{\frac{\partial^2\Delta\theta_2}{\partial x_1\,\partial y_1} R}{XY}\,dx_1\,dy_1 - \frac{1}{2\pi}\int_{h_1}^{h_2} \frac{\frac{\partial^2\Delta\theta_2}{\partial x_1\,\partial y_1}}{Y}\,dy_1 \int_{J(y_1)}^{x-BY} \frac{R}{X}\,dx_1 - \frac{1}{2\pi}\oint \frac{\frac{\partial\,\Delta\theta_2}{\partial x_1} R}{XY}\,dx_1 - \frac{B}{2}\Delta\frac{\partial\theta_2}{\partial x}$$

The second integral on the right-hand side of the preceding expression can be integrated with respect to x_1. The result of performing this integration can be expressed as

$$\frac{\partial\theta_2(x,y,0)}{\partial z} = -\frac{1}{2\pi}\iint_{\text{Wing}} \frac{\dfrac{\partial^2\Delta\theta_2}{\partial x_1\,\partial y_1}}{XY}\,dx_1\,dy_1 -$$

$$\frac{1}{2\pi}\int_{h_1}^{h_2} \frac{\partial^2\Delta\theta_2}{\partial x_1\,\partial y_1}\left[\frac{\sqrt{(x - J)^2 - B^2Y^2}}{Y} - B\cos^{-1}\frac{BY}{x - J}\right]dy_1 -$$

$$\frac{1}{2\pi}\oint \frac{\dfrac{\partial\,\Delta\theta_2}{\partial x_1}R\,dx_1}{XY} - \frac{B}{2}\Delta\frac{\partial\theta_2}{\partial x} \qquad \text{(A3)}$$

Note that $\dfrac{\partial^2\Delta\theta_2}{\partial x_1\,\partial y_1}$ may be written as a function of y_1 since $x_1 = J(y_1)$.

The expression for θ_2 as given by equation (24) is

$$\theta_2(x,y,z) = \frac{1}{B^2V}\int_{M_s}^{x} \Omega_p(\lambda,y,z)d\lambda + \frac{1}{B^2V}\int_{M_s}^{x} \Omega_w(\lambda,y,z)d\lambda$$

The lower limit of the preceding integrals is a function of y and z. In the differentiation of the preceding integrals with respect to either y or z, this variable limit must be considered.

The trailing edge of the wing may be divided into three types. The first of these is the completely supersonic trailing edge. In this type of trailing edge, the component of free-stream velocity normal to the trailing edge is always supersonic. (See fig. 73(a).) The second type of trailing edge is the completely subsonic edge. Here, the component of free-stream velocity normal to the trailing edge is subsonic. (See fig. 73(b).) The third type of trailing edge is the mixed supersonic and subsonic trailing edge. As its name implies, this type of trailing edge has both supersonic and subsonic portions. (See figs. 73(c) and 73(d).)

For supersonic trailing edges the wake has no effect upstream of the trailing edge; thus, $\Omega_p(x,y,z)$ is zero and equation (24) reduces to

$$\theta_2(x,y,z) = \frac{1}{B^2V}\int_{M_s}^{x} \Omega_w(\lambda,y,z)d\lambda \qquad \text{(A4)}$$

In order to differentiate the integral of equation (A4) with respect to y and z it is convenient to express the lower limit M_s of the integral mathematically. For all but the simplest trailing edges, the mathematical difficulties are too great to make this expression practical. A general procedure is set up, however, and a few simple cases are presented. The equation of the trailing edge has been represented by

$$x_1 = J(y_1)$$

and the Mach cone from each point on the trailing edge is given by

$$(x - J)^2 - B^2Y^2 - B^2z^2 = 0 \tag{A5}$$

The Mach sheet from the trailing edge is the envelope of the Mach cones from all the points along the trailing edge. The equation of the Mach sheet from the trailing edge can be found by eliminating y_1 from the two equations

$$(x - J)^2 - B^2(y - y_1)^2 - B^2z^2 = 0 \tag{A6}$$

$$\frac{\partial}{\partial y_1}\left[(x - J)^2 - B^2(y - y_1)^2 - B^2z^2\right] = 0 \tag{A7}$$

Such relationships follow from the mathematical procedure for finding the envelope of surfaces. (See ref. 23, p. 55.)

When the trailing edge is swept at a constant angle and the trailing-edge end points do not affect the area of the Mach surface being considered, the Mach surface is made up of two plane surfaces. For a coordinate system whose origin is located on the trailing edge, the equation of the trailing edge is given by

$$x_1 = \frac{y_1}{m_t}$$

Thus,

$$J(y_1) = \frac{y_1}{m_t}$$

and

$$\frac{\partial J(y_1)}{\partial y_1} = \frac{1}{m_t}$$

Equations (A6) and (A7) become

$$\left(x - \frac{y_1}{m_t}\right)^2 - B^2(y - y_1)^2 - B^2z^2 = 0$$

$$\left(x - \frac{y_1}{m_t}\right)\frac{1}{m_t} - B^2(y - y_1) = 0$$

The elimination of y_1 from the two preceding equations yields

$$(m_tx - y)^2 - z^2(B^2m_t^2 - 1) = 0$$

Thus, the equation for the Mach surface is

$$m_tx - y - z\sqrt{B^2m_t^2 - 1} = 0 \tag{A8}$$

when z is positive and

$$m_tx - y + z\sqrt{B^2m_t - 1} = 0 \tag{A9}$$

when z is negative. When the trailing edge is perpendicular to the stream direction, $m_t = \infty$ and equation (A8) becomes

$$x - Bz = 0 \tag{A10}$$

When the trailing edge is made up of a broken line composed of two straight-line segments, the Mach surface from the trailing edge is made up of parts of the after cones from the trailing-edge end points, parts of the after cone from the point connecting the two line segments, and the two Mach sheets from the two straight-line segments of the trailing edge. (See figs. 74 and 75.)

In the preceding paragraphs a method has been presented for the determination of the equation of the Mach surface from the trailing edge. Let the equation of the Mach surface be represented by

$$x = G(y,z)$$

Equation (A4) then can be written as

$$\theta_2(x,y,z) = \frac{1}{B^2V}\int_{G(y,z)}^{x} \Omega_w(\lambda,y,z)d\lambda \tag{A11}$$

Differentiating equation (A11) with respect to y and z yields

$$\frac{\partial\theta_2(x,y,z)}{\partial y} = \frac{1}{B^2V}\int_{G(y,z)}^{x} \frac{\partial\Omega_w(\lambda,y,z)}{\partial y}\,d\lambda - \frac{1}{B^2V}\,\Omega_w(M_s)\frac{\partial G(y,z)}{\partial y} \tag{A12}$$

$$\frac{\partial\theta_2(x,y,z)}{\partial z} = \frac{1}{B^2V}\int_{G(y,z)}^{x} \frac{\partial\Omega_w(\lambda,y,z)}{\partial z}\,d\lambda - \frac{1}{B^2V}\,\Omega_w(M_s)\frac{\partial G(y,z)}{\partial z} \tag{A13}$$

where $\Omega_w(M_s)$ is the value of $\Omega_w(\lambda,y,z)$ at the trailing-edge Mach surface obtained by approaching the Mach surface from the positive x-direction along the line $\left(y_1 = y,\ \ z_1 = z\right)$. The expression $\Omega_w(M_s)$ can be evaluated by calculating Ω_w on the line $\left(y_1 = y,\ \ z_1 = z\right)$ a small distance ϵ downstream of the trailing-edge Mach sheet and then taking the limit as ϵ approaches zero. For points behind the Mach surface from any straight-line segment of a trailing edge, the quantity $\Omega_w(M_s)$ is given by $\Omega_w\left(\frac{y^+}{m_t},y,0^+\right)$ for positive z, provided the Mach surface at the point being considered is not part of the Mach cone from an end point of the line segment.

For wings with subsonic trailing edges, Ω_p and Ω_w at the trailing-edge Mach surface are zero. Equation (24) then can be differentiated to yield

$$\frac{\partial\theta_2(x,y,z)}{\partial y} = \frac{1}{B^2V}\int_{M_s}^{x} \frac{\partial\Omega_p(\lambda,y,z)}{\partial y}\, d\lambda + \frac{1}{B^2V}\int_{M_s}^{x} \frac{\partial\Omega_w(\lambda,y,z)}{\partial y}\, d\lambda \tag{A14}$$

and

$$\frac{\partial\theta_2(x,y,z)}{\partial z} = \frac{1}{B^2V}\int_{M_s}^{x} \frac{\partial\Omega_p(\lambda,y,z)}{\partial z}\, d\lambda + \frac{1}{B^2V}\int_{M_s}^{x} \frac{\partial\Omega_w(\lambda,y,z)}{\partial z}\, d\lambda \tag{A15}$$

For wings with mixed supersonic and subsonic trailing edges, both Ω_p and Ω_w may be discontinuous through the Mach surface from the supersonic portions of the trailing edge. Expressions for $\frac{\partial\theta_2}{\partial y}$ and $\frac{\partial\theta_2}{\partial z}$ for wings with mixed trailing edges can be found in a manner similar to those used in treating wings with other types of trailing edges. The resulting expressions appear to be of little value since they require a knowledge of the induced potential on the plan form and for this reason they are not presented here.

APPENDIX B

THE UPWASH $\frac{\partial\theta_q}{\partial z}$ ALONG THE WAKE CENTER LINE OF A PITCHING TRIANGULAR WING

The upwash along the center line of the wake of a pitching triangular wing with subsonic leading edges can be found by using a number of methods. The method used here is the potential doublet method presented in reference 11. This method was chosen because certain integrals which arise from using this method have already been evaluated in reference 11.

The potential difference across the surface of a triangular wing pitching about its apex is (from ref. 24)

$$\Delta\theta_q(x_1,y_1) = 2\pi K_q x_1\sqrt{m^2x_1{}^2 - y_1{}^2} \tag{B1}$$

where the coordinate axes are located at the wing apex. (See fig. 76.)

The potential at any point in the vertical plane of symmetry can be expressed as (ref. 11)

$$\theta_q(x,0,z) = -B^2zK_q \overset{f}{\iint}_{\text{Wing}} \frac{x_1\sqrt{m^2x_1{}^2 - y_1{}^2}}{\left[(x - x_1)^2 - B^2(y_1{}^2 + z^2)\right]^{3/2}}\,dx_1\,dy_1 -$$

$$B^2zcK_q \overset{f}{\iint}_{\text{Wake}} \frac{\sqrt{m^2c^2 - y_1{}^2}}{\left[(x - x_1)^2 - B^2(y^2 + z^2)\right]^{3/2}}\,dx_1\,dy_1 \tag{B2}$$

Equation (B2) can also be expressed as

$$\theta_q(x,0,z) = B^2zK_q \,{}^{f}\!\!\iint_{\text{Wing}} \frac{(x - x_1)\sqrt{m^2x_1^{\,2} - y_1^{\,2}}}{\left[(x - x_1)^2 - B^2\left(y_1^{\,2} + z^2\right)\right]^{3/2}}\,dx_1\,dy_1 \;-$$

$$B^2zxK_q \,{}^{f}\!\!\iint_{\text{Wing}} \frac{\sqrt{m^2x_1^{\,2} - y_1^{\,2}}}{\left[(x - x_1)^2 - B^2\left(y_1^{\,2} + z^2\right)\right]^{3/2}}\,dx_1\,dy_1 \;-$$

$$B^2zcK_q \,{}^{f}\!\!\iint_{\text{Wake}} \frac{\sqrt{m^2c^2 - y_1^{\,2}}}{\left[(x - x_1)^2 - B^2\left(y_1^{\,2} + z^2\right)\right]^{3/2}}\,dx_1\,dy_1 \qquad \text{(B3)}$$

The upwash along the center line of the wake is

$$w(x,0,0) = \lim_{z \to 0} \frac{\theta_q}{\partial z}$$

$$= \lim_{z \to 0} B^2K_q \frac{\partial}{\partial z} \,{}^{f}\!\!\iint_{\text{Wing}} \frac{z(x - x_1)\sqrt{m^2x_1^{\,2} - y_1^{\,2}}}{\left[(x - x_1)^2 - B^2\left(y_1^{\,2} + z^2\right)\right]^{3/2}}\,dx_1\,dy_1 \;-$$

$$\lim_{z \to 0} B^2xK_q \frac{\partial}{\partial z} \,{}^{f}\!\!\iint_{\text{Wing}} \frac{z\sqrt{m^2x_1^{\,2} - y_1^{\,2}}}{\left[(x - x_1)^2 - B^2\left(y_1^{\,2} + z^2\right)\right]^{3/2}}\,dx_1\,dy_1 \;-$$

$$\lim_{z \to 0} B^2cK_q \frac{\partial}{\partial z} \,{}^{f}\!\!\iint_{\text{Wake}} \frac{z\sqrt{m^2c^2 - y_1^{\,2}}}{\left[(x - x_1)^2 - B^2\left(y_1^{\,2} + z^2\right)\right]^{3/2}}\,dx_1\,dy_1$$

(B4)

The first integral of equation (B4) can be evaluated to yield

$$\lim_{z \to 0} B^2 K_q \frac{\partial}{\partial z} {}^{f}\!\iint_{\text{Wing}} \frac{z(x - x_1)\sqrt{m^2 x_1^2 - y_1^2}}{\left[(x - x_1)^2 - B^2(y_1^2 + z^2)\right]^{3/2}} \, dx_1 \, dy_1 = 2K_q Bmx \left[\int_0^1 \frac{K(k_1) - E(k_1)}{(Bm + k_1)^2} \, dk_1 - \int_1^{k_3} \frac{K(k_2) - E(k_2)}{k_2(Bmk_2 + 1)^2} \, dk_2\right] \tag{B5}$$

for $c \leqq x \leqq (Bm + 1)c$, and

$$\lim_{z \to 0} B^2 K_q \frac{\partial}{\partial z} {}^{f}\!\iint_{\text{Wing}} \frac{z(x - x_1)\sqrt{m^2 x_1^2 - y_1^2}}{\left[(x - x_1)^2 - B^2(y_1^2 + z^2)\right]^{3/2}} \, dx_1 \, dy_1 = 2K_q c \left\{Bmk_4 K(k_4) + \frac{x - c}{c}\left[E(k_4) - K(k_4)\right] - \frac{B^2 m^2 x}{c} \int_0^{k_4} \frac{k_1}{(Bm + k_1)^2} K(k_1) \, dk_1\right\} \tag{B6}$$

for $(Bm + 1)c \leqq x$. The last two integrals in equation (B4) arise in evaluating the potential in the vertical plane of symmetry from a triangular wing. These two integrals were evaluated in reference 11. From reference 11, the values of these expressions are found to be given by

$$-\lim_{z \to 0} B^2 x K_q \frac{\partial}{\partial z} {}^{f}\!\iint_{\text{Wing}} \frac{z\sqrt{m^2 x_1^2 - y_1^2}}{\left[(x - x_1)^2 - B^2(y_1^2 + z^2)\right]^{3/2}} \, dx_1 \, dy_1 = -2K_q x \left[\int_0^1 \frac{K(k_1) - E(k_1)}{k_1 + Bm} \, dk_1 - \int_1^{k_3} \frac{K(k_2) - E(k_2)}{k_2^2(1 + Bmk_2)} \, dk_2\right] \tag{B7}$$

for $c \leqq x \leqq (Bm + 1)c$,

$$-\lim_{z \to 0} B^2 x K_q \frac{\partial}{\partial z} {}^{f}\!\iint_{\text{Wing}} \frac{z\sqrt{m^2 x_1^2 - y_1^2}}{\left[(x - x_1)^2 - B^2(y_1^2 + z^2)\right]^{3/2}} \, dx_1 \, dy_1 = -2K_q x \int_0^{k_4} \frac{K(k_1) - E(k_1)}{k_1 + Bm} \, dk_1 \tag{B8}$$

for $(Bm + 1)c \leqq x$,

$$-\lim_{z \to 0} B^2 c K_q \frac{\partial}{\partial z} {}^{f}\!\iint_{\text{Wake}} \frac{z\sqrt{m^2 c^2 - y_1^2}}{\left[(x - x_1)^2 - B^2(y_1^2 + z^2)\right]^{3/2}} \, dx_1 \, dy_1 = -\frac{2BmK_q c^2}{x - c}\left[E(k_3) - (1 - k_3^2)K(k_3)\right] \tag{B9}$$

for $c \leqq x \leqq (Bm + 1)c$, and

$$-\lim_{z \to 0} B^2 c K_q \frac{\partial}{\partial z} {}^{f}\!\iint_{\text{Wake}} \frac{z\sqrt{m^2 c^2 - y_1^2}}{\left[(x - x_1)^2 - B^2(y_1^2 + z^2)\right]^{3/2}} \, dx_1 \, dy_1 = -2K_q c E(k_3) \tag{B10}$$

for $(Bm + 1)c \leqq x$.

The upwash along the wake center line is (from eqs. (B4) to (B10))

$$\frac{\partial\theta_q(x,0,0)}{\partial z} = -2K_q c\left\{\frac{x}{c}\int_0^1 \frac{k_1\left[K\left(k_1\right) - E\left(k_1\right)\right]}{\left(Bm + k_1\right)^2}\,dk_1 - \frac{x}{c}\int_1^{k_3} \frac{K\left(k_2\right) - E\left(k_2\right)}{k_2^{\,2}\left(Bmk_2 + 1\right)^2}\,dk_2 - \frac{\left(1 - k_3^{\,2}\right)K\left(k_3\right) - E\left(k_3\right)}{k_3}\right\} \tag{B11}$$

for $c \leqq x \leqq (Bm + 1)c$, and

$$\frac{\partial\theta_q(x,0,0)}{\partial z} = -2K_q c\left(\frac{x}{c}\int_0^{k_4}\left\{\frac{\left[\left(B^2m^2 + 1\right)k_1 + Bm\right]K\left(k_1\right)}{\left(Bm + k_1\right)^2} - \frac{E\left(k_1\right)}{Bm + k_1}\right\}dk_1 + \left(2 - \frac{x}{c}\right)E\left(k_4\right) + \frac{Bm\left(1 - k_4^{\,2}\right)K\left(k_4\right)}{k_4}\right) \tag{B12}$$

for $(Bm + 1)c \leqq x$.

APPENDIX C

THE UPWASH COMPONENT $\frac{\partial\theta_2}{\partial z}$ ALONG THE CENTER LINE OF THE WAKE OF A TRIANGULAR WING

The upwash component $\frac{\partial\theta_2}{\partial z}$ can be determined by the methods previously presented. For this case, however, the upwash can be determined relatively easily by the use of potential doublets and therefore this method is used.

The difference in the x-derivative of the potential across the wake is given by

$$\Delta\frac{\partial\theta_2}{\partial x} = \frac{2\dot{\alpha}\sqrt{m^2c^2 - {y_1}^2}}{B^2E'(Bm)} \tag{C1}$$

The potential difference across the wake is

$$\Delta\theta_2 = \int_c^{x_1} \Delta\frac{\partial\theta_2}{\partial x}\,dx = \frac{2\dot{\alpha}\left(x_1 - c\right)\sqrt{m^2c^2 - {y_1}^2}}{B^2E'(Bm)} \tag{C2}$$

The upwash component $\frac{\partial\theta_2}{\partial z}$ along the center line of the wake is given by

$$\frac{\partial\theta_2(x,0,0)}{\partial z} = -\lim_{z\longrightarrow 0} \frac{\dot{\alpha}}{\pi E'(Bm)}\,\frac{\partial}{\partial z}\,{}^{f}\!\iint_{\text{Wake}} \frac{z\left(x_1 - c\right)\sqrt{m^2c^2 - {y_1}^2}}{\left[\left(x - x_1\right)^2 - B^2\left({y_1}^2 + z^2\right)\right]^{3/2}}\,dx_1\,dy_1 \tag{C3}$$

If the indicated operations in equation (C3) are performed, the following equations result:

$$\frac{\partial\theta_2}{\partial z} = -\frac{2\dot{\alpha}mc}{\pi BE'(Bm)}\left[2E\left(k_3\right) - \left(1 - k_3{}^2\right)K\left(k_3\right)\right] \qquad (C4)$$

for $c \leqq x \leqq (Bm + 1)c$, and

$$\frac{\partial\theta_2}{\partial z} = -\frac{2\dot{\alpha}(x - c)}{\pi B^2E'(Bm)}\left[2E\left(k_4\right) - \left(1 - k_4{}^2\right)K\left(k_4\right)\right] \qquad (C5)$$

for $(Bm + 1)c \leqq x$.

APPENDIX D

EXPRESSIONS FOR THE MOMENT ON CERTAIN HORIZONTAL-TAIL SURFACES

If the type of arguments utilized in references 22 and 25 are followed, expressions may be found for the lift and moment (about the trailing edge) on surfaces which have supersonic leading edges and trailing edges which are perpendicular to the free-stream direction (see fig. 77(a)) for the case of an angle-of-attack distribution which varies linearly with time.

Consider a two-dimensional airfoil (as shown in fig. 78(a)) which has an angle of attack given by

$$\sigma = -\dot{\sigma}(t - t_o)h(x) \tag{D1}$$

By symmetry it is clear that the lift and moment coefficients based on the area with the variable angle of attack for the wings shown in figures 78(a), 78(b), and 78(c) are the same. The wing shown in figure 78(d) can be obtained as a simple combination of the wings shown in figures 78(a), 78(b), and 78(c). The lift and moment coefficients based on the area with the variable angle of attack therefore are the same as the lift and moment coefficients for the two-dimensional wing.

The potential function for the flow over the upper surface of the two-dimensional wing illustrated in figure 78(a) is (from eq. (13))

$$\phi = \frac{\dot{\sigma}M^2}{B^3}\int_0^{x-Bz} \xi h(\xi)d\xi + \frac{\dot{\sigma}V}{B}\left[(t - t_o) - \frac{M^2x}{B^2V}\right]\int_0^{x-Bz} h(\xi)d\xi \tag{D2}$$

where x is the distance downstream from the leading edge of the airfoil.

The pressure-difference coefficient is

$$\Delta C_p = \frac{4}{B}\left[\dot{\sigma}(t - t_o)h(x) - \frac{\dot{\sigma}}{B^2V}\int_0^x h(\xi)d\xi\right] \tag{D3}$$

The lift and moment coefficients are, for $t = t_0$,

$$C_L = \frac{\text{Lift/Unit length}}{\frac{\rho}{2} V^2 \bar{c}} = -\frac{4\dot{\sigma}}{B^3 \bar{c} V} \int_0^c dx \int_0^x h(\xi) d\xi \qquad \text{(D4)}$$

$$C_m = \frac{\text{Moment/Unit length}}{\frac{\rho}{2} V^2 \bar{c}^2} = \frac{4\dot{\sigma}}{B^3 \bar{c}^2 V} \int_0^c (c - x) dx \int_0^x h(\xi) d\xi \qquad \text{(D5)}$$

where the moment is taken about the trailing edge of the airfoil.

The lift produced by a deflected strip such as is illustrated in figure 77(b) is the same as that produced by the strip illustrated in figure 78(d) and hence the same as a strip of the same width on the two-dimensional airfoil illustrated in figure 78(a). The total lift and moment coefficients for the type of airfoil illustrated in figure 77(a) therefore are

$$C_L = -\frac{4\dot{\sigma}}{B^3 S V} \iint_{\text{Airfoil surface}} \left[\int_{\text{L.E.}}^x h(\xi) d\xi\right] ds \qquad \text{(D6)}$$

$$C_m = \frac{4\dot{\sigma}}{B^3 S \bar{c} V} \iint_{\text{Airfoil surface}} \left[\lambda \int_{\text{L.E.}}^x h(\xi) d\xi\right] ds \qquad \text{(D7)}$$

where λ is the distance upstream to the element of area ds. (See fig. 77(b).)

In the case where the airfoil illustrated in figure 77(a) is a tail surface and the wing-tail combination has a constant vertical acceleration, the time-dependent angle-of-attack distribution on the tail surface is given by

$$\sigma = \dot{\alpha}\left(1 + \frac{\partial}{\partial z} \frac{\Omega\alpha}{\alpha V}\right) t$$

In this case equations (D6) and (D7) become

$$C_L = \frac{\text{Lift}}{\frac{\rho}{2} V^2 S_t} = - \frac{4\dot{\alpha}}{B^3 S_t V} \iint_{\text{Tail surface}} \left[\int_{\text{L.E.}}^{x} \left(1 + \frac{\partial}{\partial z} \frac{\Omega_\alpha}{\alpha V} \right) d\xi \right] ds \qquad \text{(D8)}$$

$$C_m = \frac{\text{Moment}}{\frac{\rho}{2} V^2 S_t \bar{c}_t} = \frac{4\dot{\alpha}}{B^3 S_t \bar{c}_t V} \iint_{\text{Tail surface}} \left[\lambda \int_{\text{L.E.}}^{x} \left(1 + \frac{\partial}{\partial z} \frac{\Omega_\alpha}{\alpha V} \right) d\xi \right] ds \qquad \text{(D9)}$$

REFERENCES

1. Ribner, Herbert S., and Malvestuto, Frank S., Jr.: Stability Derivatives of Triangular Wings at Supersonic Speeds. NACA Rep. 908, 1948. (Supersedes NACA TN 1572.)

2. Malvestuto, Frank S., Jr., and Margolis, Kenneth: Theoretical Stability Derivatives of Thin Sweptback Wings Tapered to a Point With Sweptback or Sweptforward Trailing Edges for a Limited Range of Supersonic Speeds. NACA Rep. 971, 1950. (Supersedes NACA TN 1761.)

3. Harmon, Sidney M.: Stability Derivatives at Supersonic Speeds of Thin Rectangular Wings With Diagonals Ahead of Tip Mach Lines. NACA Rep. 925, 1949. (Supersedes NACA TN 1706.)

4. Jones, Arthur L.: The Theoretical Lateral-Stability Derivatives for Wings at Supersonic Speeds. Jour. Aero. Sci., vol. 17, no. 1, Jan. 1950, pp. 39-46.

5. Malvestuto, Frank S., Jr., Margolis, Kenneth, and Ribner, Herbert S.: Theoretical Lift and Damping in Roll at Supersonic Speeds of Thin Sweptback Tapered Wings With Streamwise Tips, Subsonic Leading Edges, and Supersonic Trailing Edges. NACA Rep. 970, 1950. (Supersedes NACA TN 1860.)

6. Harmon, Sidney M., and Jeffreys, Isabella: Theoretical Lift and Damping in Roll of Thin Wings With Arbitrary Sweep and Taper at Supersonic Speeds - Supersonic Leading and Trailing Edges. NACA TN 2114, 1950.

7. Cohen, Doris: Formulas for the Supersonic Loading, Lift and Drag of Flat Swept-Back Wings With Leading Edges Behind the Mach Lines. NACA Rep. 1050, 1951.

8. Martin, John C., Margolis, Kenneth, and Jeffreys, Isabella: Calculation of Lift and Pitching Moments Due to Angle of Attack and Steady Pitching Velocity at Supersonic Speeds for Thin Sweptback Tapered Wings With Streamwise Tips and Supersonic Leading and Trailing Edges. NACA TN 2699, 1952.

9. Margolis, Kenneth: Theoretical Lift and Damping in Roll of Thin Sweptback Tapered Wings With Raked-In and Cross-Stream Wing Tips at Supersonic Speeds. Subsonic Leading Edges. NACA TN 2048, 1950.

10. Lagerstrom, P. A., Graham, Martha E., and Grosslight, G.: Downwash and Sidewash Induced by Three-Dimensional Lifting Wings in Supersonic Flow. Rep. No. SM-13007, Douglas Aircraft Co., Inc., Apr. 14, 1947.

11. Lomax, Harvard, Sluder, Loma, and Heaslet, Max. A.: The Calculation of Downwash Behind Supersonic Wings With an Application to Triangular Plan Forms. NACA Rep. 957, 1950. (Supersedes NACA TN 1620 and NACA TN 1803.)

12. Robinson, A., and Hunter-Tod, J. H.: Bound and Trailing Vortices in the Linearized Theory of Supersonic Flow, and the Downwash in the Wake of a Delta Wing. Rep. No. 10, College of Aero., Cranfield (British), Oct. 1947.

13. Mirels, Harold, and Haefeli, Rudolph C.: Line-Vortex Theory for Calculation of Supersonic Downwash. NACA Rep. 983, 1950. (Supersedes NACA TN 1925.)

14. Ward, G. N.: Calculation of Downwash Behind a Supersonic Wing. The Aeronautical Quarterly, vol. I, pt. I, May 1949, pp. 35-38.

15. Martin, John C.: The Calculation of Downwash Behind Wings of Arbitrary Plan Form at Supersonic Speeds. NACA TN 2135, 1950.

16. Ribner, Herbert S.: Time-Dependent Downwash at the Tail and the Pitching Moment Due to Normal Acceleration at Supersonic Speeds. NACA TN 2042, 1950.

17. Mirels, Harold: Theoretical Method for Solution of Aerodynamic Forces on Thin Wings in Nonuniform Supersonic Stream With an Application to Tail Surfaces. NACA TN 1736, 1948.

18. Graham, Martha E.: Some Linearized Computations of Supersonic Wing-Tail Interference. Rep. No. SM-13430, Douglas Aircraft Co., Inc., Dec. 23, 1948.

19. Miles, John W.: The Application of Unsteady Flow Theory to the Calculation of Dynamic Stability Derivatives. Aerophysics Lab. Rep. AL-957, North American Aviation, Inc., Sept. 8, 1950.

20. Mirels, Harold: A Lift-Cancellation Technique in Linearized Supersonic-Wing Theory. NACA Rep. 1004, 1951. (Supersedes NACA TN 2145.)

21. Cowley, W. L., and Glauert, H.: The Effect of the Lag of the Downwash on the Longitudinal Stability of an Aeroplane and on the Rotary Derivative M_q. R. & M. No. 718, British A.R.C., 1921.

22. Lomax, Harvard, Heaslet, Max. A., Fuller, Franklyn B., and Sluder, Loma: Two- and Three-Dimensional Unsteady Lift Problems in High-Speed Flight. NACA Rep. 1077, 1952. (Supersedes NACA TN 2403 by Lomax, Heaslet, Sluder, TN 2387 by Lomax, Heaslet, Fuller; contains material from TN 2256 by Lomax, Heaslet, Fuller.)

23. Miller, Frederic H.: Partial Differential Equations. John Wiley & Sons, Inc., 1941.

24. Brown, Clinton E., and Adams, Mac C.: Damping in Pitch and Roll of Triangular Wings at Supersonic Speeds. NACA Rep. 892, 1948. (Supersedes NACA TN 1566.)

25. Lagerstrom, P. A., and Van Dyke, M. D.: General Considerations About Planar and Non-Planar Lifting Systems. Rep. No. SM-13432, Douglas Aircraft Co., Inc., June 1949.

TABLE I.- FORMULAS FOR TRANSFORMATION OF THE STABILITY DERIVATIVES C_{m_α}, C_{L_q}, C_{m_q}, $C_{L_{\dot{\alpha}}}$, AND $C_{m_{\dot{\alpha}}}$ FROM BODY TO STABILITY AXES

Body axes; origin[1] at $x = 0$, $y = 0$, $\overline{z} = 0$	Body axes; origin at $x = d$, $y = 0$, $z = 0$		Stability axes; origin at $x = d$, $y = 0$, $z = 0$	
Stability derivative	Stability derivative[2]	Shift in origin from (0,0,0) to (d,0,0)	Stability derivative[3]	Origin at (d,0,0); rotation through angle α
C_{m_α}	$C_{m_\alpha}{}^*$	$C_{m_\alpha} + \frac{d}{\overline{c}_w} C_{L_\alpha}$	$C_{m_\alpha}{}'$	$C_{m_\alpha}{}^*$ (approx.)
C_{L_q}	$C_{L_q}{}^*$	$C_{L_q} - \frac{2d}{\overline{c}_w} C_{L_\alpha}$	$C_{L_q}{}'$	$C_{L_q}{}^*$ (approx.)
C_{m_q}	$C_{m_q}{}^*$	$C_{m_q} + \frac{d}{\overline{c}_w} C_{L_q} - \frac{2d}{\overline{c}_w} C_{m_\alpha} - \frac{2d^2}{\overline{c}_w{}^2} C_{L_\alpha}$	$C_{m_q}{}'$	$C_{m_q}{}^*$
$C_{L_{\dot{\alpha}}}$	$C_{L_{\dot{\alpha}}}{}^*$	$C_{L_{\dot{\alpha}}}$	$C_{L_{\dot{\alpha}}}{}'$	$C_{L_{\dot{\alpha}}}{}^*$ (approx.)
$C_{m_{\dot{\alpha}}}$	$C_{m_{\dot{\alpha}}}{}^*$	$C_{m_\alpha} + \frac{d}{\overline{c}} C_{L_{\dot{\alpha}}}$	$C_{m_{\dot{\alpha}}}{}'$	$C_{m_{\dot{\alpha}}}{}^*$

[1] The origin refers to a system of Cartesian coordinates used in the analysis. (See fig. 25(a).)

[2] These coefficients are for a system of body axes located at (d,0,0) in the system used in the analysis. (See fig. 25(a).)

[3] These coefficients are for a system of stability axes located at (d,0,0) in the system used in the analysis. (See fig. 25(b).)

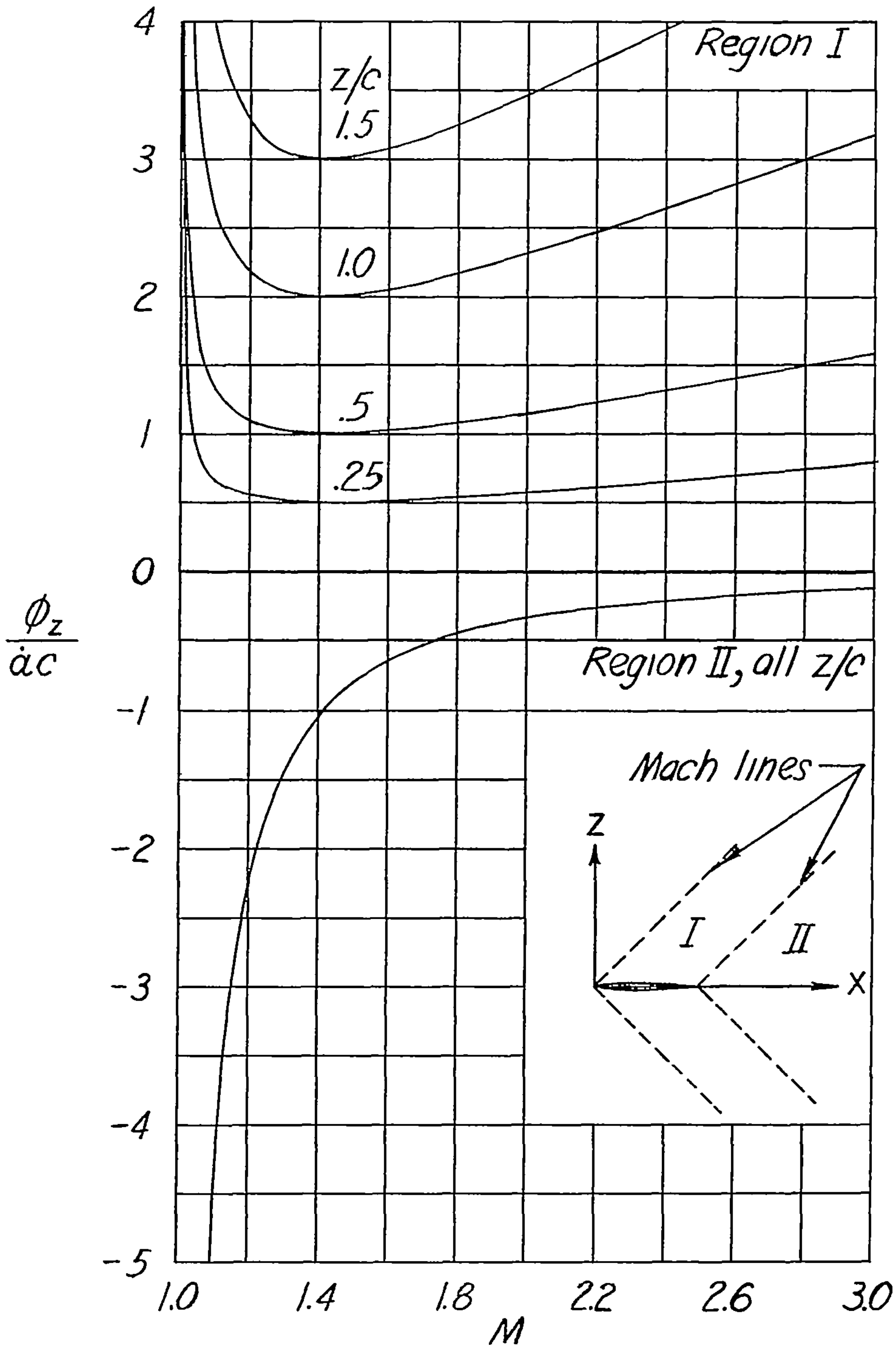

Figure 1.- Variation of $\frac{\phi_z}{\dot{\alpha}c}$ behind a two-dimensional airfoil with Mach number for various values of $\frac{z}{c}$ for $t = t_o$.

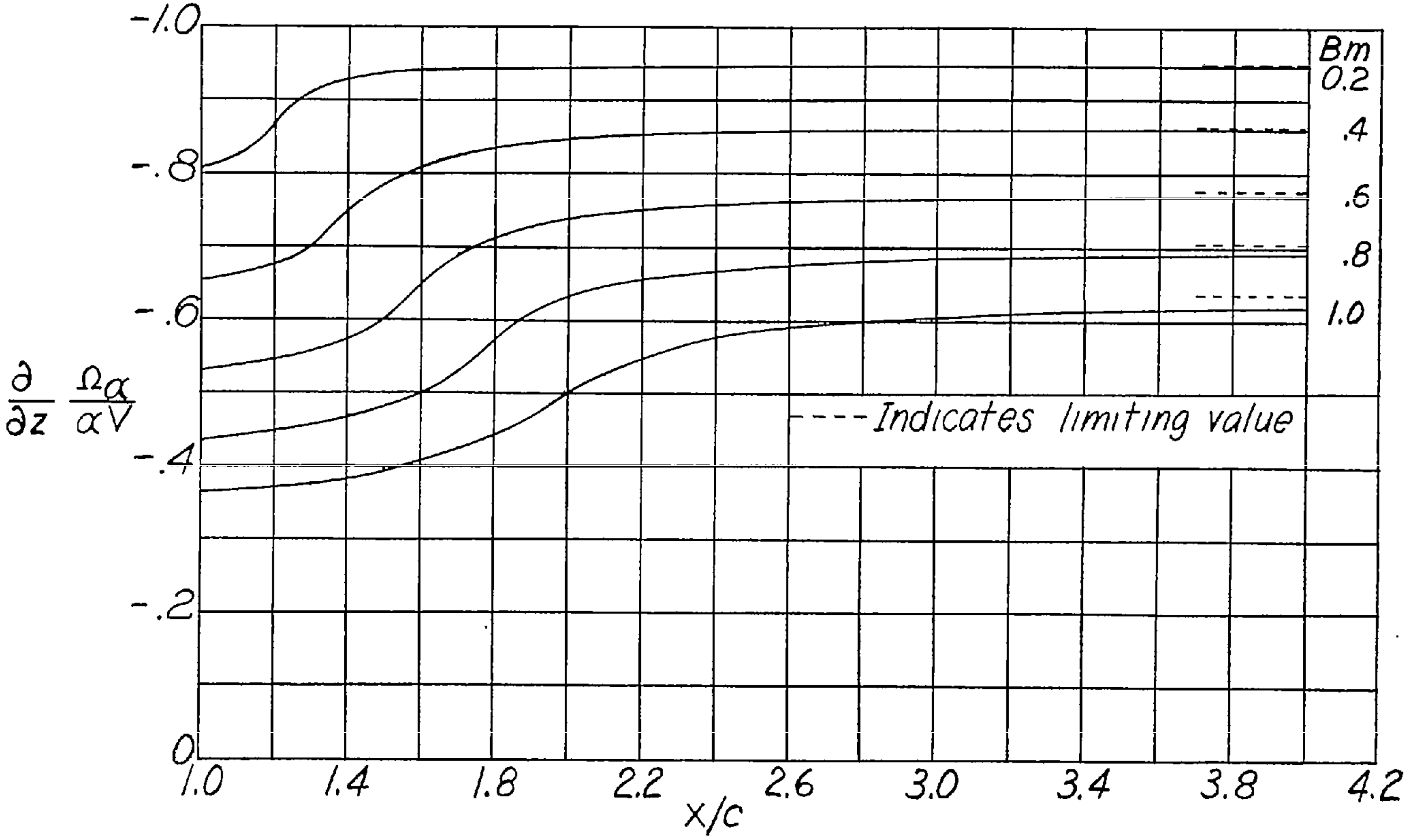

Figure 2.- Variation of $\frac{\partial}{\partial z}\frac{\Omega_\alpha}{\alpha V}$ along the wake center line of a triangular wing. (Values are taken from refs. 11 and 12.)

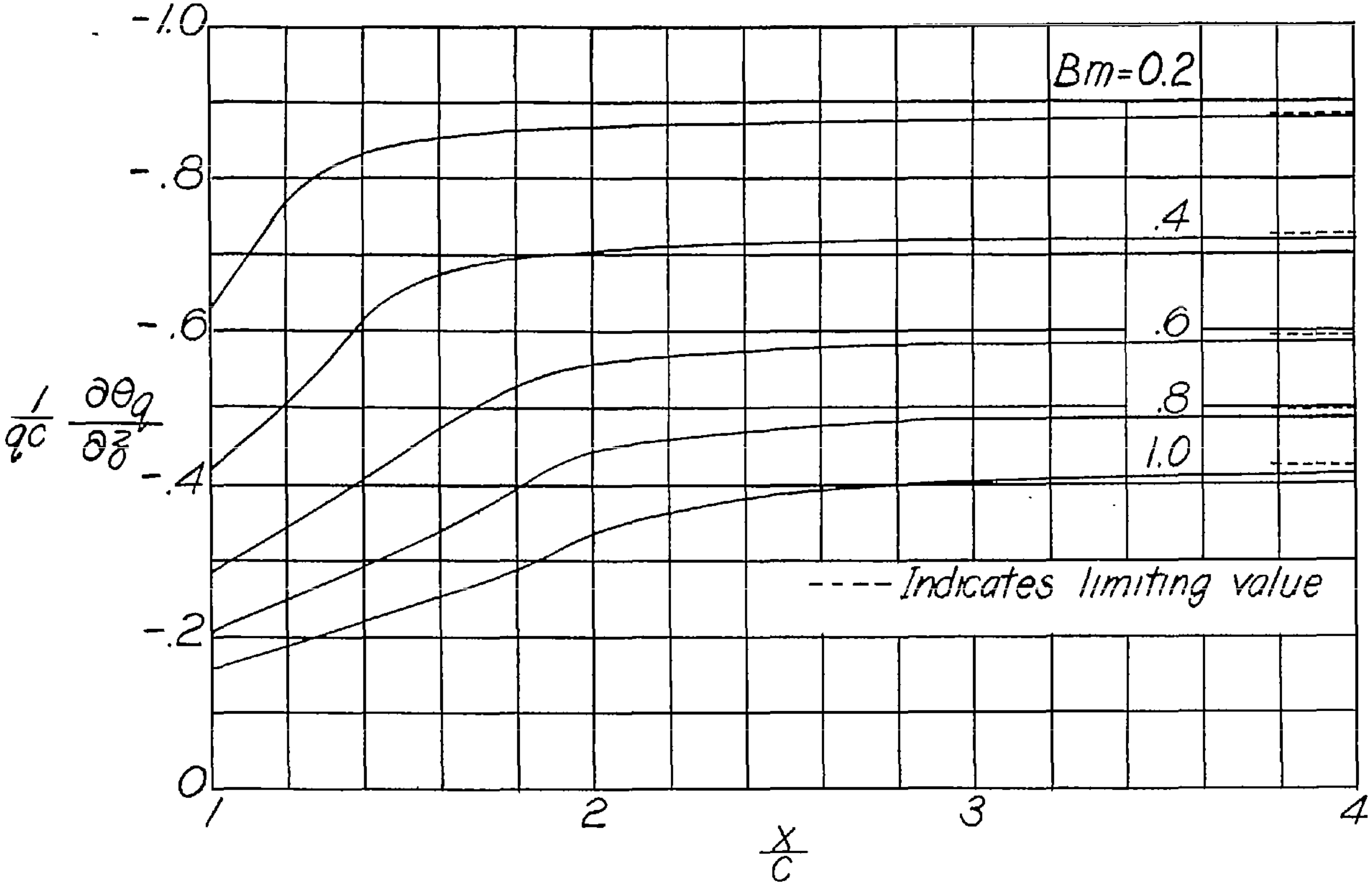

Figure 3.- Variation of $\frac{1}{qc}\frac{\partial\theta_q}{\partial z}$ along the wake center line of a triangular wing pitching about its apex.

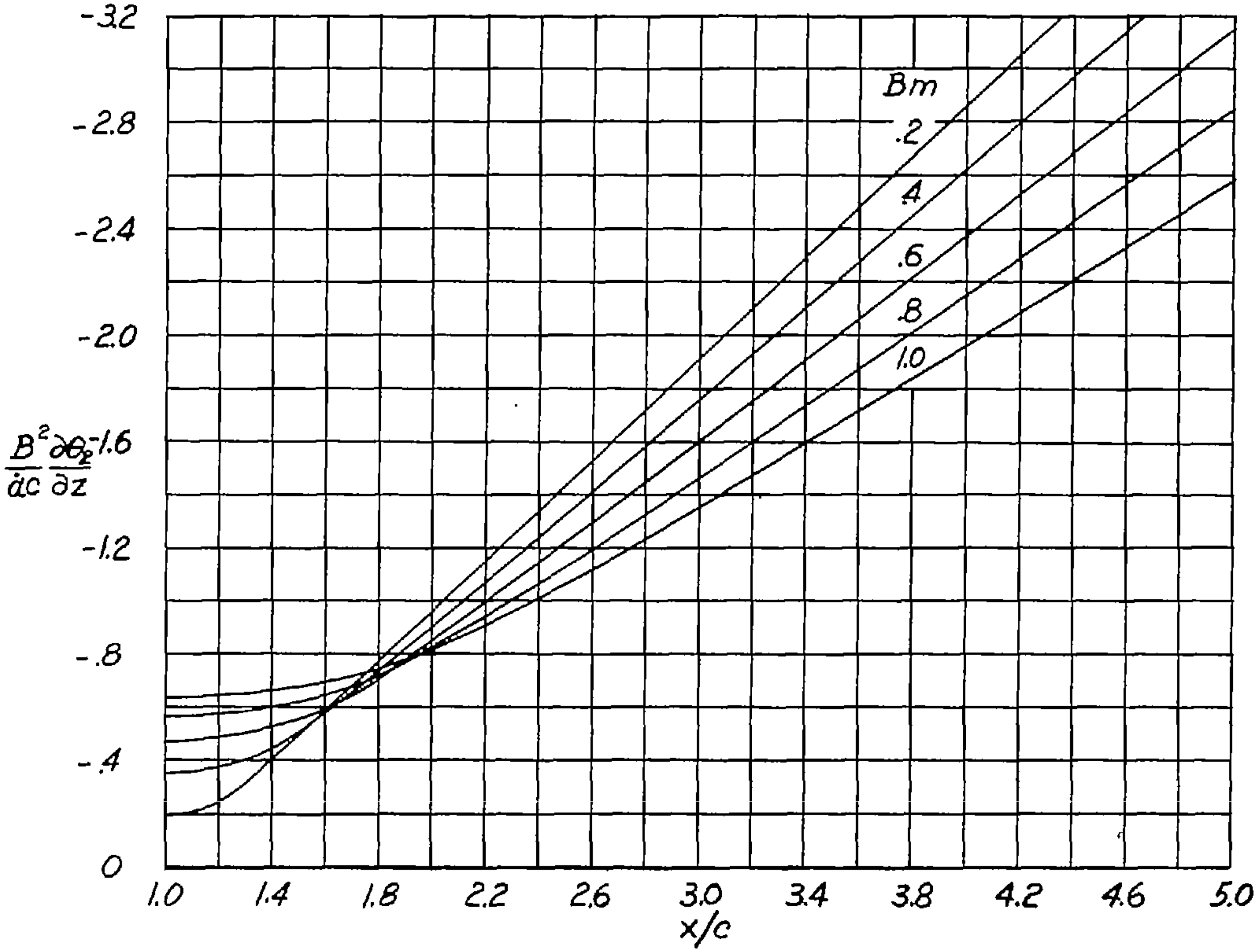

Figure 4.- The variation of the upwash component $\frac{B^2}{\dot{\alpha}c}\frac{\partial\theta_2}{\partial z}$ along the center line of the wake from a triangular wing with subsonic leading edges for various values of the parameter Bm.

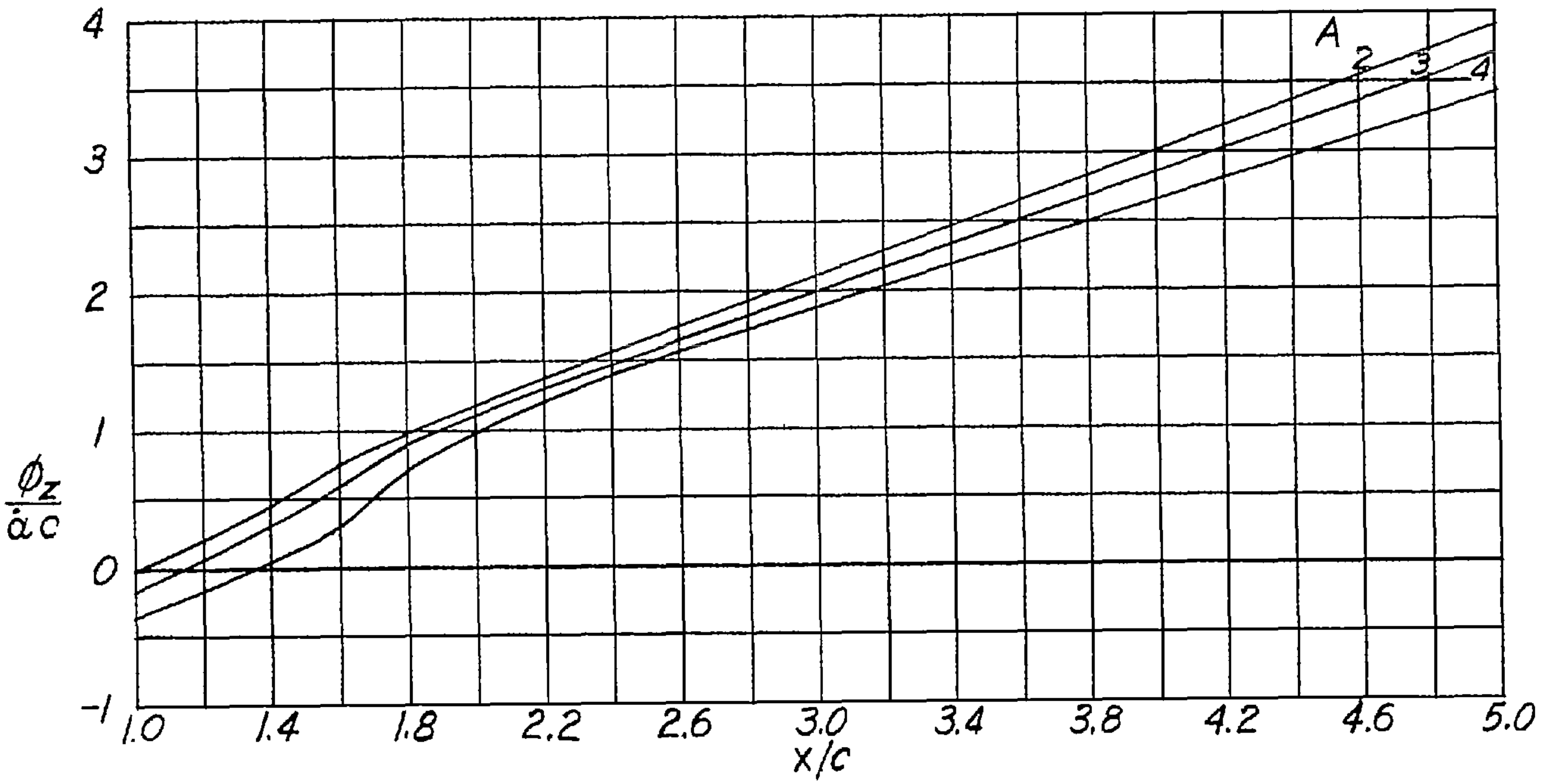

(a) M = 1.20.

Figure 5.- The variation of upwash along the center line of the wake at $t = t_0$ of a triangular wing with a constant vertical acceleration for various aspect ratios.

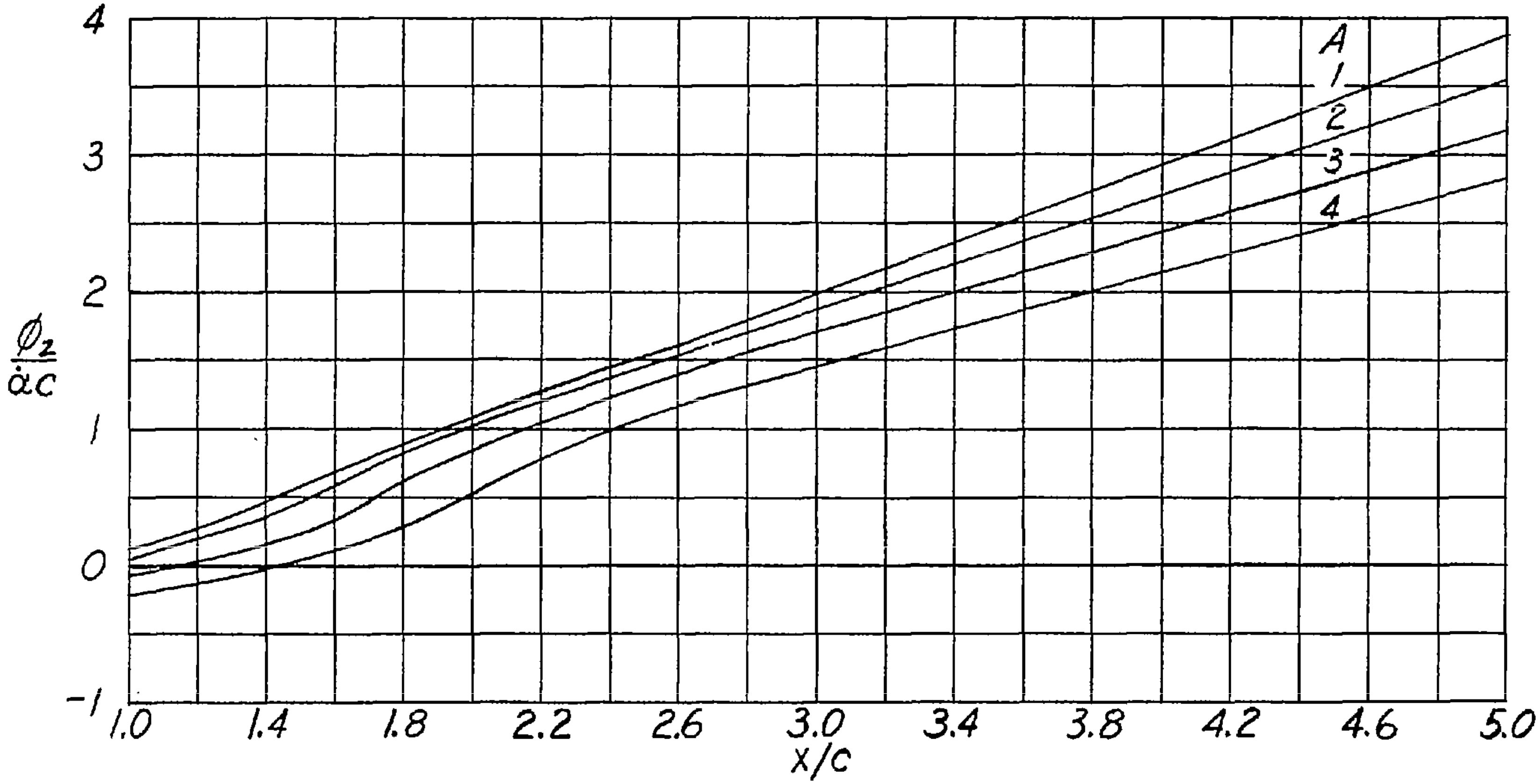

(b) M = 1.414.

Figure 5.- Continued.

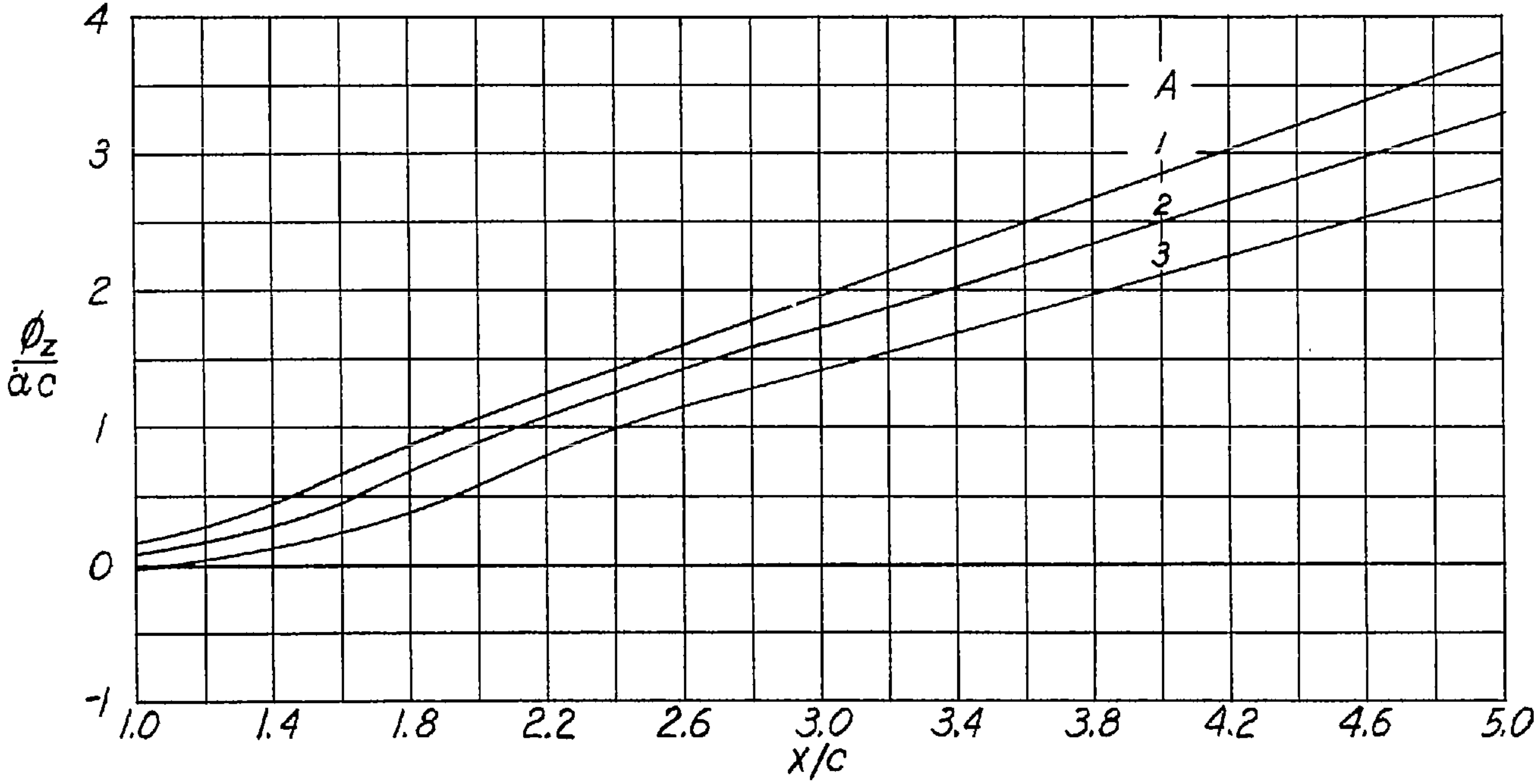

(c) M = 1.67.

Figure 5.– Continued.

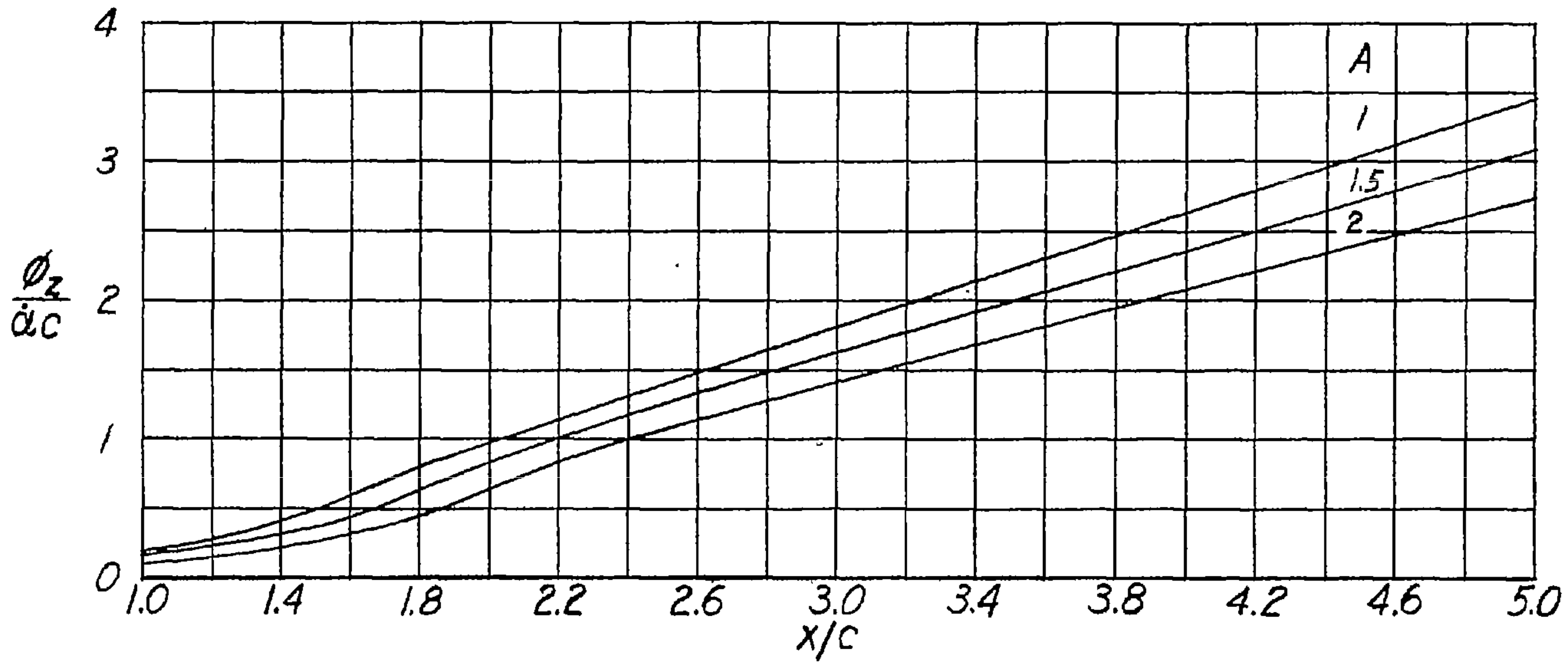

(d) M = 2.24.

Figure 5.- Concluded.

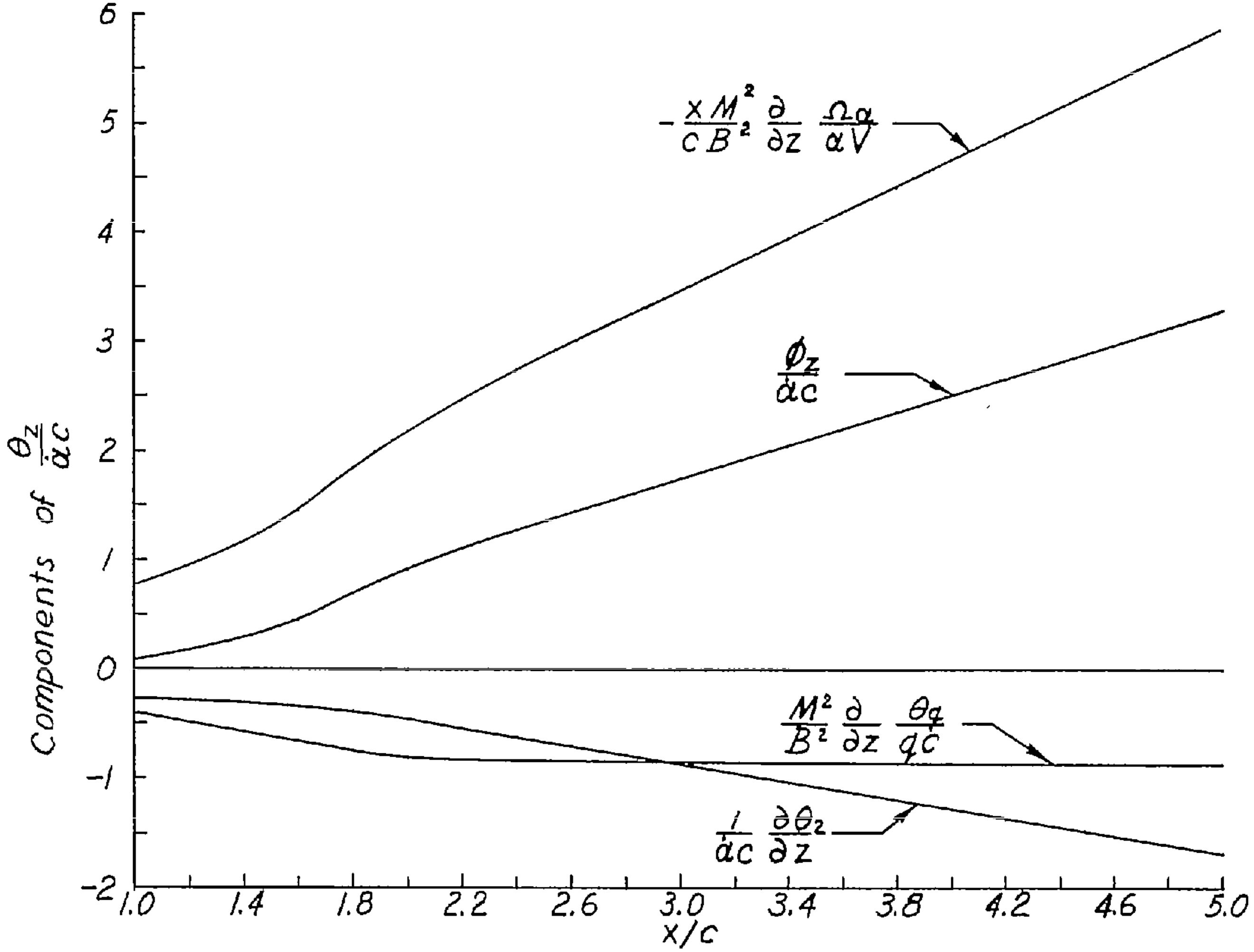

Figure 6.- Components of the upwash along the center line of the wake at $t = t_0$ behind a triangular wing of aspect ratio 2 with a constant vertical acceleration at $M = 1.67$.

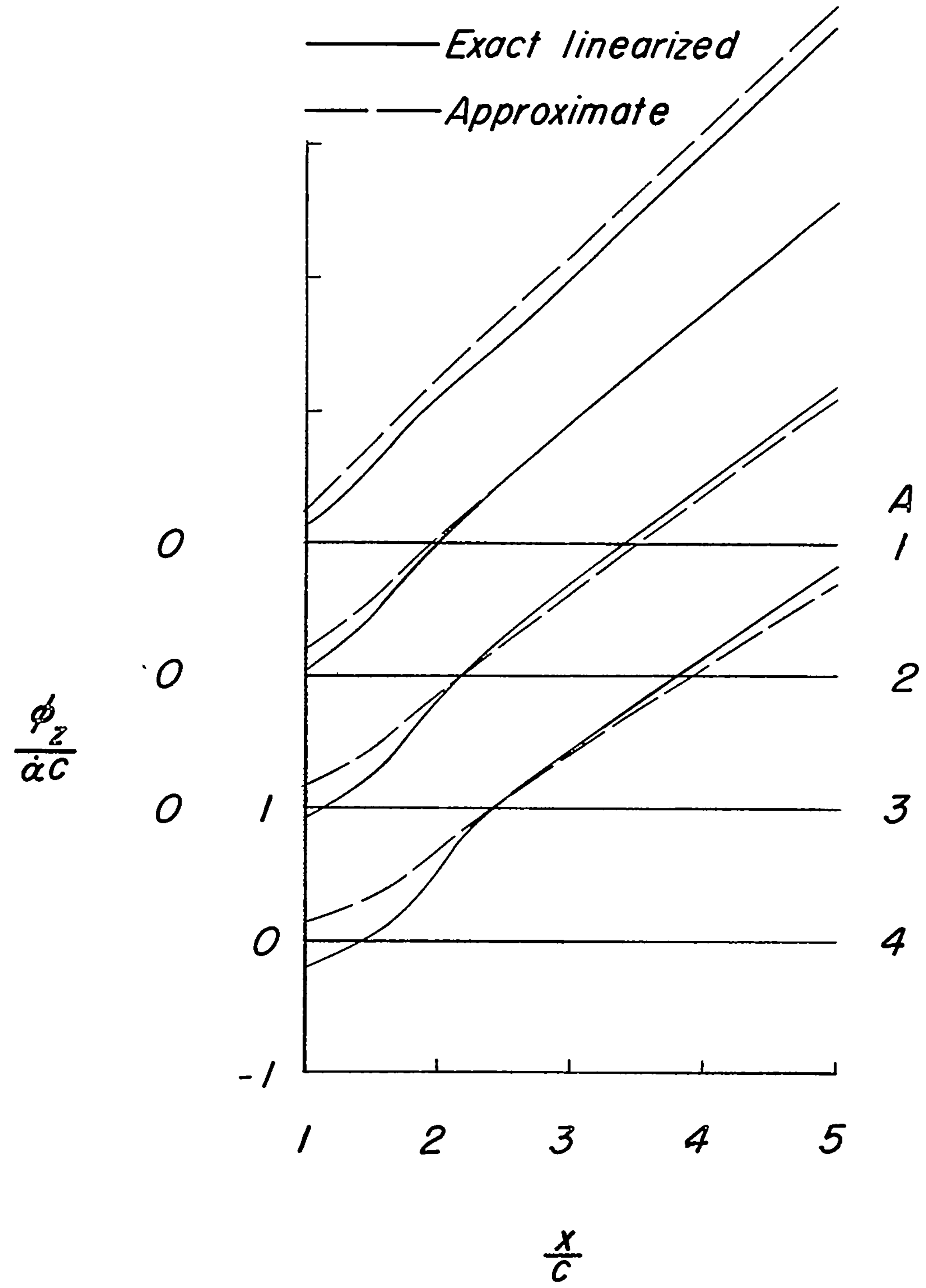

Figure 7.- Exact (linearized) and approximate (eq. (37b)) values of upwash at $t = t_0$ along the center line of the wake behind a triangular wing with constant vertical acceleration for various aspect ratios. $M = 1.414$.

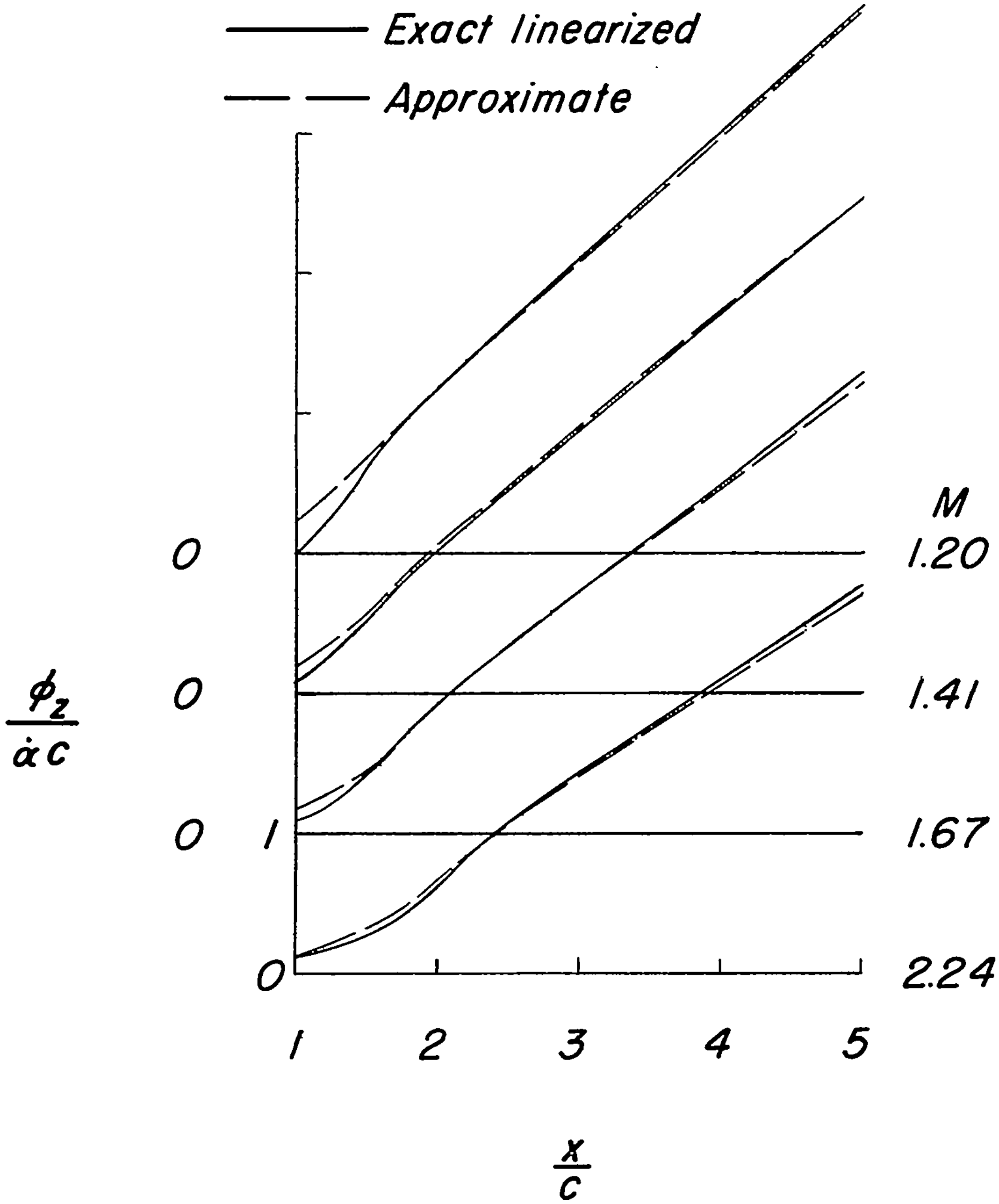

Figure 8.- Exact (linearized) and approximate (eq. (37b)) values of upwash at $t = t_0$ along the center line of the wake behind a triangular wing with constant vertical acceleration for various Mach numbers. A = 2.

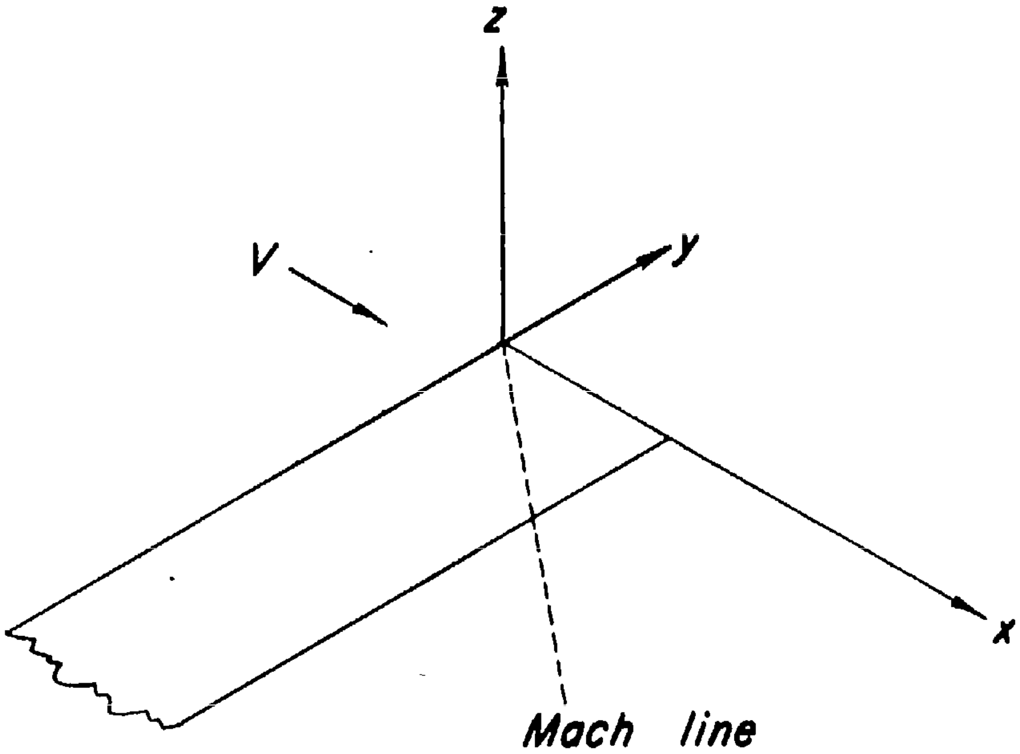

Figure 9.- Location of coordinate axes used in treating a rectangular wing tip.

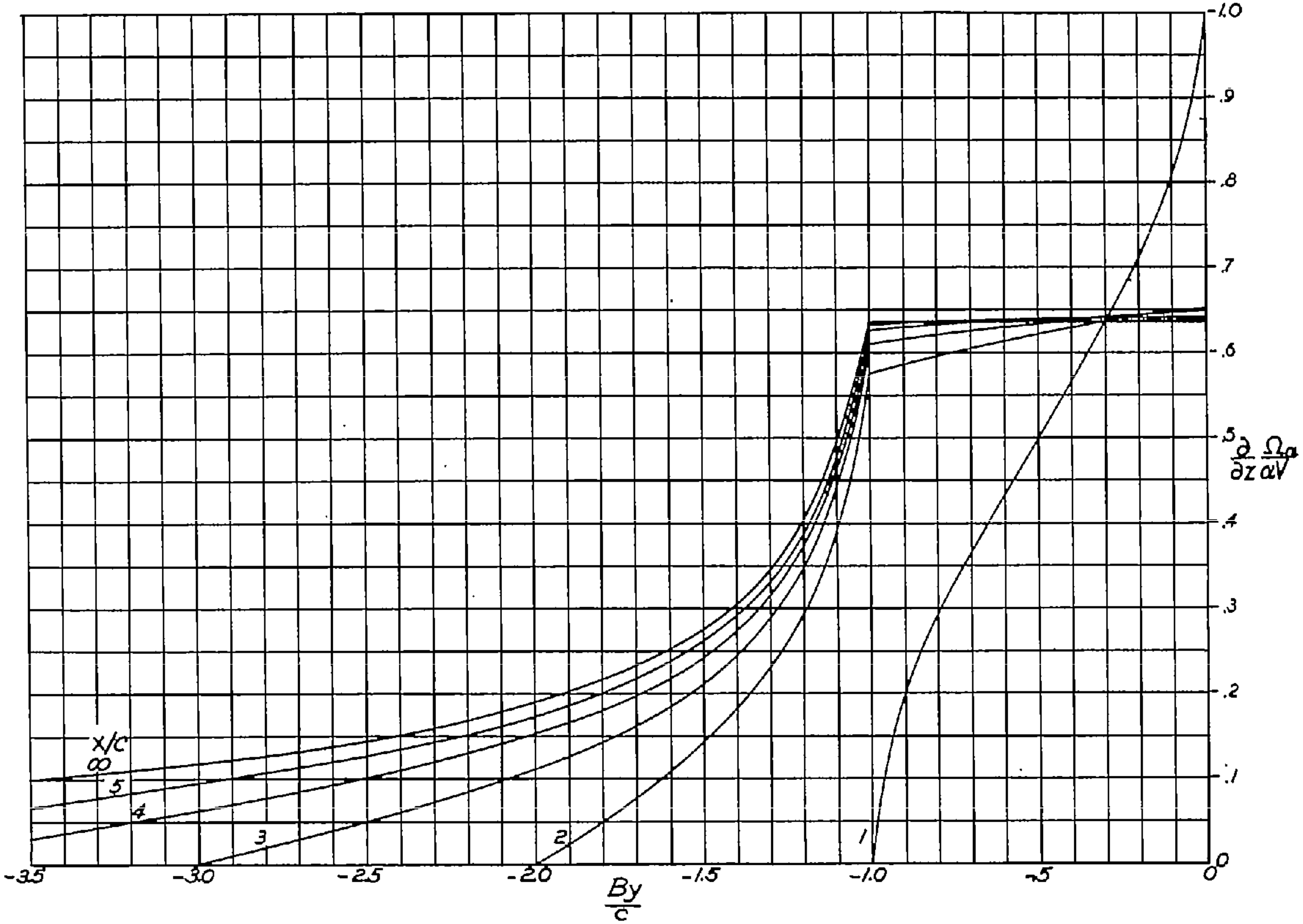

Figure 10.- The variation of upwash in the plane of the wing behind one tip of a semi-infinite rectangular wing at a constant angle of attack (from ref. 10).

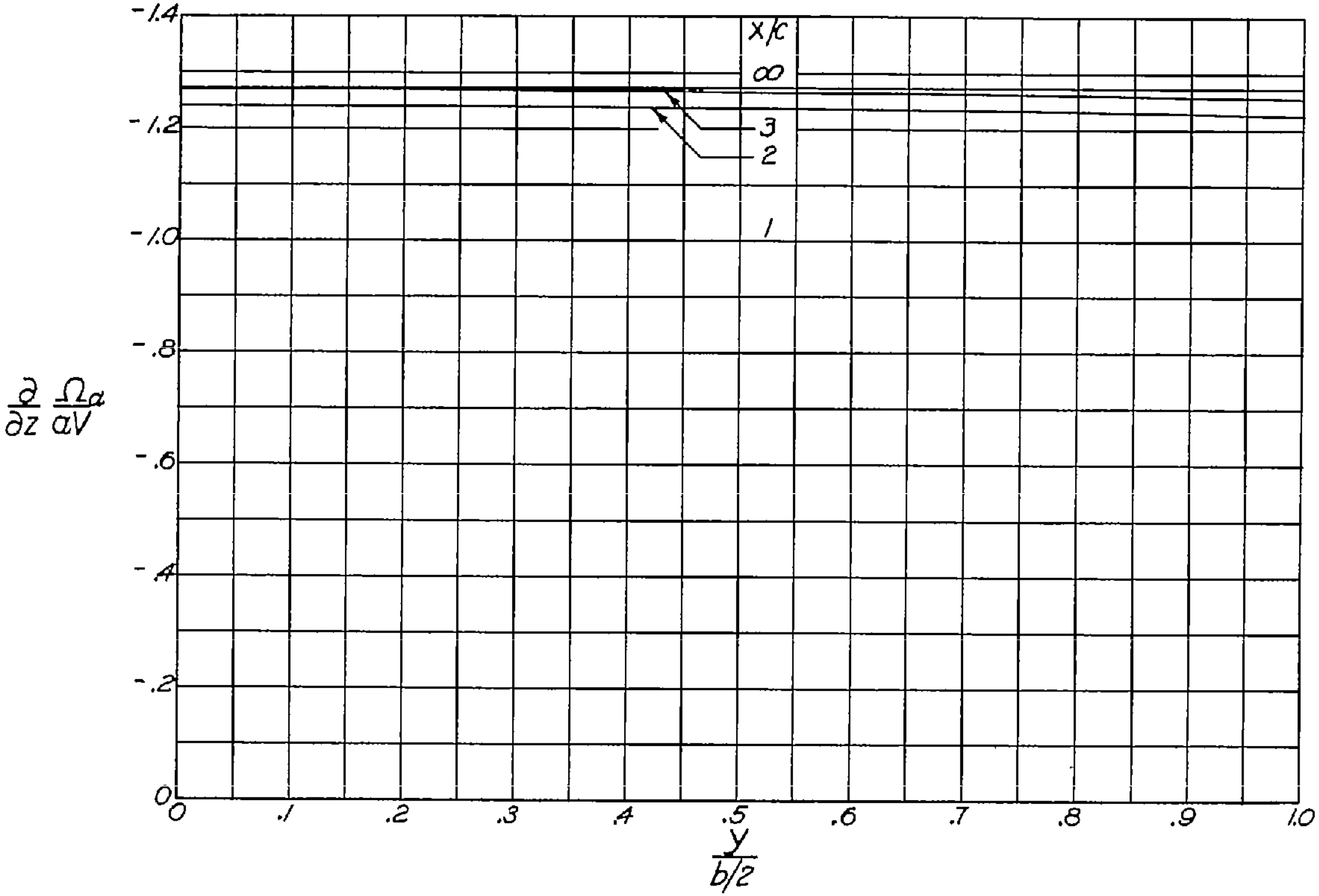

(a) AB = 1.

Figure 11.- The variation of upwash in the plane of the wing behind a rectangular wing at a constant angle of attack for various values of the parameter AB.

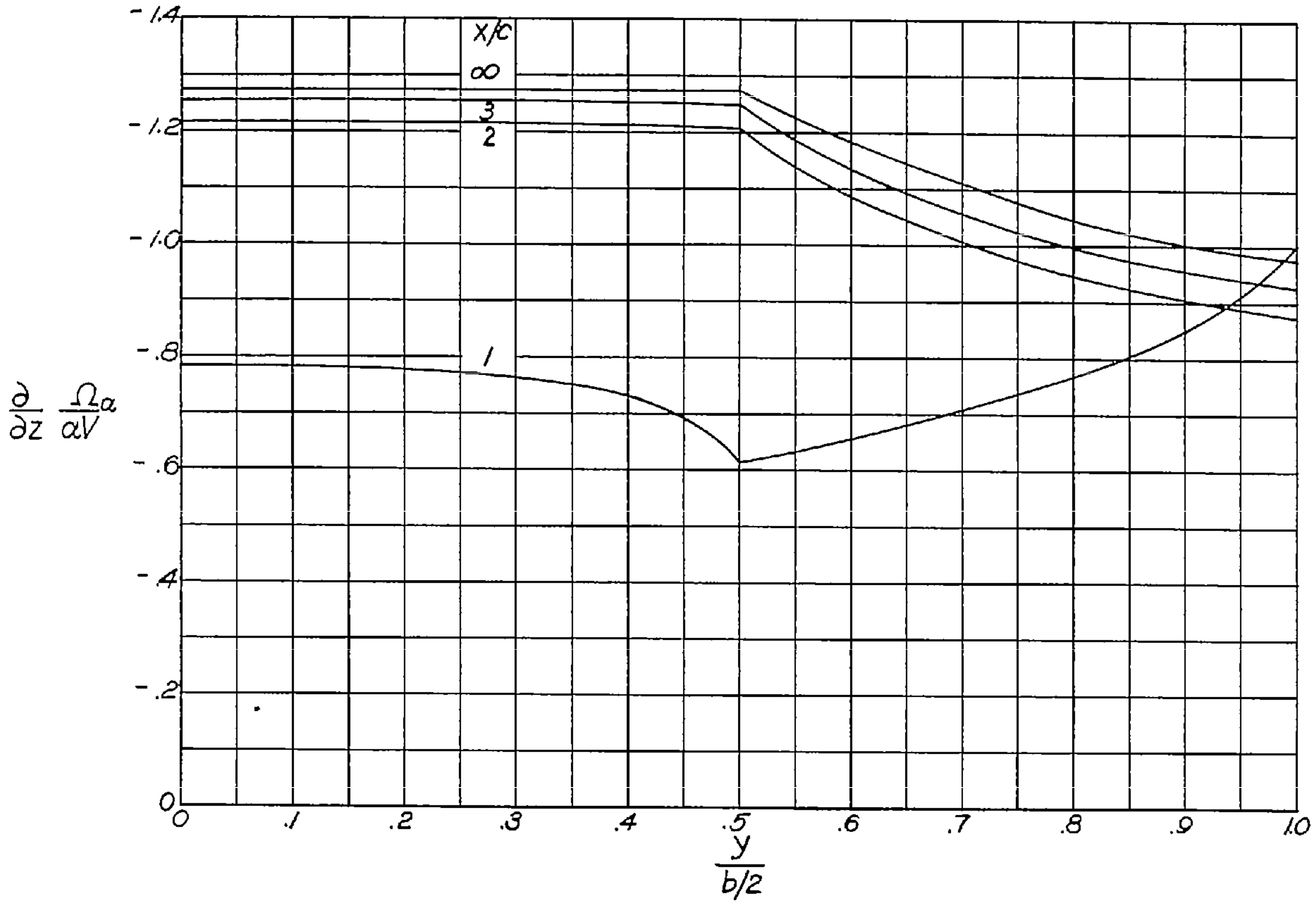

(b) AB = 1.33.

Figure 11.- Continued.

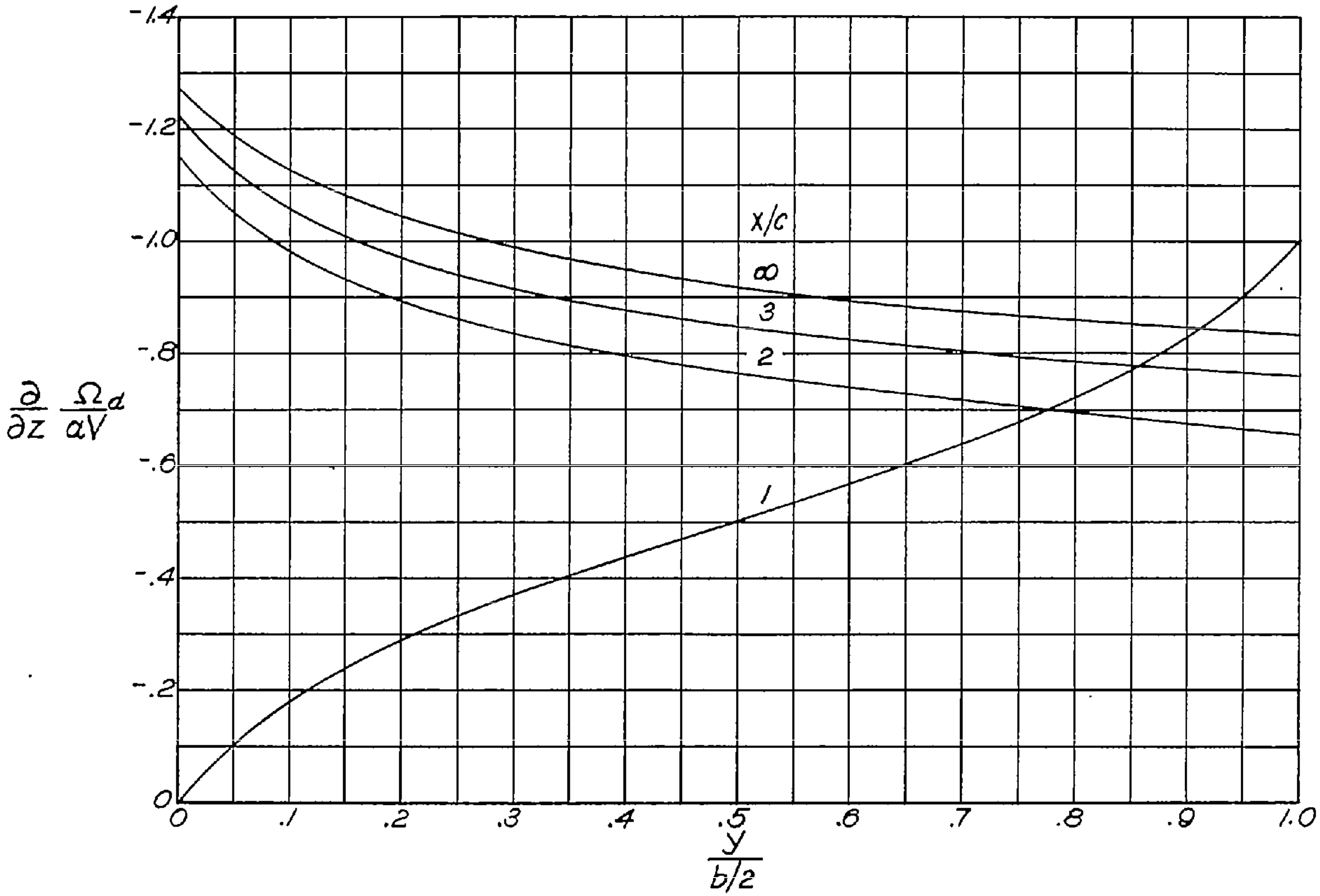

(c) AB = 2.

Figure 11.- Continued.

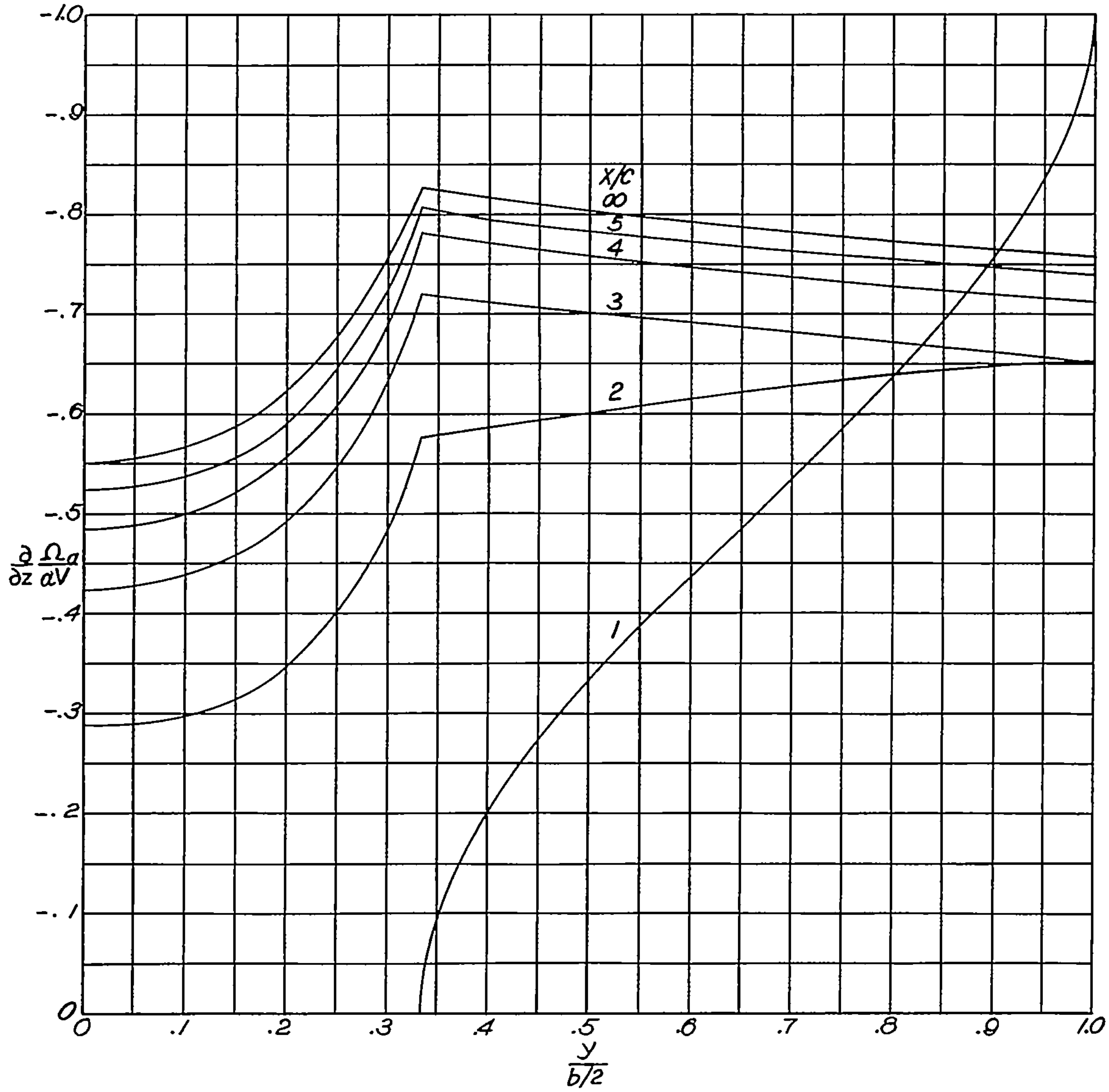

(d) AB = 3.

Figure 11.- Continued.

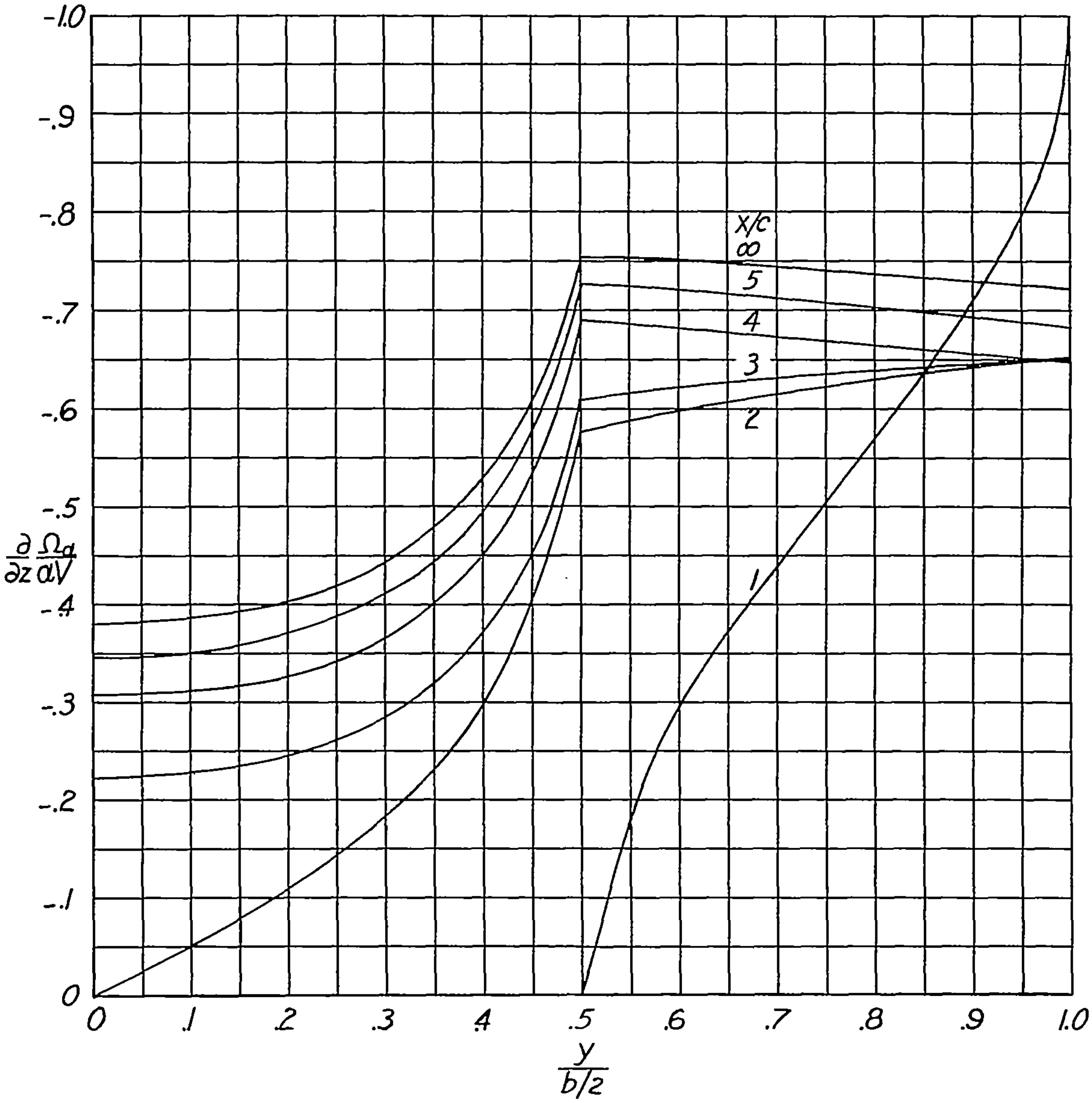

(e) AB = 4.

Figure 11.- Continued.

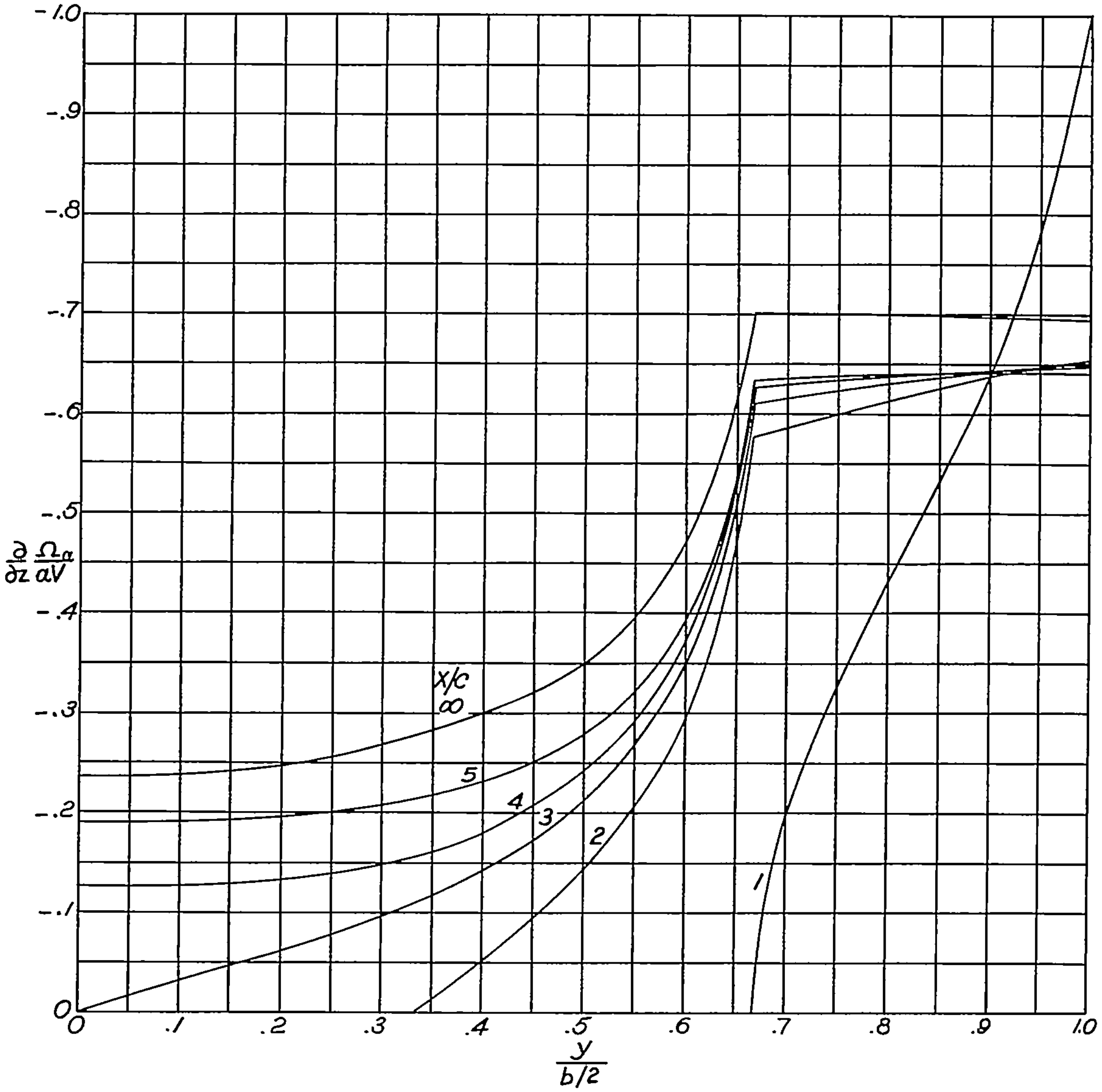

(f) AB = 6.

Figure 11.- Continued.

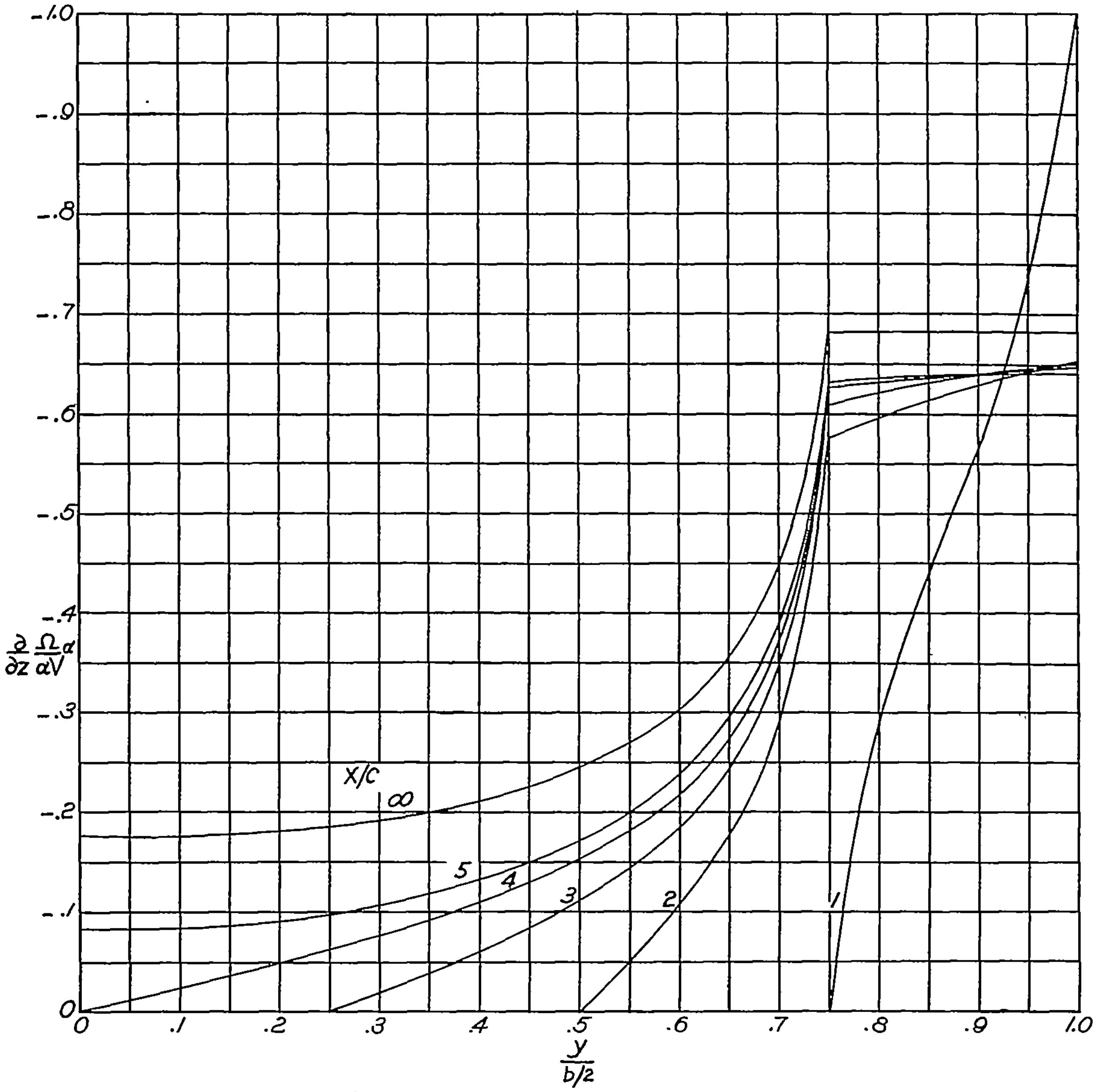

(g) AB = 8.

Figure 11.- Concluded.

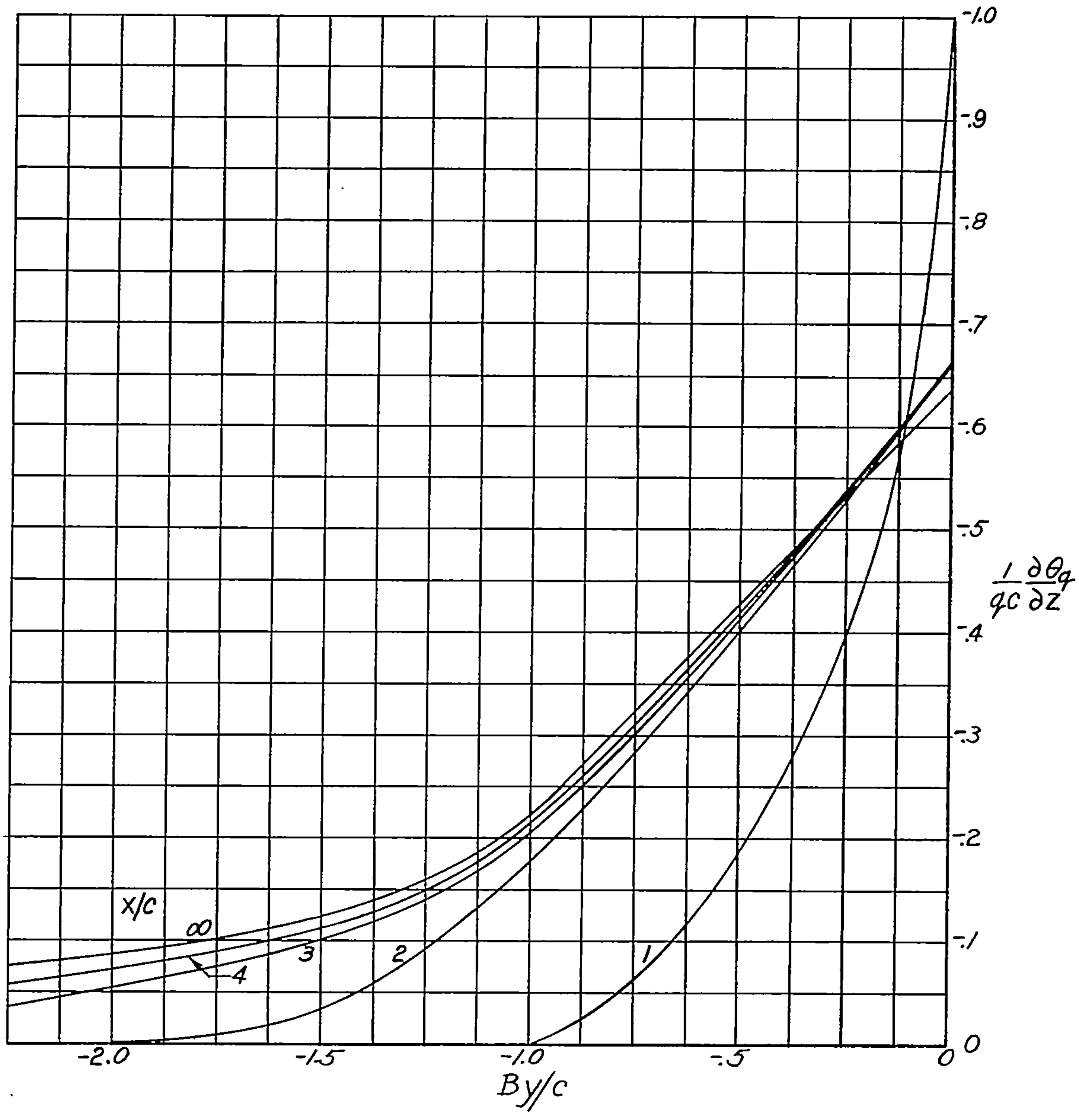

Figure 12.- The variation of the upwash in the plane of the wing behind a semi-infinite rectangular wing pitching about its leading edge (from ref. 15).

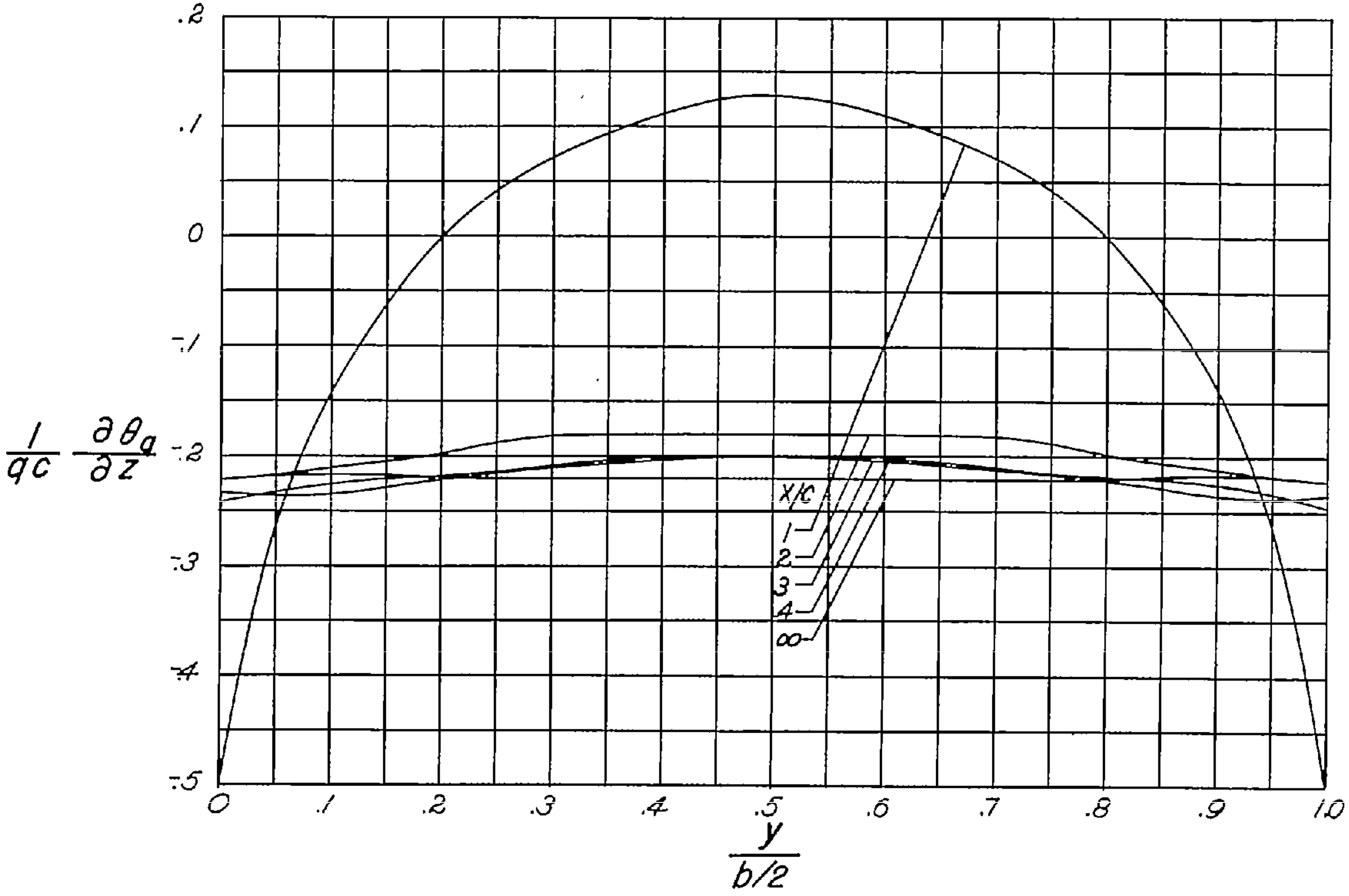

(a) AB = 1.

Figure 13.- Variation of the upwash in the plane of the wing behind a rectangular wing pitching about its midchord point for various values of the parameter AB.

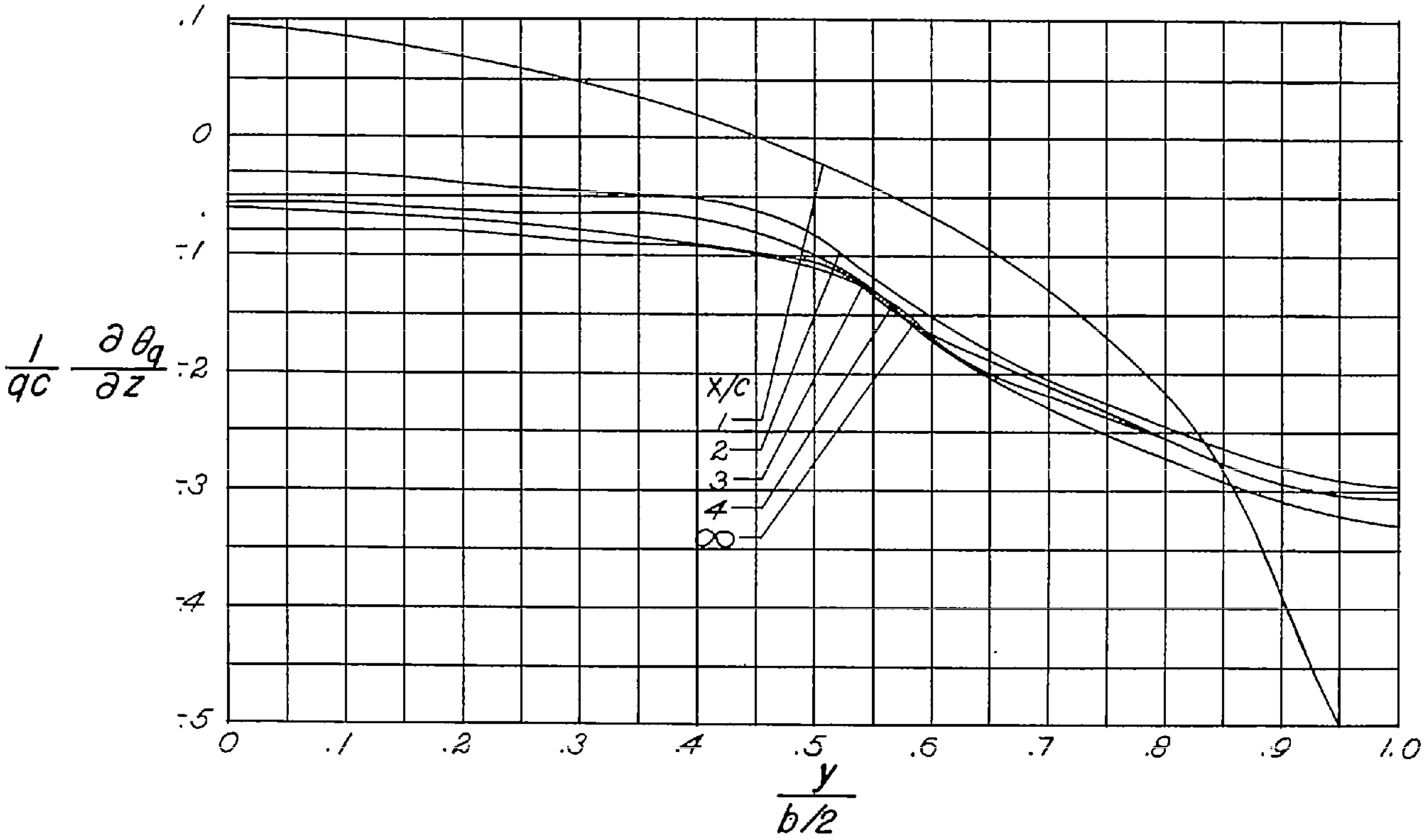

(b) AB = 1.33.

Figure 13.- Continued.

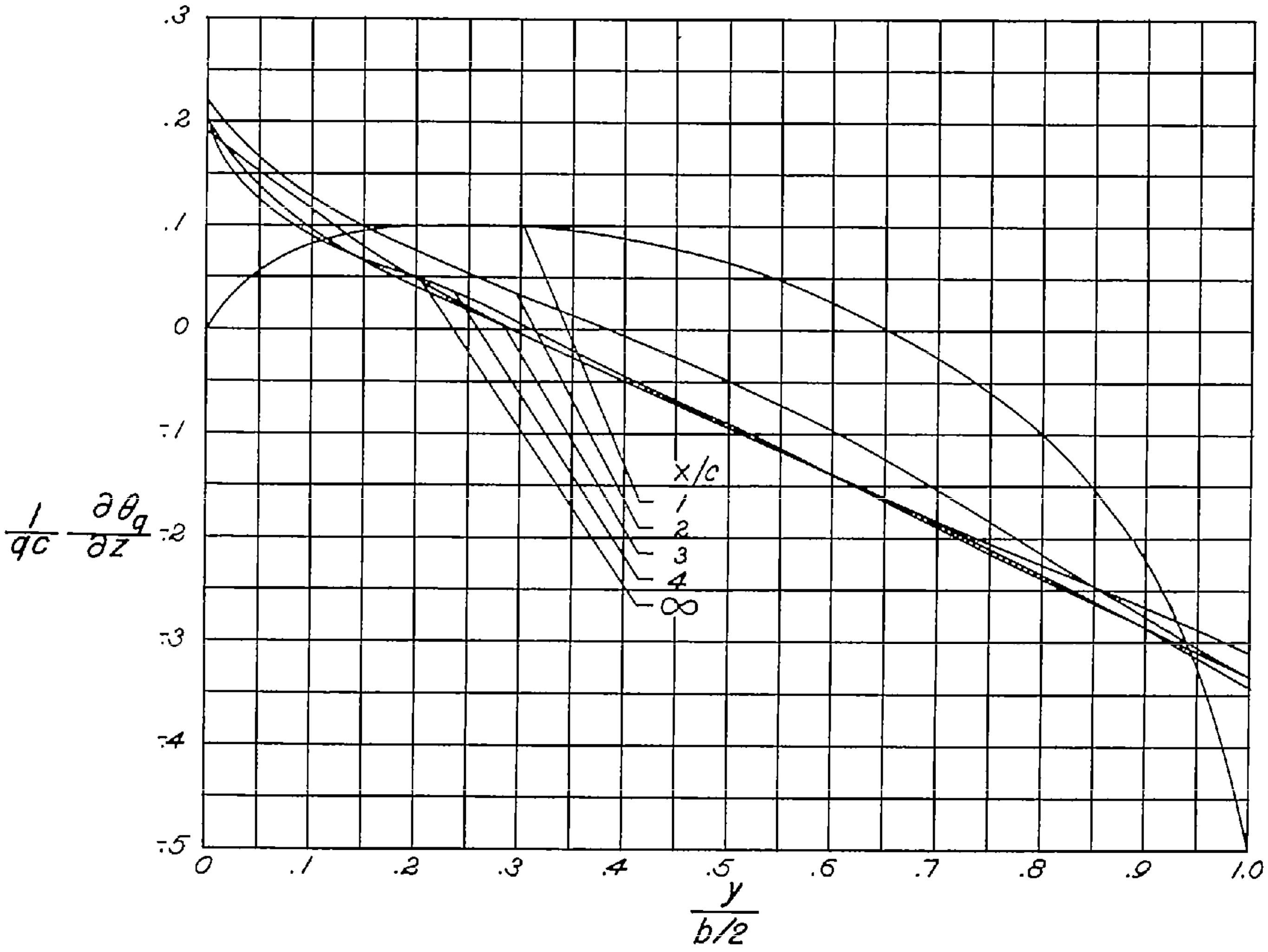

(c) AB = 2.

Figure 13.- Continued.

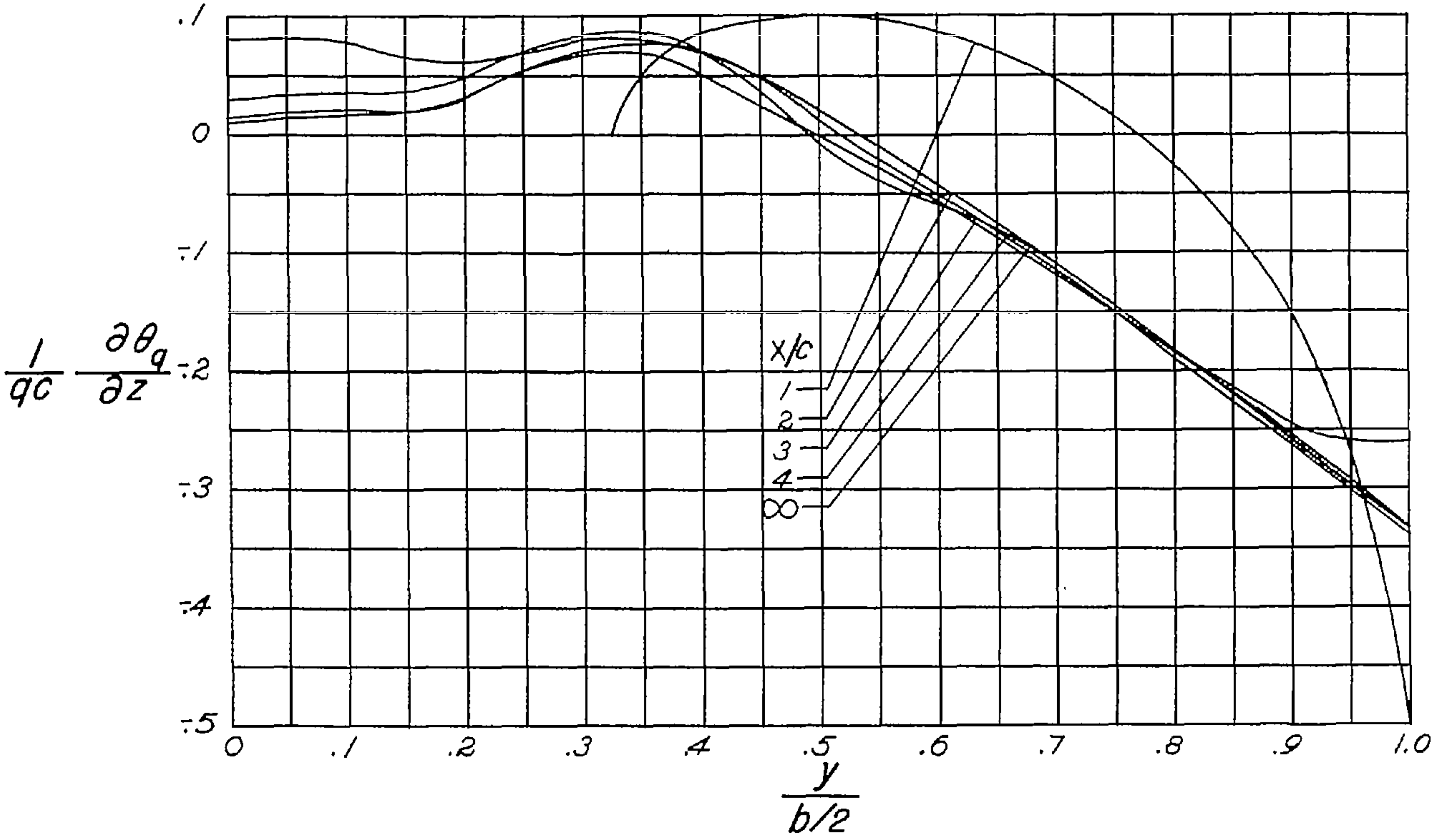

(d) AB = 3.

Figure 13.- Continued.

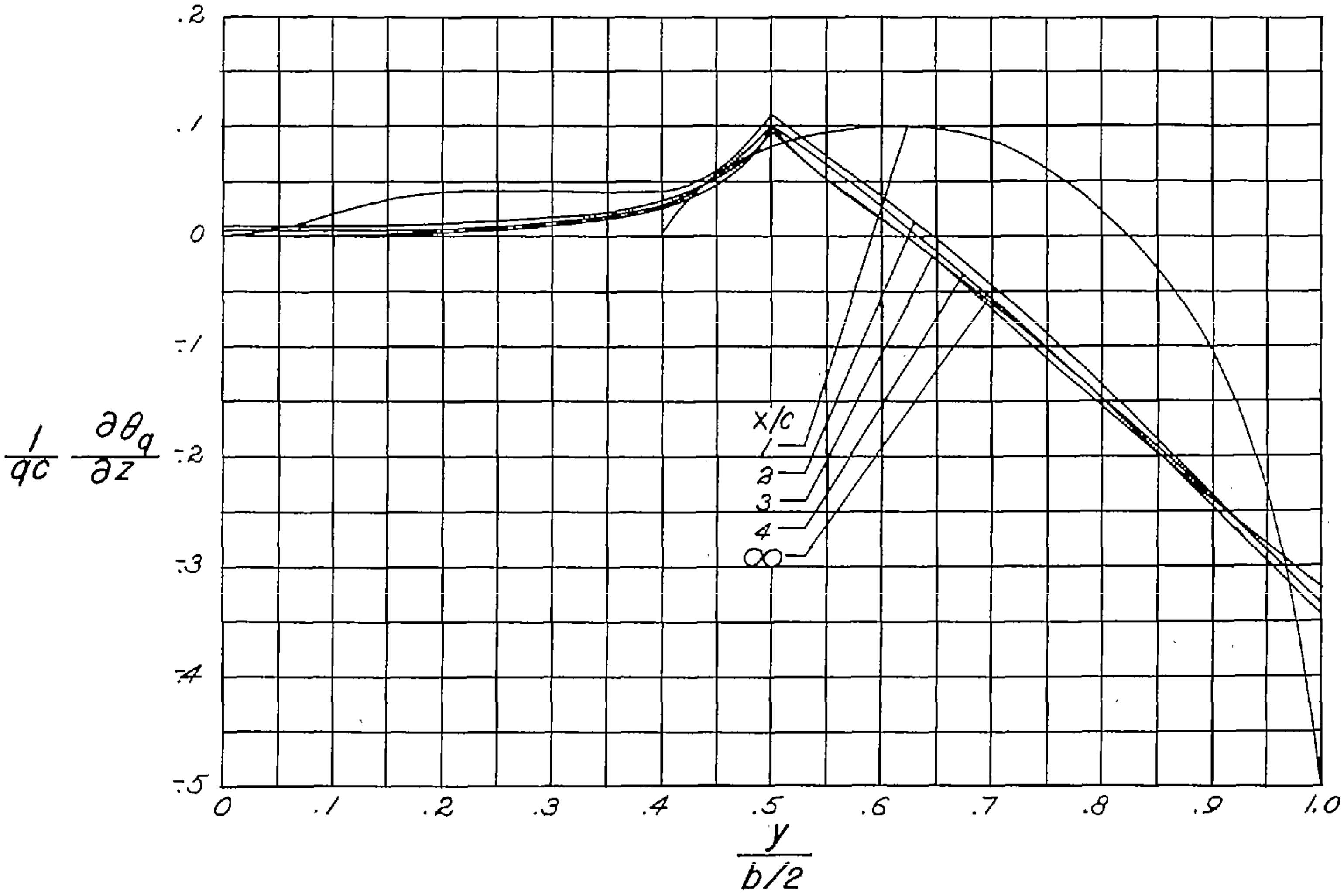

(e) AB = 4.

Figure 13.- Continued.

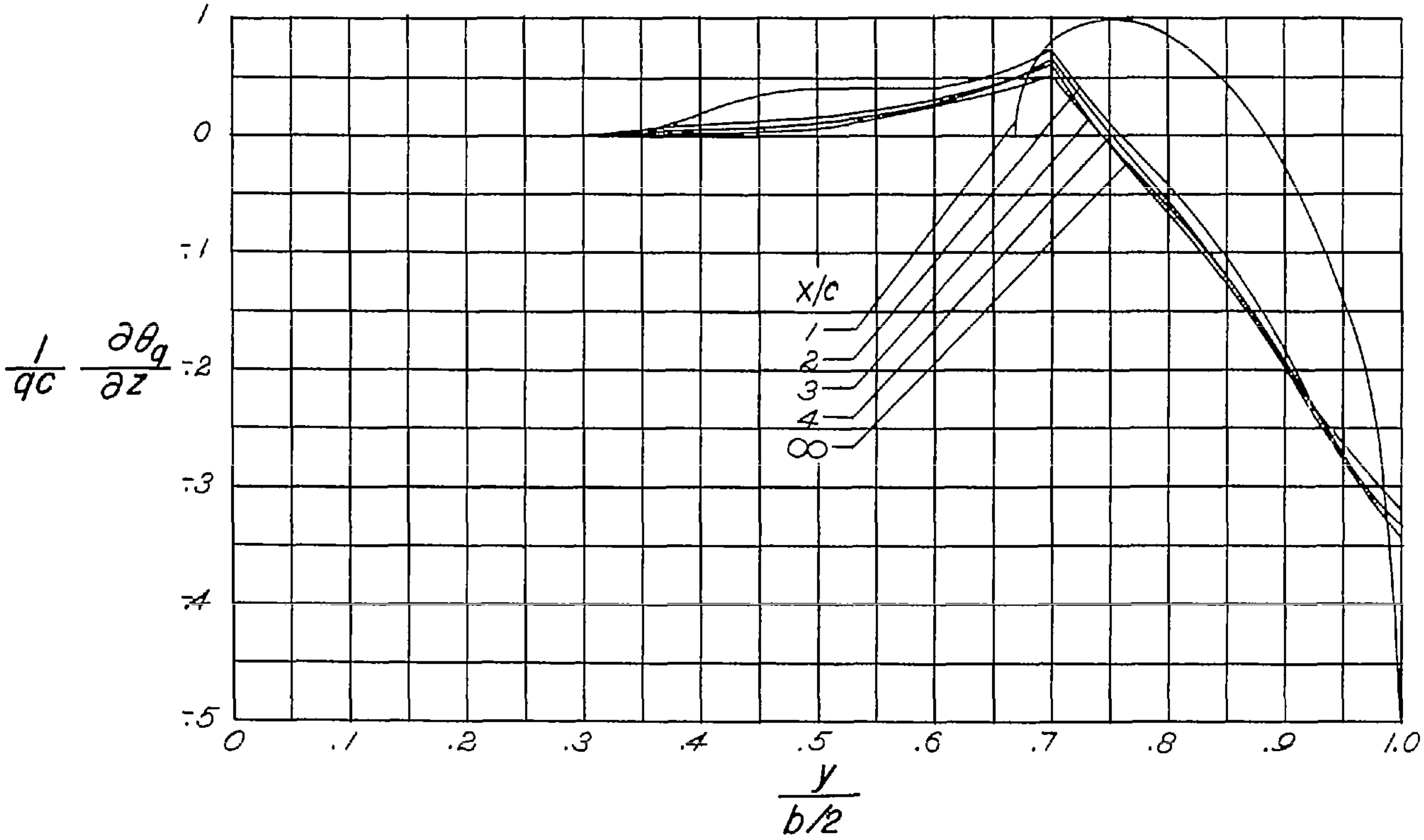

(f) AR = 6.

Figure 13.- Continued.

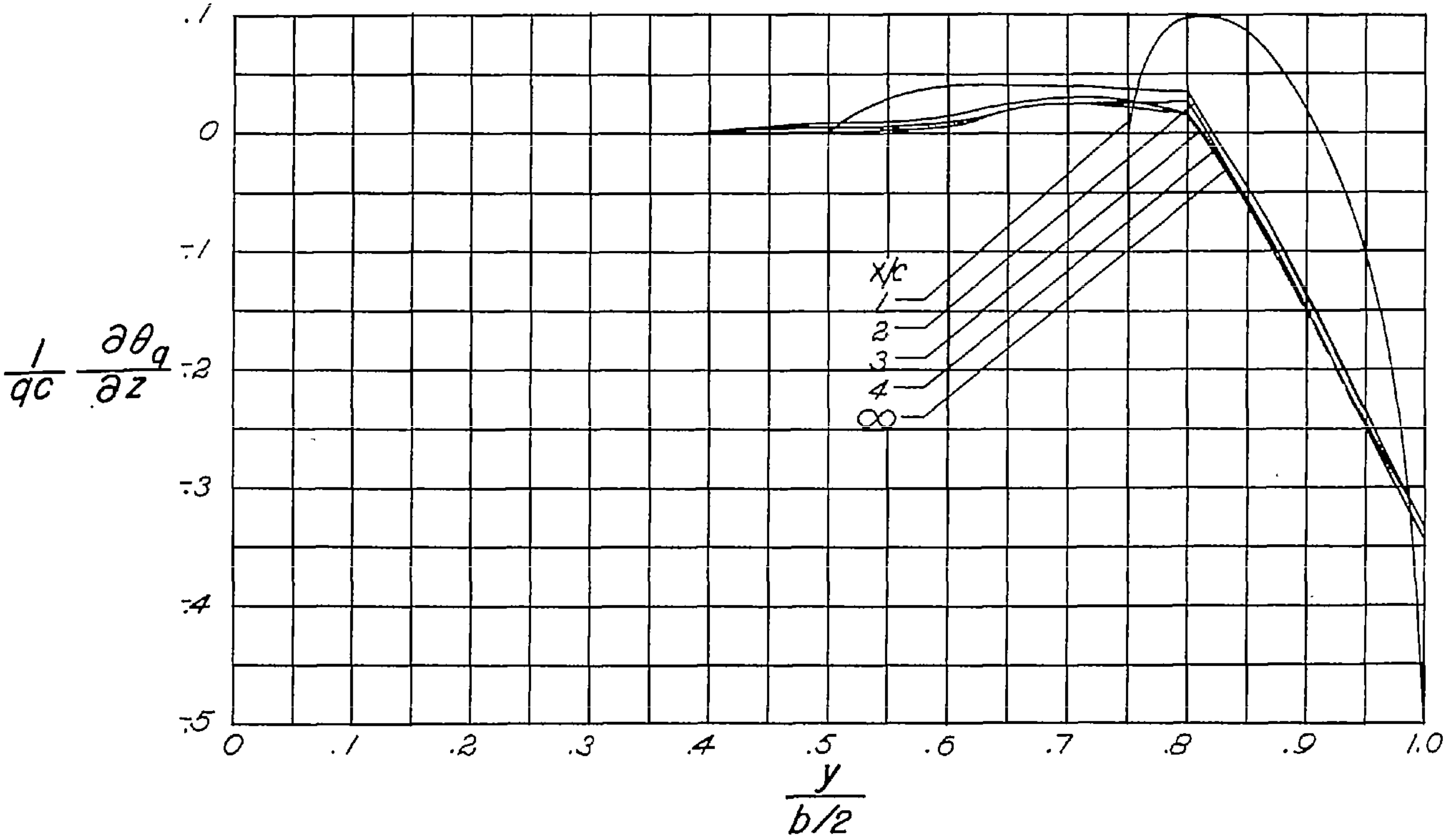

(g) AB = 8.

Figure 13.- Concluded.

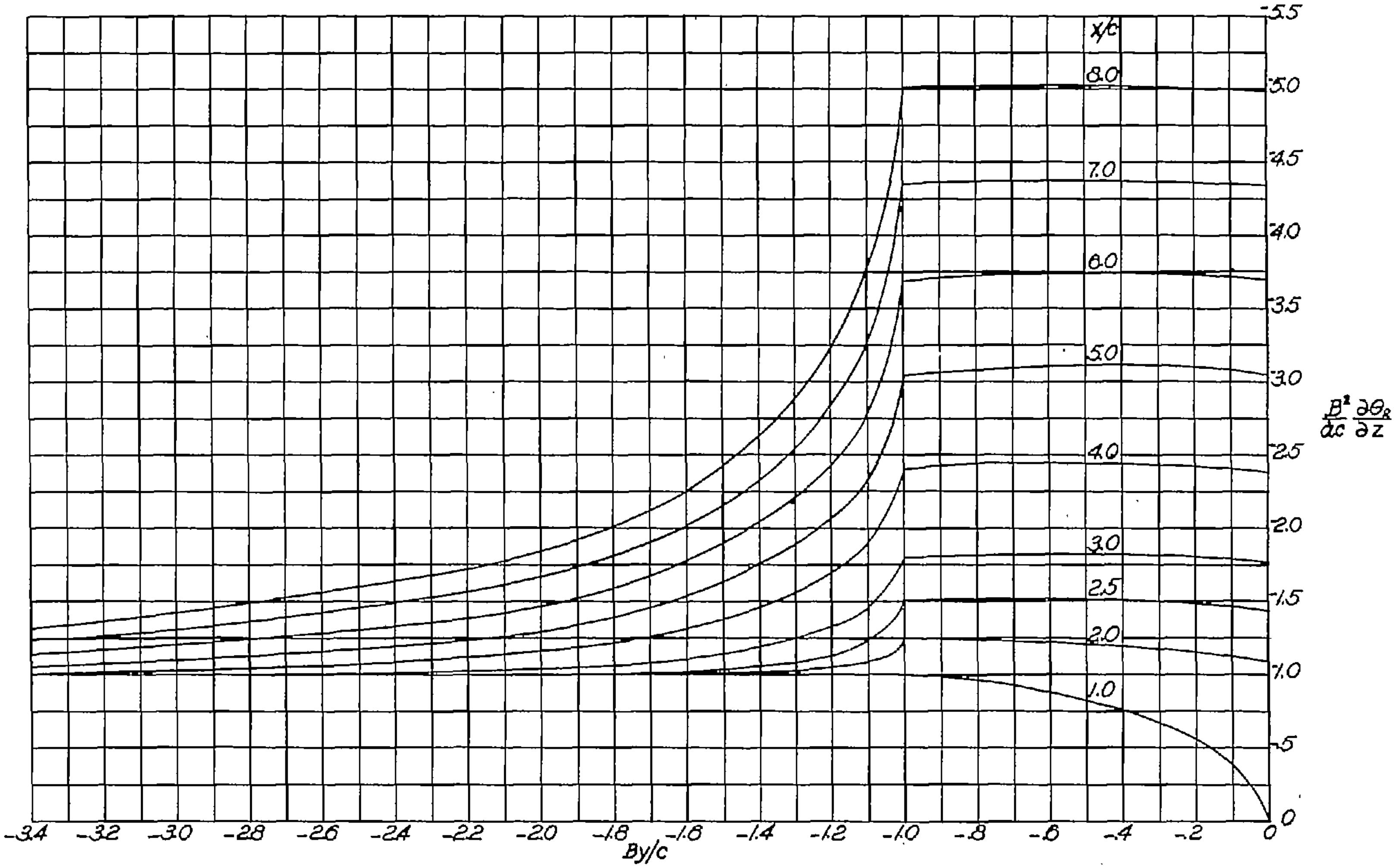

Figure 14.- The variation of the upwash component $\frac{B^2}{dc}\frac{\partial\theta_2}{\partial z}$ in the plane of the wing behind a semi-infinite rectangular wing.

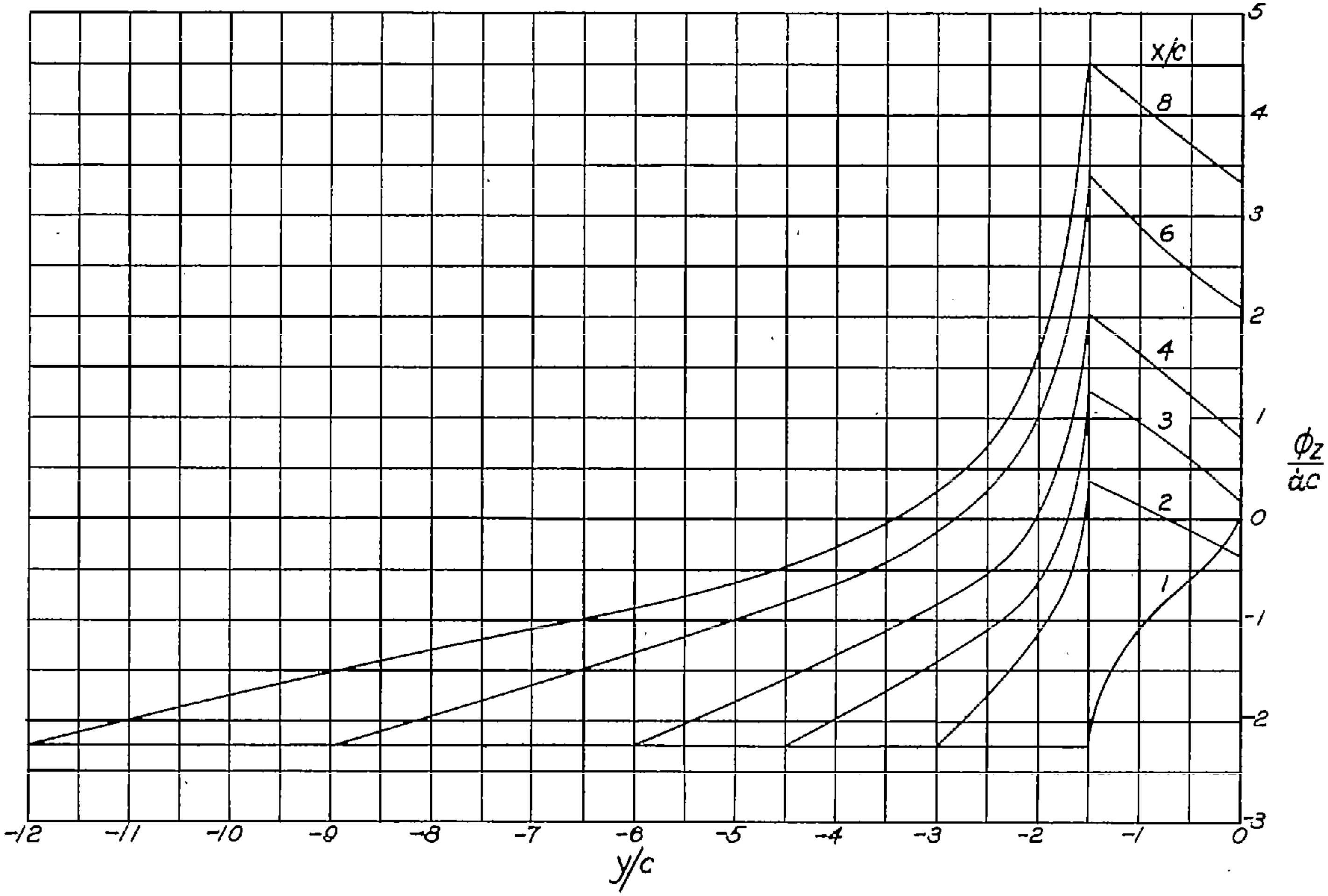

(a) M = 1.20.

Figure 15.- The variation of the upwash at $t = t_o$ in the plane of the wing behind a semi-infinite rectangular wing with a constant vertical acceleration for various Mach numbers.

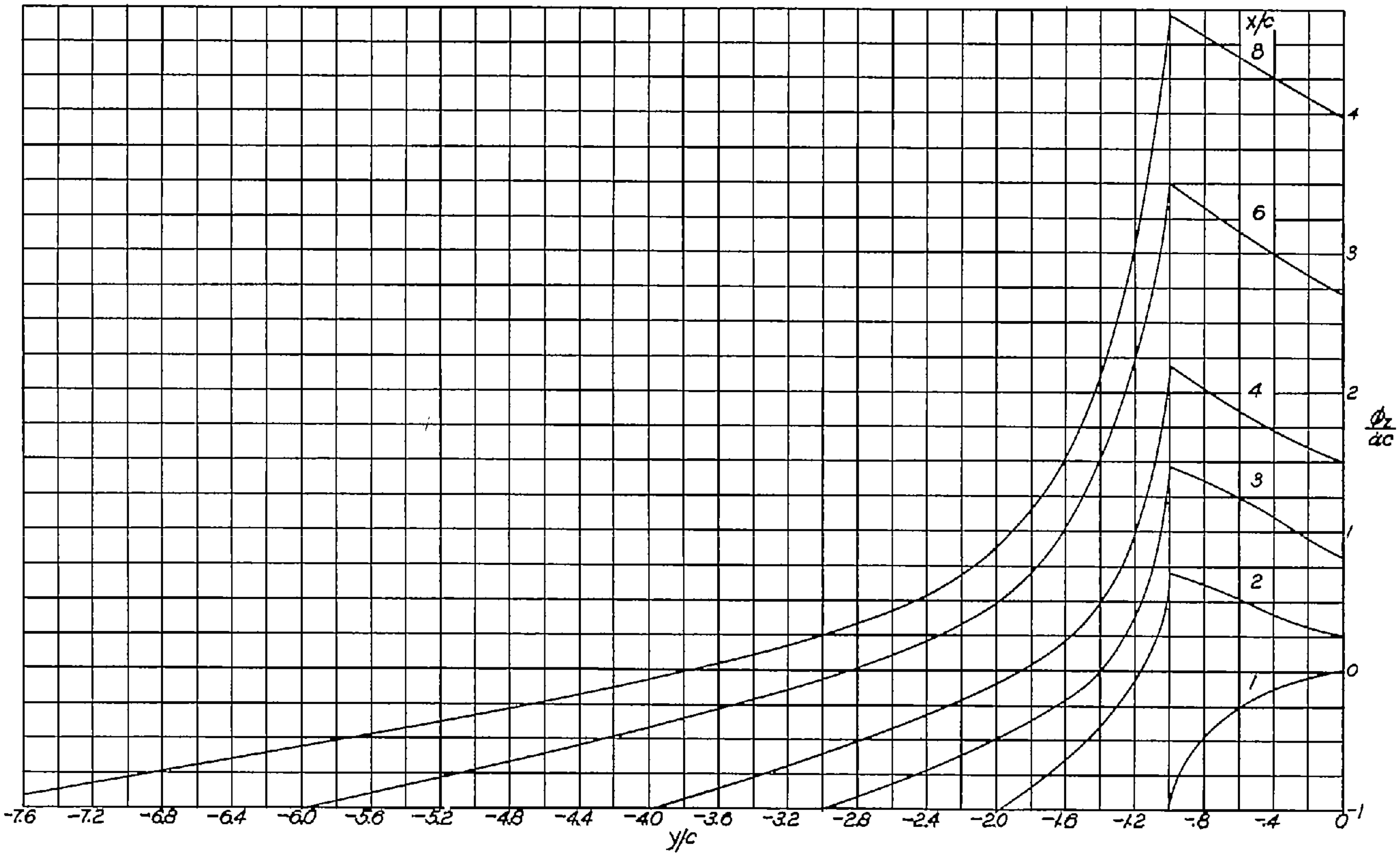

(b) M = 1.414.

Figure 15.- Continued.

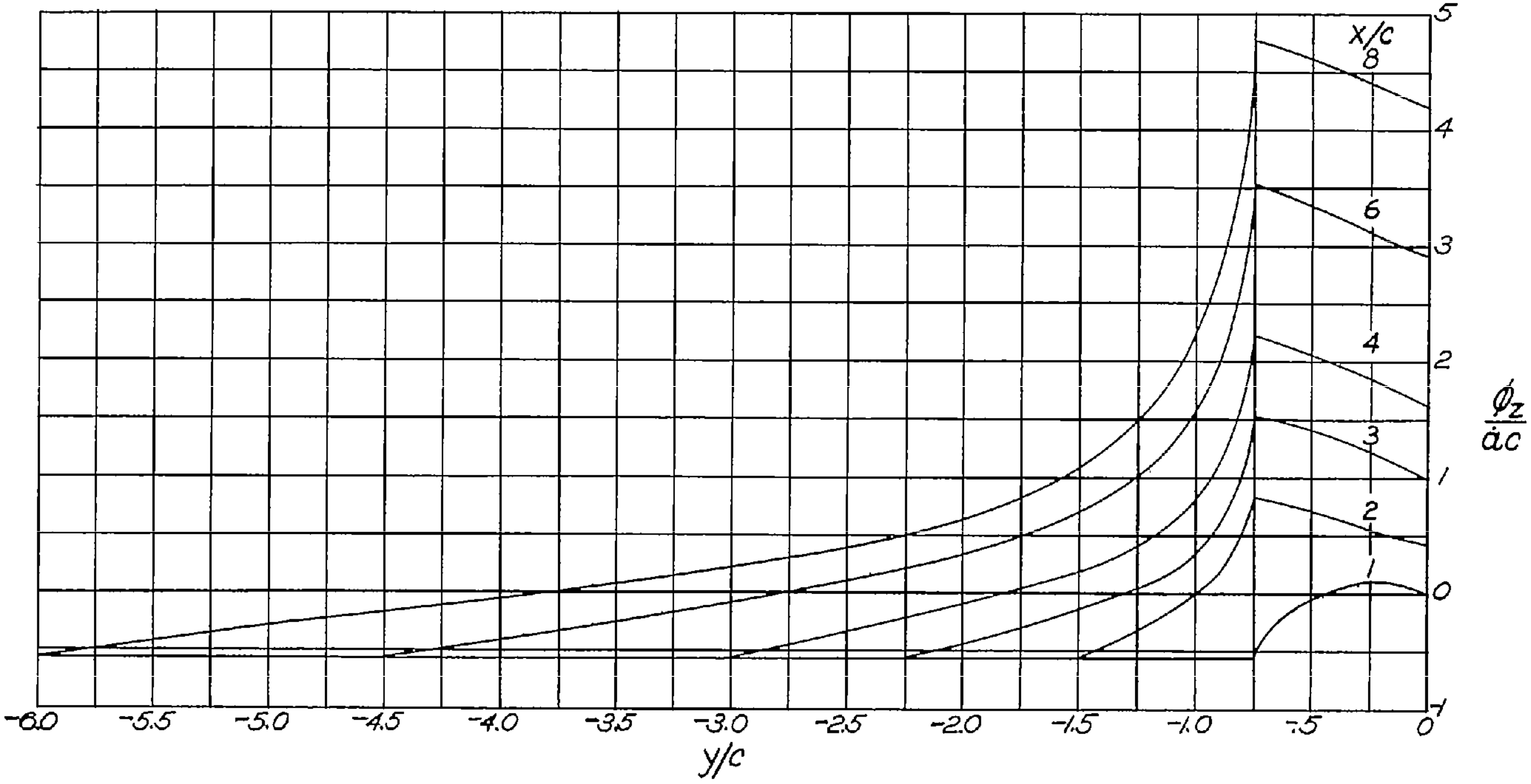

(c) M = 1.667.

Figure 15.- Continued.

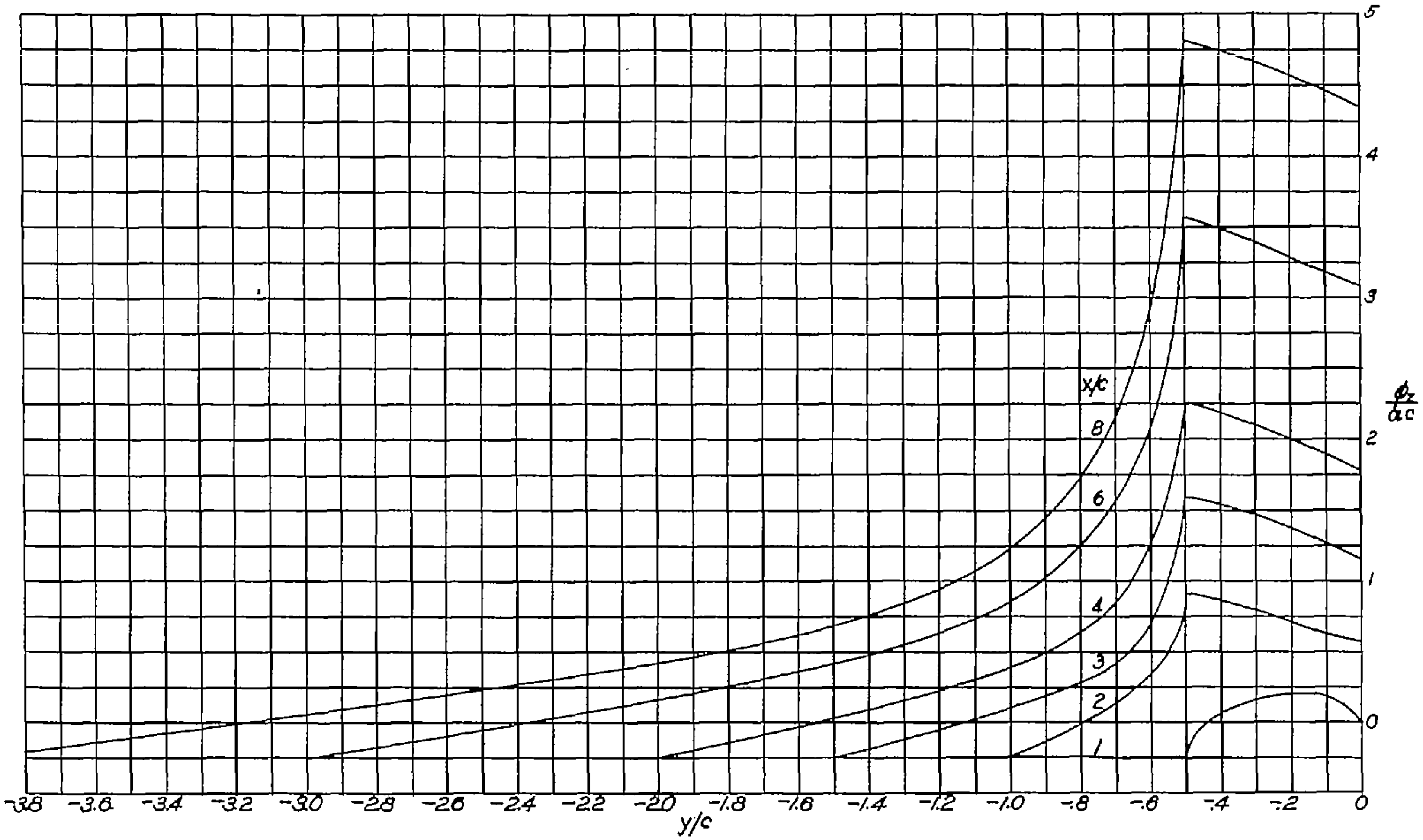

(d) M = 2.24.

Figure 15.- Concluded.

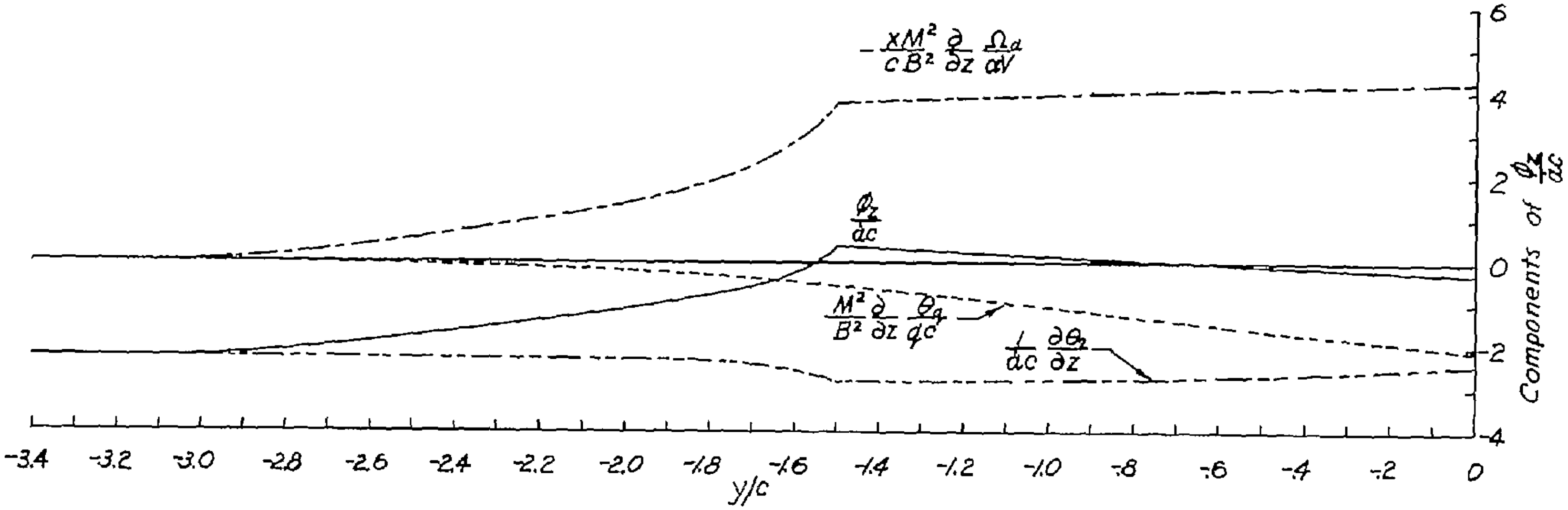

(a) x = 2c; M = 1.20.

Figure 16.- The contribution of each component of upwash in the plane of the wing at $t = t_0$ for a semi-infinite rectangular wing with a constant vertical acceleration.

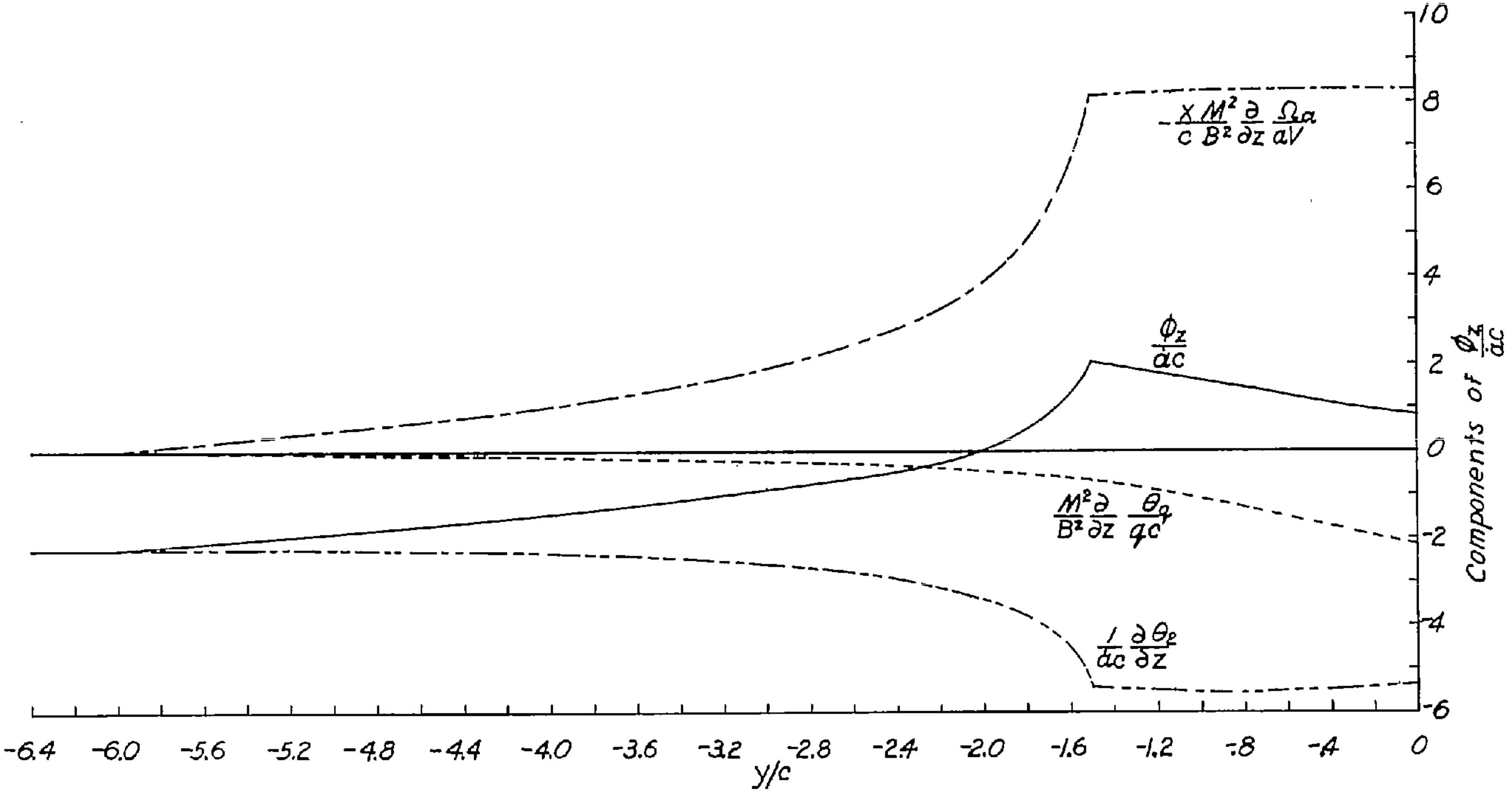

(b) x = 4c; M = 1.20.

Figure 16.- Continued.

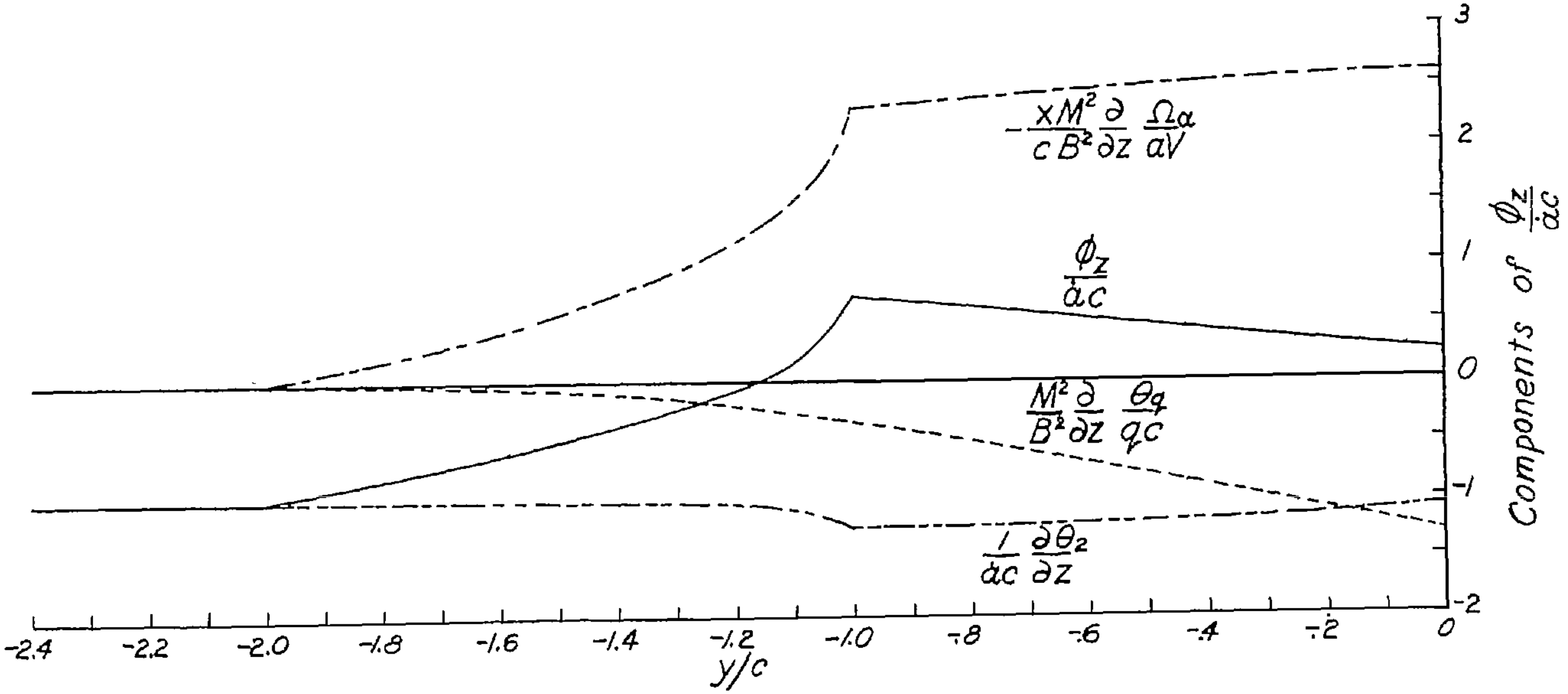

(c) x = 2c; M = 1.414.

Figure 16.- Continued.

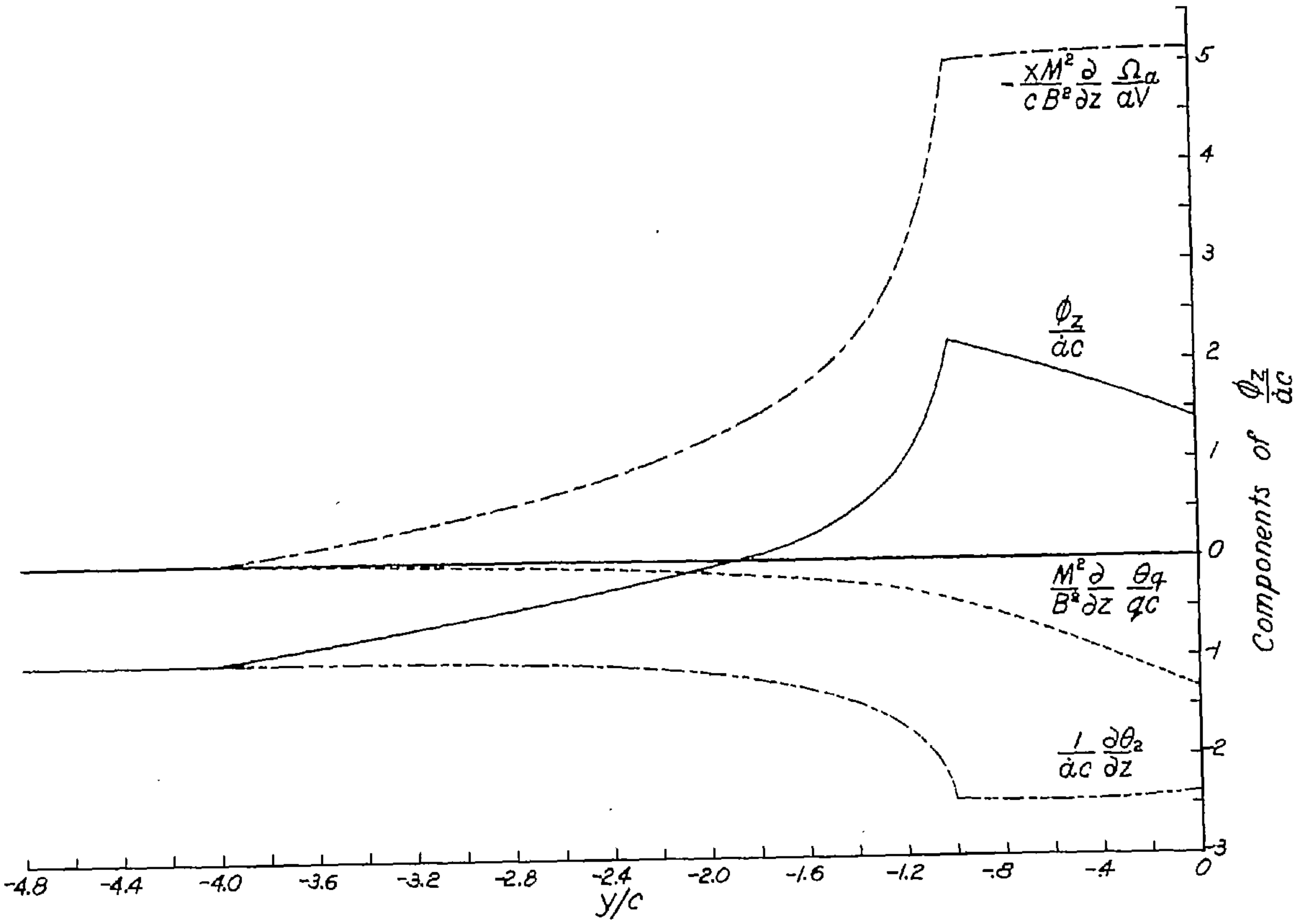

(d) x = 4c; M = 1.414.

Figure 16.- Continued.

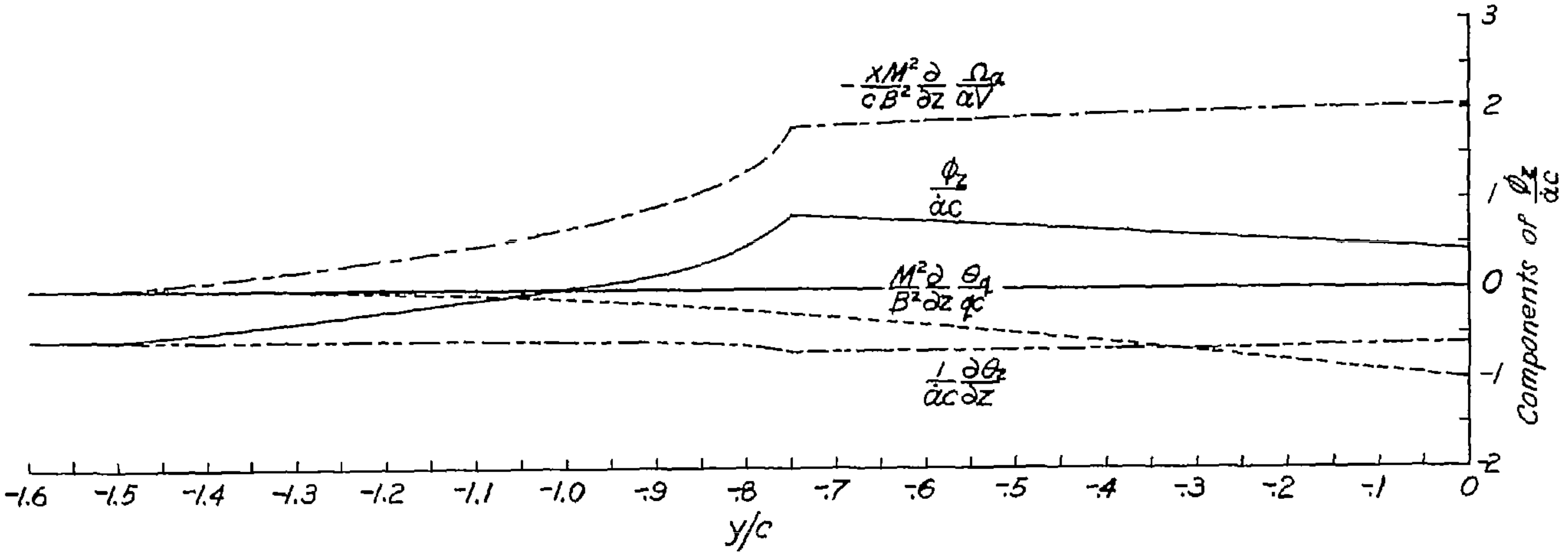

(e) x = 2c; M = 1.667.

Figure 16.- Continued.

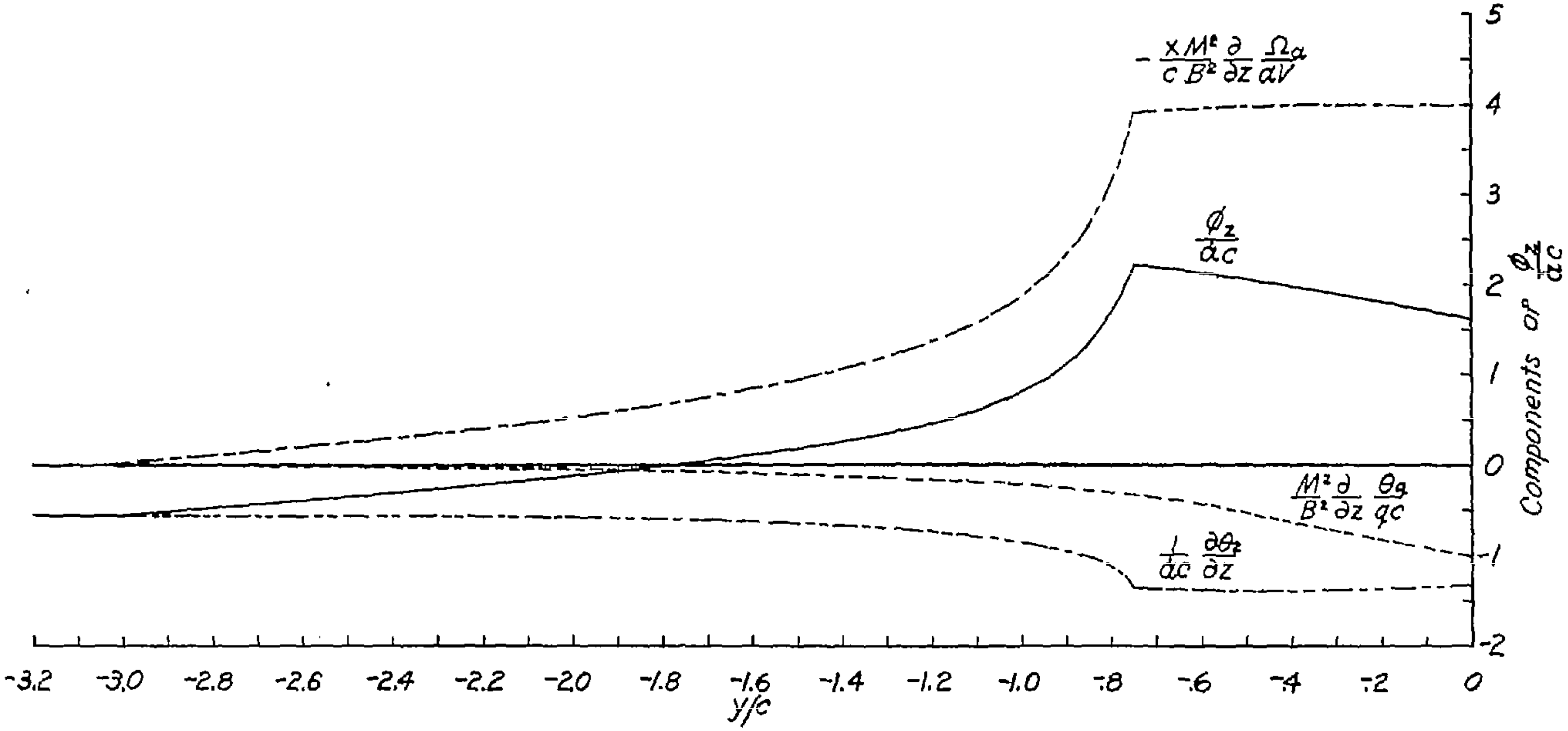

(f) x = 4c; M = 1.667.

Figure 16.- Continued.

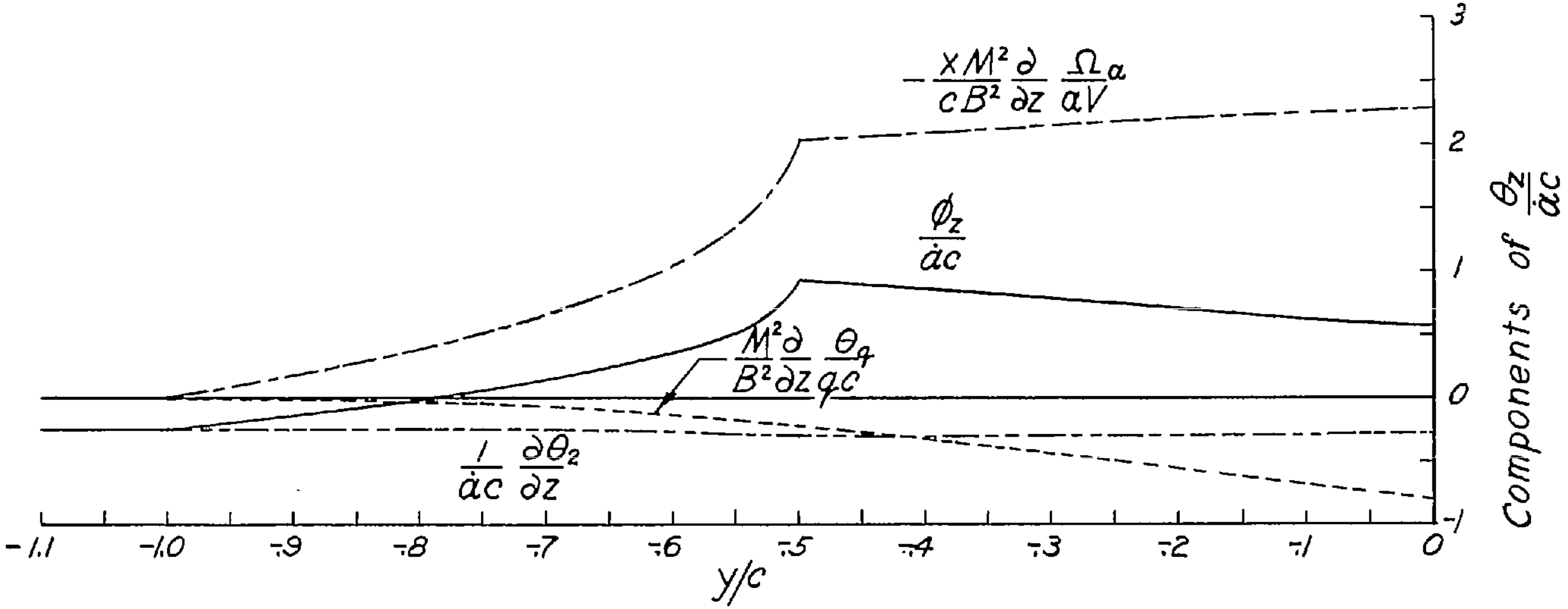

(g) x = 2c; M = 2.24.

Figure 16.- Continued.

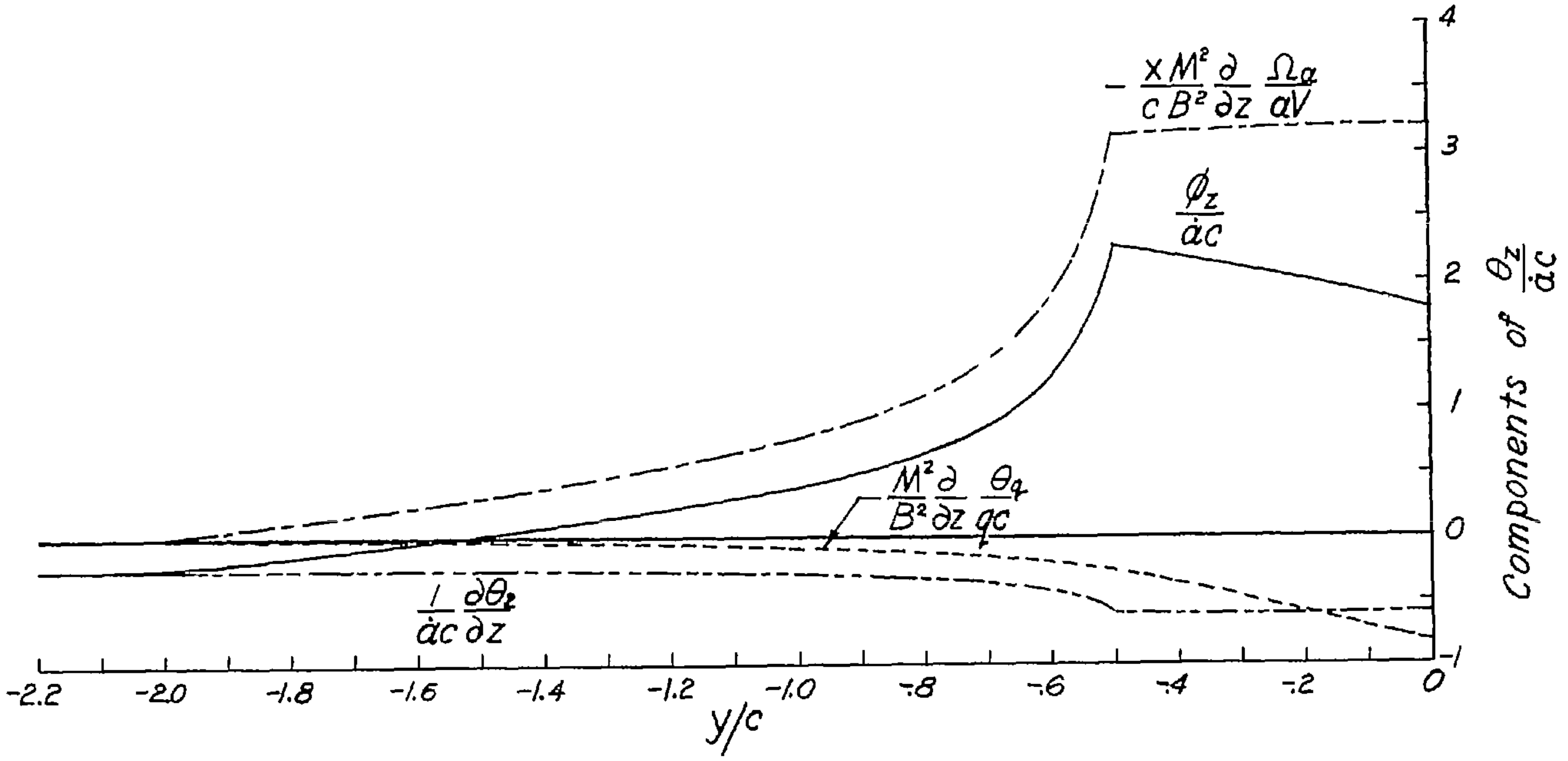

(h) x = 4c; M = 2.24.

Figure 16.- Concluded.

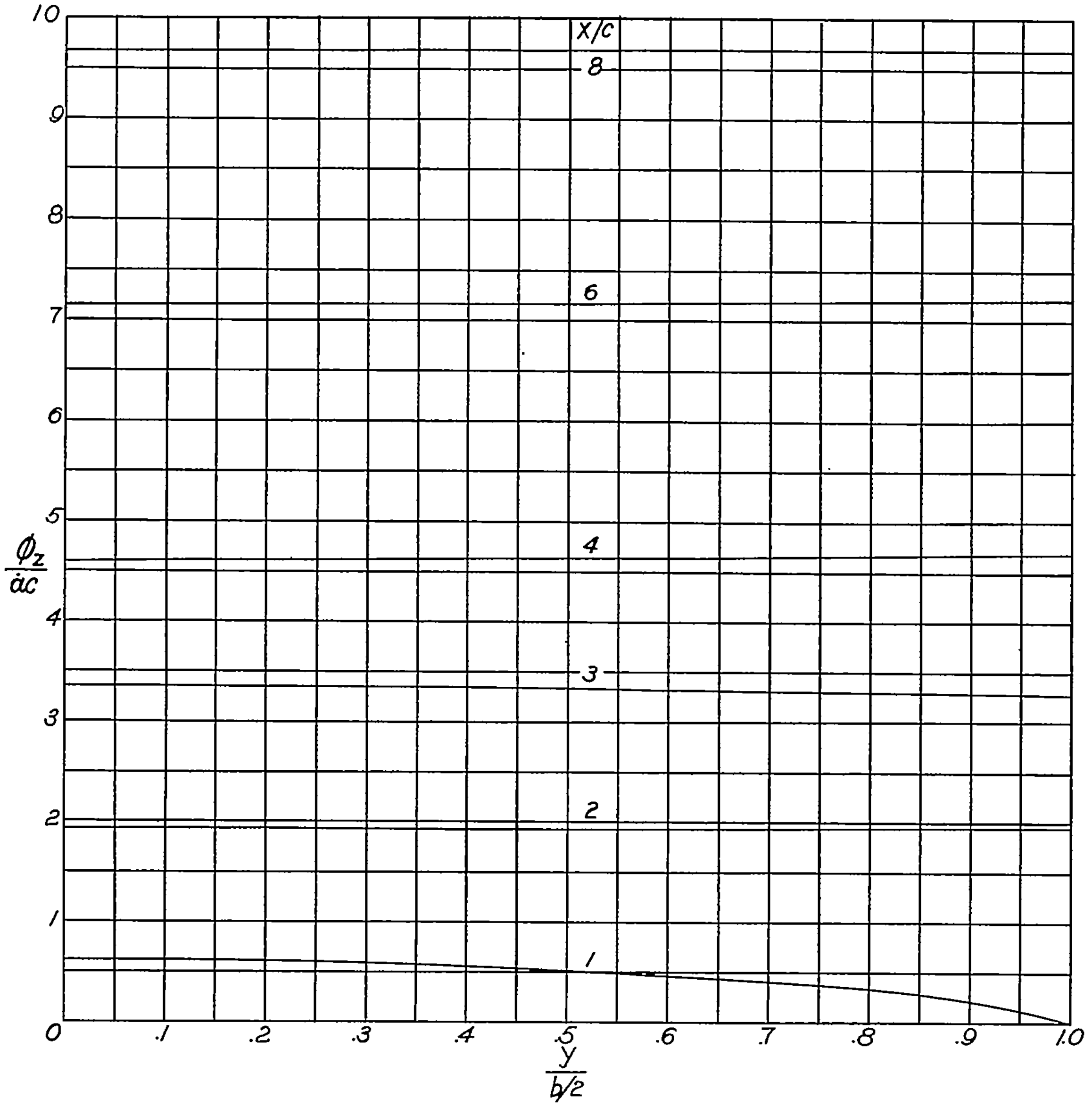

(a) $M = 1.414$.

Figure 17.- The upwash distribution at $t = t_o$ in the plane of the wing behind a rectangular wing with a constant vertical acceleration with $A = 1$ for various Mach numbers.

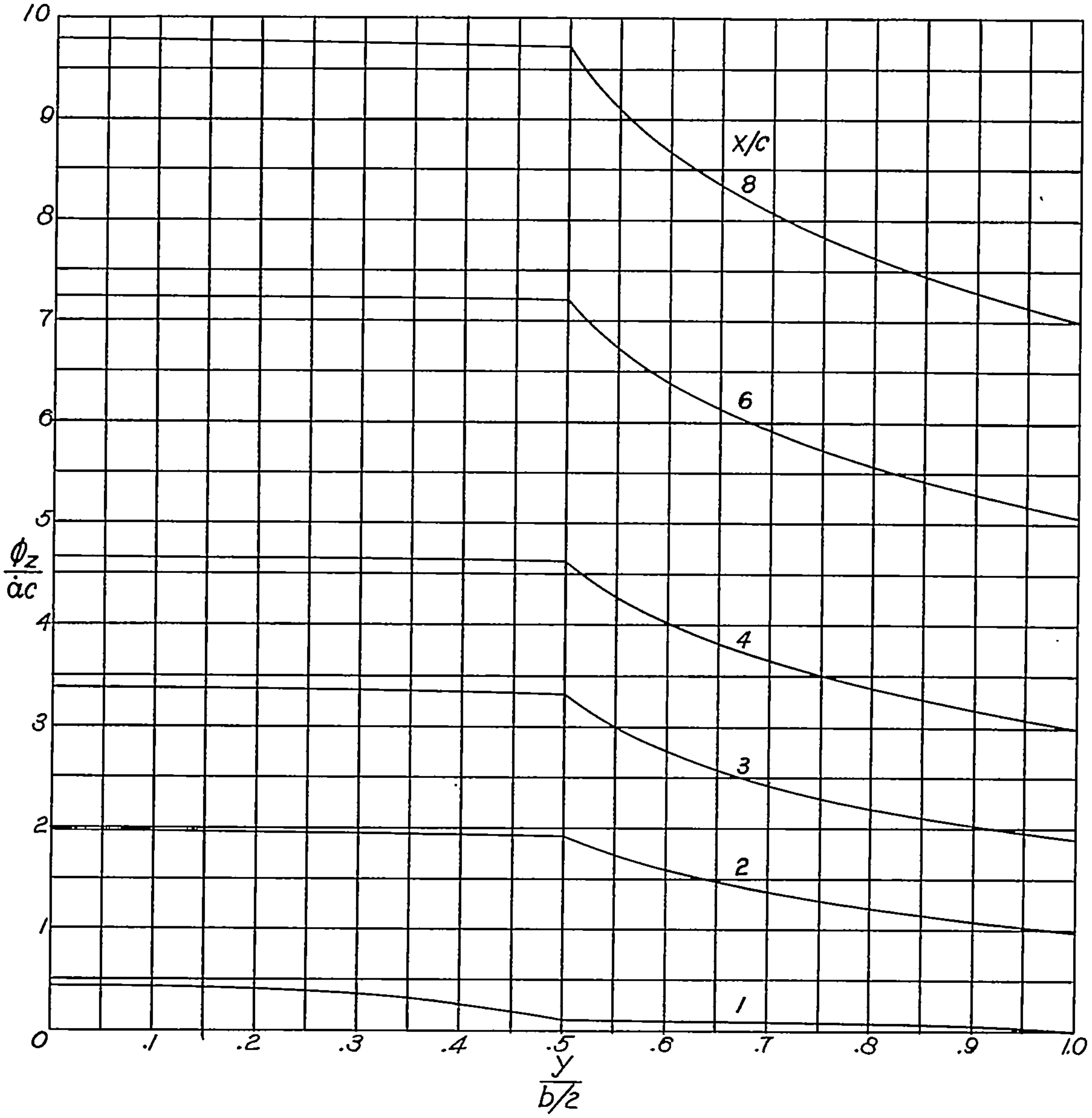

(b) M = 1.667.

Figure 17.- Continued.

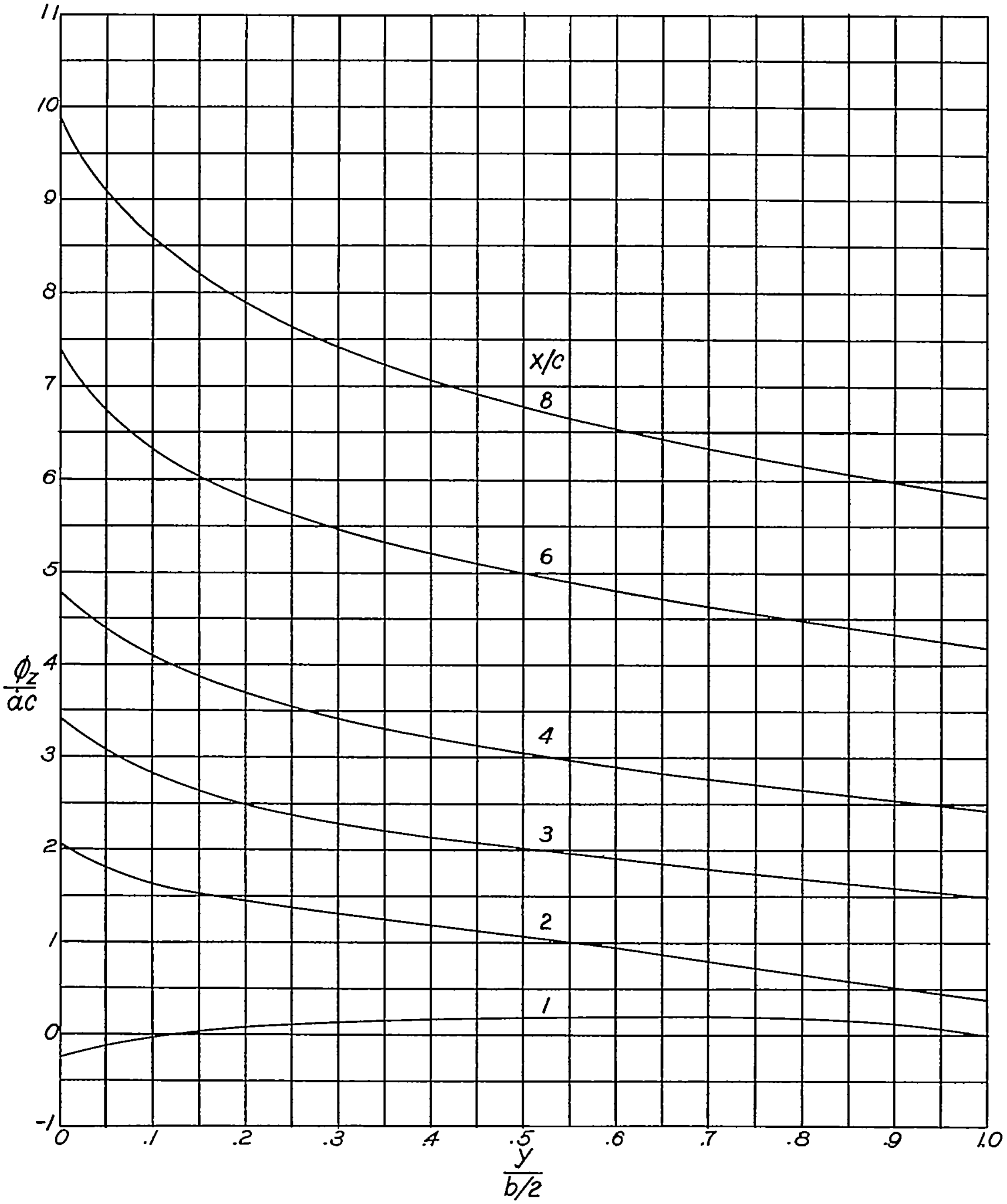

(c) M = 2.24.

Figure 17.- Concluded.

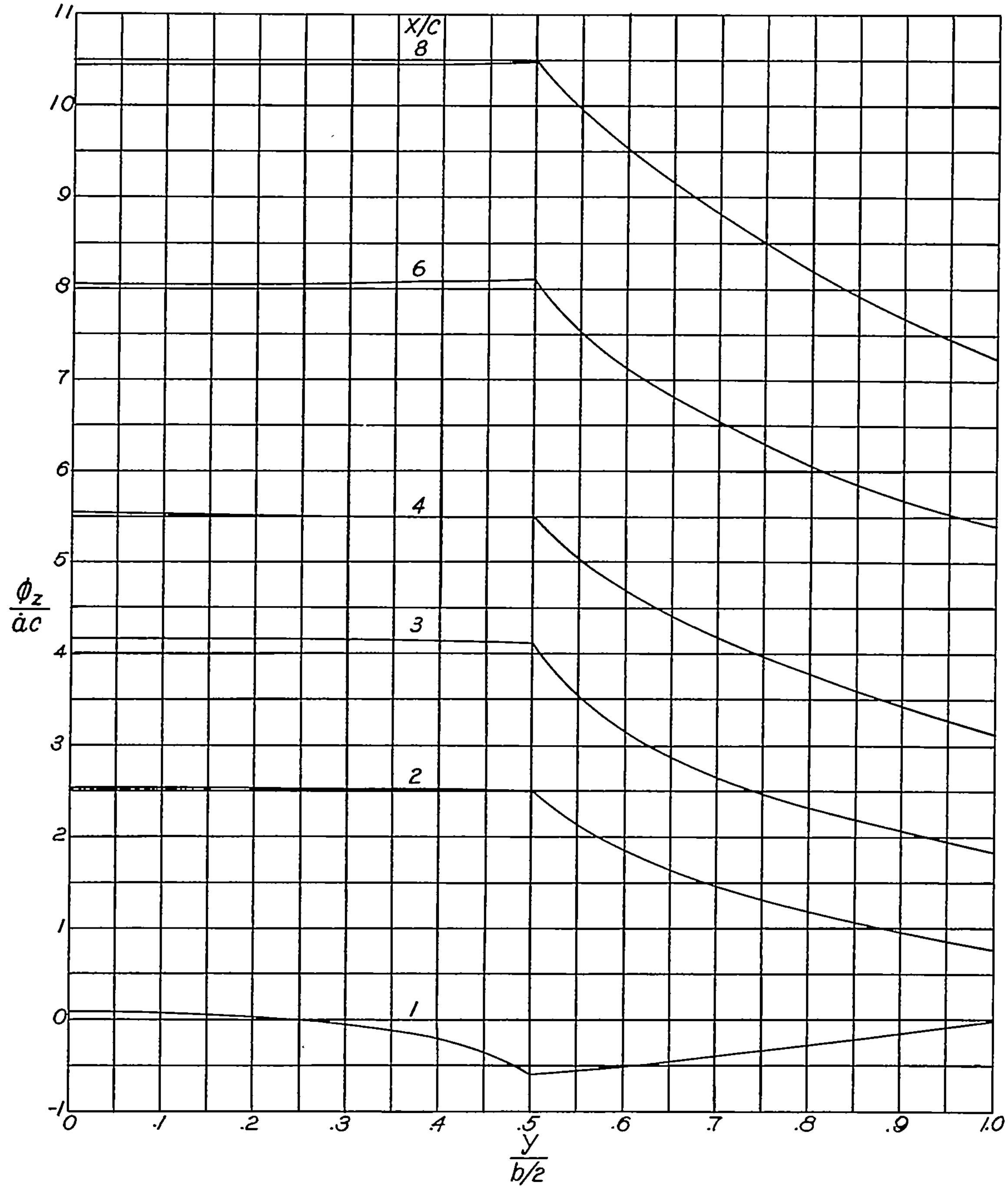

(a) M = 1.20.

Figure 18.- The upwash distribution at $t = t_o$ in the plane of the wing behind a rectangular wing with a constant vertical acceleration with $A = 2$ for various Mach numbers.

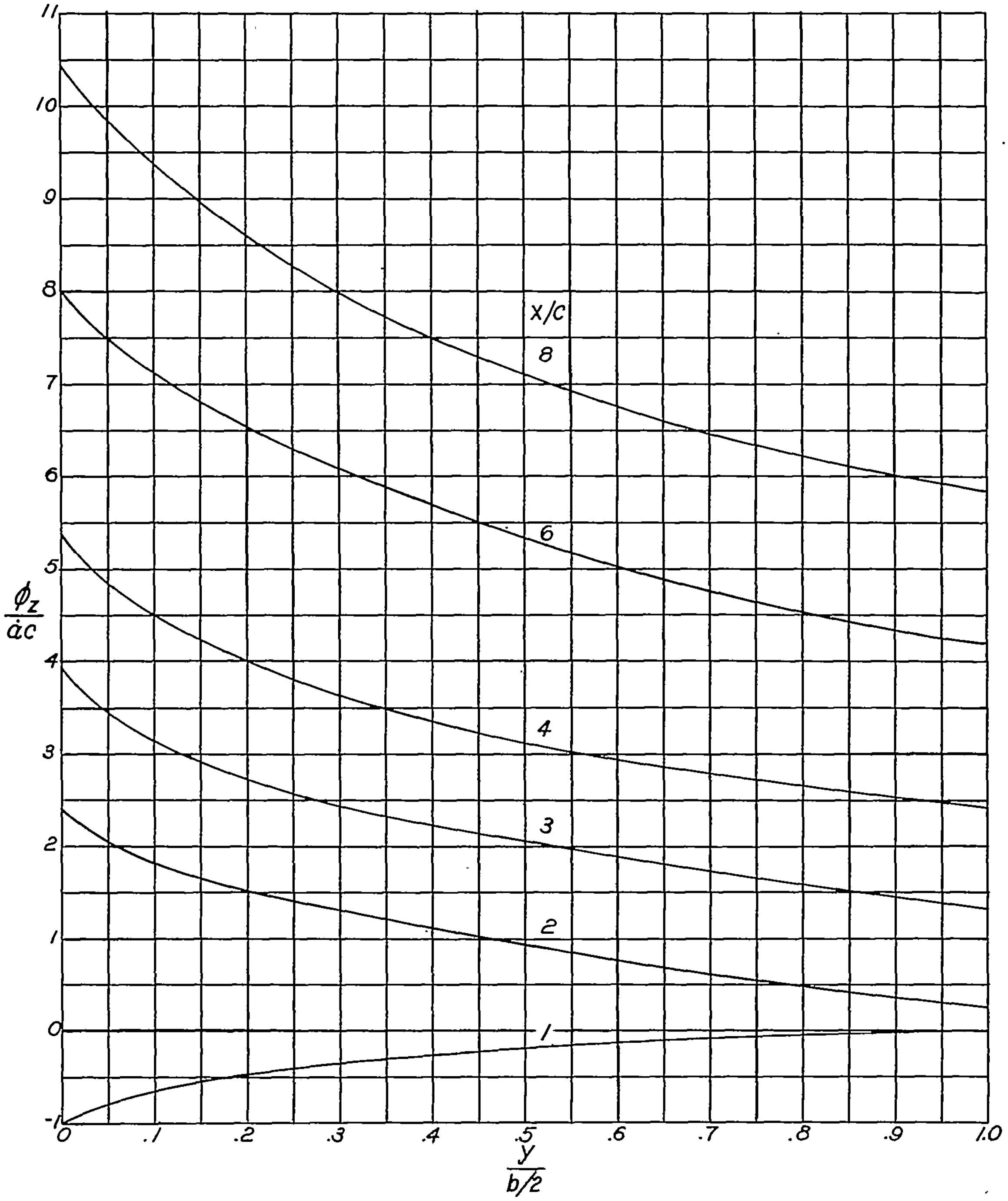

(b) M = 1.414.

Figure 18.- Continued.

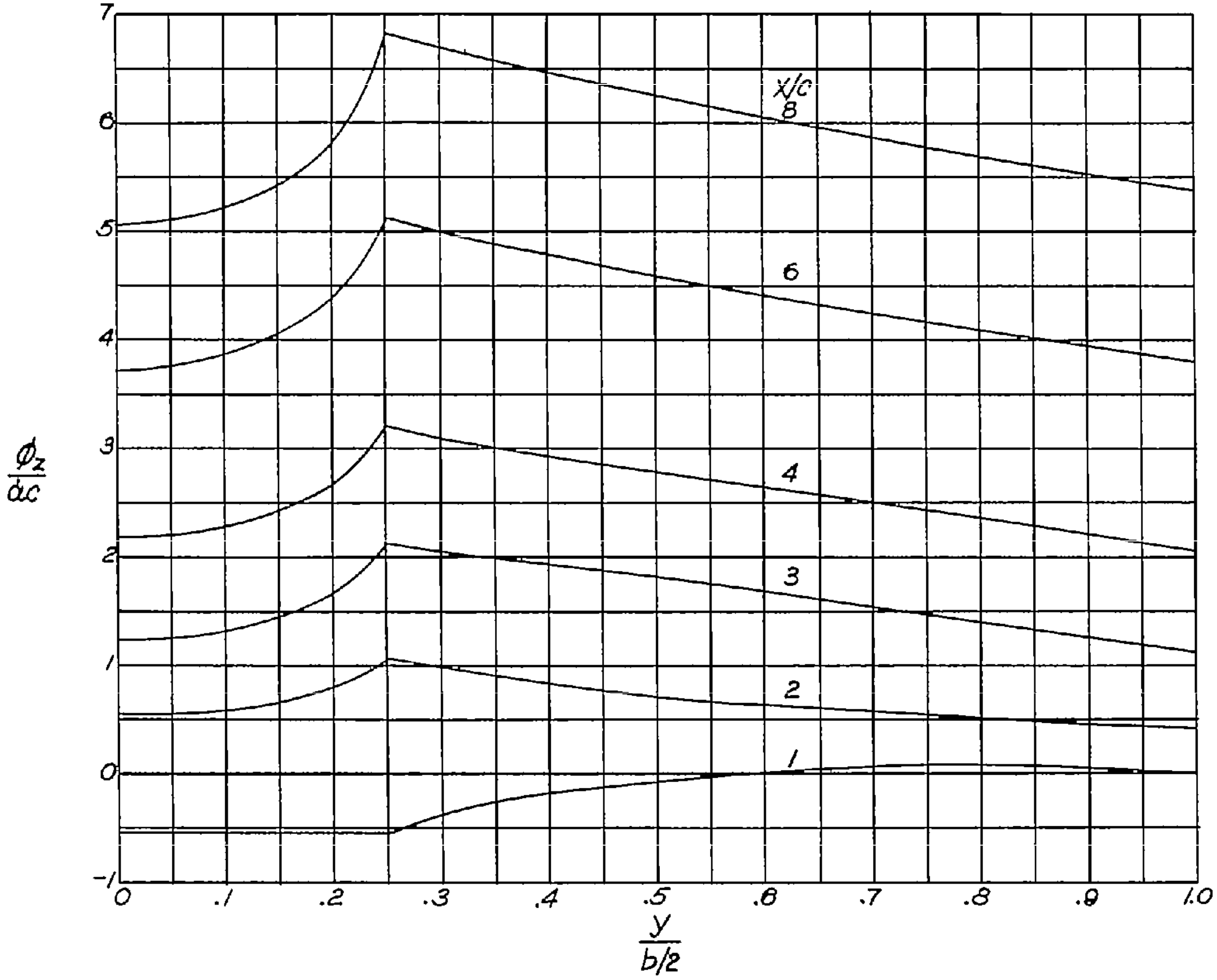

(c) M = 1.667.

Figure 18.- Continued.

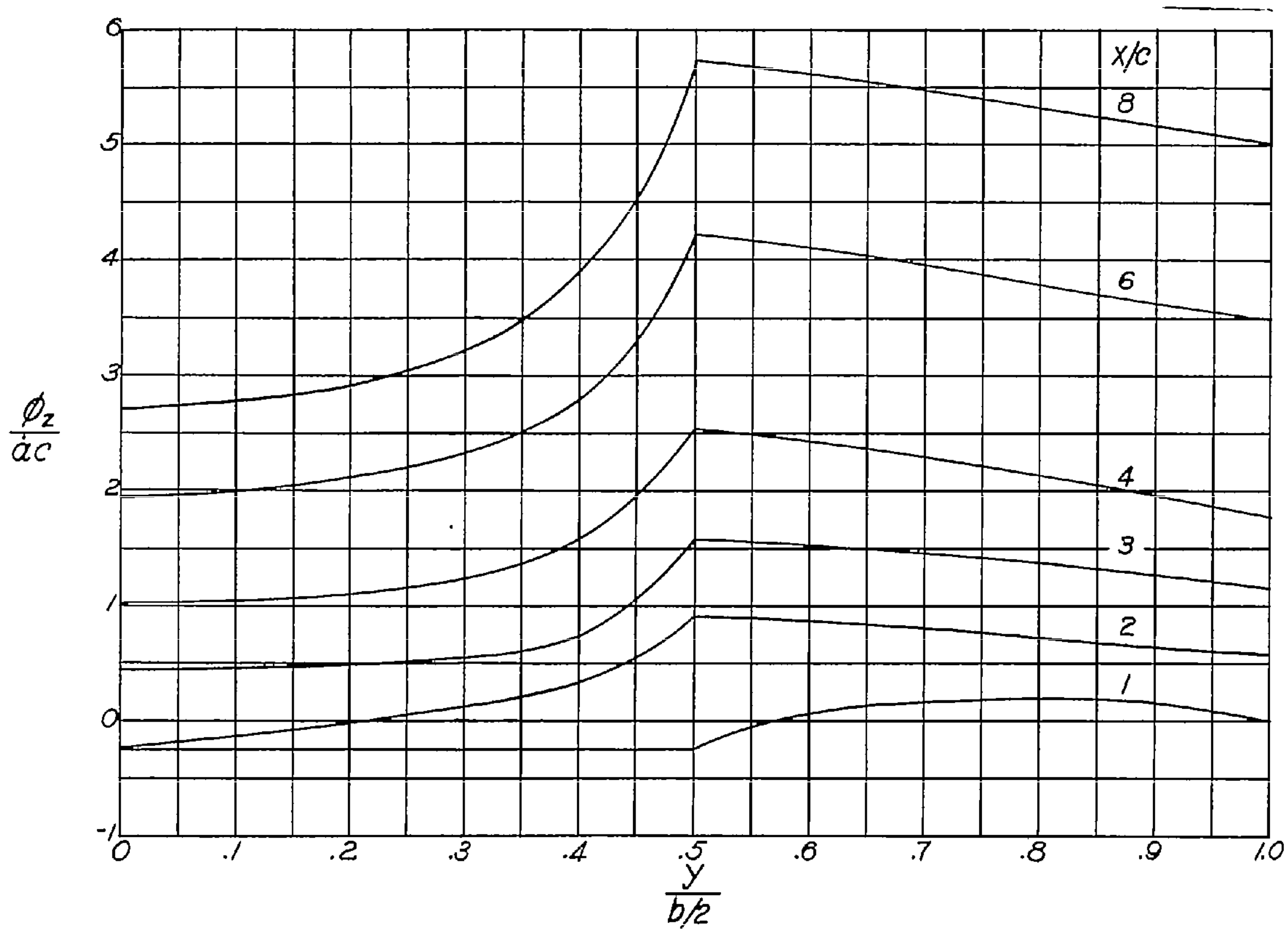

(d) M = 2.24.

Figure 18.- Concluded.

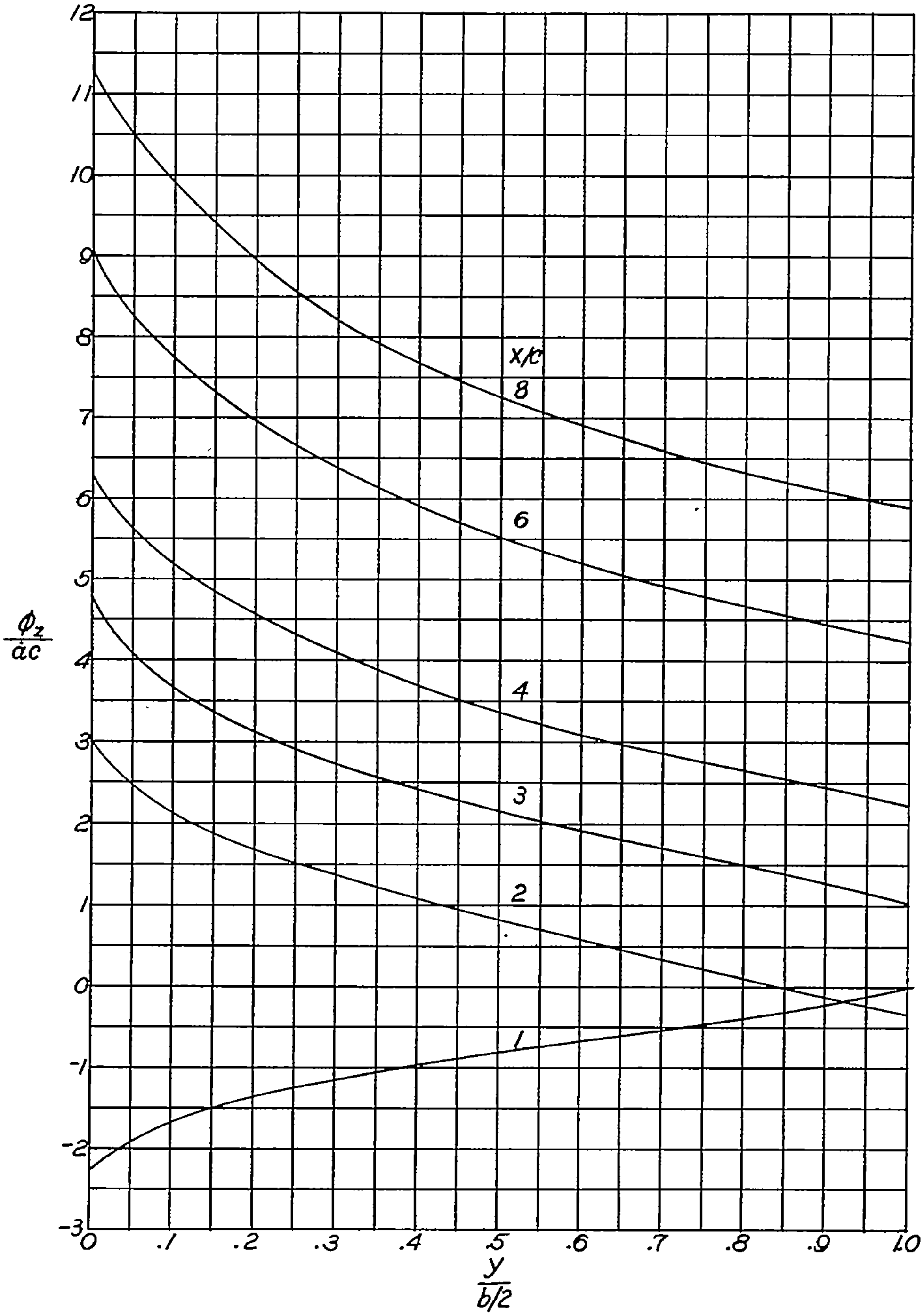

(a) M = 1.20.

Figure 19.- The upwash distribution at $t = t_o$ in the plane of the wing behind a rectangular wing with a constant vertical acceleration with A = 3 for various Mach numbers.

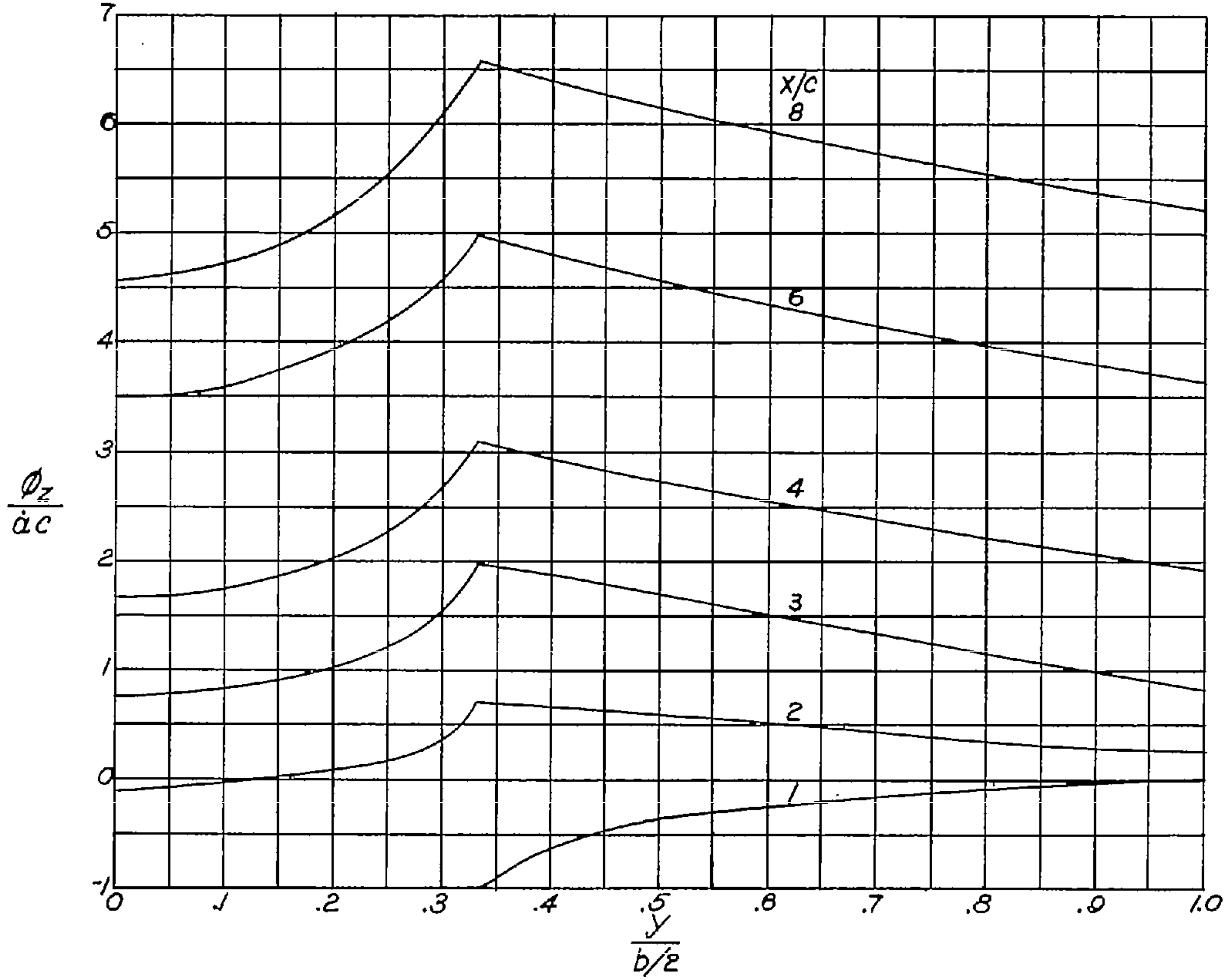

(b) M = 1.414.

Figure 19.- Continued.

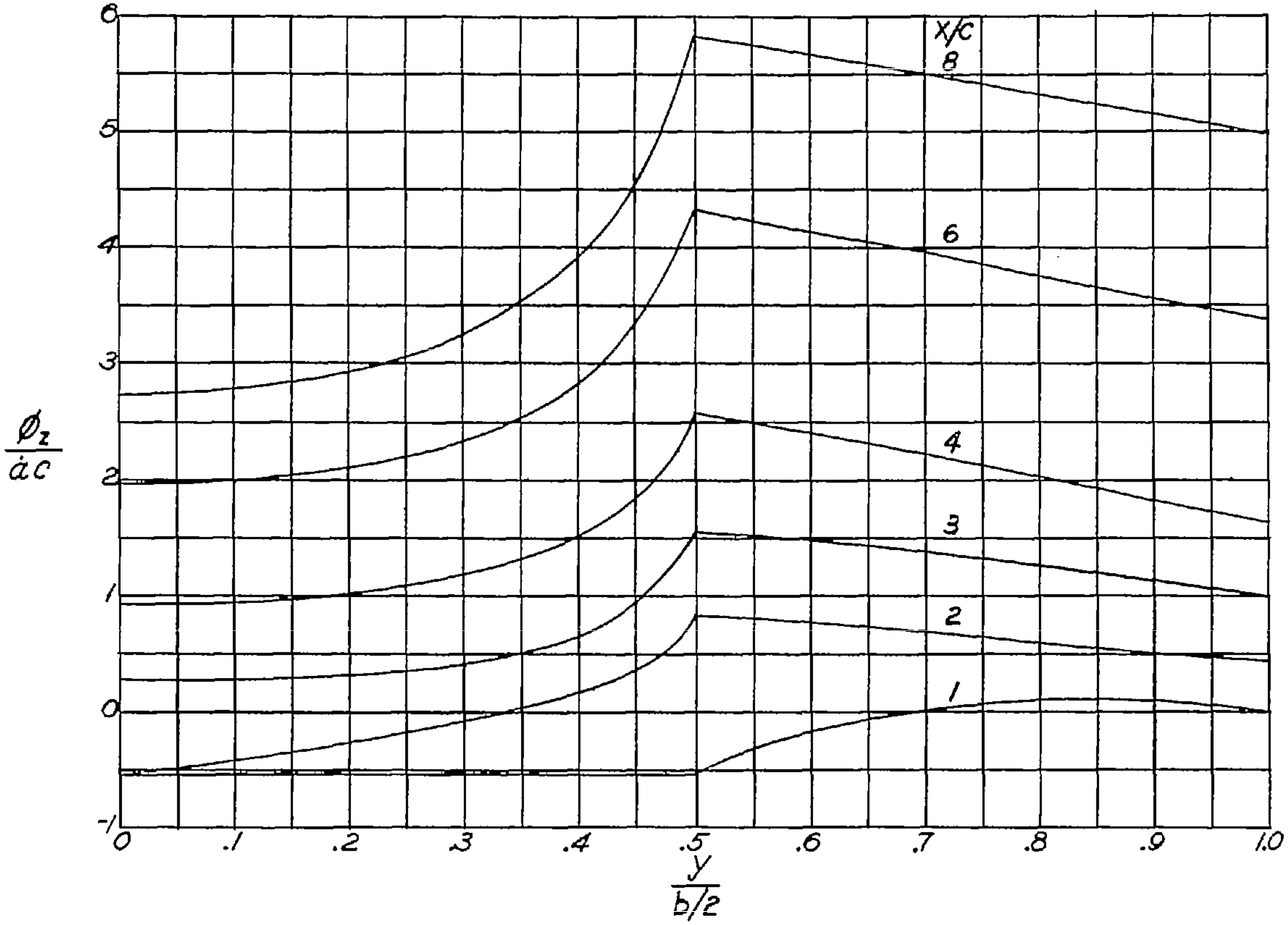

(c) M = 1.667.

Figure 19.- Continued.

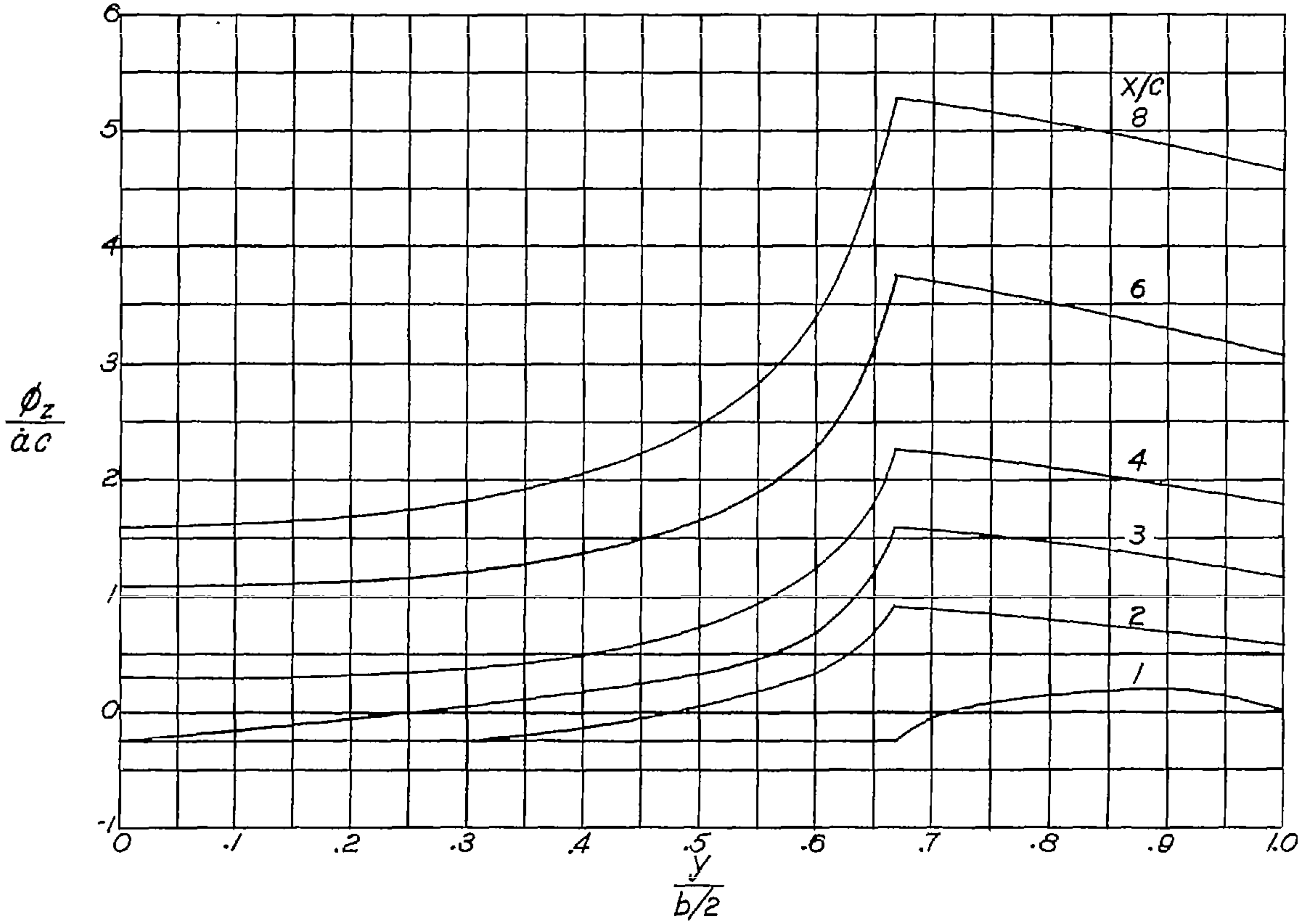

(d) M = 2.24.

Figure 19.- Concluded.

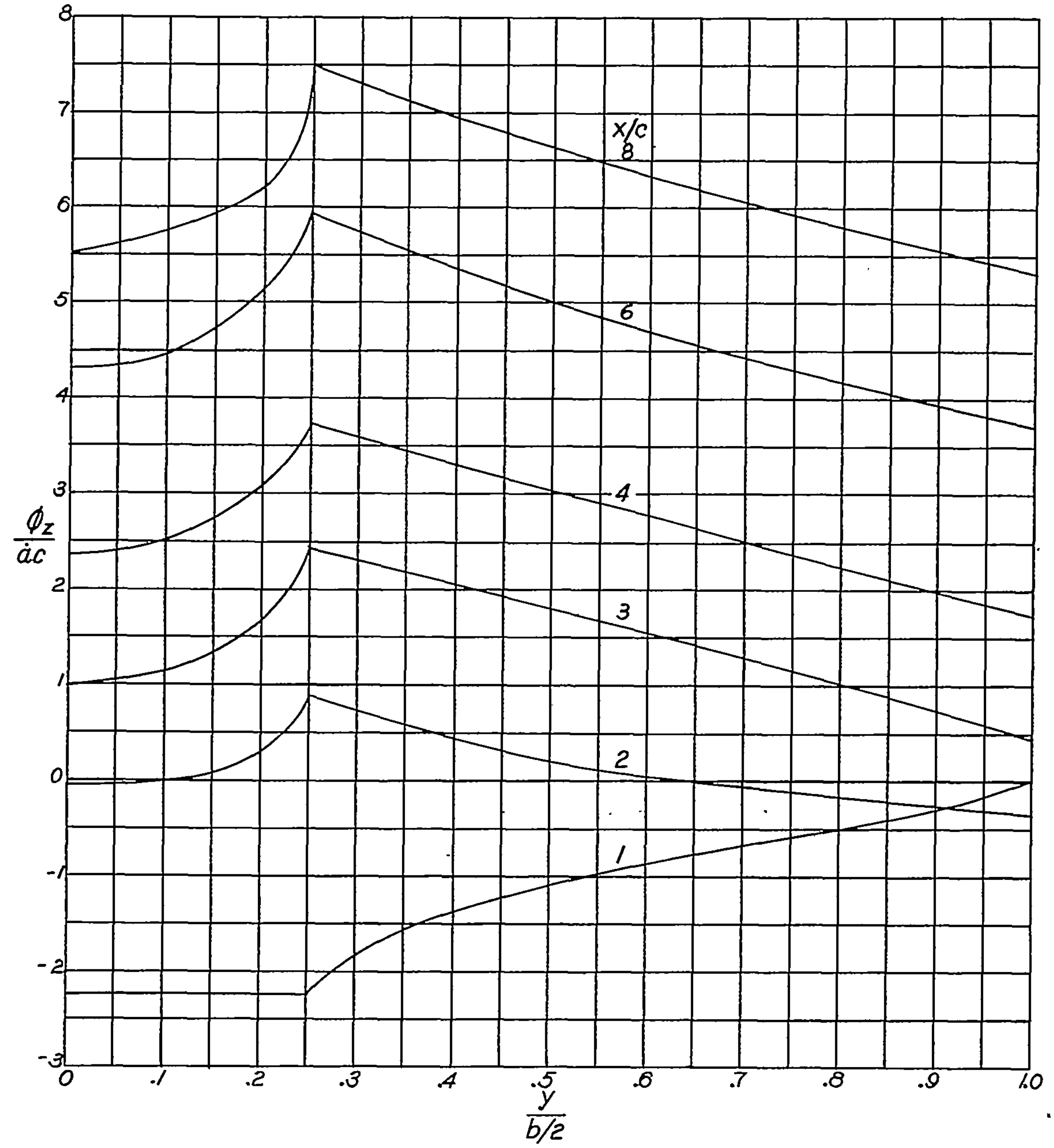

(a) M = 1.20.

Figure 20.- The upwash distribution at $t = t_0$ in the plane of the wing behind a rectangular wing with a constant vertical acceleration with $A = 4$ for various Mach numbers.

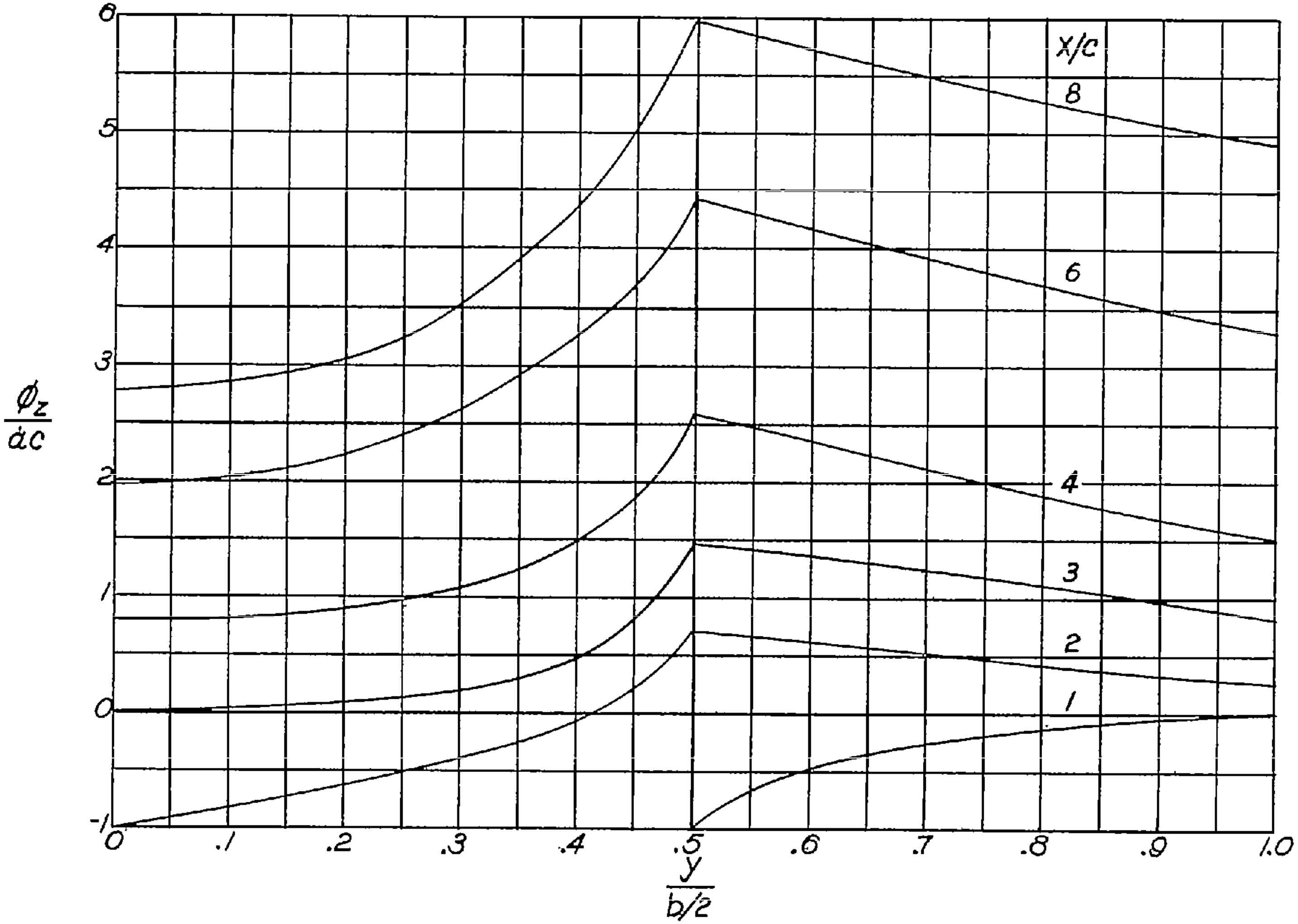

(b) M = 1.414.

Figure 20.- Continued.

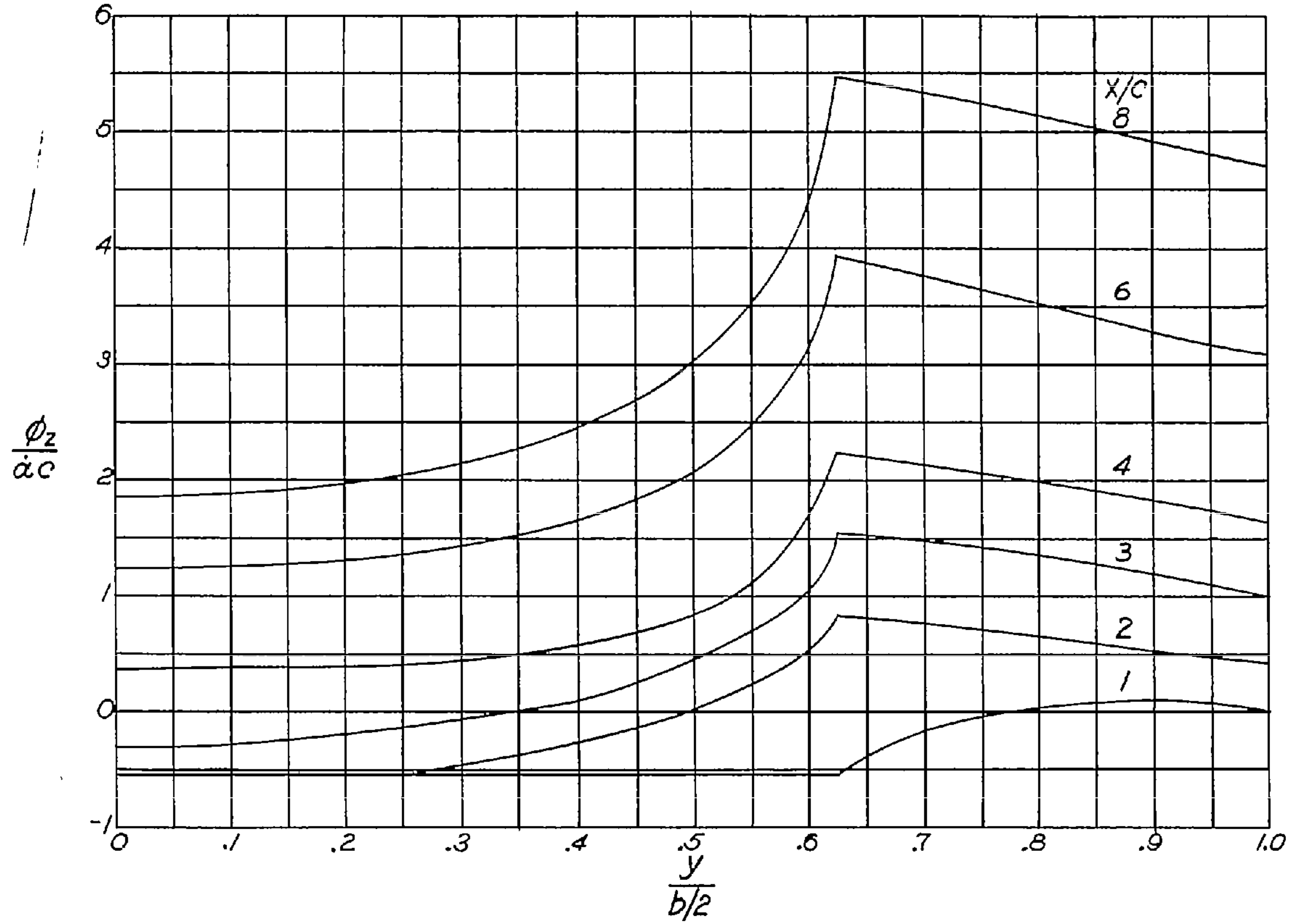

(c) M = 1.667.

Figure 20.- Continued.

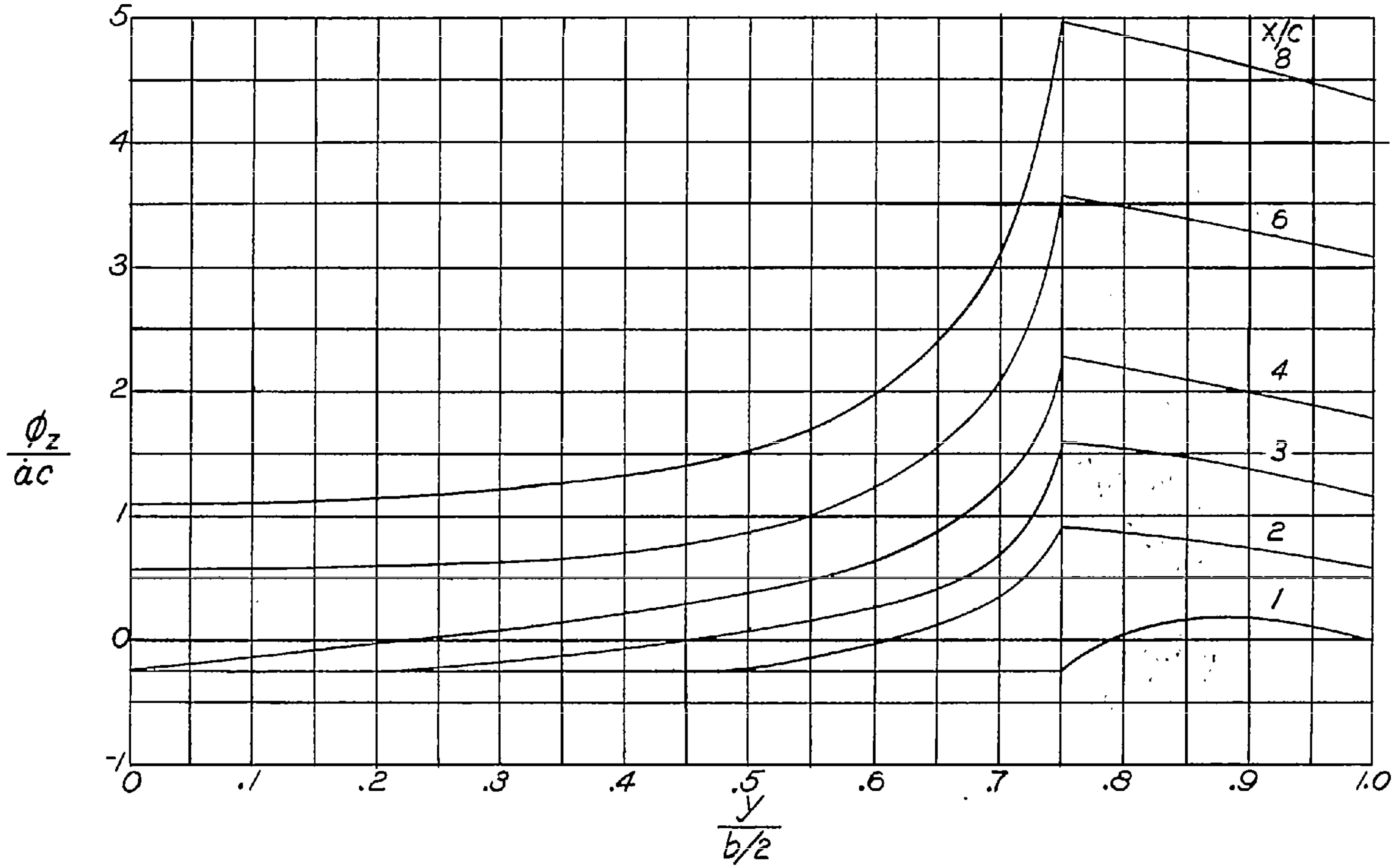

(d) M = 2.24.

Figure 20.- Concluded.

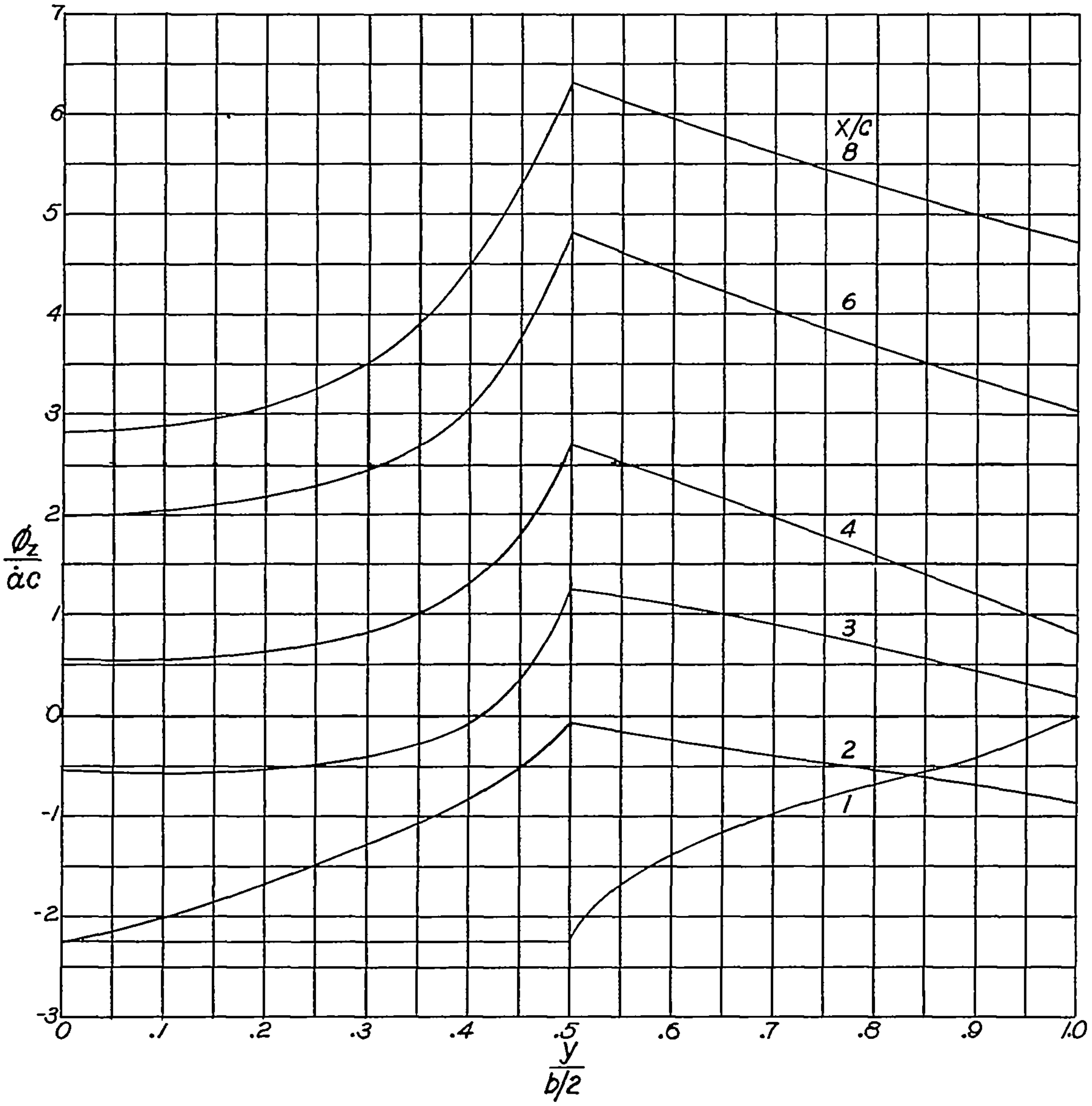

(a) M = 1.20.

Figure 21.- The upwash distribution at $t = t_0$ in the plane of the wing behind a rectangular wing with a constant vertical acceleration with $A = 6$ for various Mach numbers.

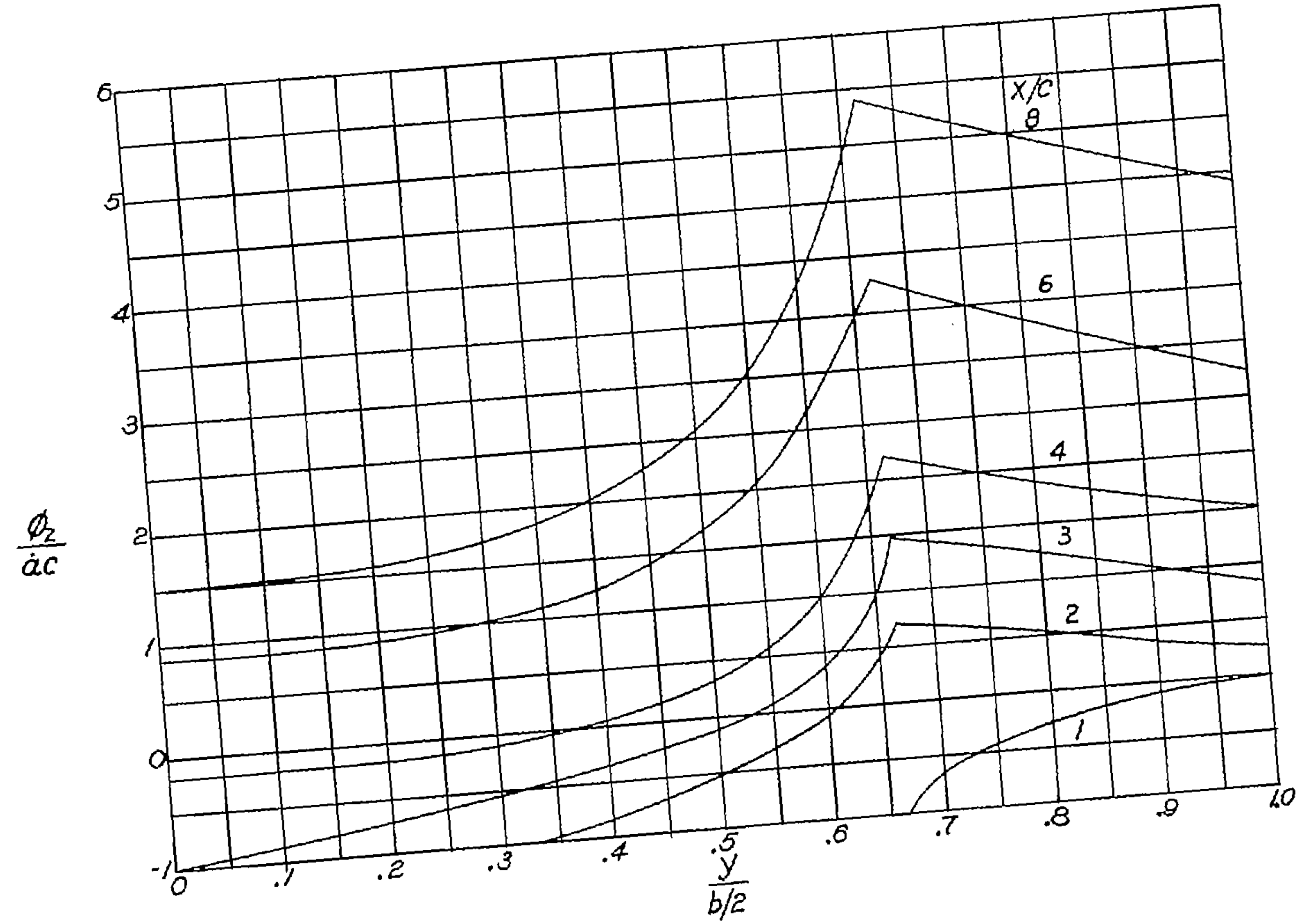

(b) M = 1.414.

Figure 21.- Continued.

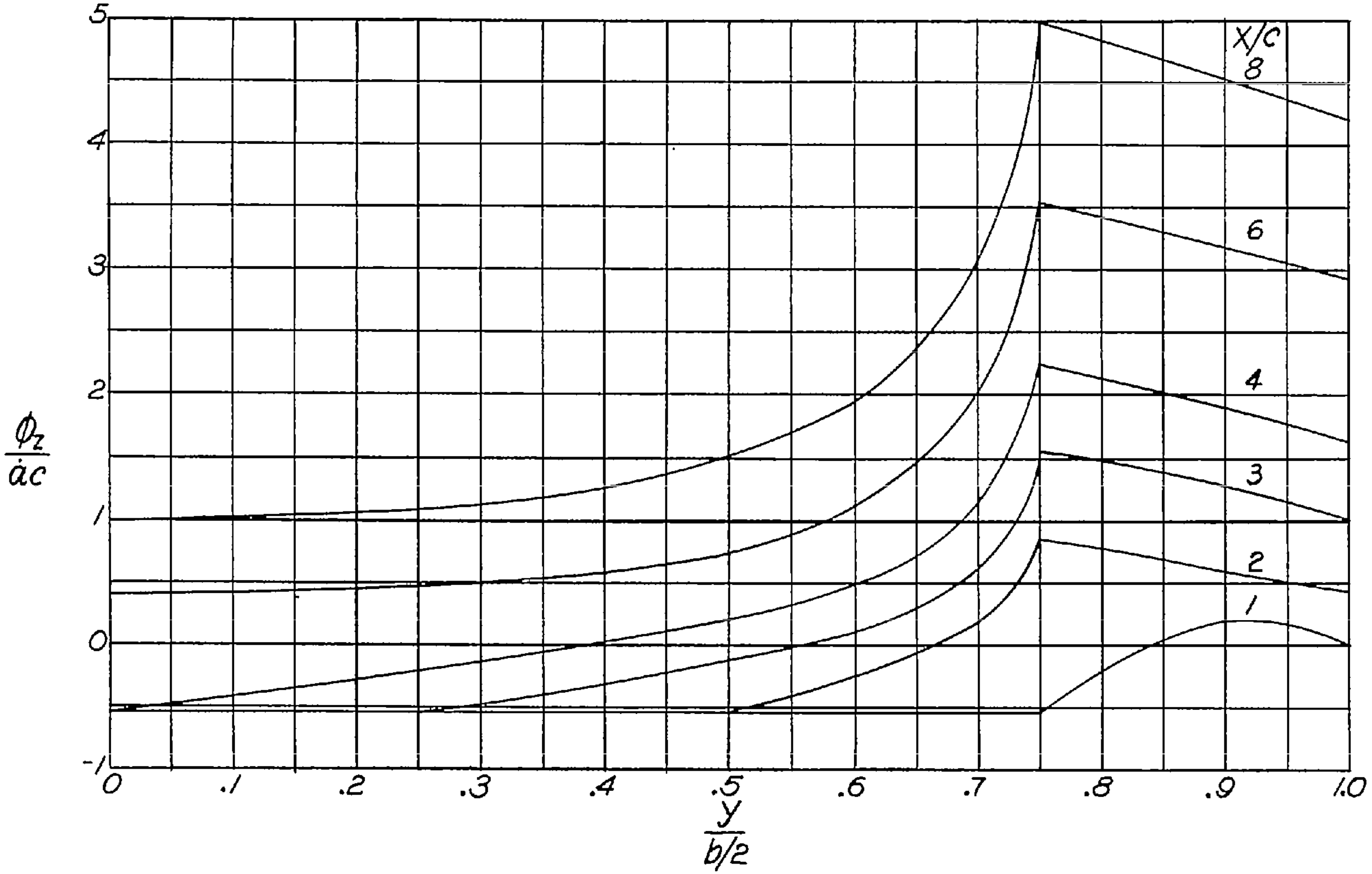

(c) M = 1.667.

Figure 21.- Continued.

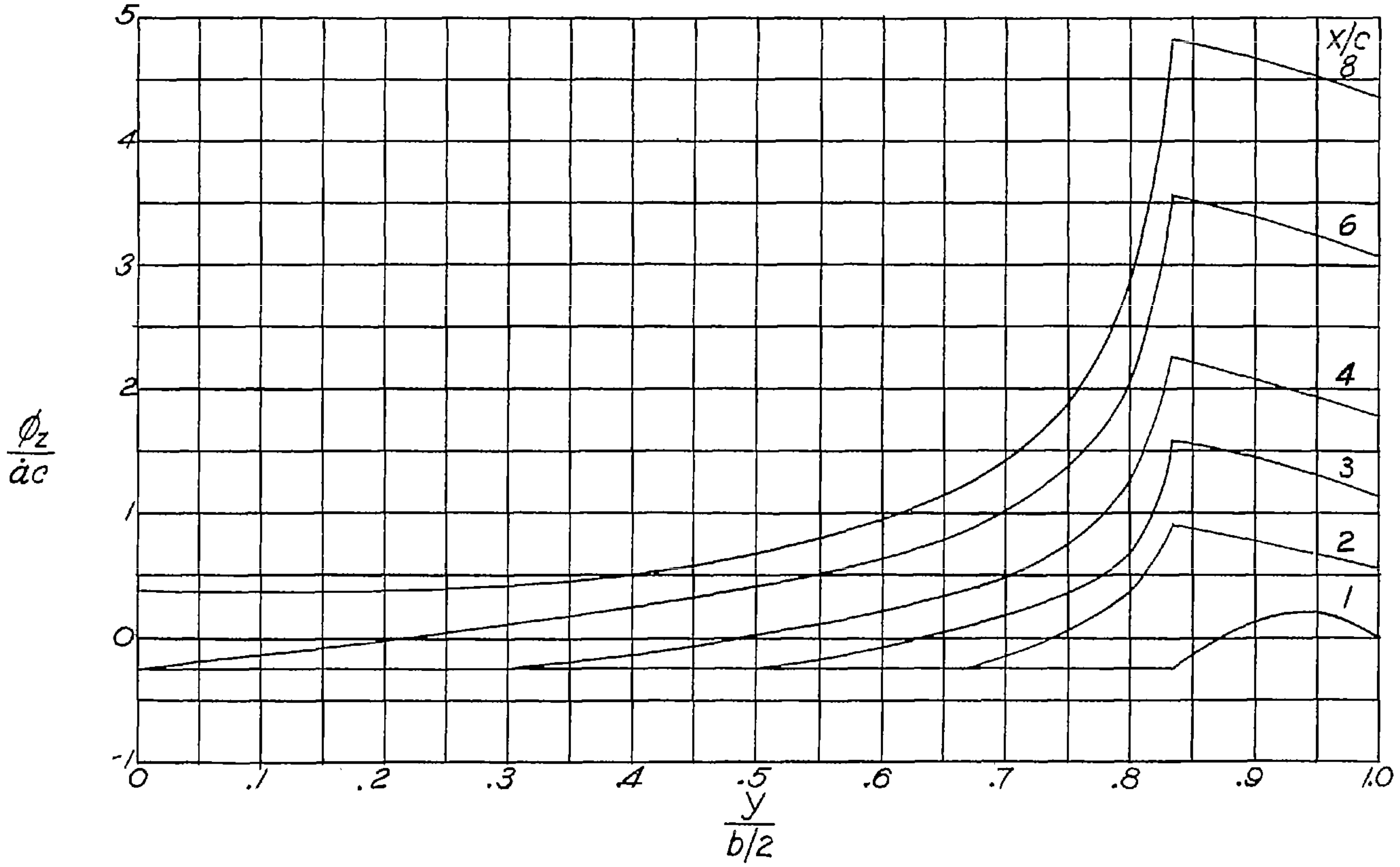

(d) M = 2.24.

Figure 21.- Concluded.

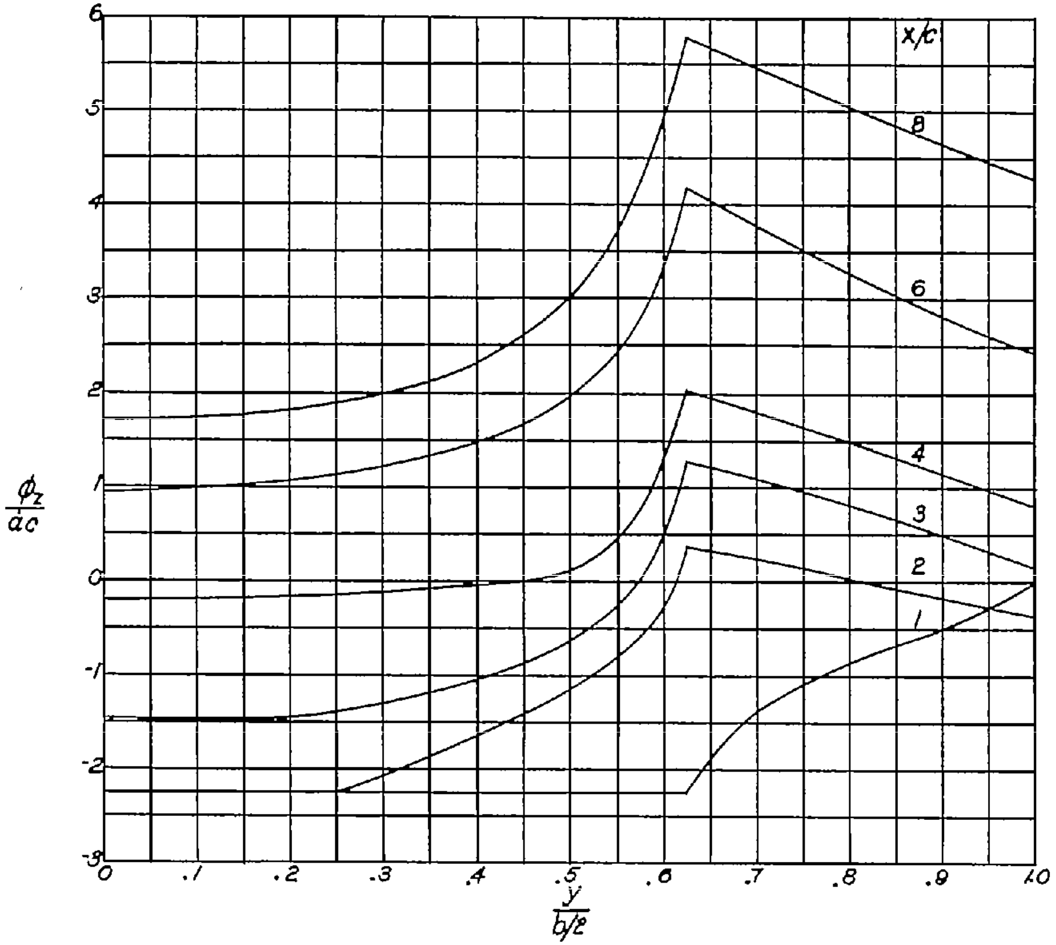

(a) M = 1.20.

Figure 22.- The upwash distribution at $t = t_o$ in the plane of the wing behind a rectangular wing with a constant vertical acceleration with $A = 8$ for various Mach numbers.

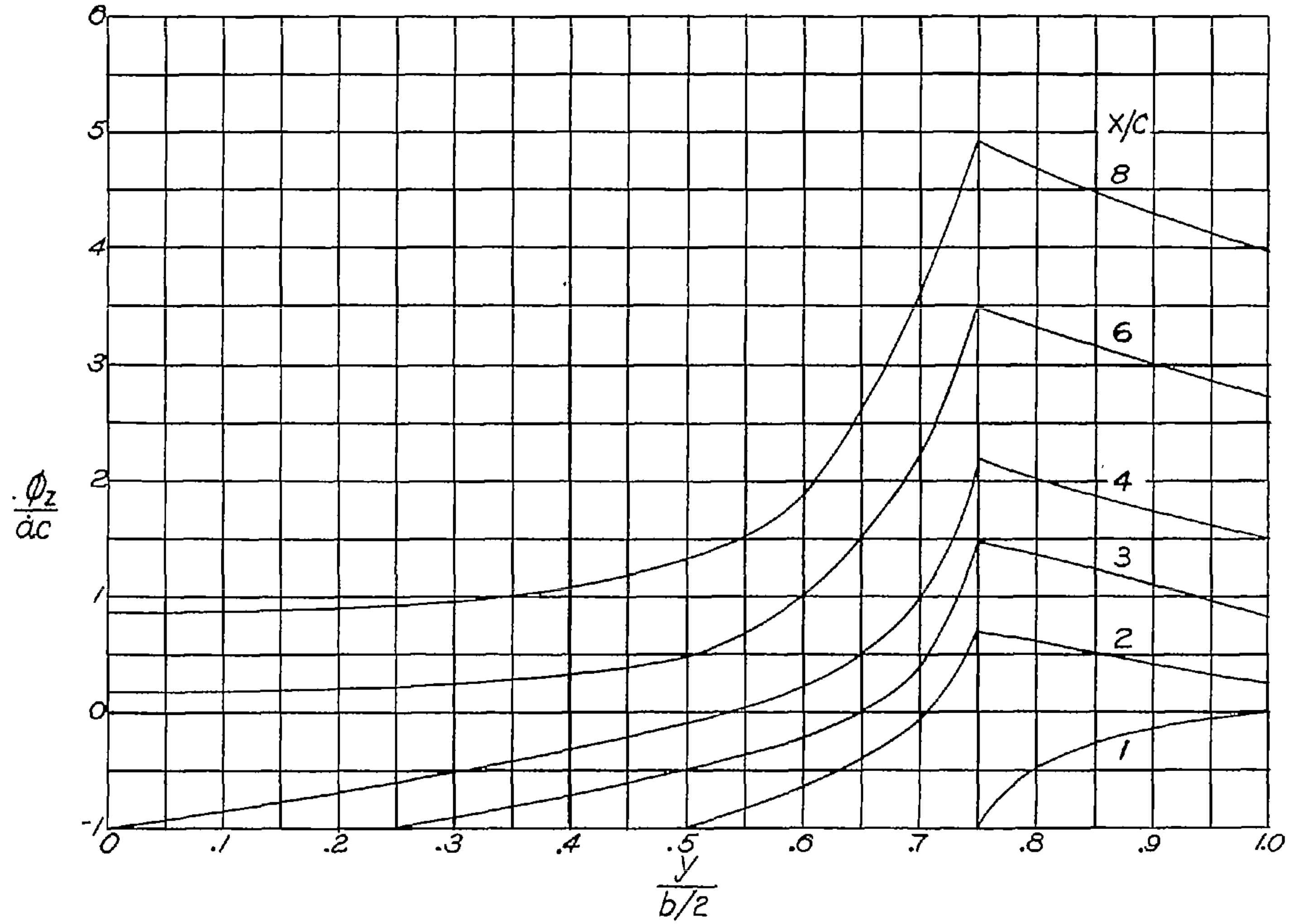

(b) M = 1.414.

Figure 22.- Continued.

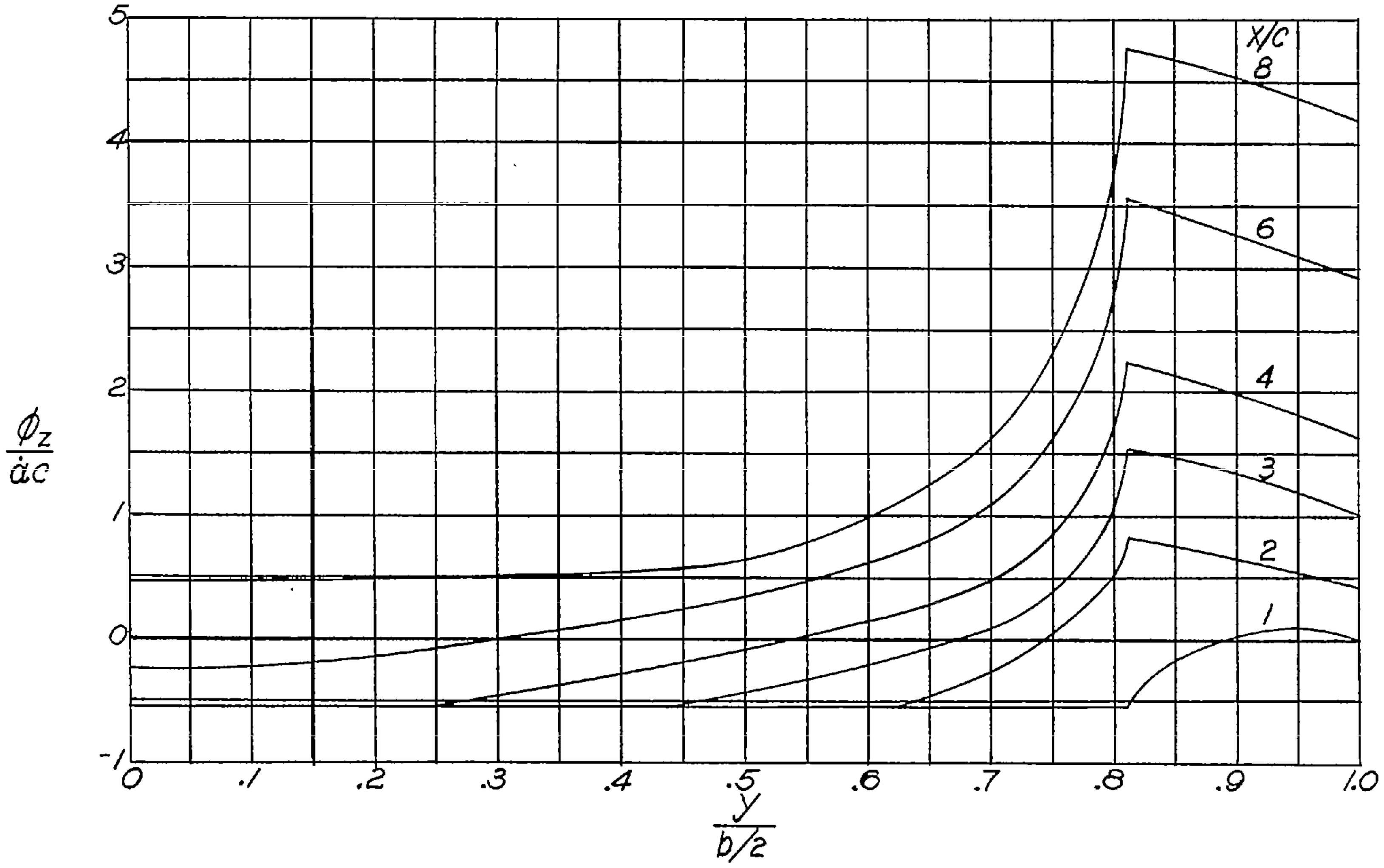

(c) M = 1.667.

Figure 22.- Continued.

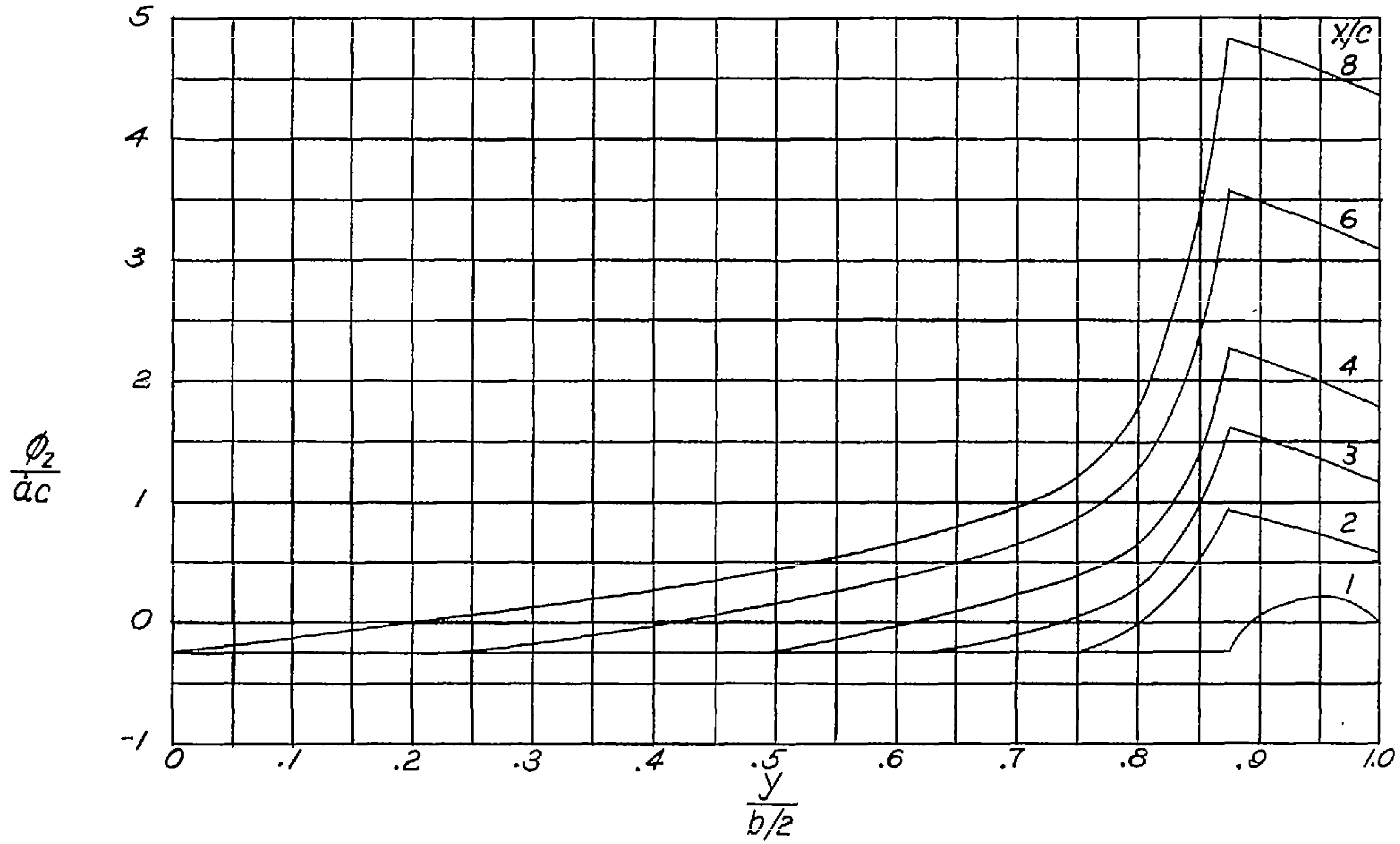

(d) M = 2.24.

Figure 22.- Concluded.

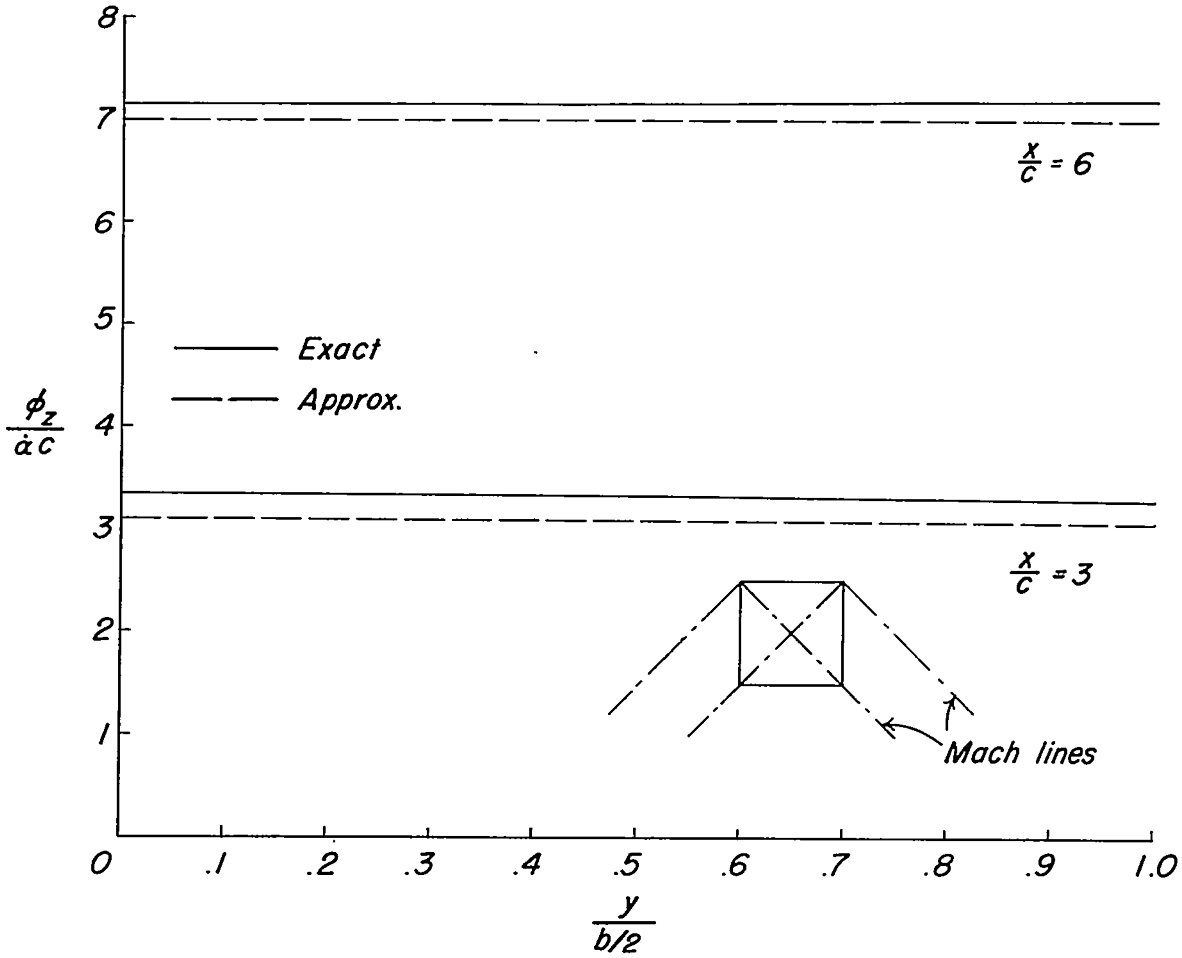

(a) M = 1.414.

Figure 23.- Exact (linearized) and approximate (eq. (37b)) values of upwash at $t = t_0$ in the plane of the wing behind a rectangular wing for two Mach numbers. A = 1.

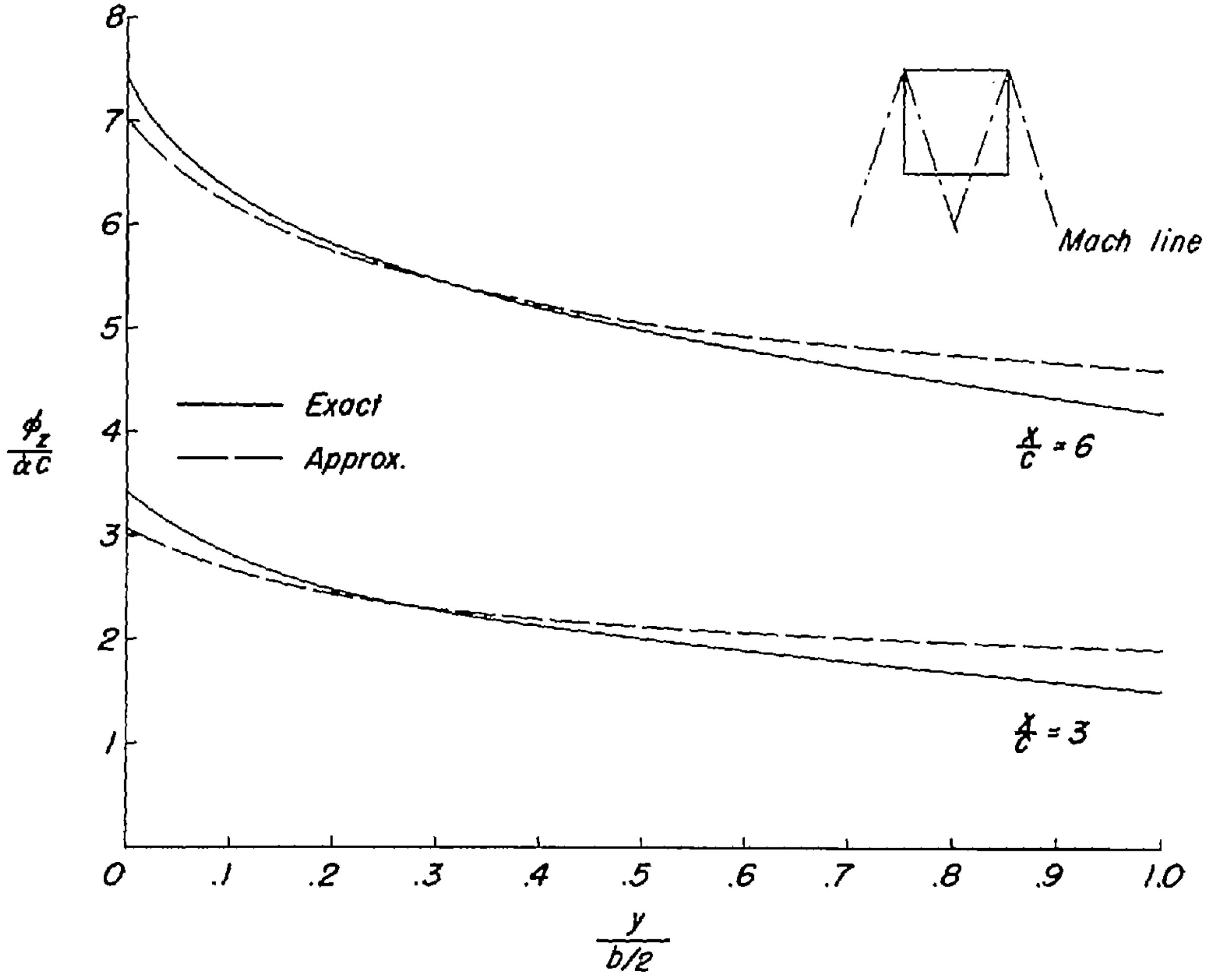

(b) M = 2.24.

Figure 23.- Concluded.

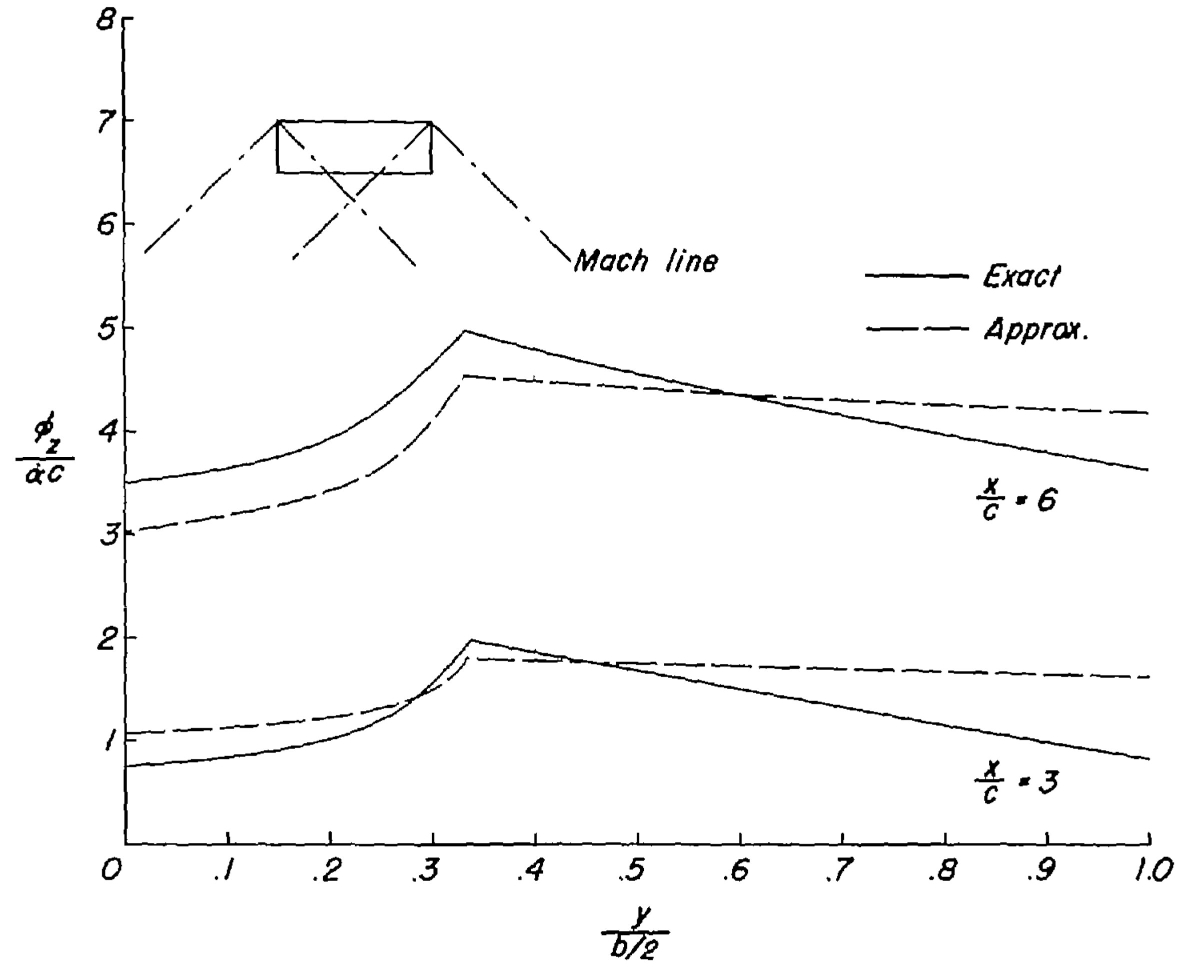

(a) $M = 1.414$.

Figure 24.- Exact (linearized) and approximate (eq. (37b)) values of upwash at $t = t_o$ in the plane of the wing behind a rectangular wing for two Mach numbers. $A = 3$.

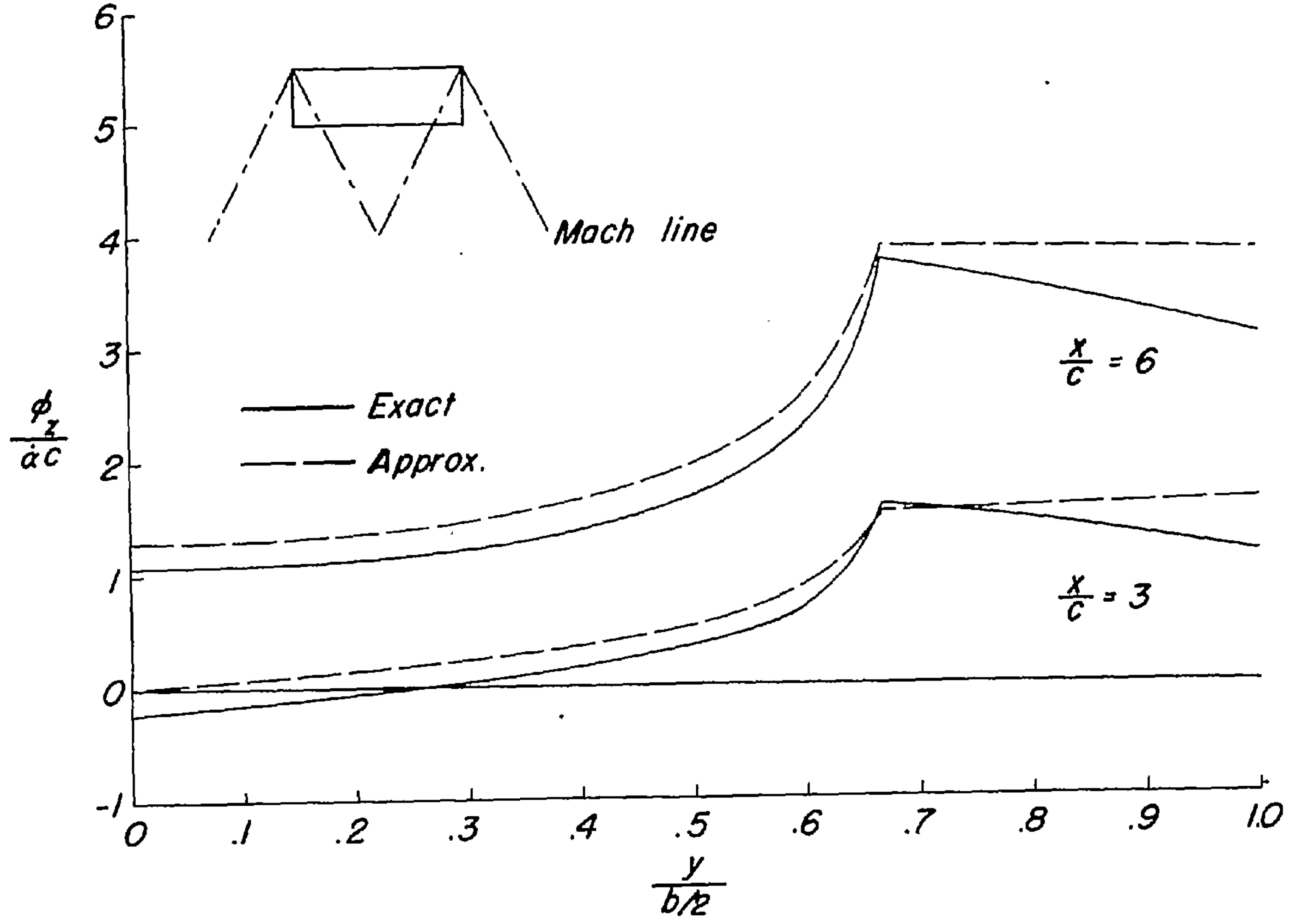

(b) M = 2.24.

Figure 24.- Concluded.

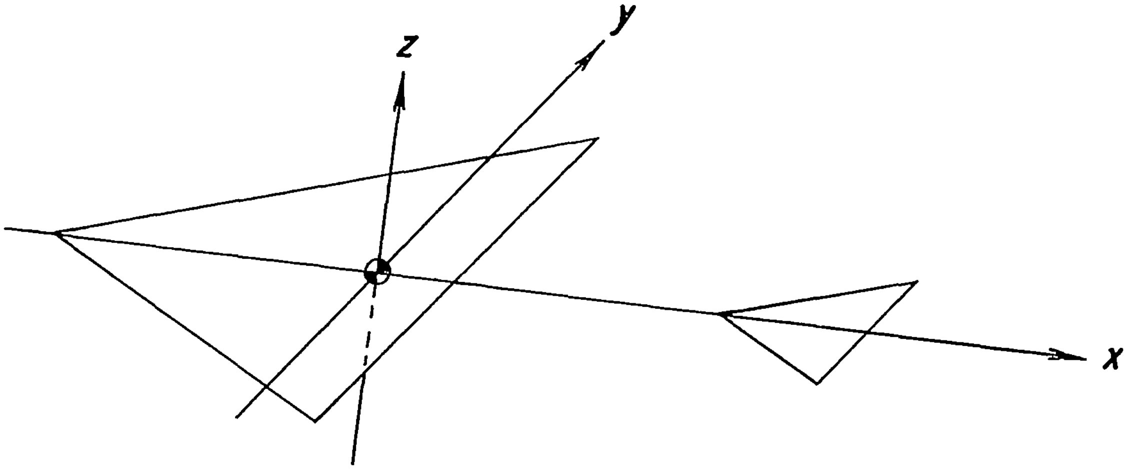

(a) Body axes used in determining aerodynamic coefficients.

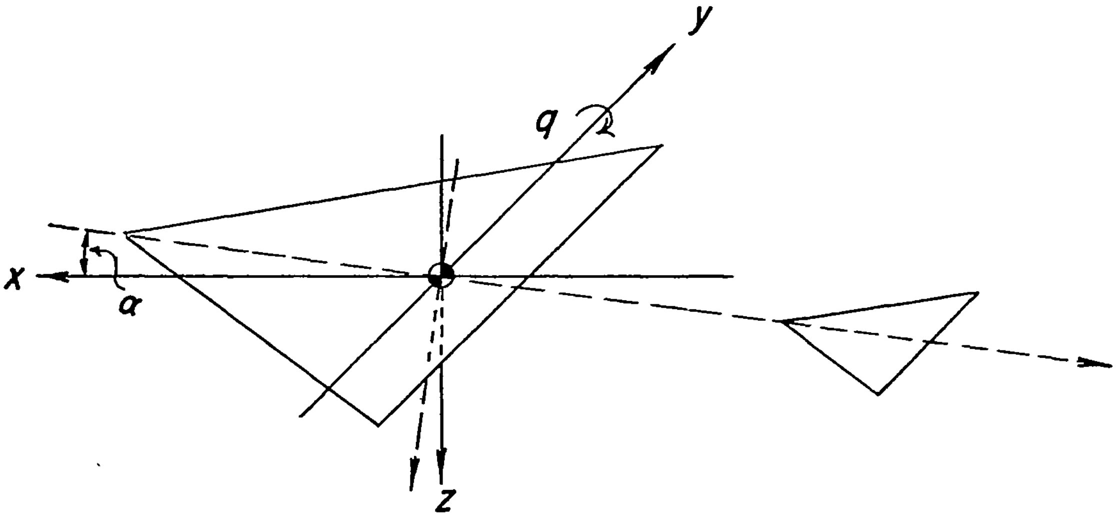

(b) Stability axes (principal body axes dashed for comparison).

Figure 25.- Systems of axes and associated data.

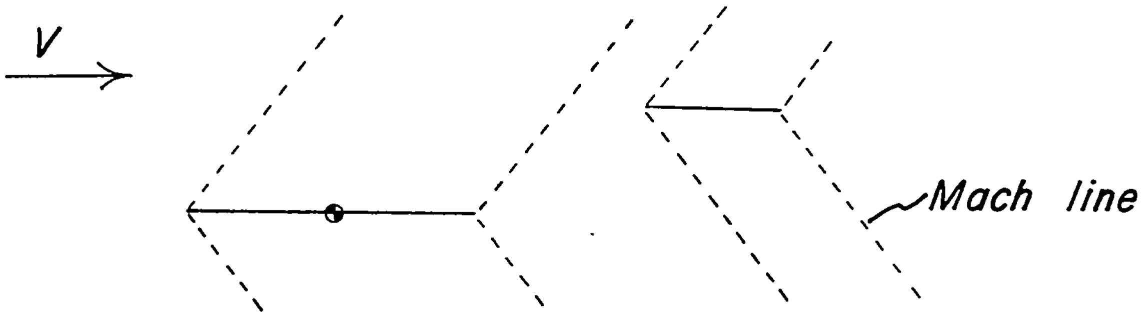

(a) Tail lies downstream of Mach sheet from trailing edge of wing.

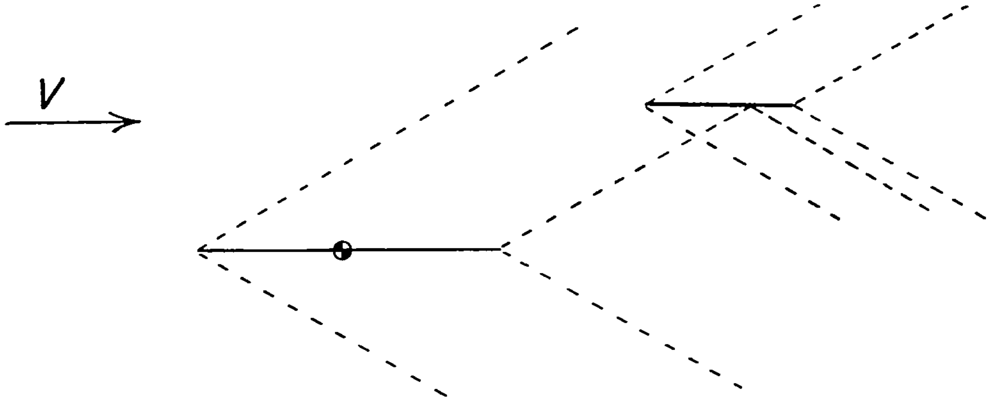

(b) Mach sheet from wing trailing edge intersects tail.

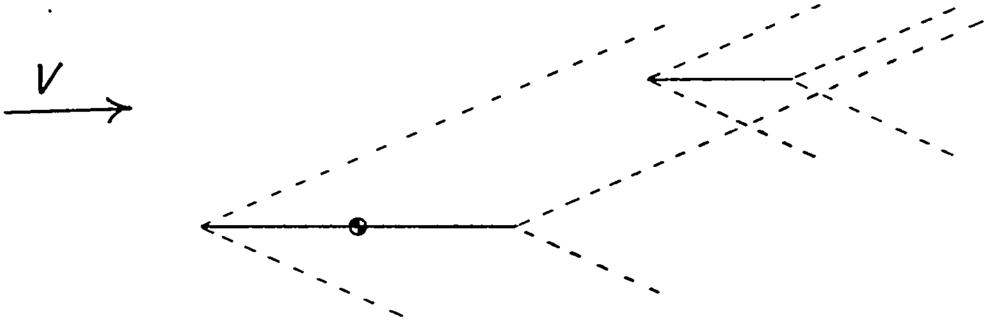

(c) Tail surface lies between Mach sheet from leading edge of wing and Mach sheet from trailing edge of wing.

Figure 26.- Types of flow treated for the two-dimensional wing-tail combination.

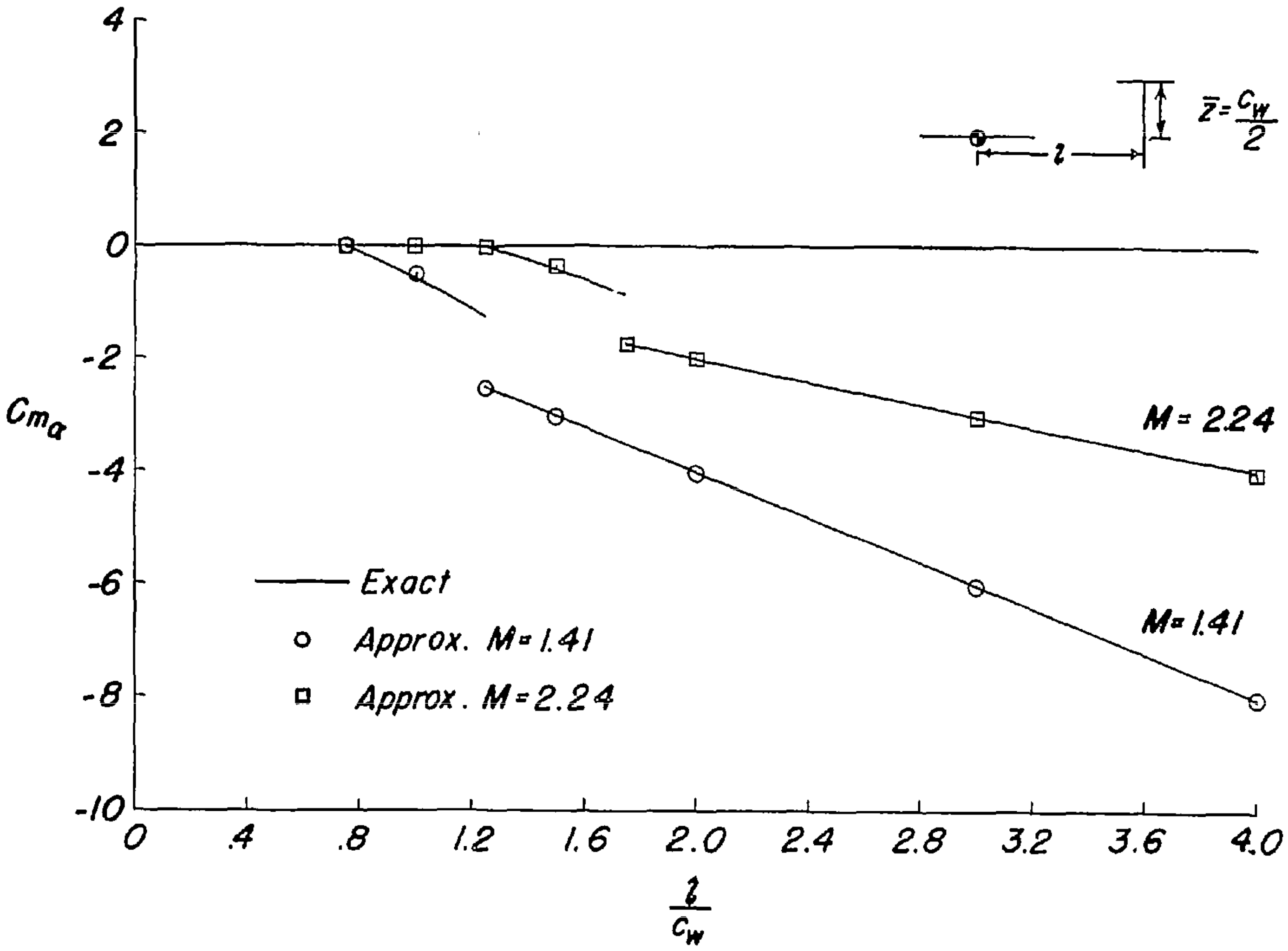

Figure 27.- Comparison of exact (linearized) and approximate (eq. (53)) values of C_{m_α} for a two-dimensional wing-tail combination at two Mach numbers. $\bar{x} = c_t = \frac{c_w}{2}$.

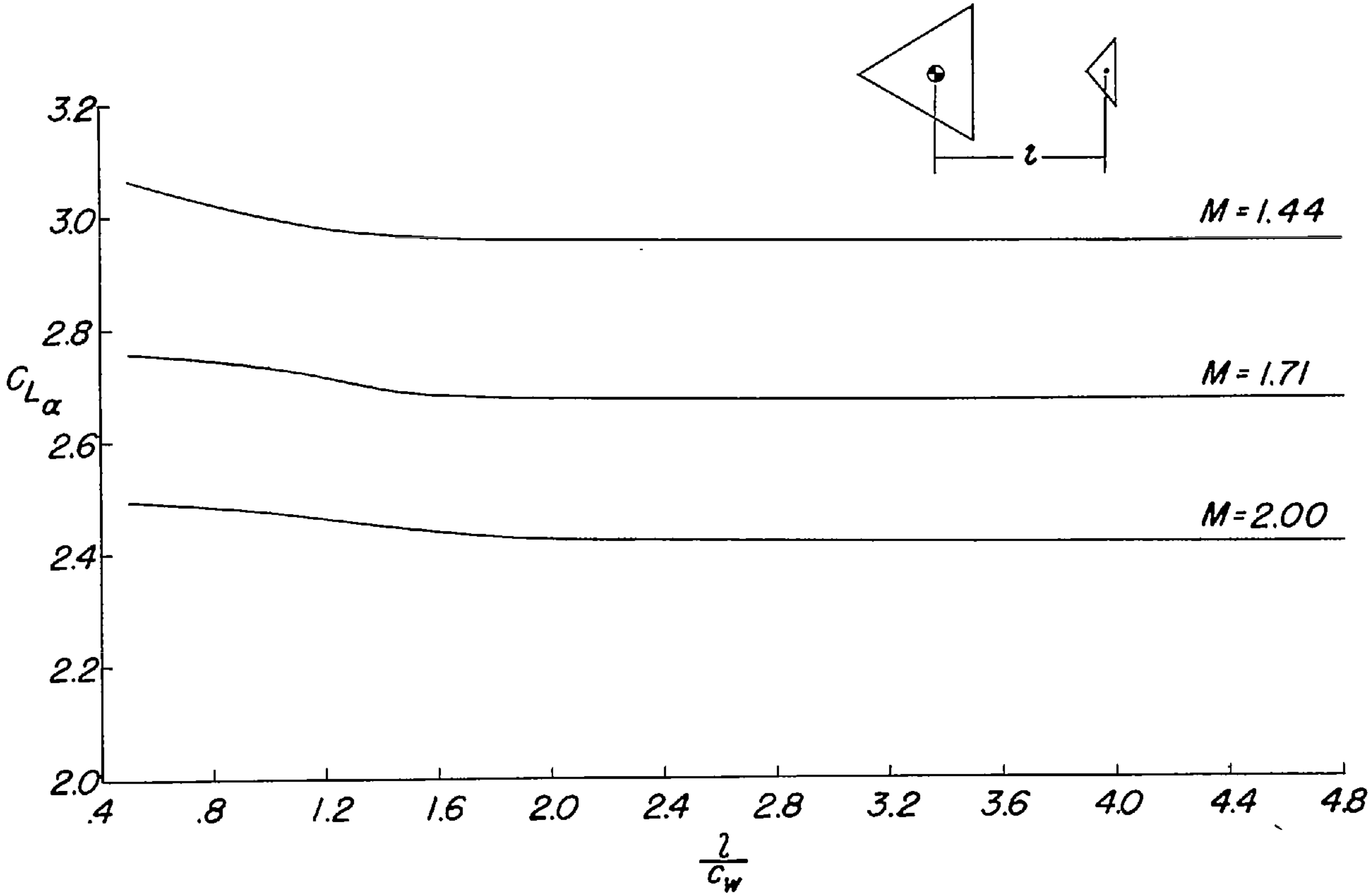

Figure 28.- Variation of C_{L_α} with l/c_w for three Mach numbers for a triangular wing-tail combination.

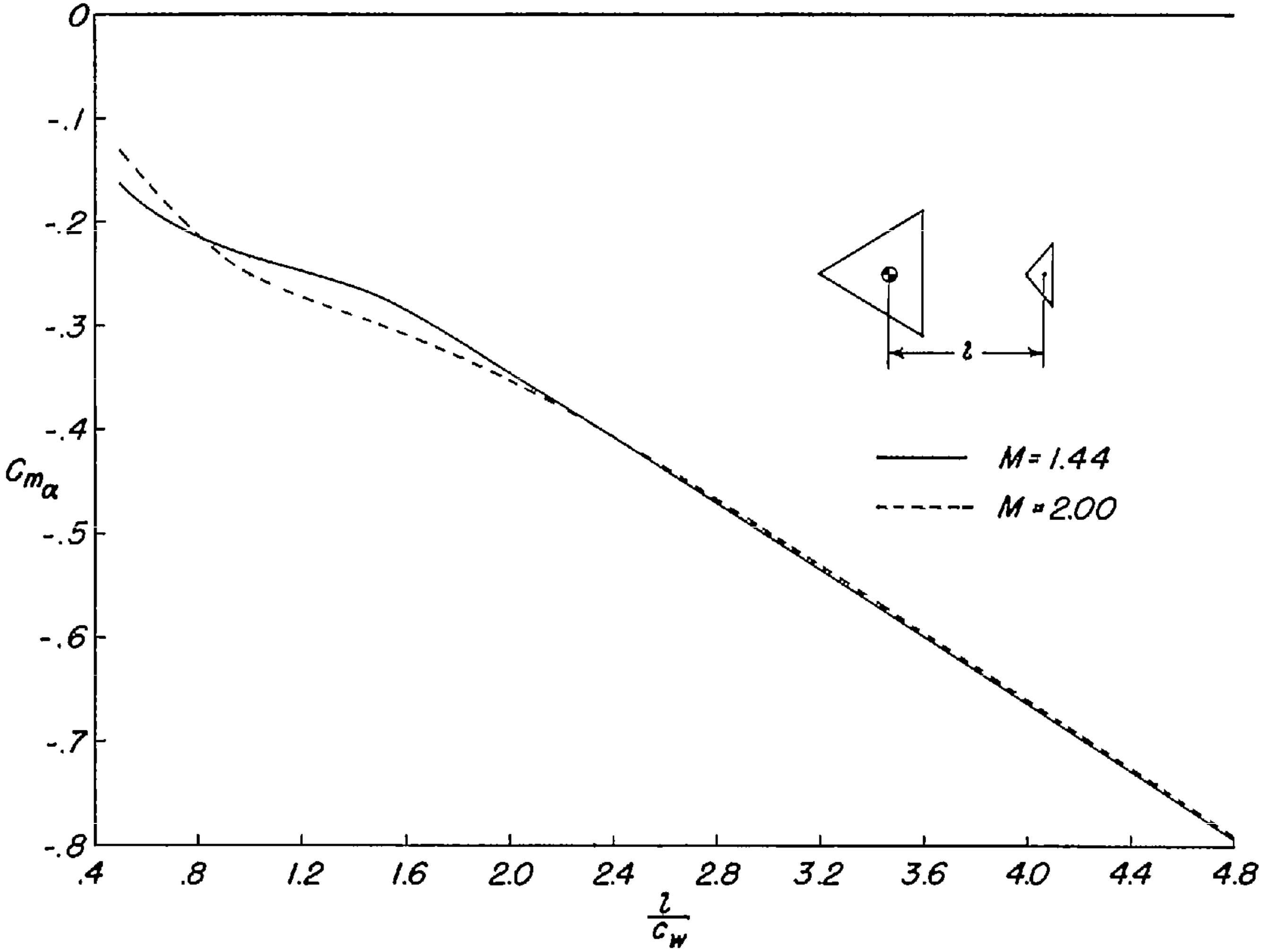

Figure 29.- Variation of C_{m_α} with l/c_w for two Mach numbers for a triangular wing-tail combination.

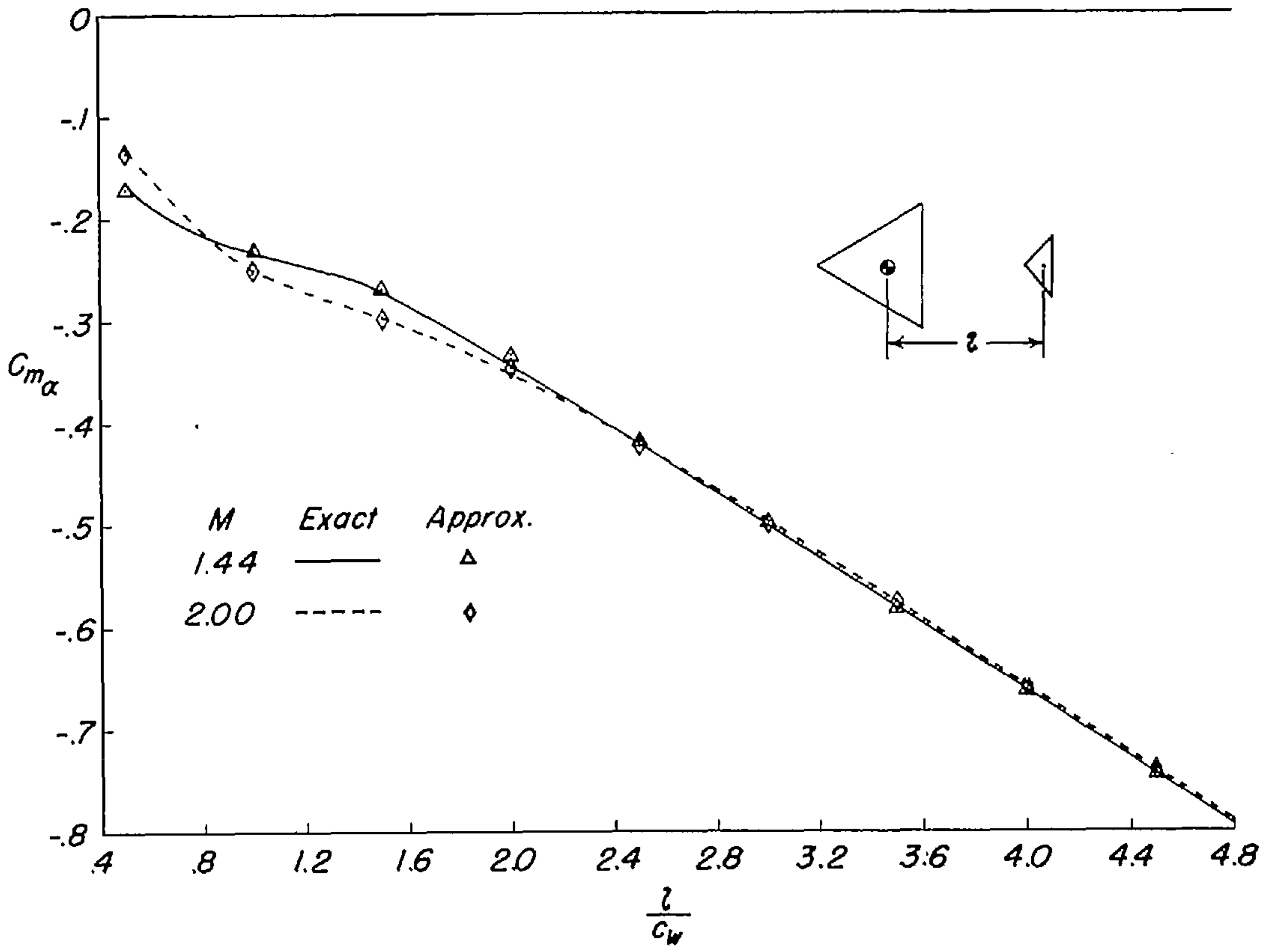

Figure 30.- Comparison of exact (linearized) and approximate (eq. (53)) values of C_{m_α} for a triangular wing-tail combination at two Mach numbers.

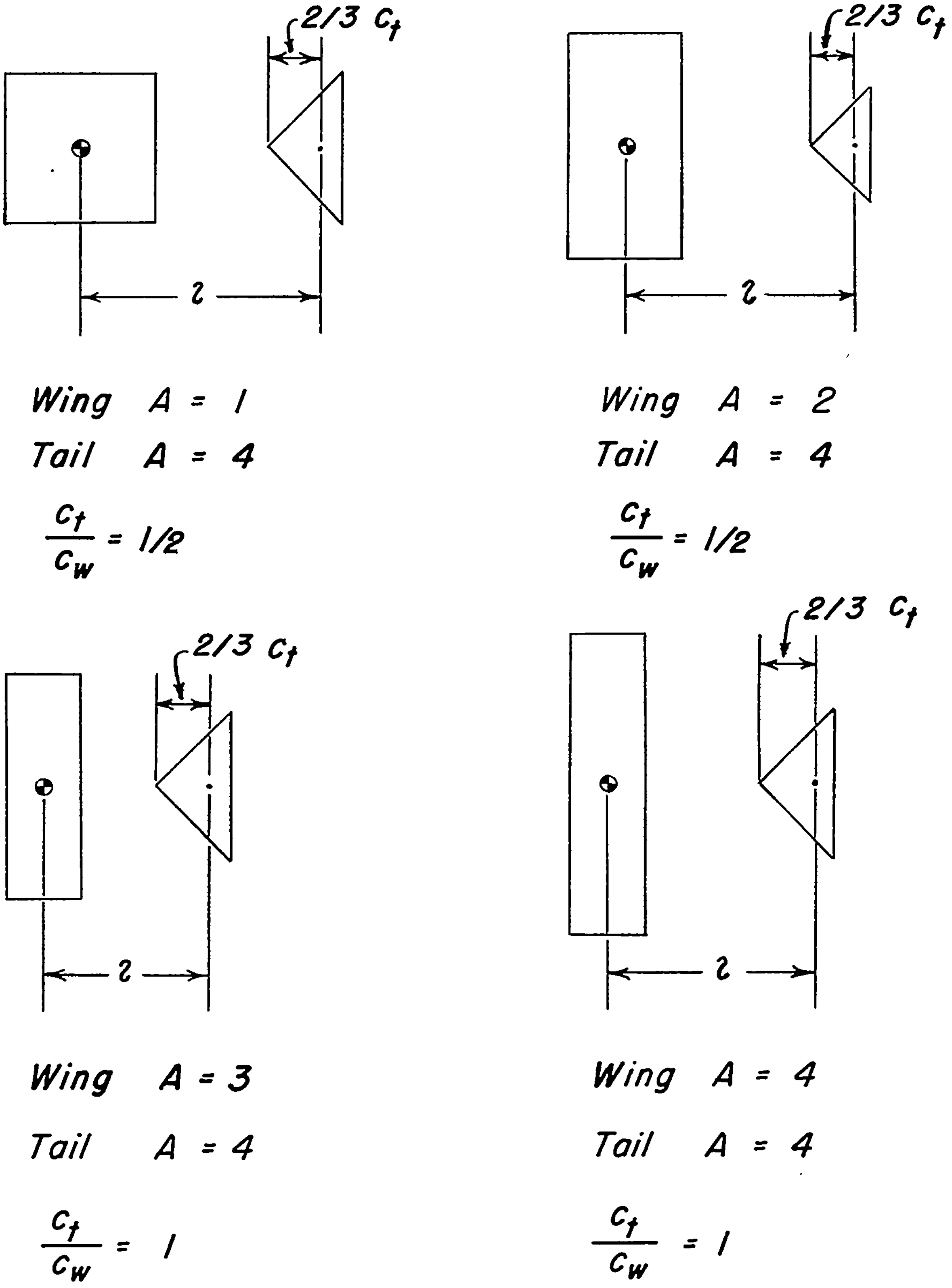

Wing $A = 1$
Tail $A = 4$
$\frac{c_t}{c_w} = 1/2$

Wing $A = 2$
Tail $A = 4$
$\frac{c_t}{c_w} = 1/2$

Wing $A = 3$
Tail $A = 4$
$\frac{c_t}{c_w} = 1$

Wing $A = 4$
Tail $A = 4$
$\frac{c_t}{c_w} = 1$

Figure 31.- Several rectangular-wing—triangular-tail combinations and associated data.

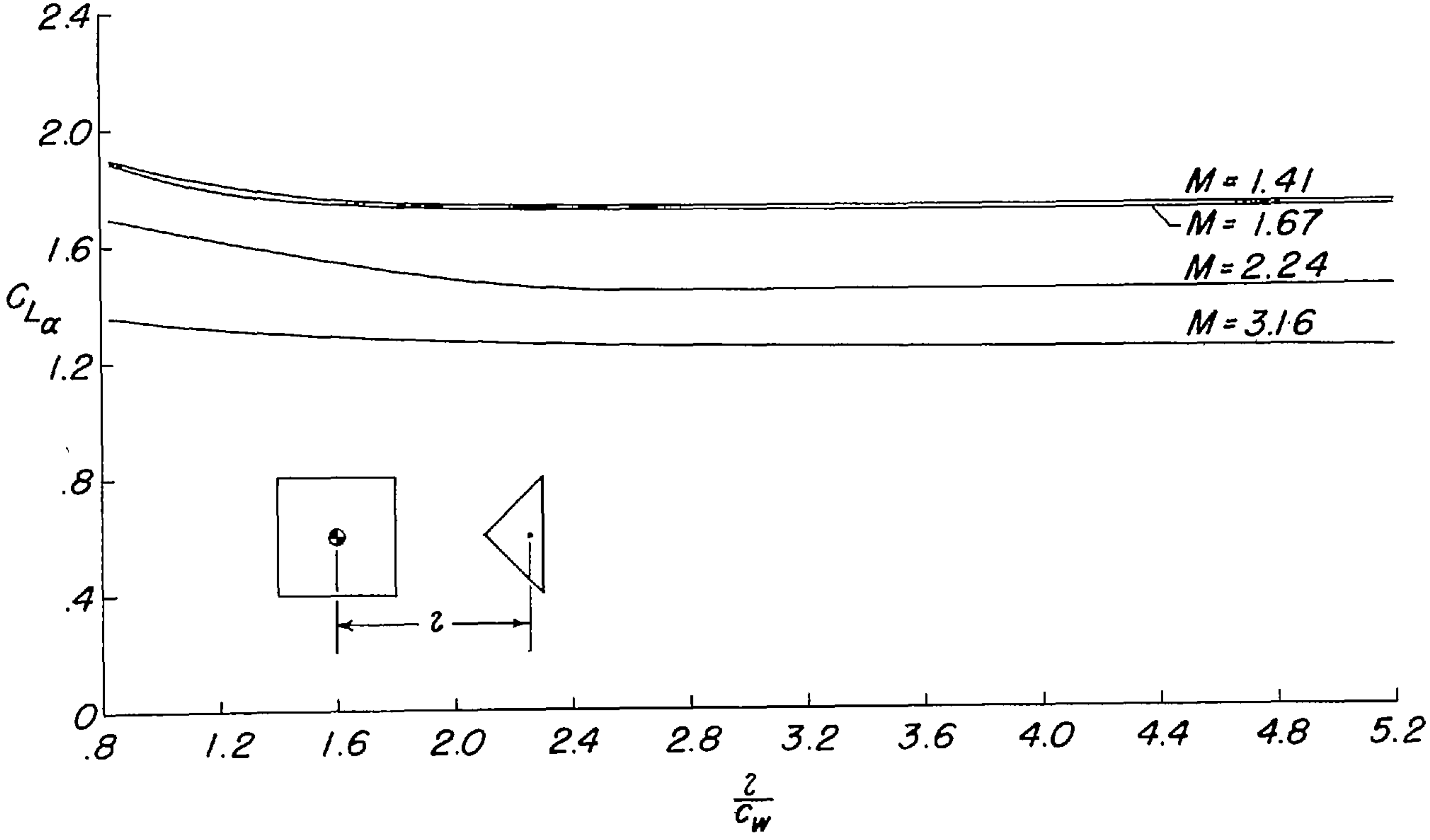

(a) Wing aspect ratio 1; $\frac{c_t}{c_w} = \frac{1}{2}$.

Figure 32.- Variation of C_{L_α} with l/c_w for several rectangular-wing—triangular-tail combinations and several Mach numbers.

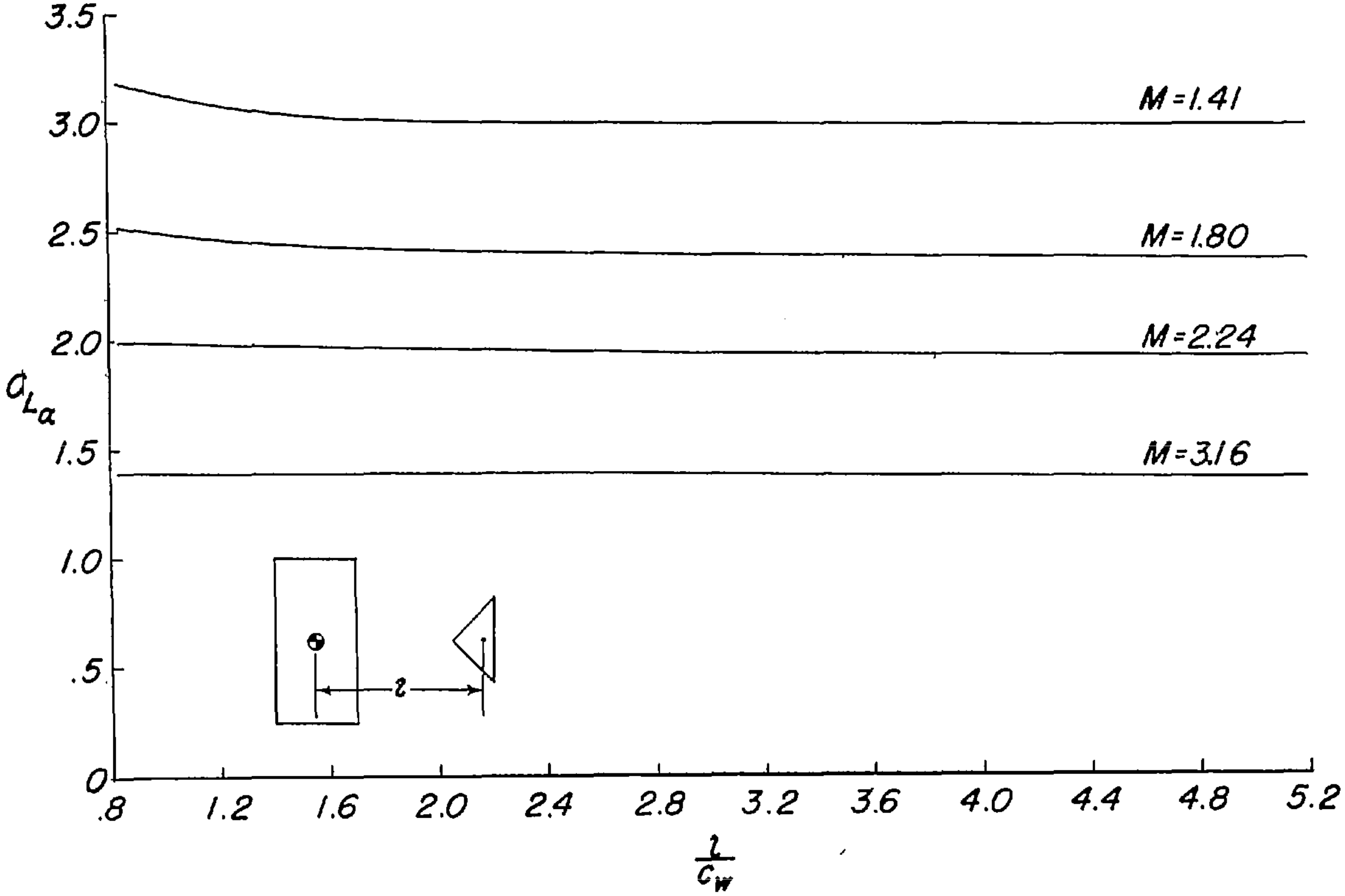

(b) Wing aspect ratio 2; $\frac{c_t}{c_w} = \frac{1}{2}$.

Figure 32.- Continued.

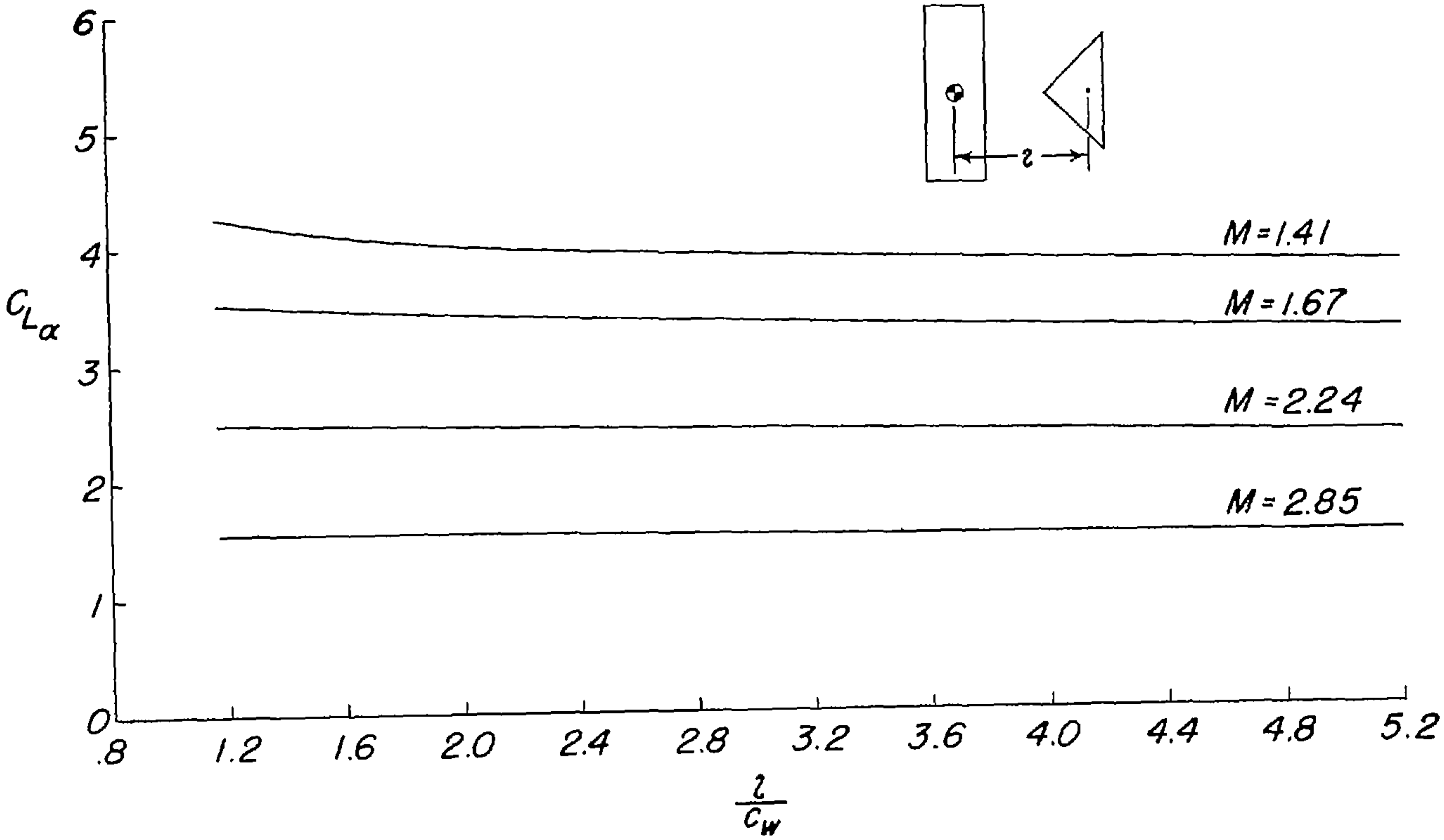

(c) Wing aspect ratio 3; $\frac{c_t}{c_w} = 1$.

Figure 32.- Continued.

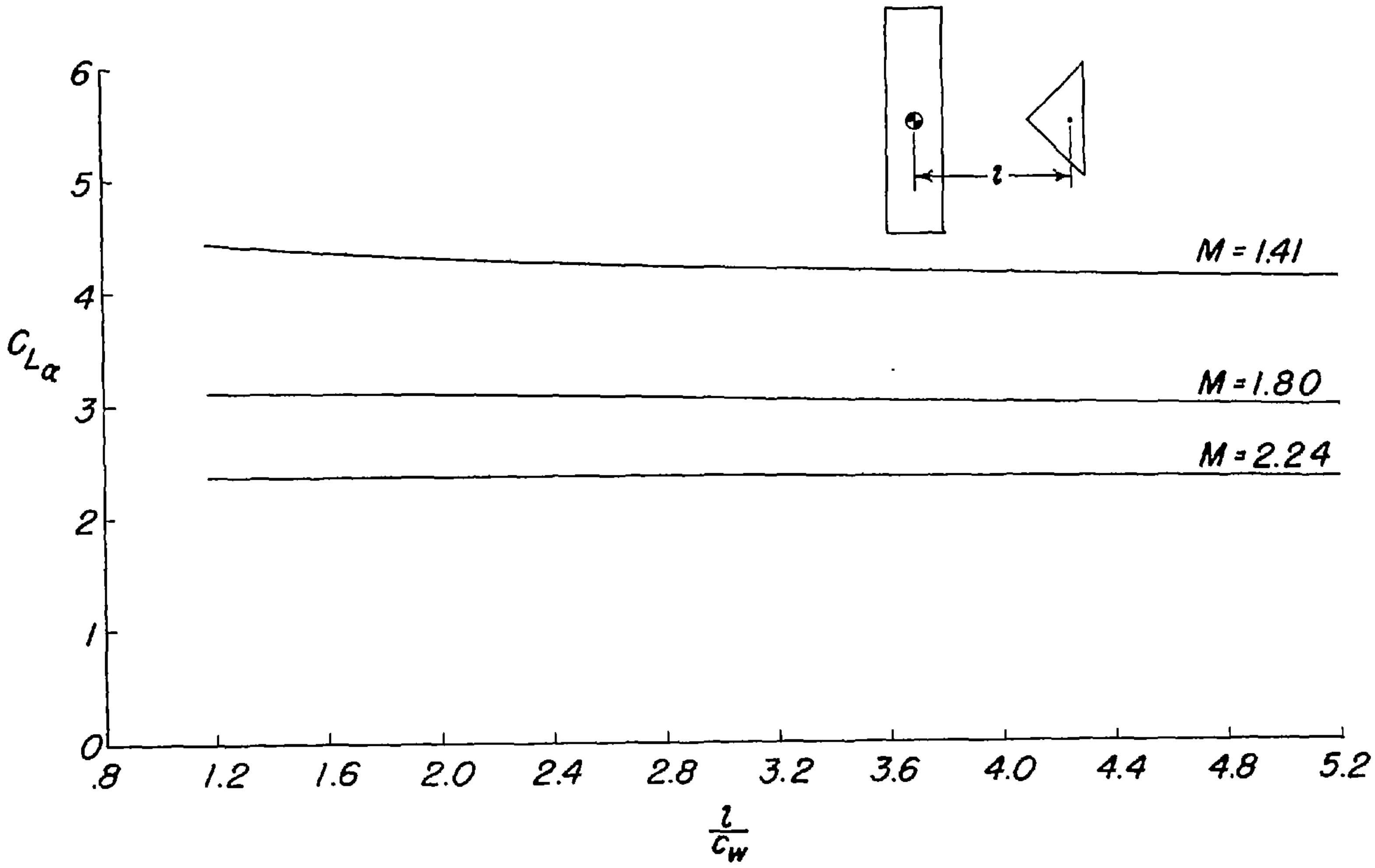

(d) Wing aspect ratio 4; $\frac{c_t}{c_w} = 1$.

Figure 32.- Concluded.

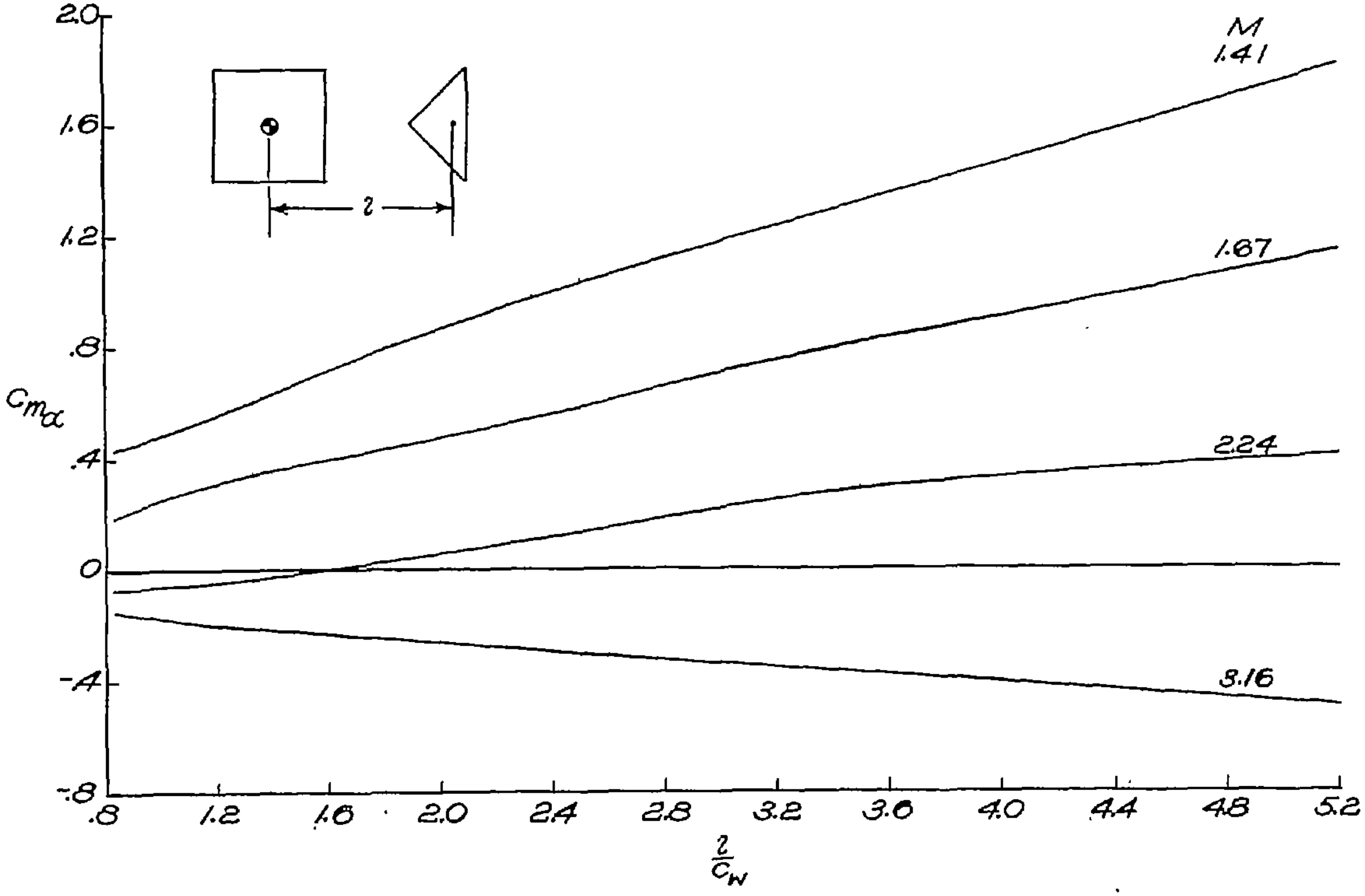

(a) Wing aspect ratio 1; $\frac{c_t}{c_w} = \frac{1}{2}$.

Figure 33.- Variation of C_{m_α} with l/c_w for several rectangular-wing—triangular-tail combinations and several Mach numbers.

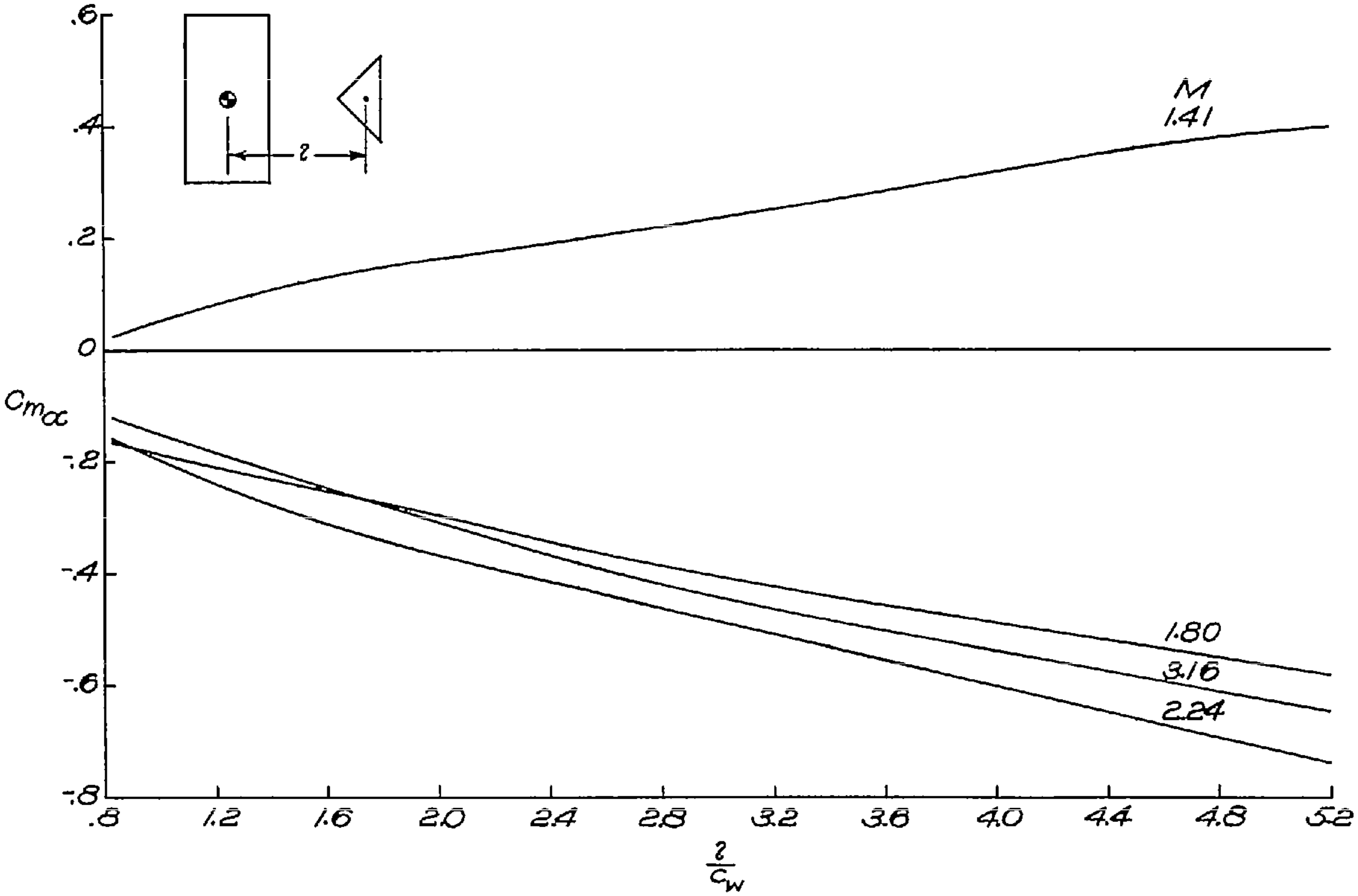

(b) Wing aspect ratio 2; $\frac{c_t}{c_w} = \frac{1}{2}$.

Figure 33.- Continued.

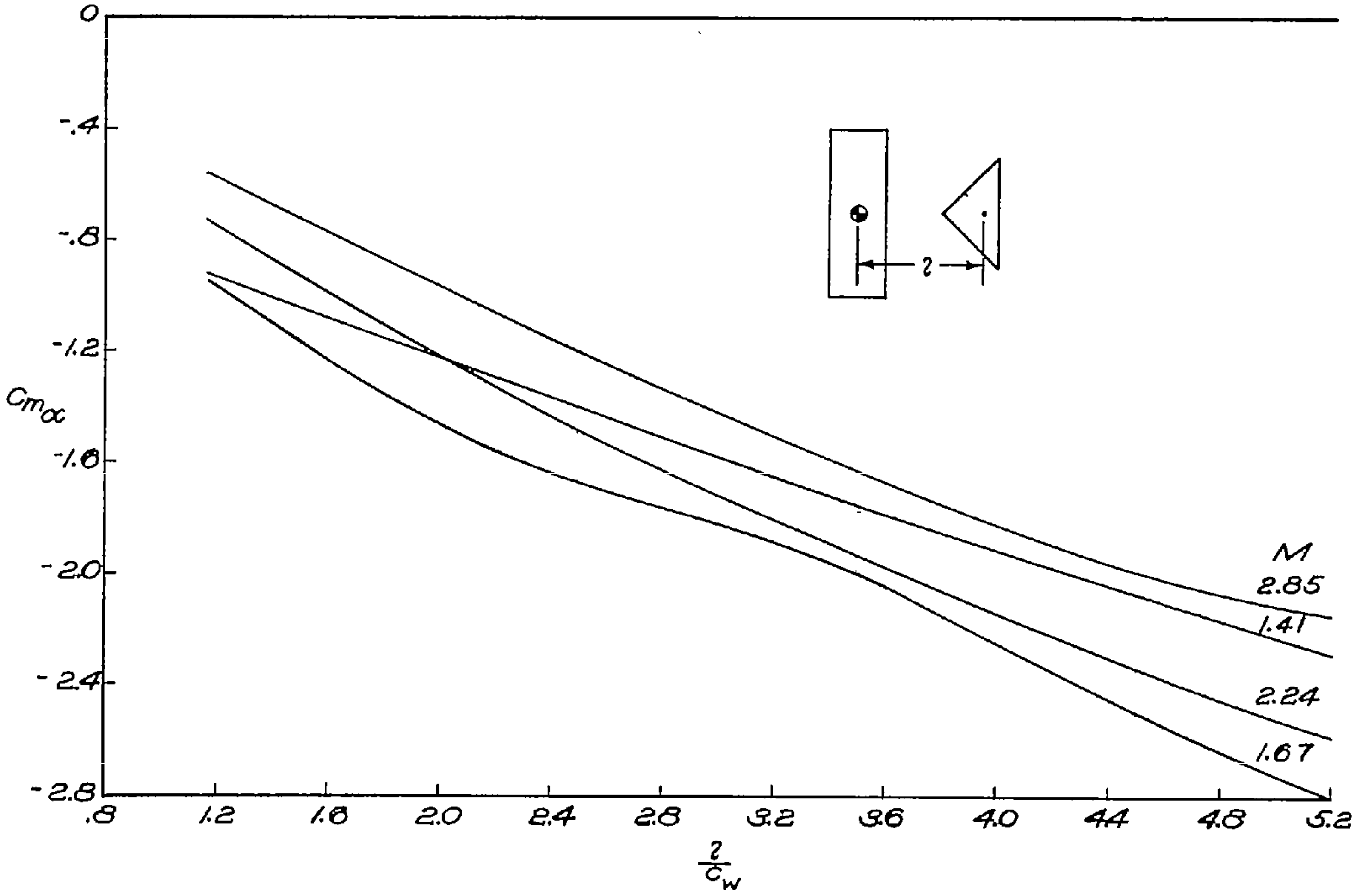

(c) Wing aspect ratio 3; $\frac{c_t}{c_w} = 1$.

Figure 33.- Continued.

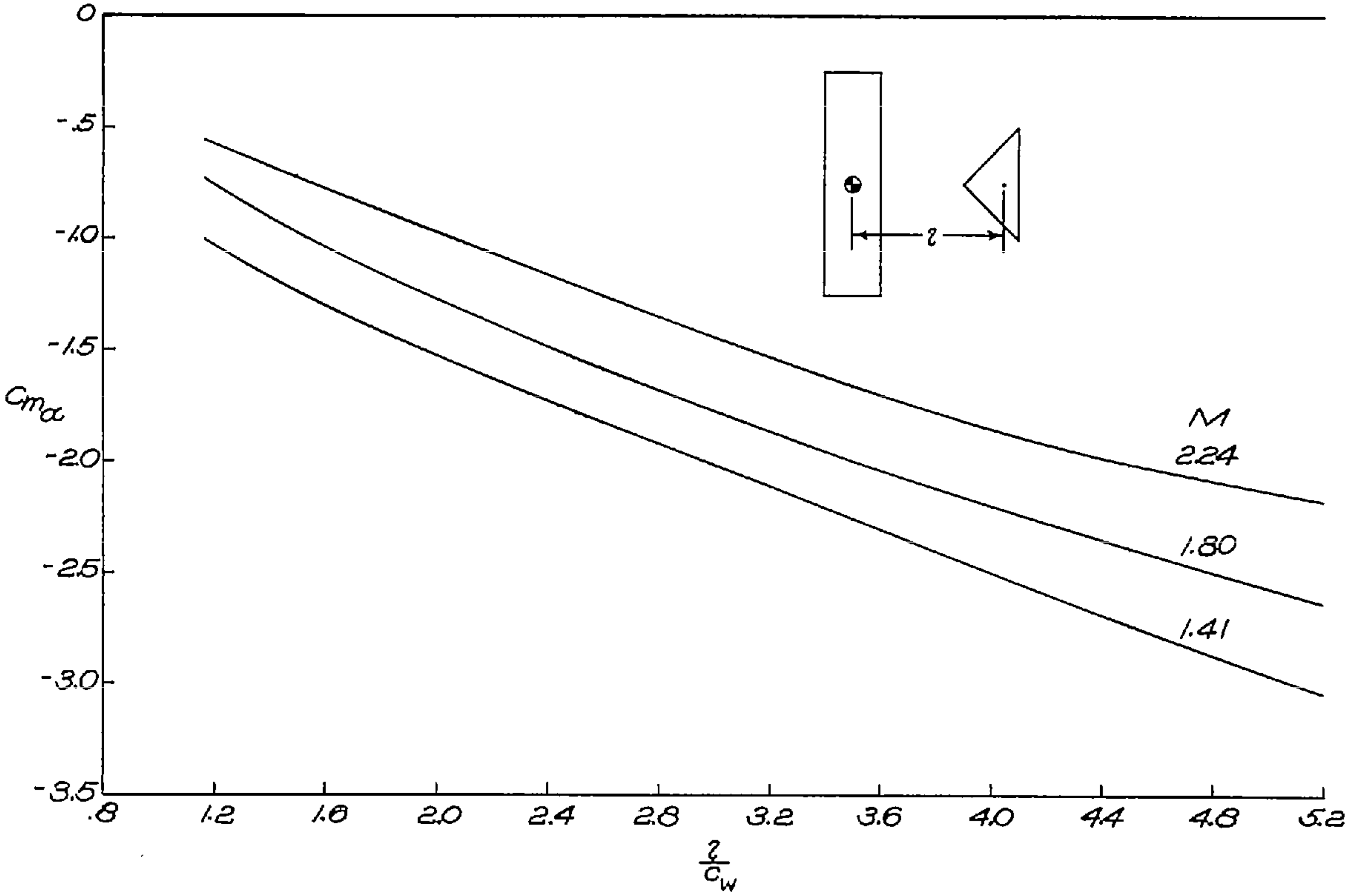

(d) Wing aspect ratio 4; $\frac{c_t}{c_w} = 1$.

Figure 33.- Concluded.

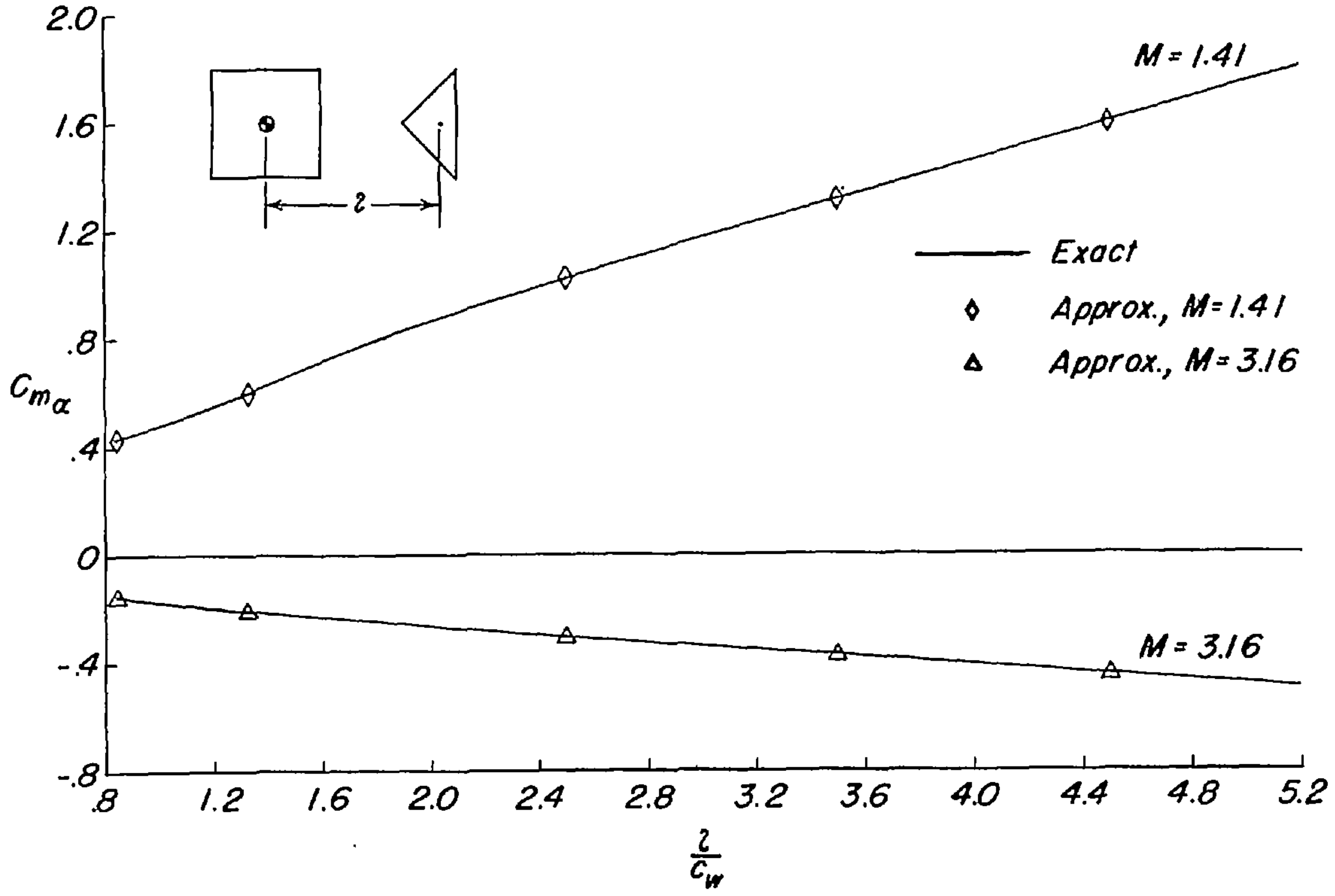

(a) Wing aspect ratio 1; $\frac{c_t}{c_w} = \frac{1}{2}$.

Figure 34.- Comparison of exact (linearized) and approximate (eq. (53)) values of C_{m_α} for two rectangular-wing—triangular-tail combinations.

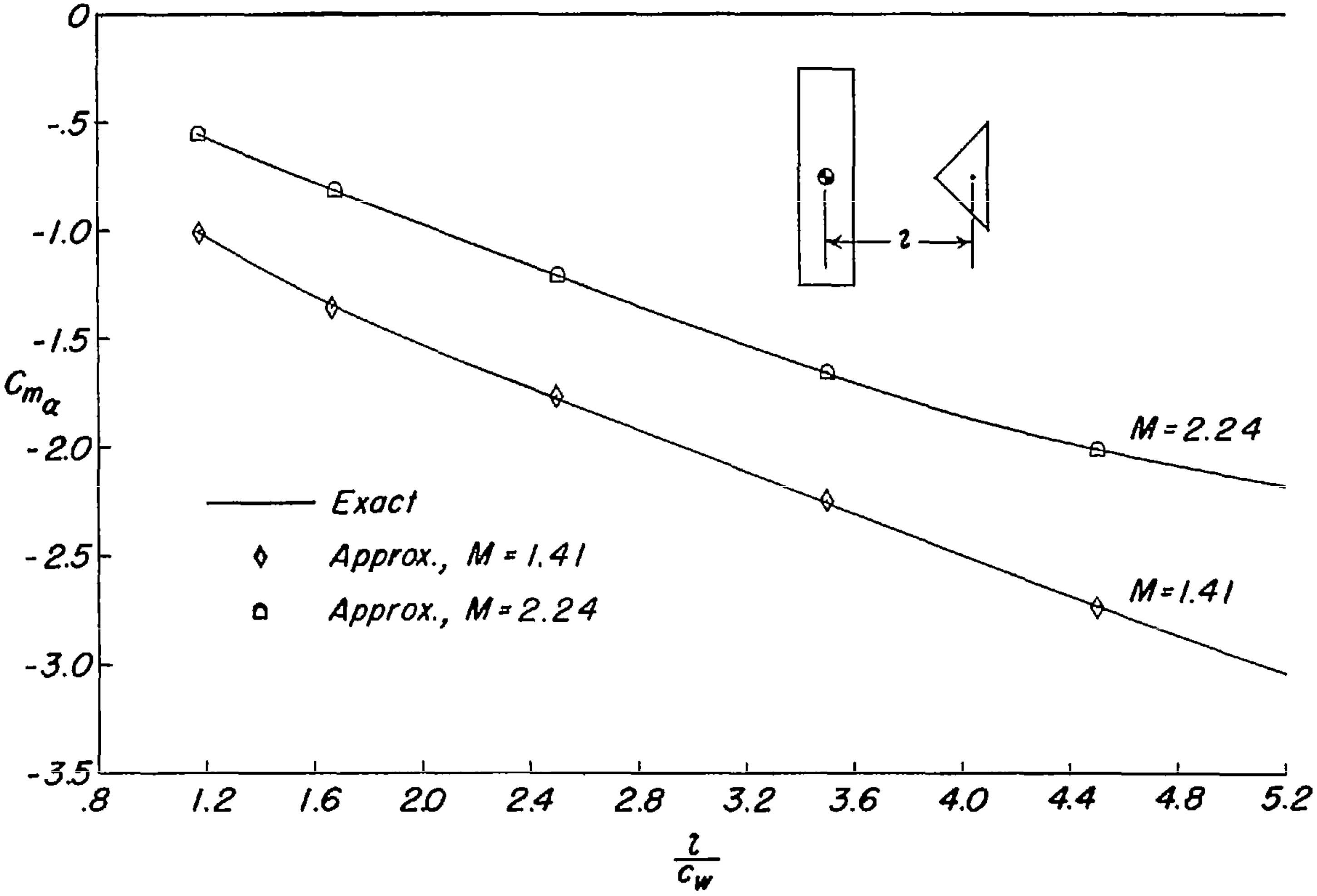

(b) Wing aspect ratio 4; $\frac{c_t}{c_w} = 1$.

Figure 34.- Concluded.

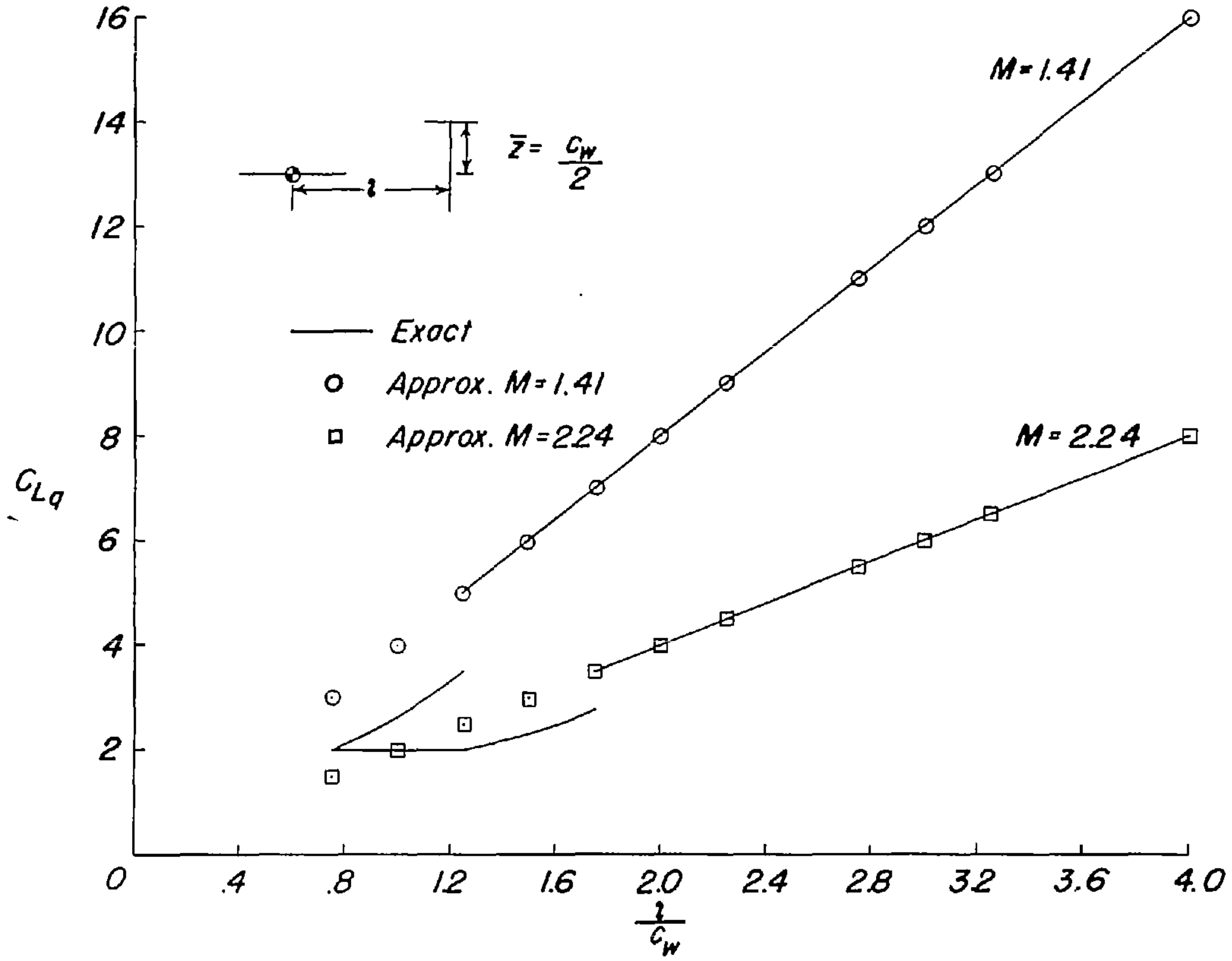

Figure 35.- Comparison of exact (linearized) and approximate (eq. (65)) values of C_{L_q} for a two-dimensional wing-tail combination for two Mach numbers. $\bar{z} = c_t = \frac{c_W}{2}$.

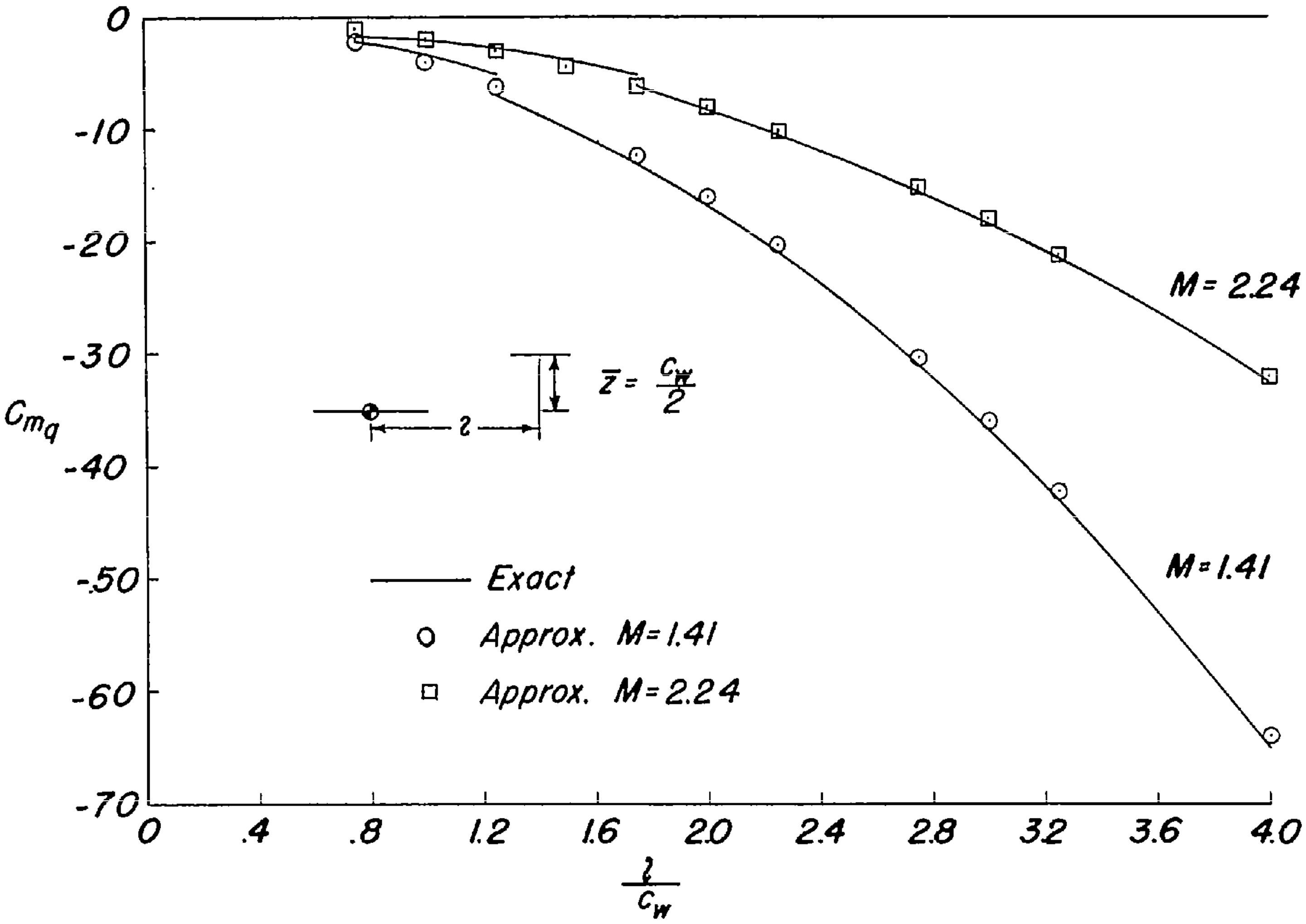

Figure 36.- Comparison of exact (linearized) and approximate (eq. (66)) values of C_{m_q} for a two-dimensional wing-tail combination for two Mach numbers. $\bar{x} = c_t = \frac{c_w}{2}$.

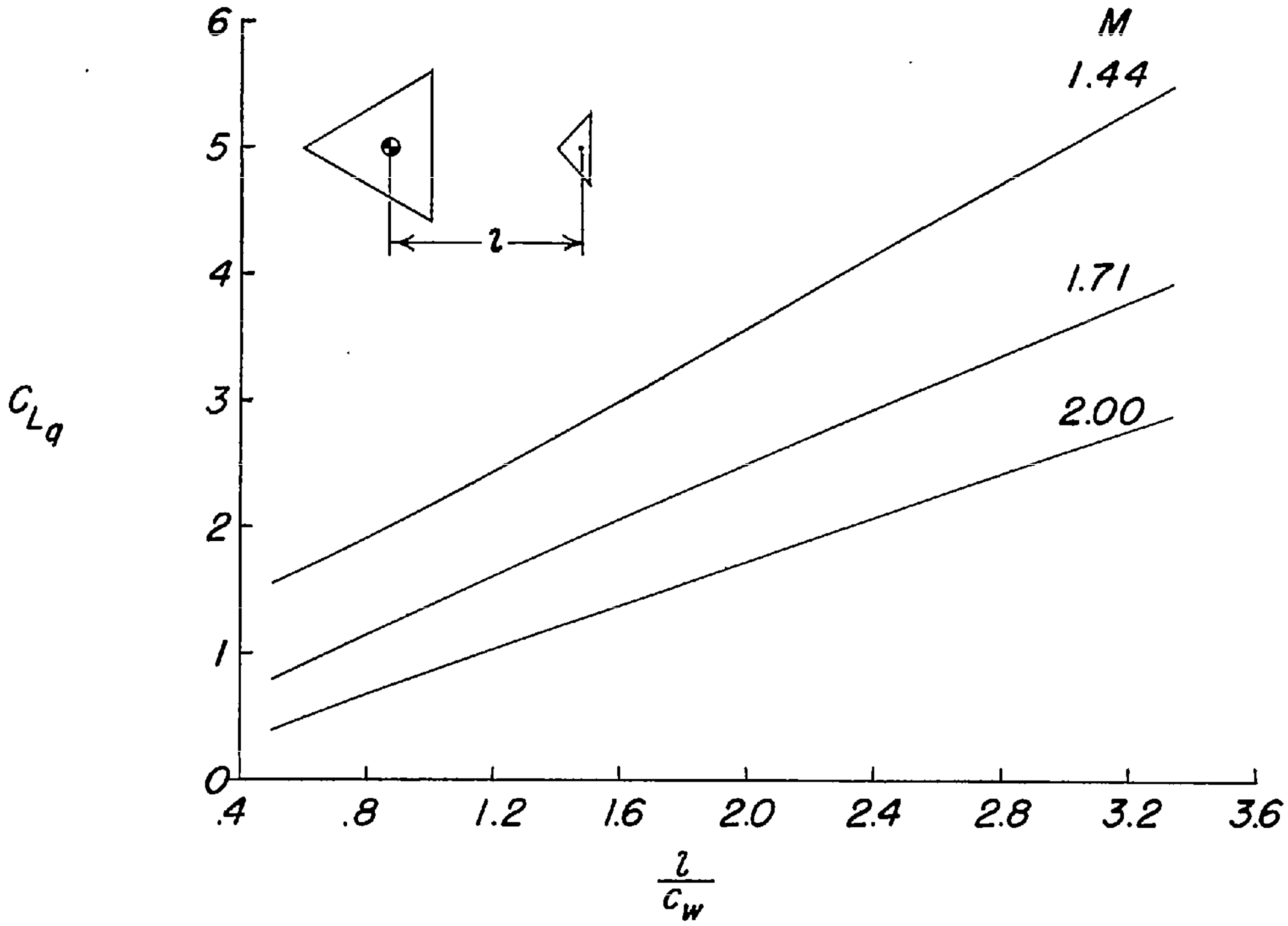

Figure 37.- Variation of C_{L_q} with l/c_w for three Mach numbers for a triangular wing-tail combination.

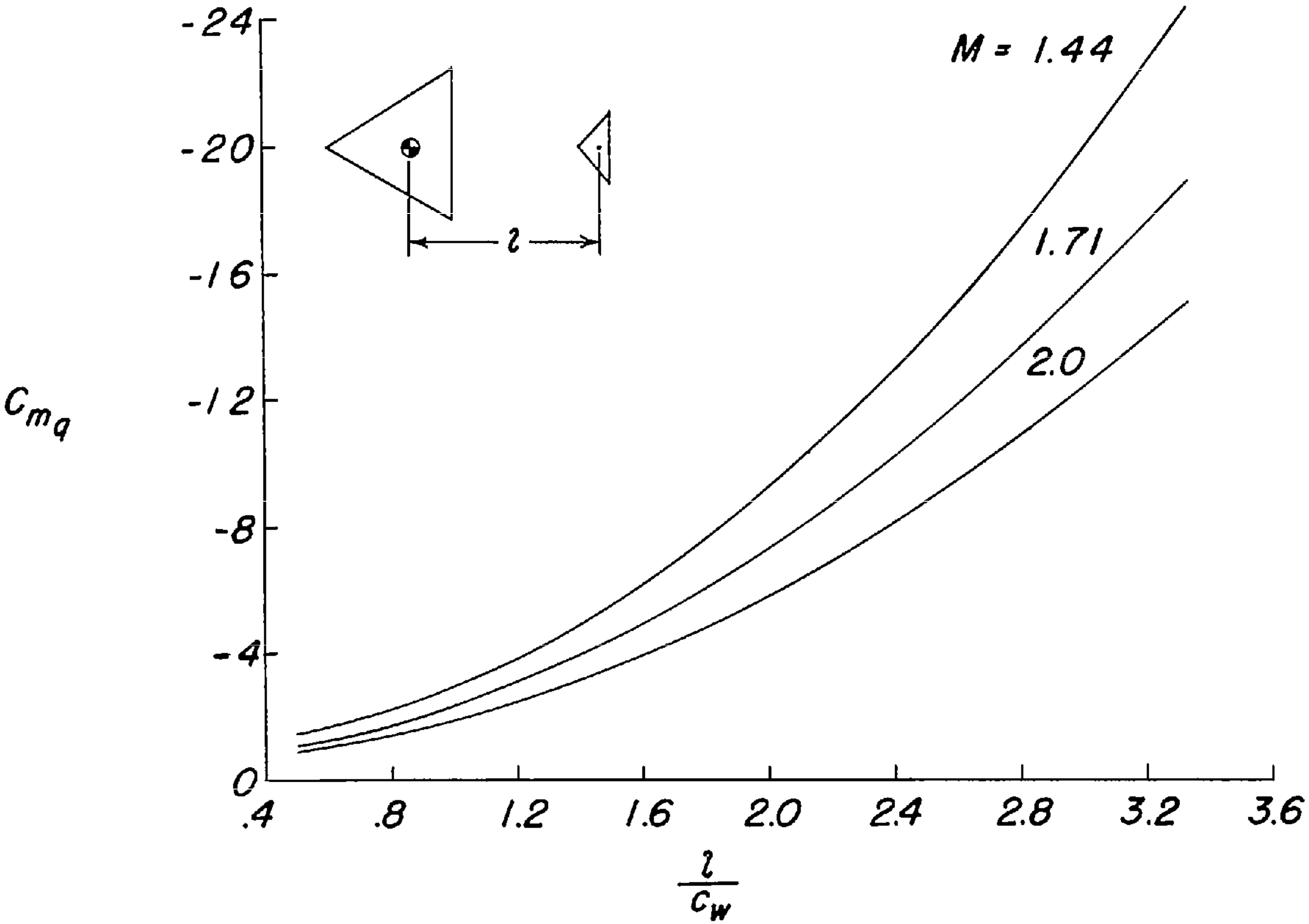

Figure 38.- Variation of C_{m_q} with l/c_w for three Mach numbers for a triangular wing-tail combination.

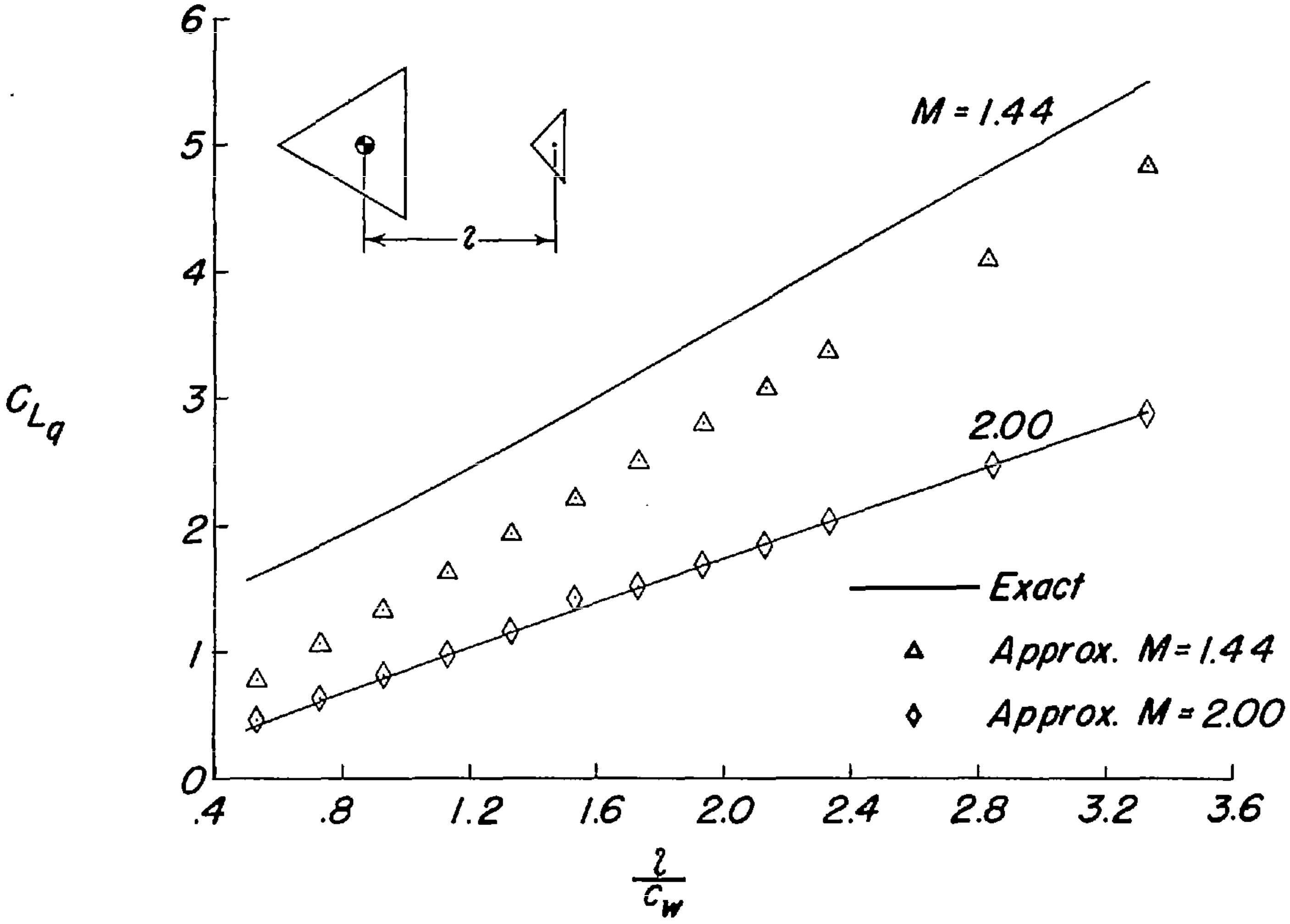

Figure 39.- Comparison of exact (linearized) and approximate (eq. (65)) values of C_{L_q} for a triangular wing-tail combination at two Mach numbers.

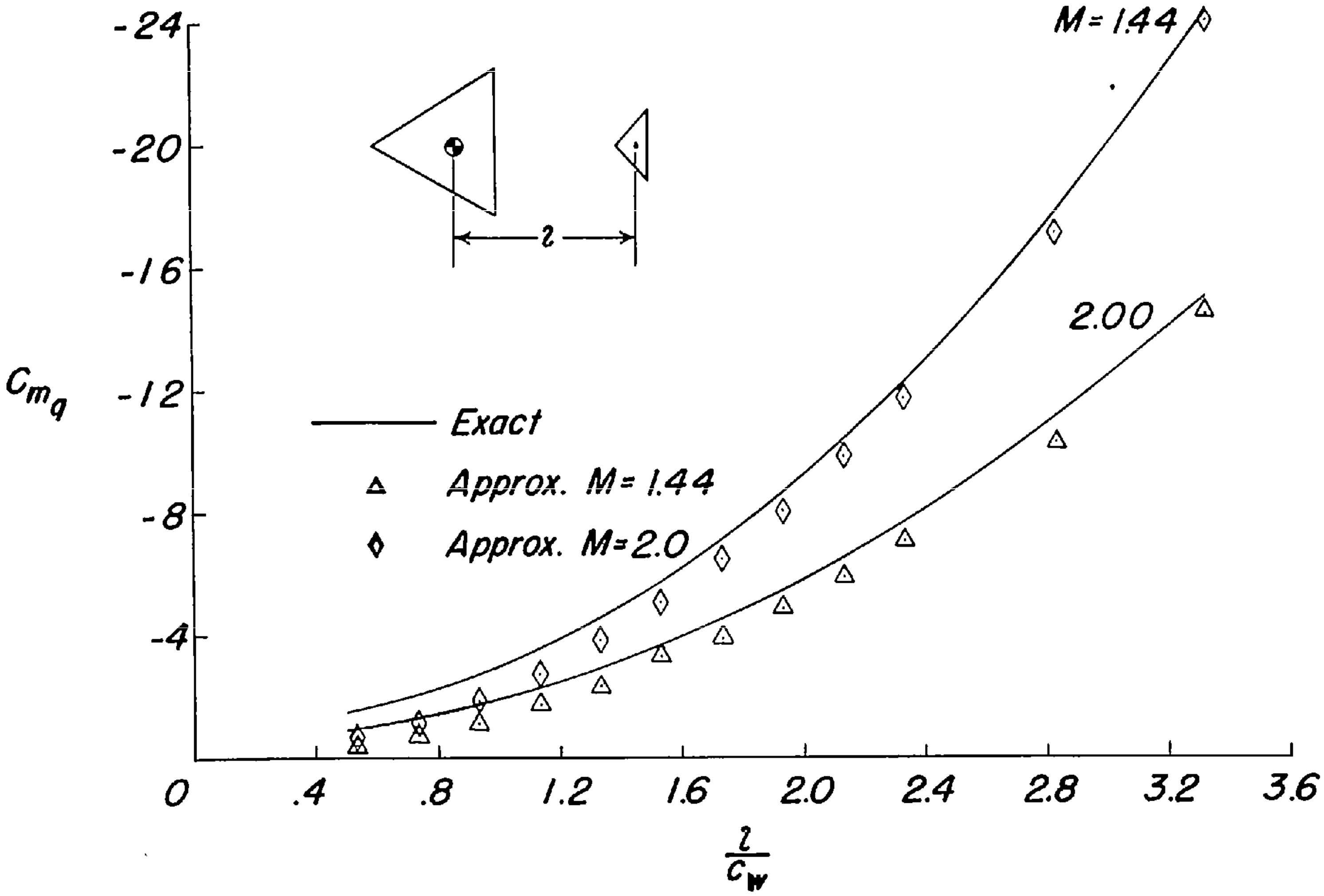

Figure 40.- Comparison of exact (linearized) and approximate (eq. (66)) values of C_{m_q} for a triangular wing-tail combination at two Mach numbers.

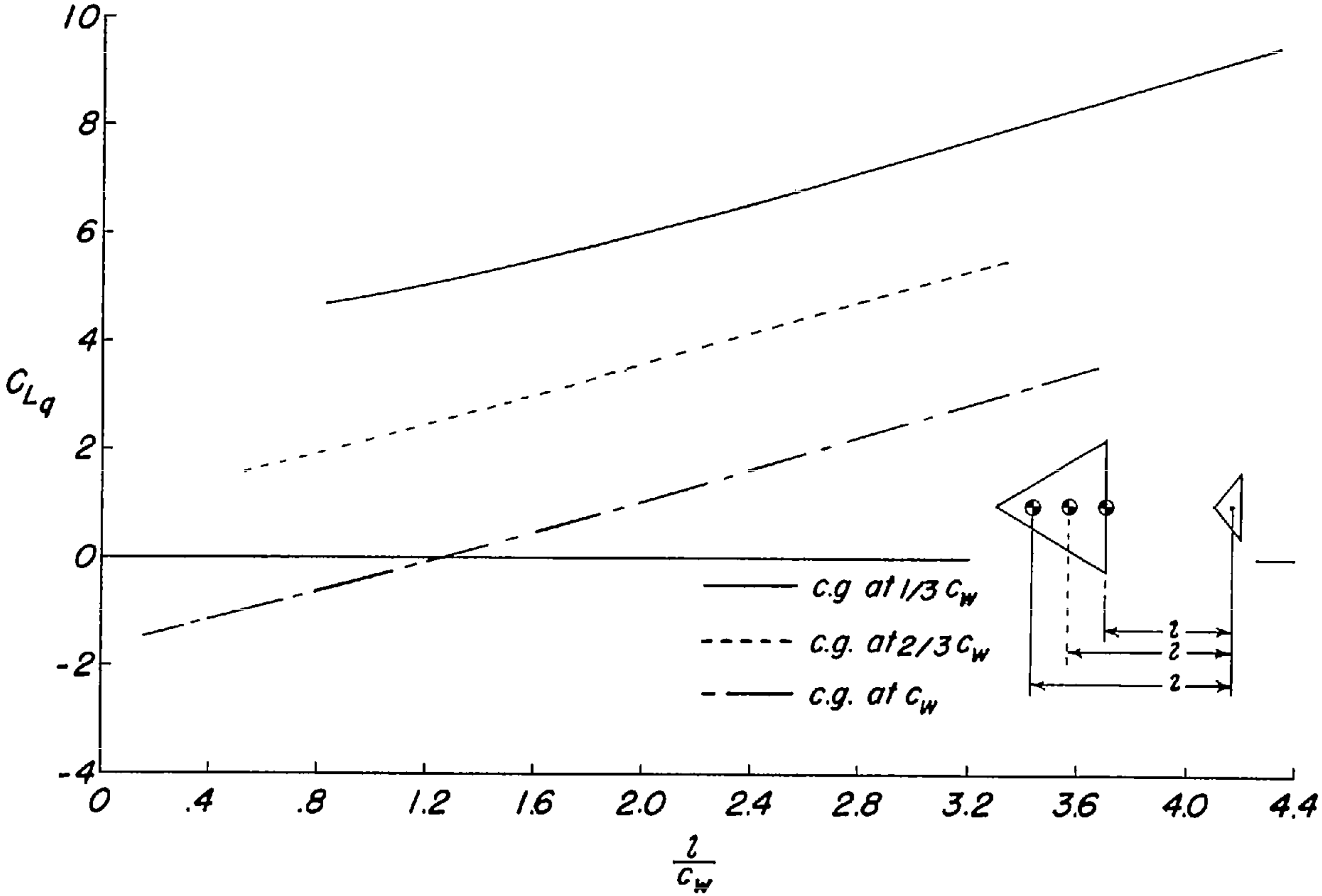

Figure 41.- Variation of C_{L_q} with l/c_w for three center-of-gravity locations for a triangular wing-tail combination. M = 1.44.

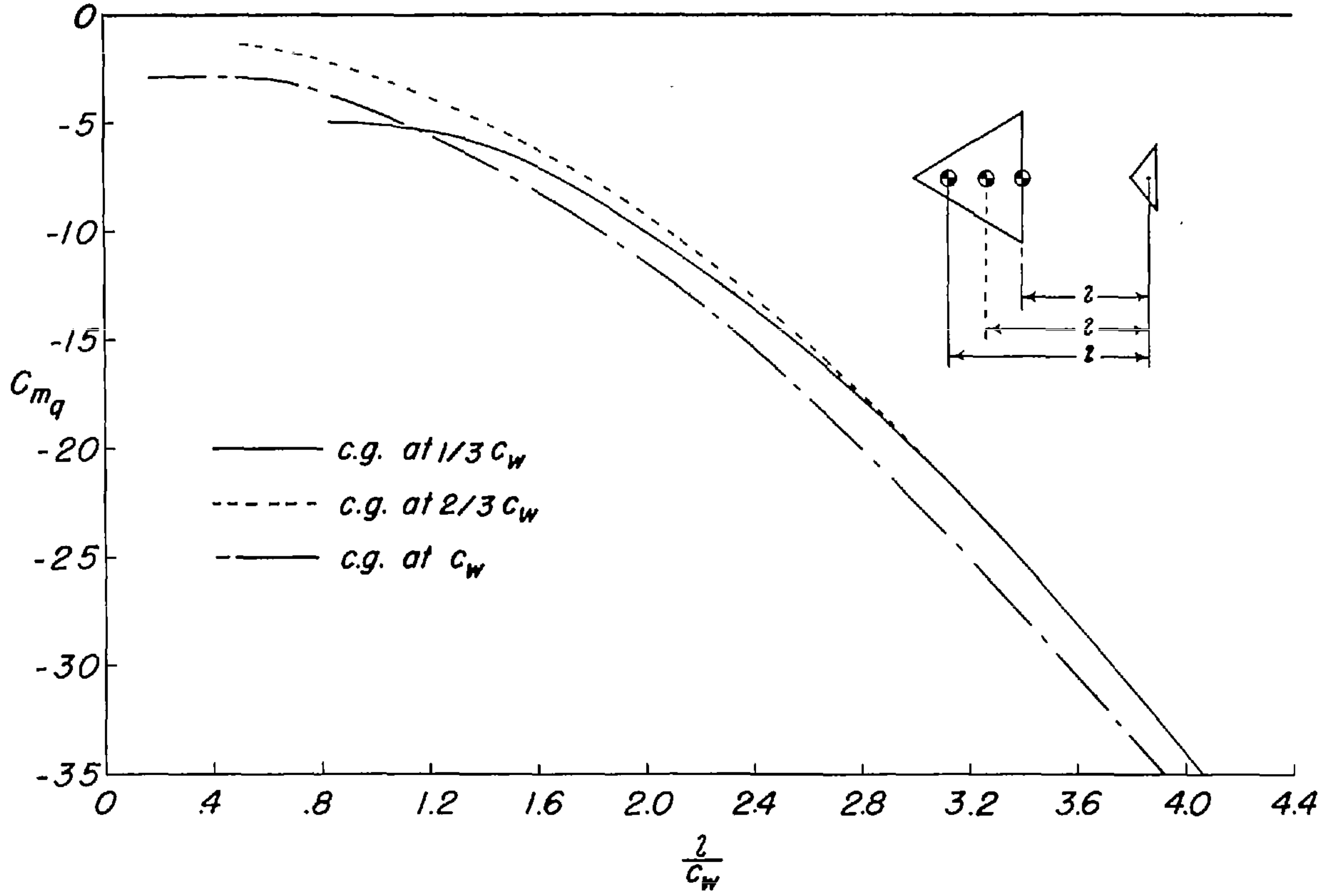

Figure 42.- Variation of C_{m_q} with l/c_w for three center-of-gravity locations for a triangular wing-tail combination. M = 1.44.

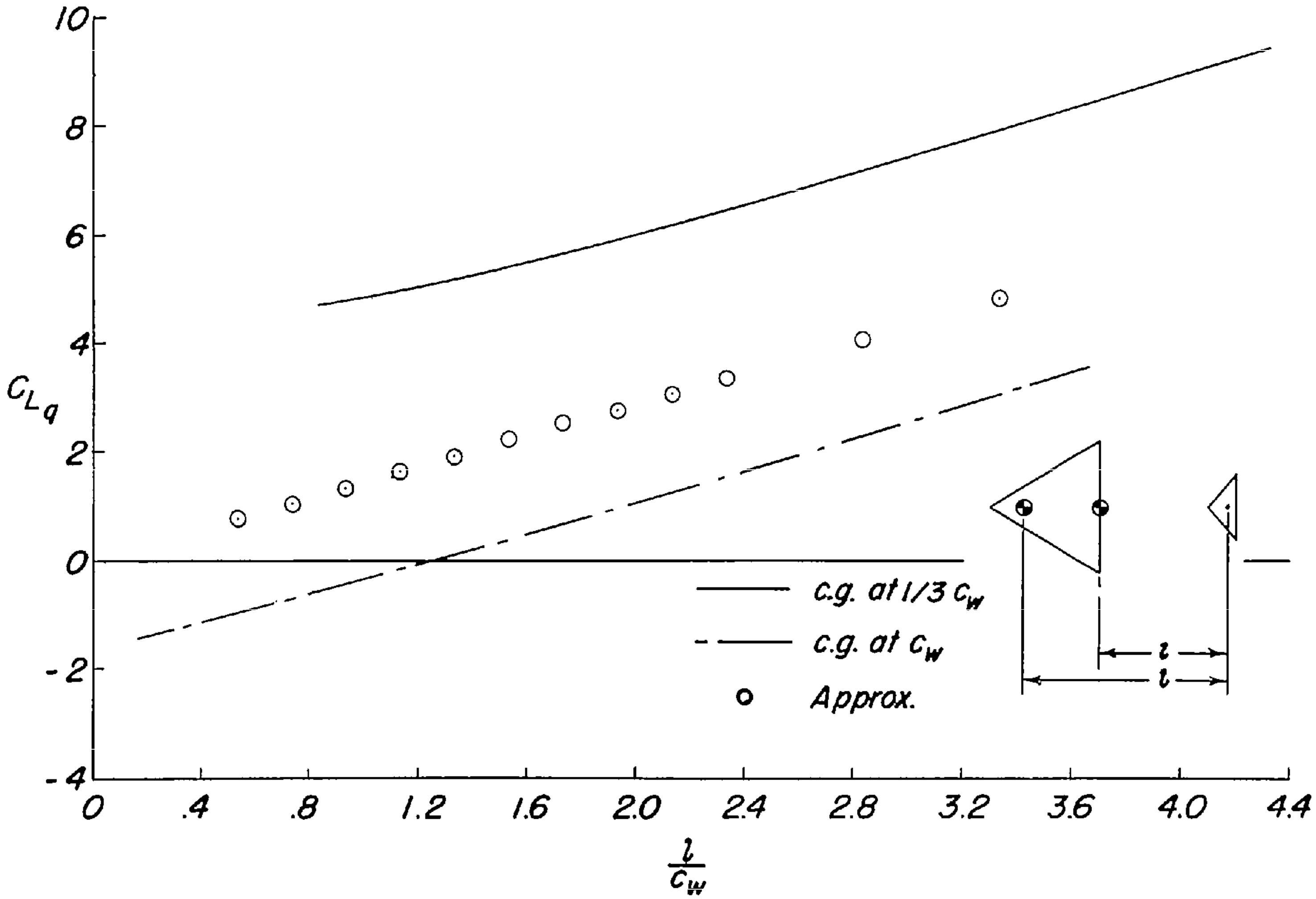

Figure 43.- Comparison of exact (linearized) and approximate (eq. (65)) values of C_{L_q} for two center-of-gravity locations for a triangular wing-tail combination. M = 1.44.

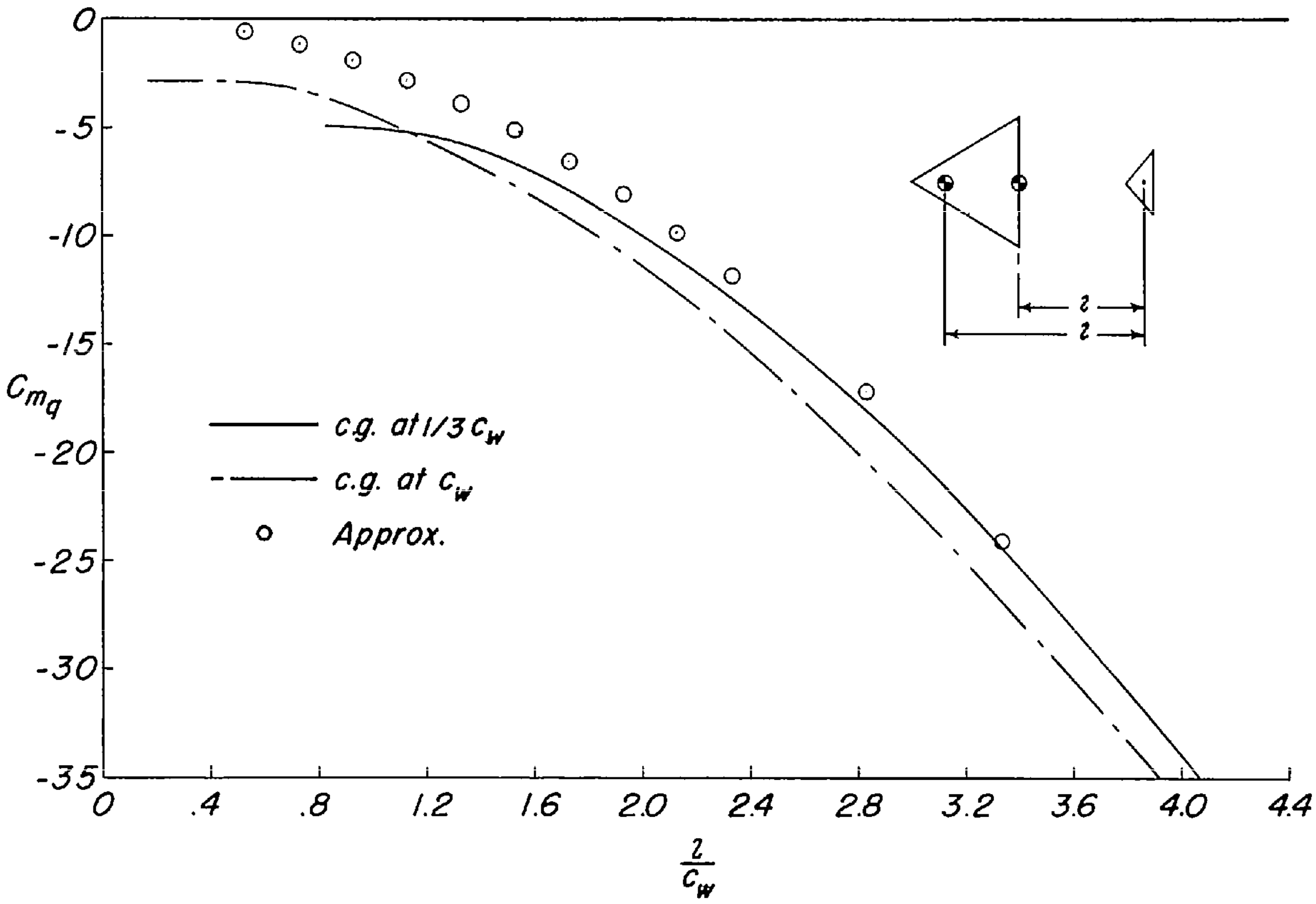

Figure 44.- Comparison of exact (linearized) and approximate (eq. (66)) values of C_{m_q} for two center-of-gravity locations for a triangular wing-tail combination. M = 1.44.

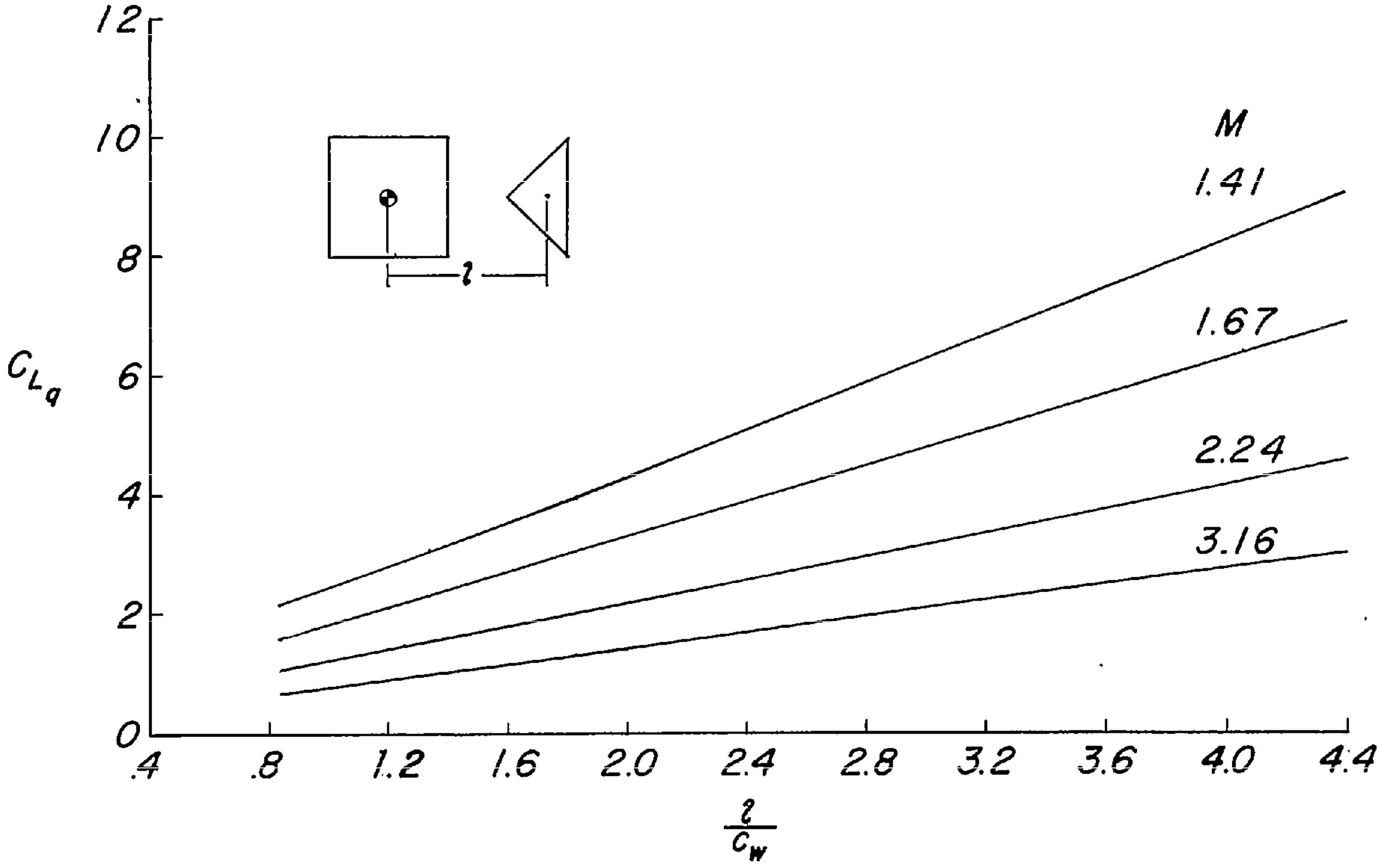

(a) Wing aspect ratio 1; $\frac{c_t}{c_w} = \frac{1}{2}$.

Figure 45.- Variation of C_{L_q} with l/c_w for several rectangular-wing—triangular-tail combinations.

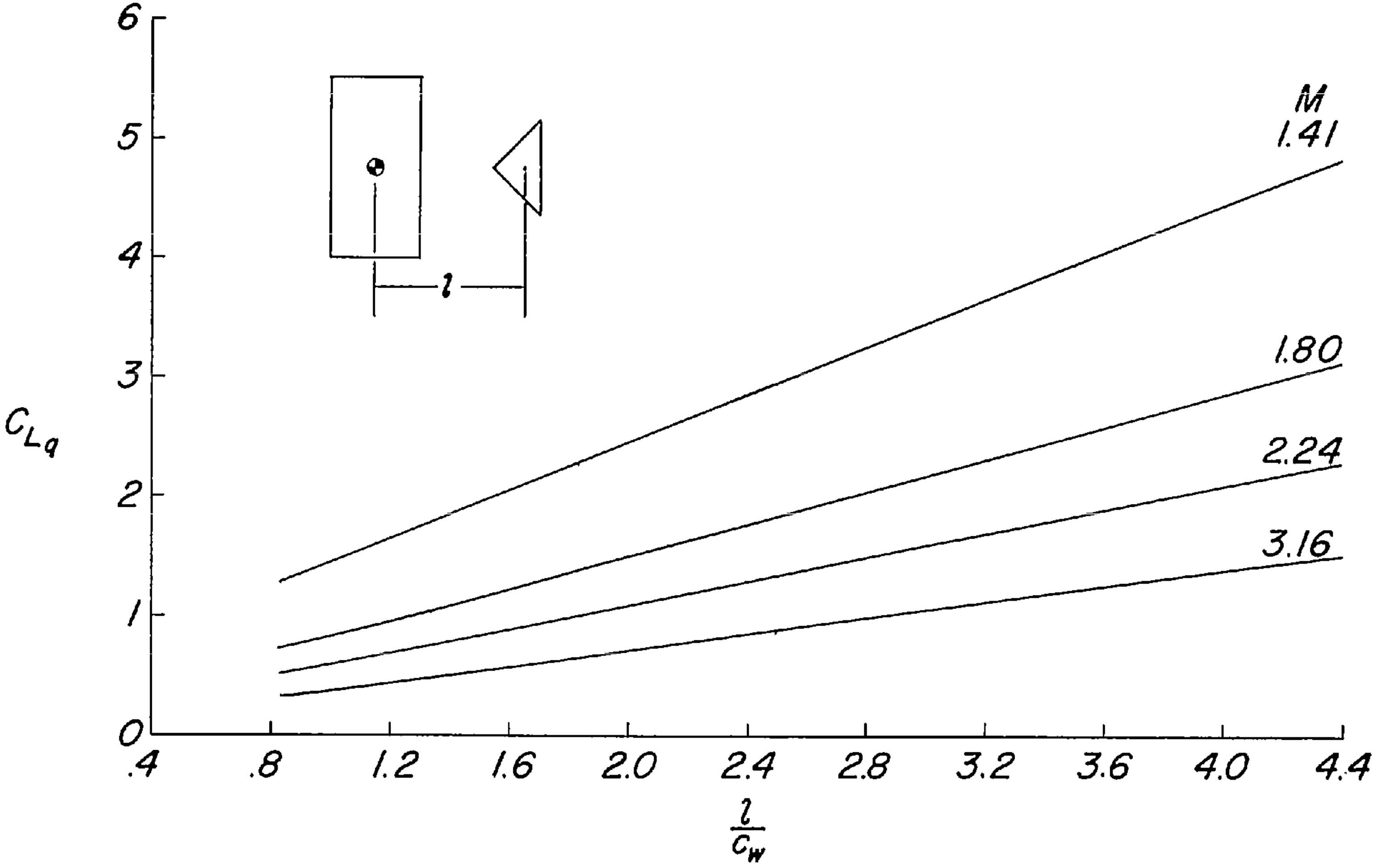

(b) Wing aspect ratio 2; $\frac{c_t}{c_w} = \frac{1}{2}$.

Figure 45.- Continued.

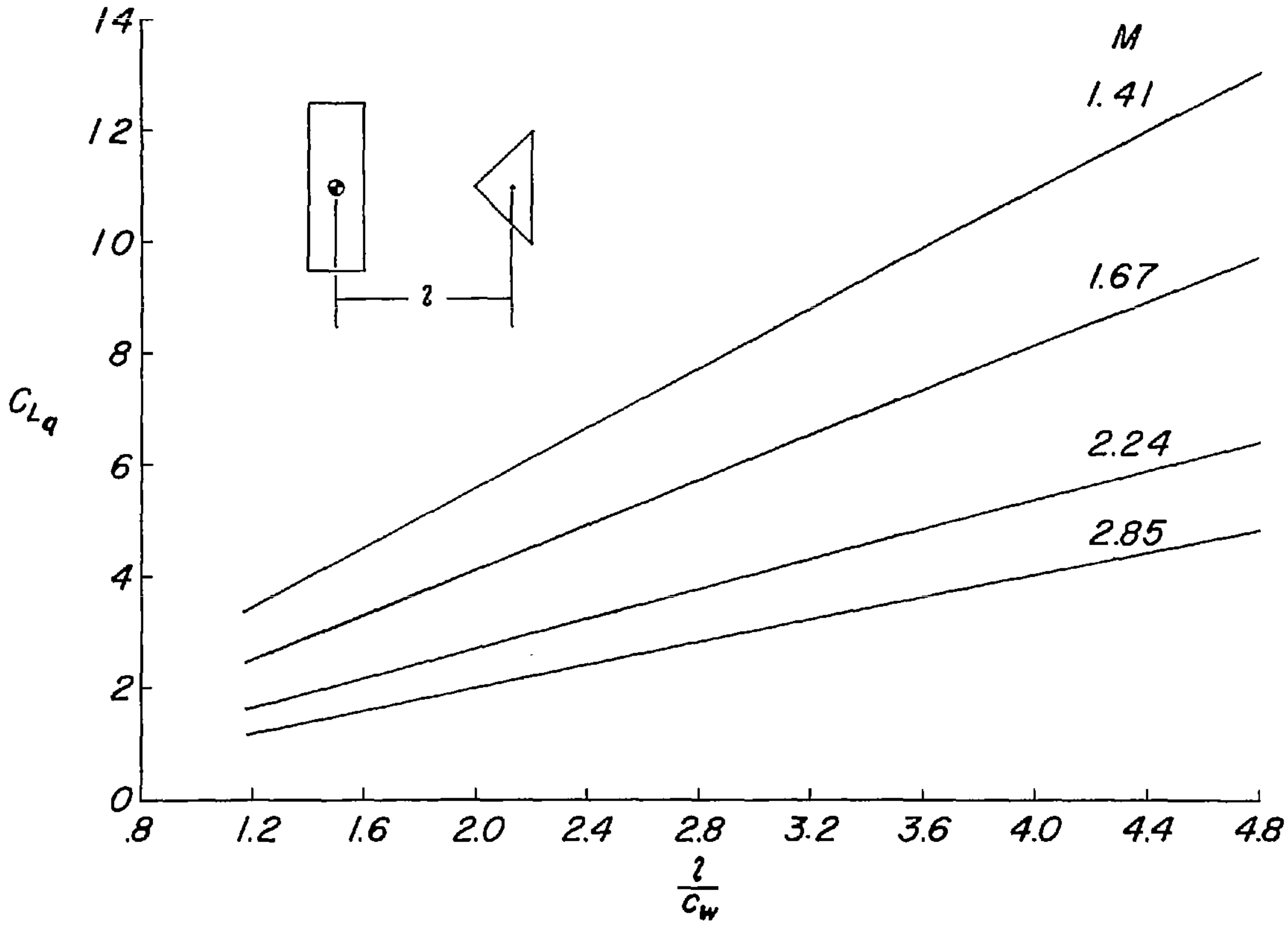

(c) Wing aspect ratio 3; $\frac{c_t}{c_w} = 1$.

Figure 45.- Continued.

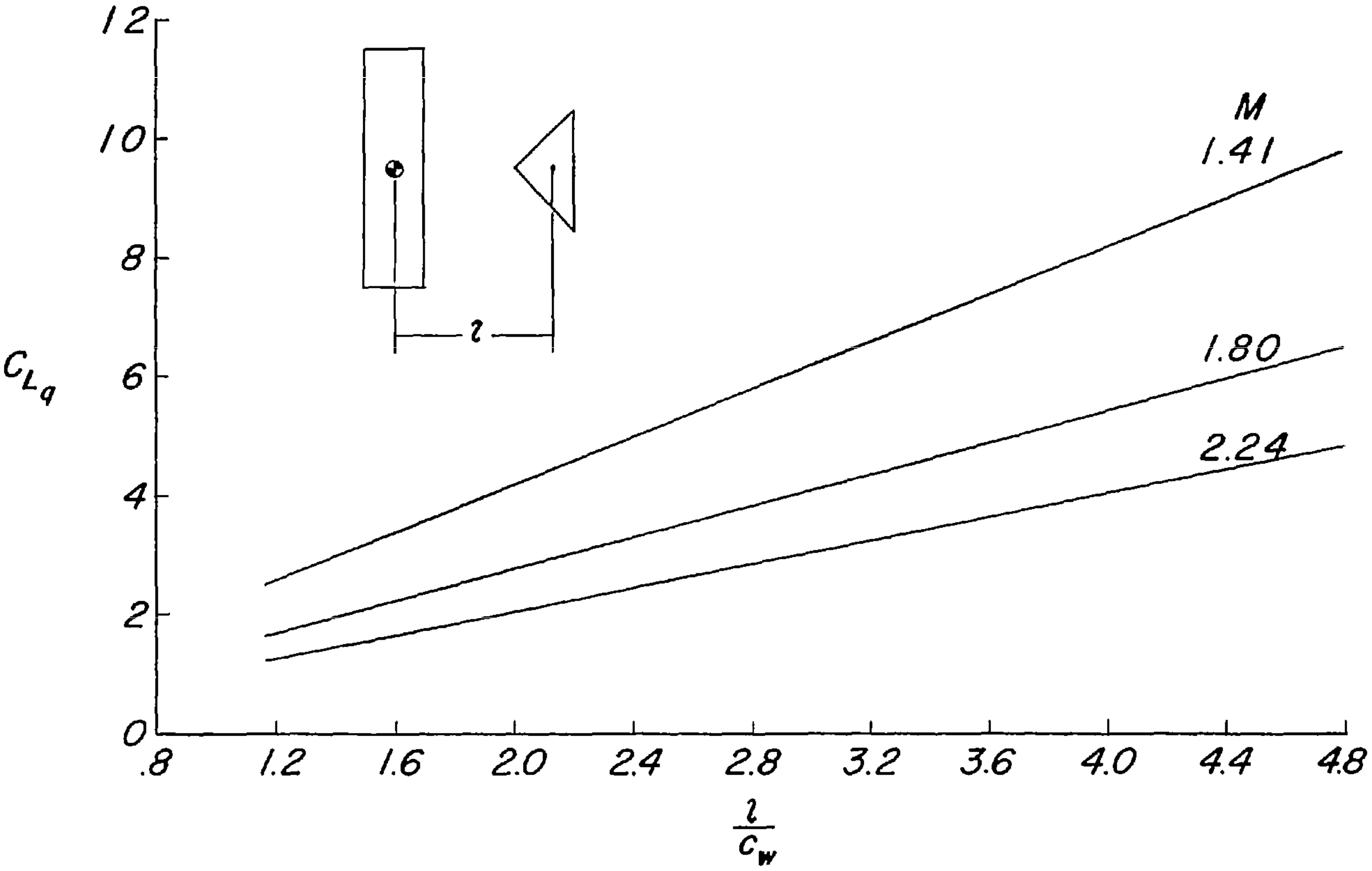

(d) Wing aspect ratio 4; $\frac{c_t}{c_w} = 1$.

Figure 45.- Concluded.

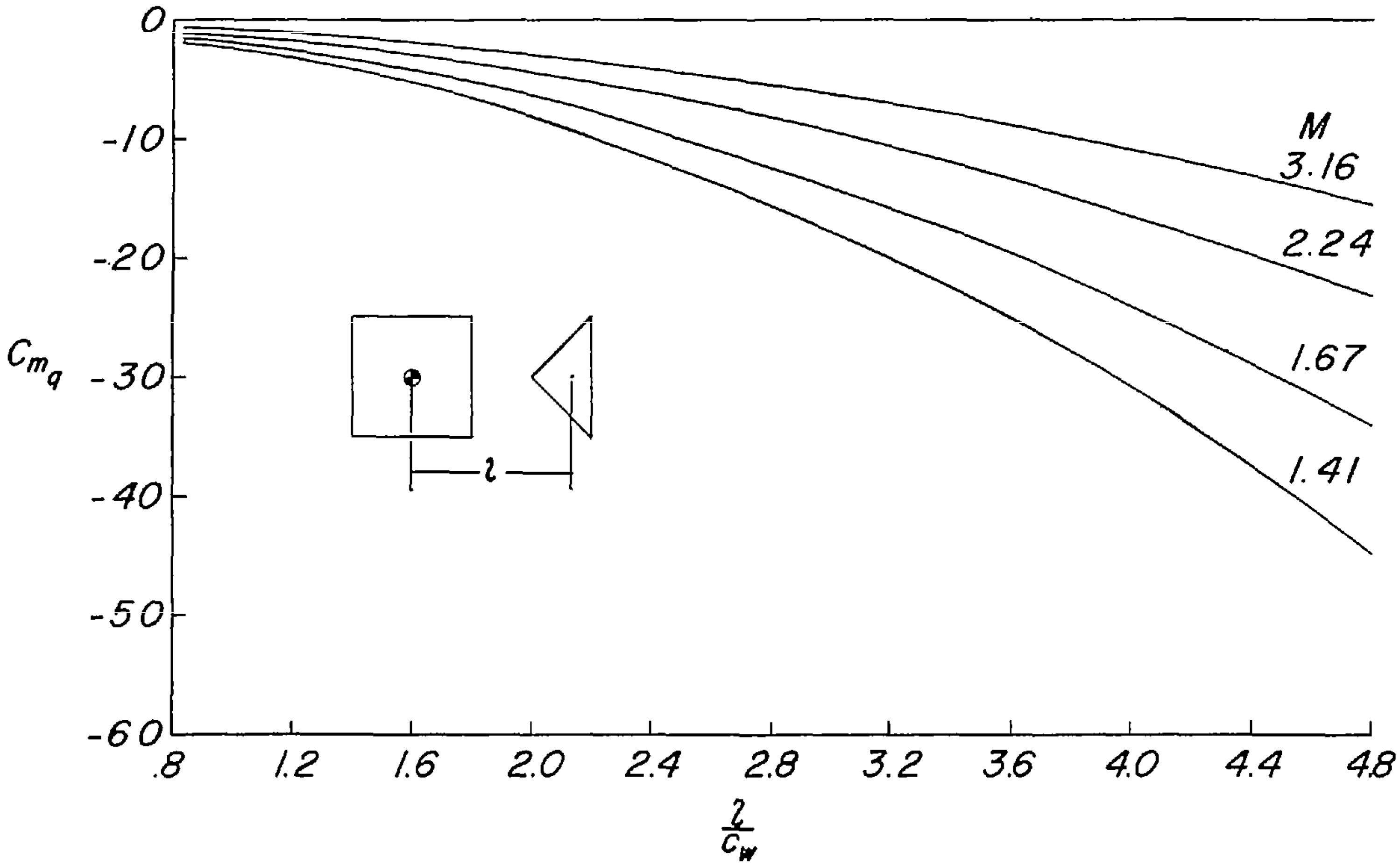

(a) Wing aspect ratio 1; $\frac{c_t}{c_w} = \frac{1}{2}$.

Figure 46.- Variation of C_{m_q} with l/c_w for several rectangular-wing—triangular-tail combinations.

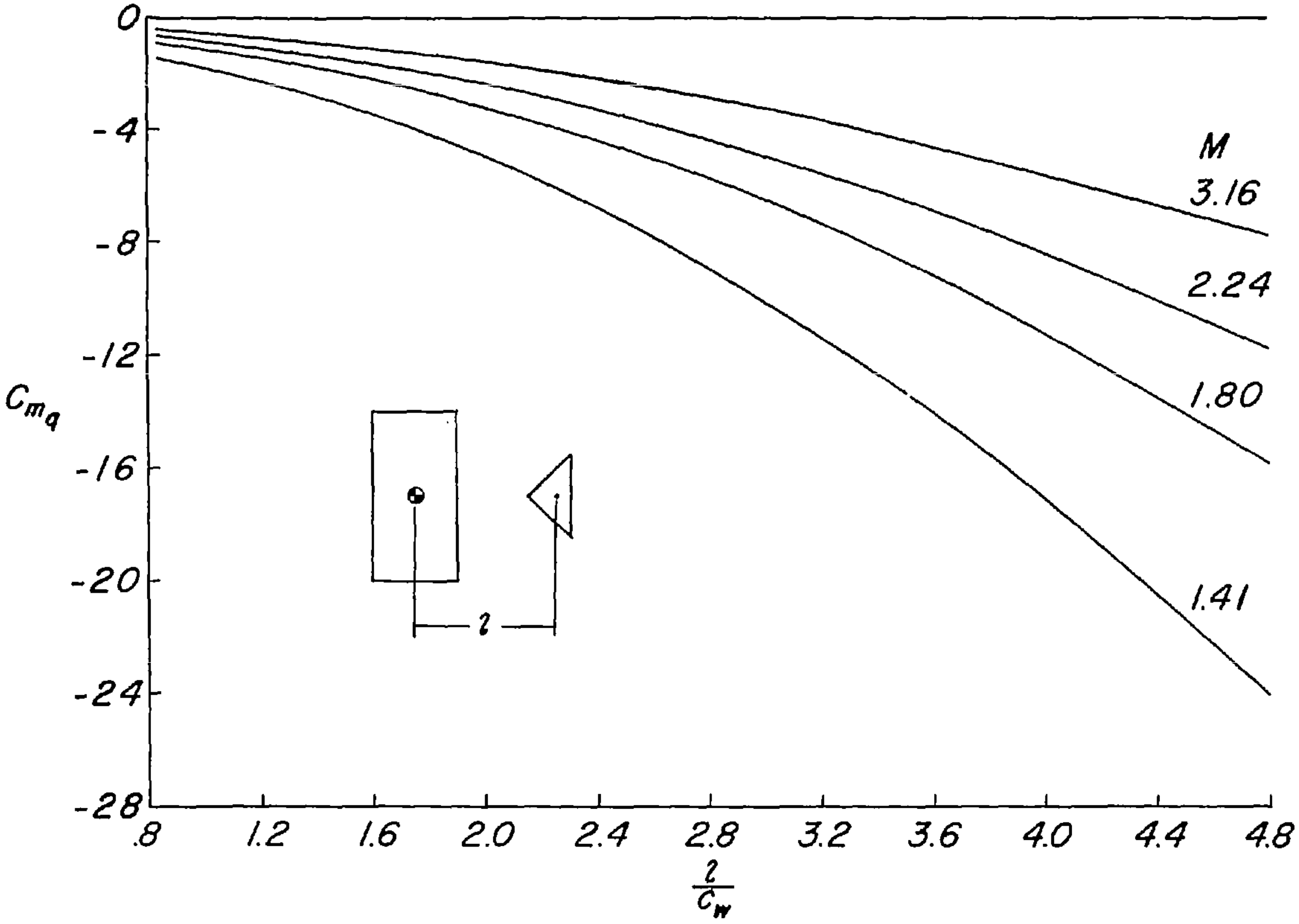

(b) Wing aspect ratio 2; $\frac{c_t}{c_w} = \frac{1}{2}$.

Figure 46.- Continued.

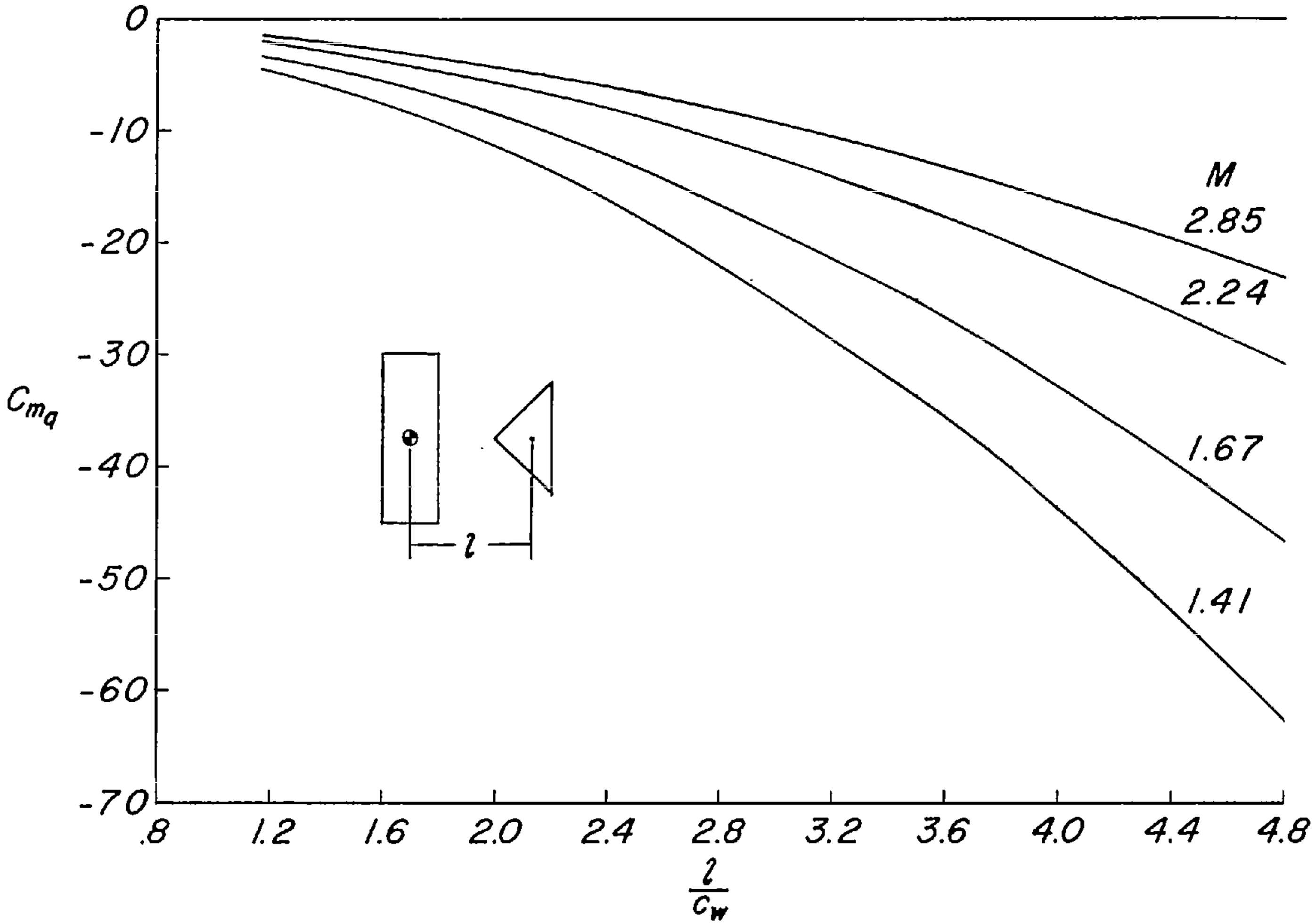

(c) Wing aspect ratio 3; $\frac{c_t}{c_w} = 1$.

Figure 46.- Continued.

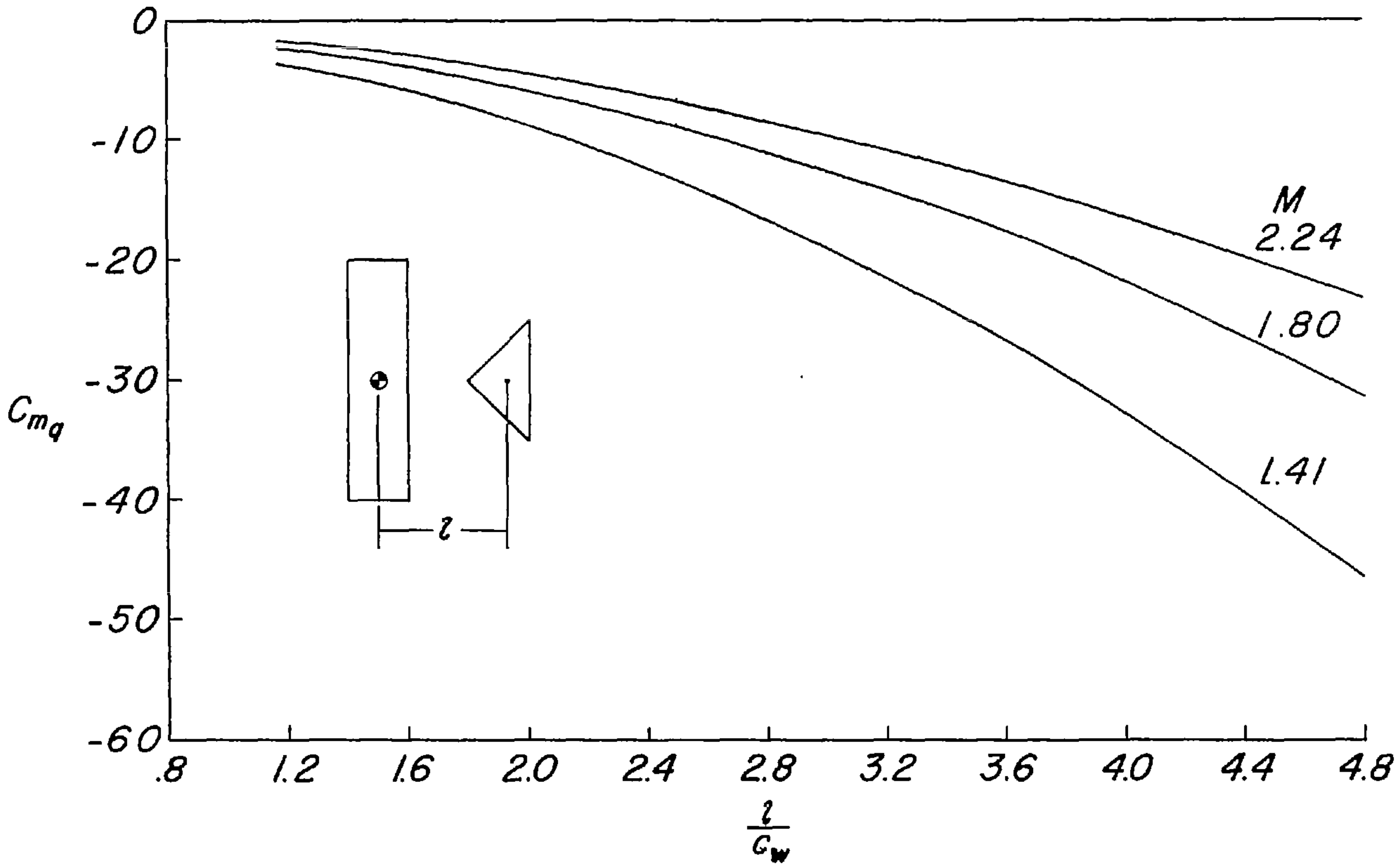

(d) Wing aspect ratio 4; $\frac{c_t}{c_w} = 1$.

Figure 46.- Concluded.

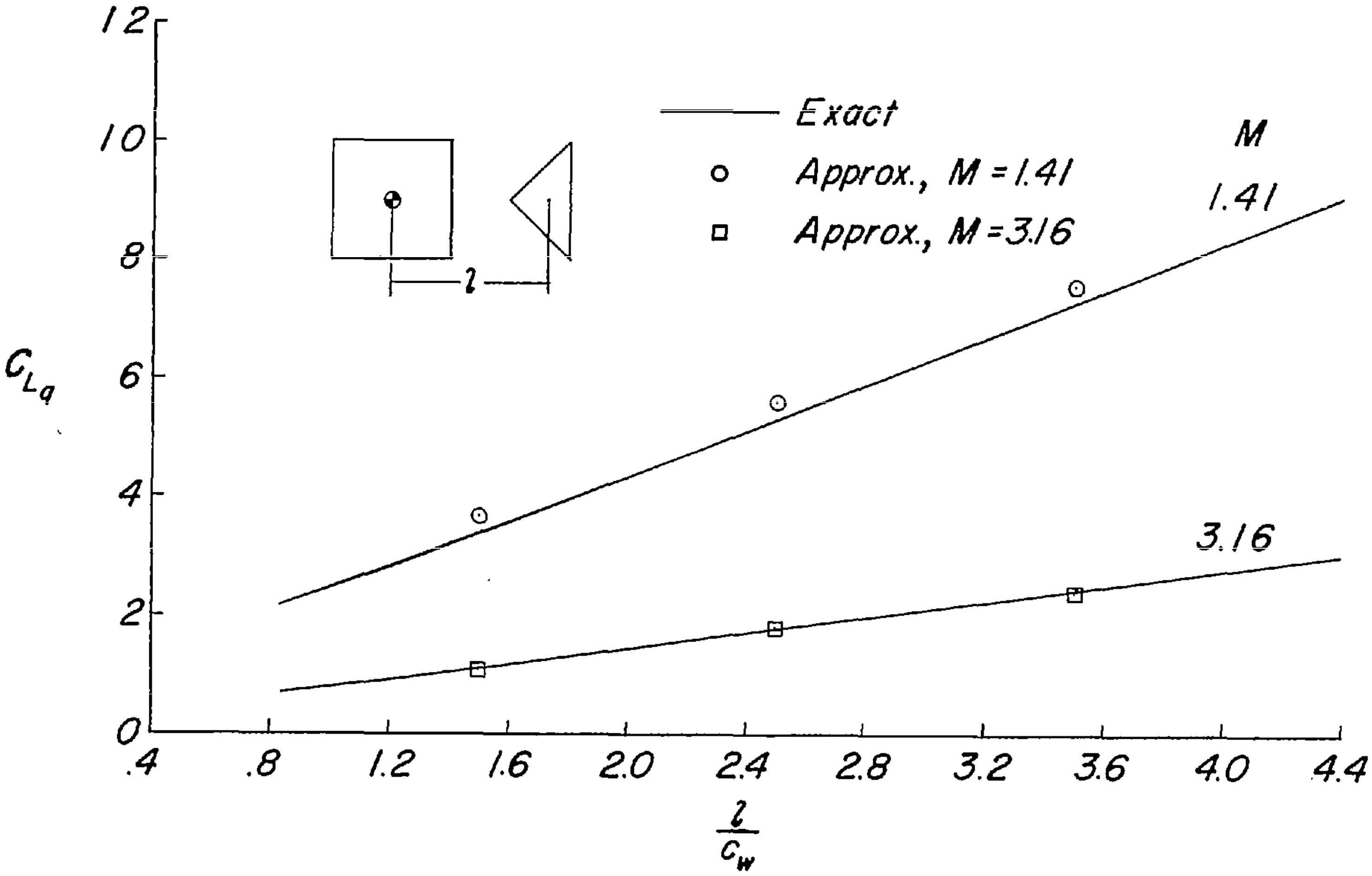

(a) Wing aspect ratio 1; $\frac{c_t}{c_w} = \frac{1}{2}$.

Figure 47.- Comparison of exact (linearized) and approximate (eq. (65)) values of C_{L_q} for two rectangular-wing—triangular-tail combinations.

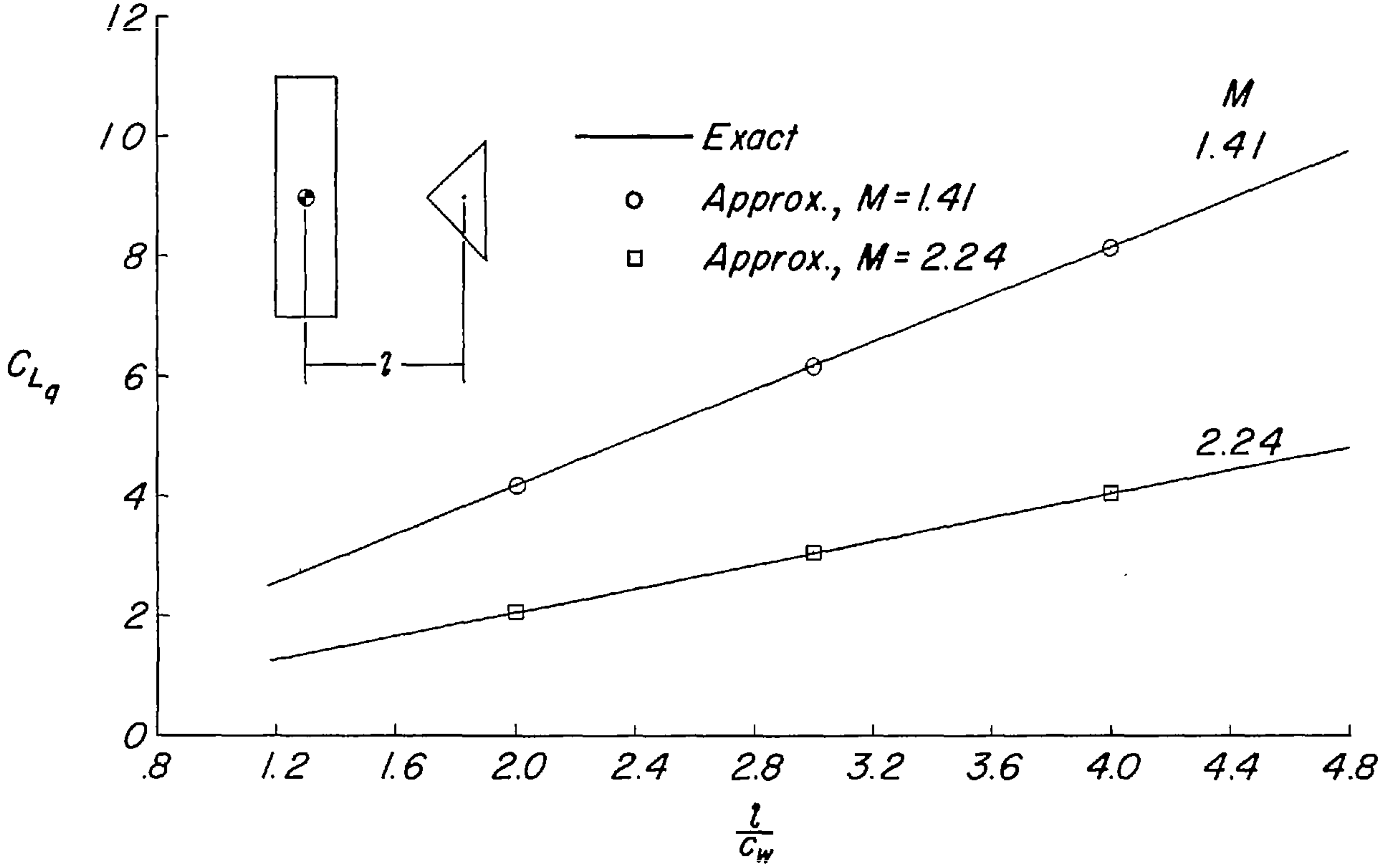

(b) Wing aspect ratio 4; $\frac{c_t}{c_w} = 1$.

Figure 47.- Concluded.

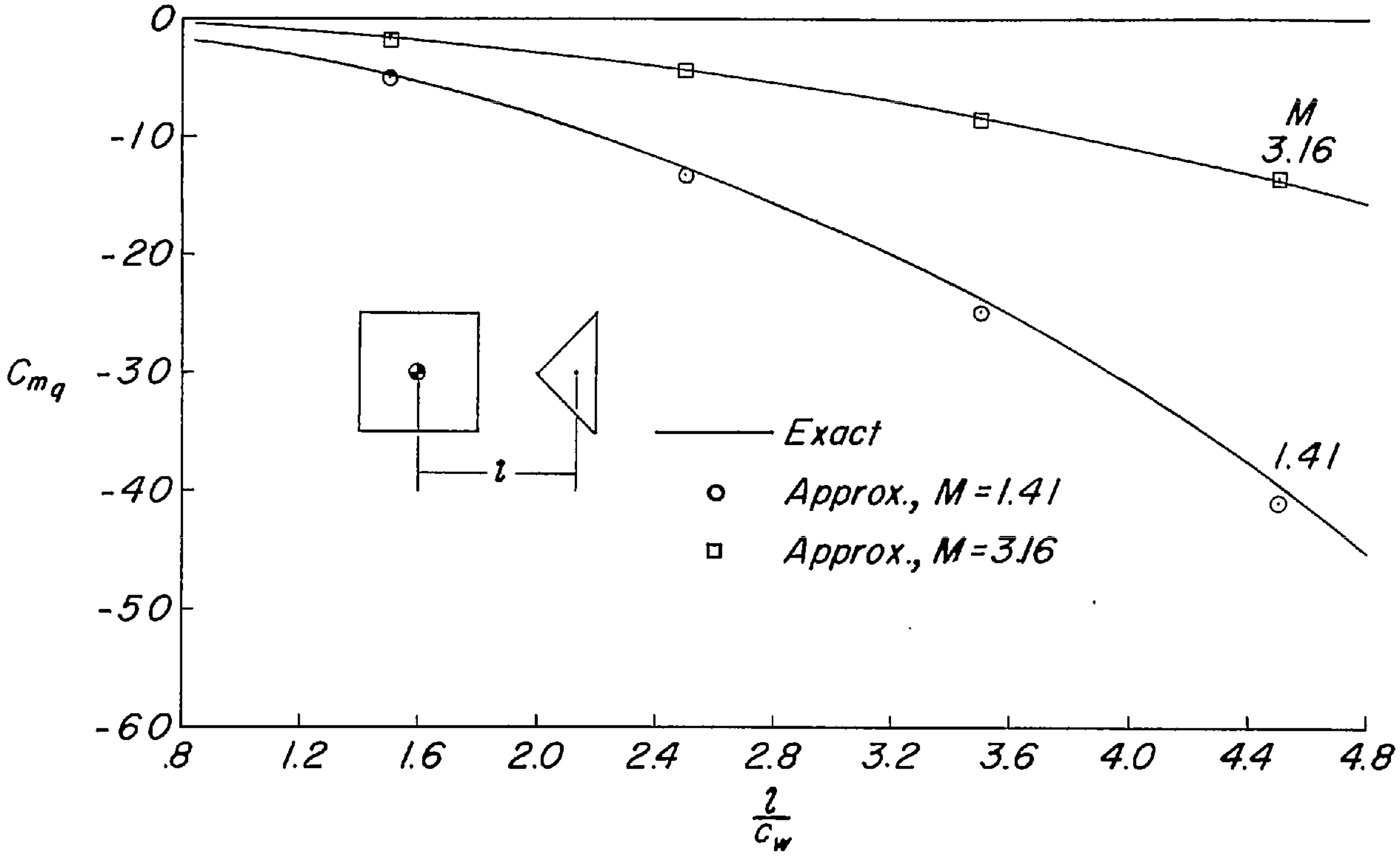

(a) Wing aspect ratio 1; $\frac{c_t}{c_w} = 1$.

Figure 48.- Comparison of exact (linearized) and approximate (eq. (66)) values of C_{m_q} for two rectangular-wing—triangular-tail combinations.

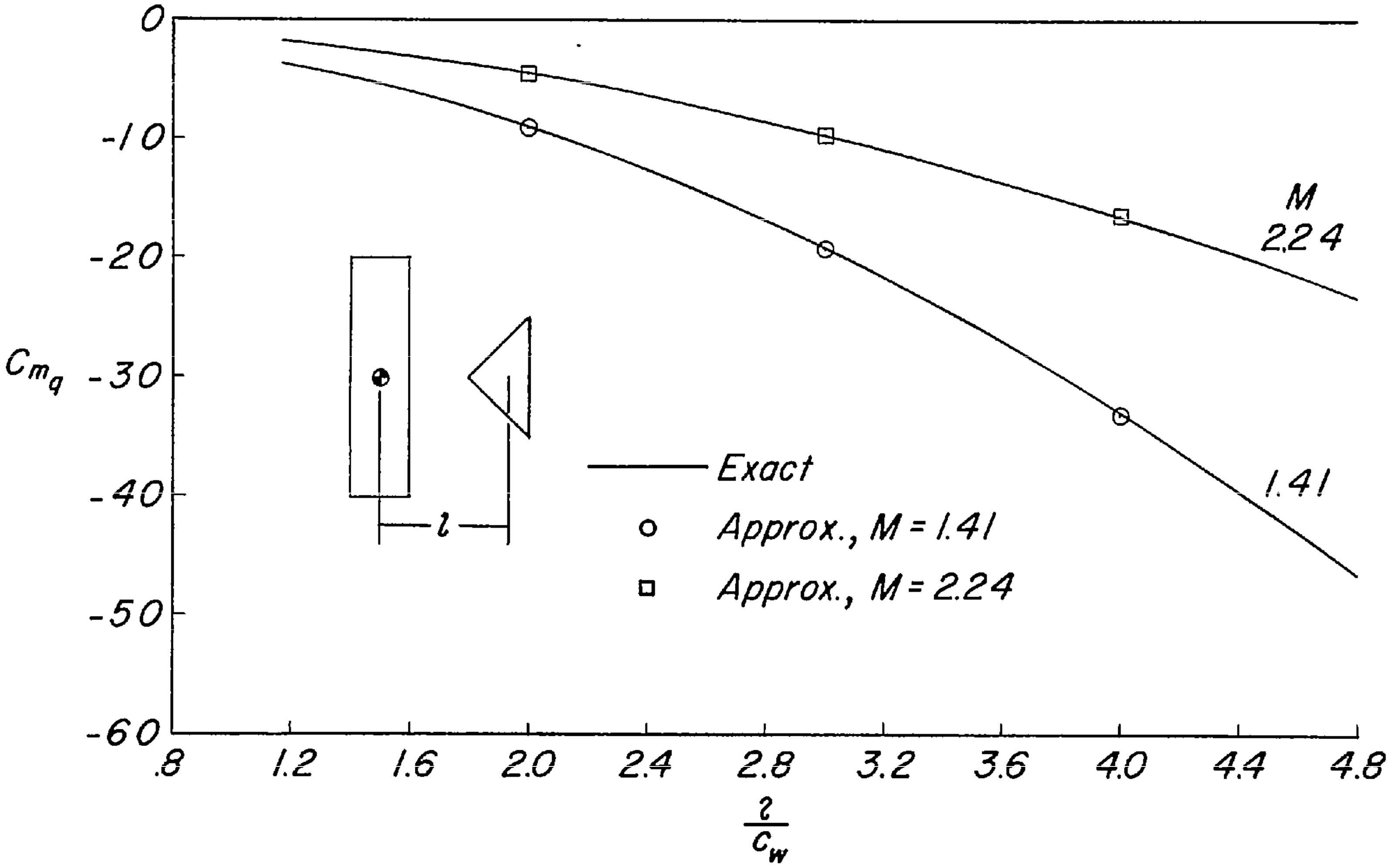

(b) Wing aspect ratio 4; $\frac{c_t}{c_w} = 1$.

Figure 48.- Concluded.

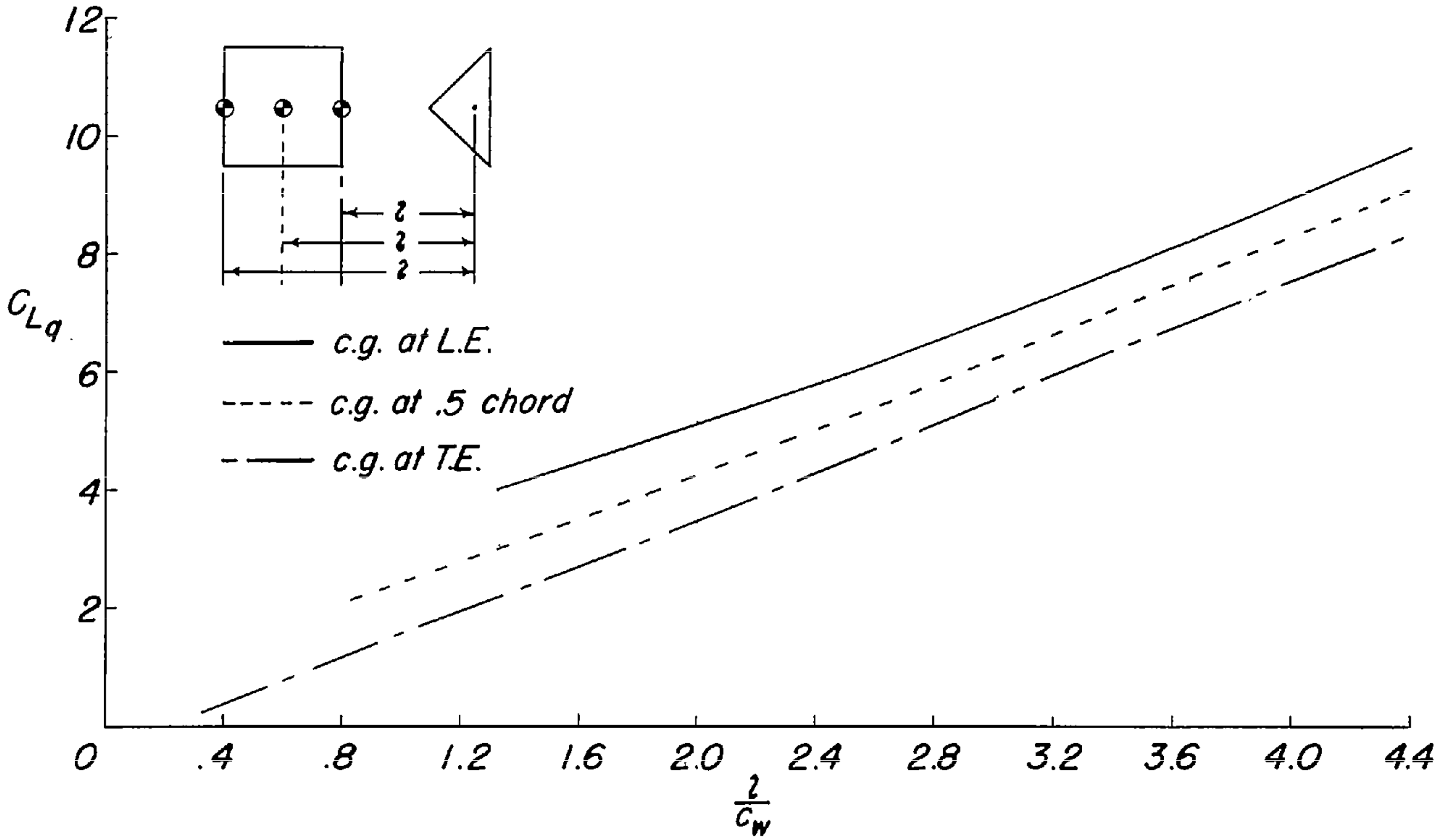

(a) Wing aspect ratio 1; $\frac{c_t}{c_w} = \frac{1}{2}$.

Figure 49.- Variation of C_{L_q} with l/c_w for three center-of-gravity locations for two rectangular-wing—triangular-tail combinations. M = 1.414.

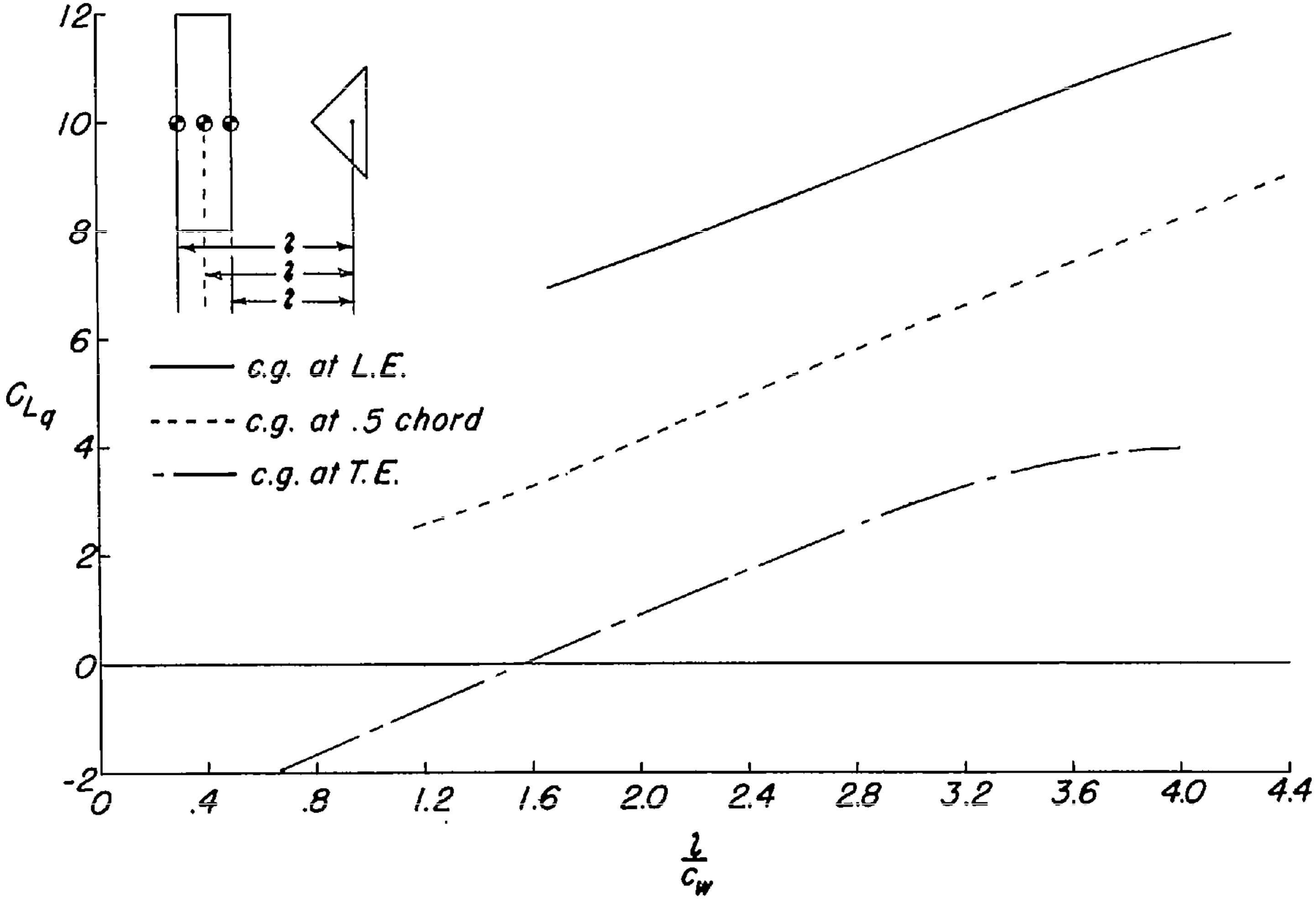

(b) Wing aspect ratio 4; $\frac{c_t}{c_w} = 1$.

Figure 49.- Concluded.

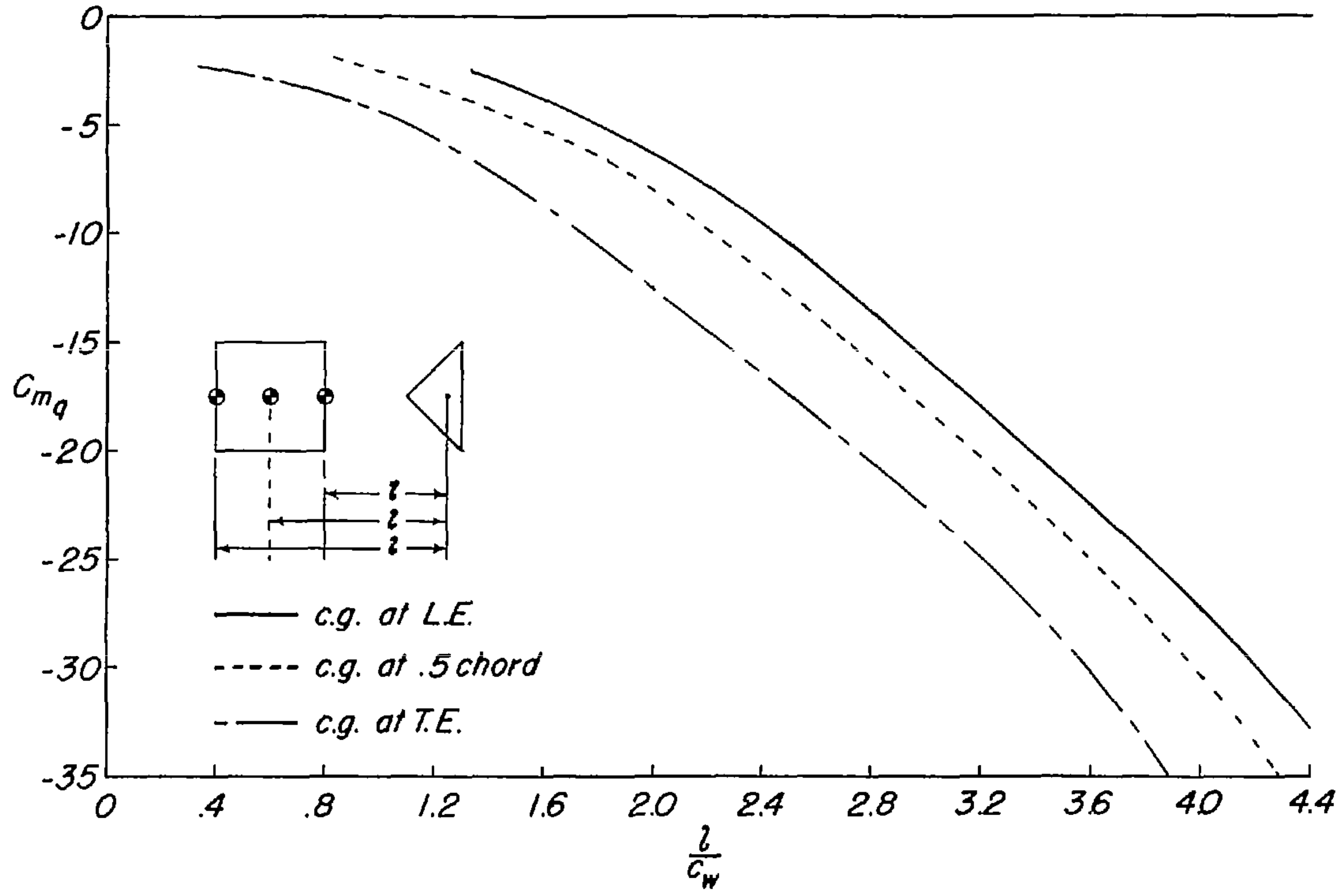

(a) Wing aspect ratio 1; $\frac{c_t}{c_w} = \frac{1}{2}$.

Figure 50.- Variation of C_{m_q} with l/c_w for three center-of-gravity locations for two rectangular-wing—triangular-tail combinations. $M = 1.414$.

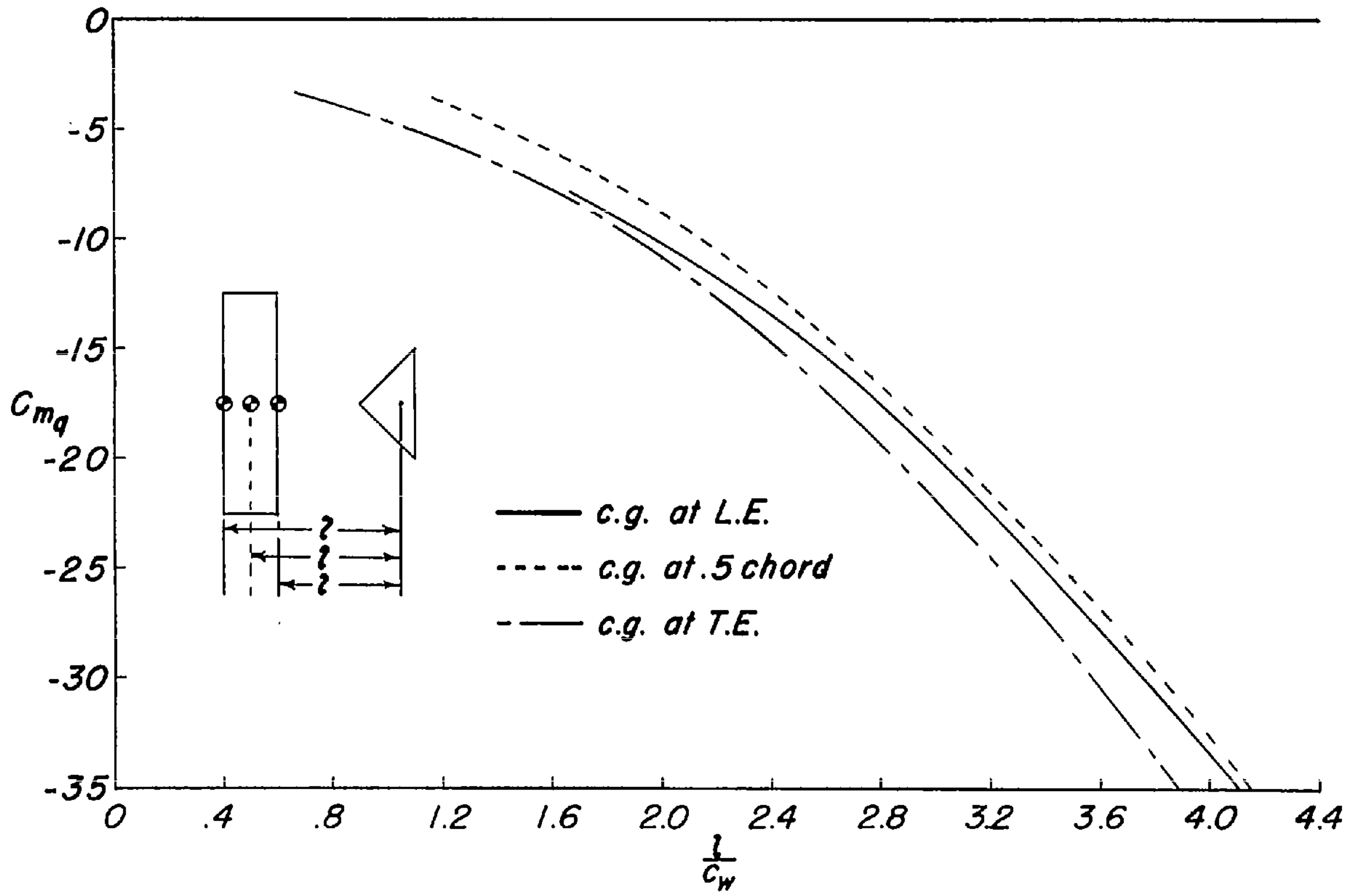

(b) Wing aspect ratio 4; $\frac{c_t}{c_w} = 1$.

Figure 50.- Concluded.

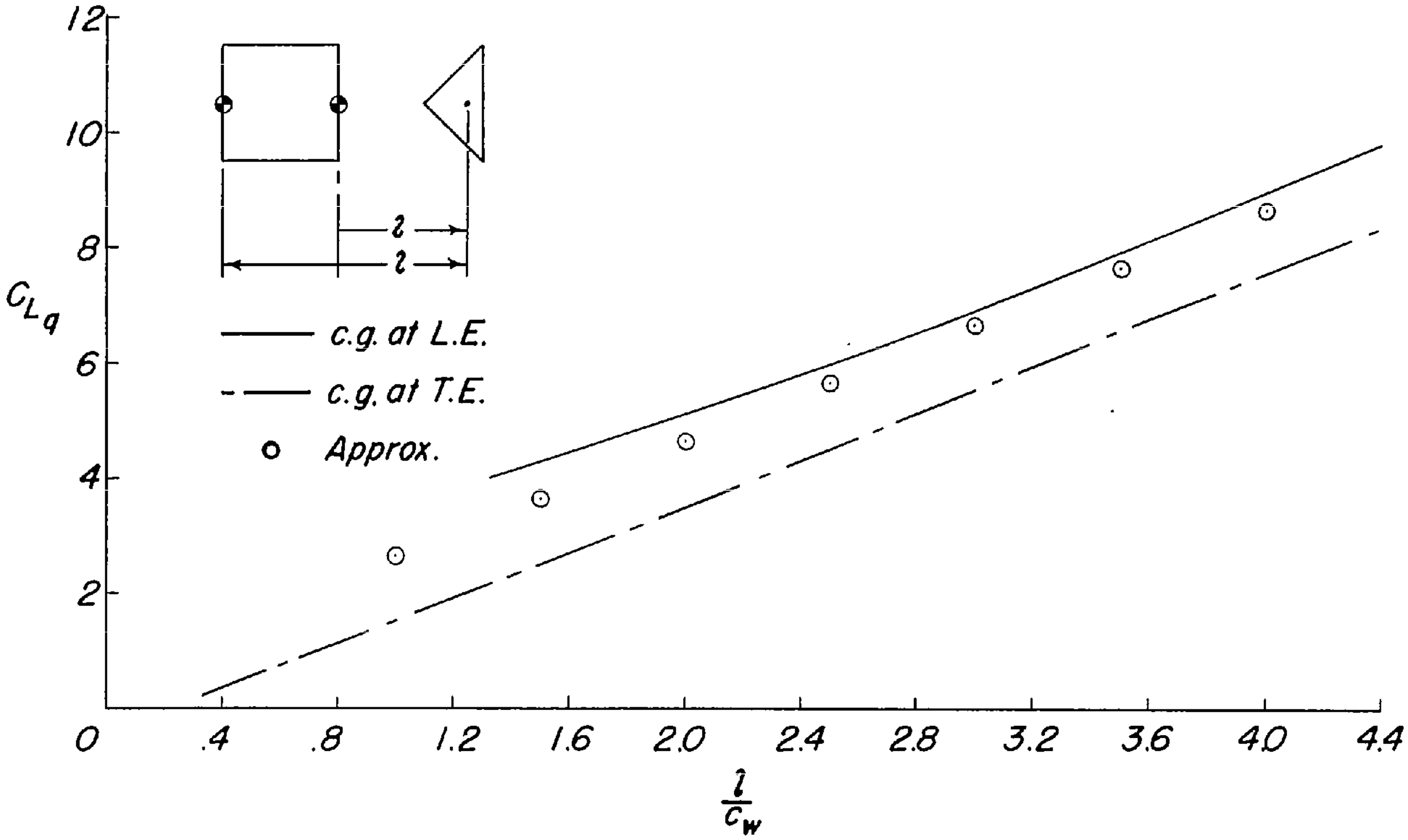

(a) Wing aspect ratio 1; $\frac{c_t}{c_w} = \frac{1}{2}$.

Figure 51.- Comparison of exact (linearized) and approximate (eq. (65)) values of C_{L_q} for two center-of-gravity locations for two rectangular-wing—triangular-tail combinations. M = 1.414.

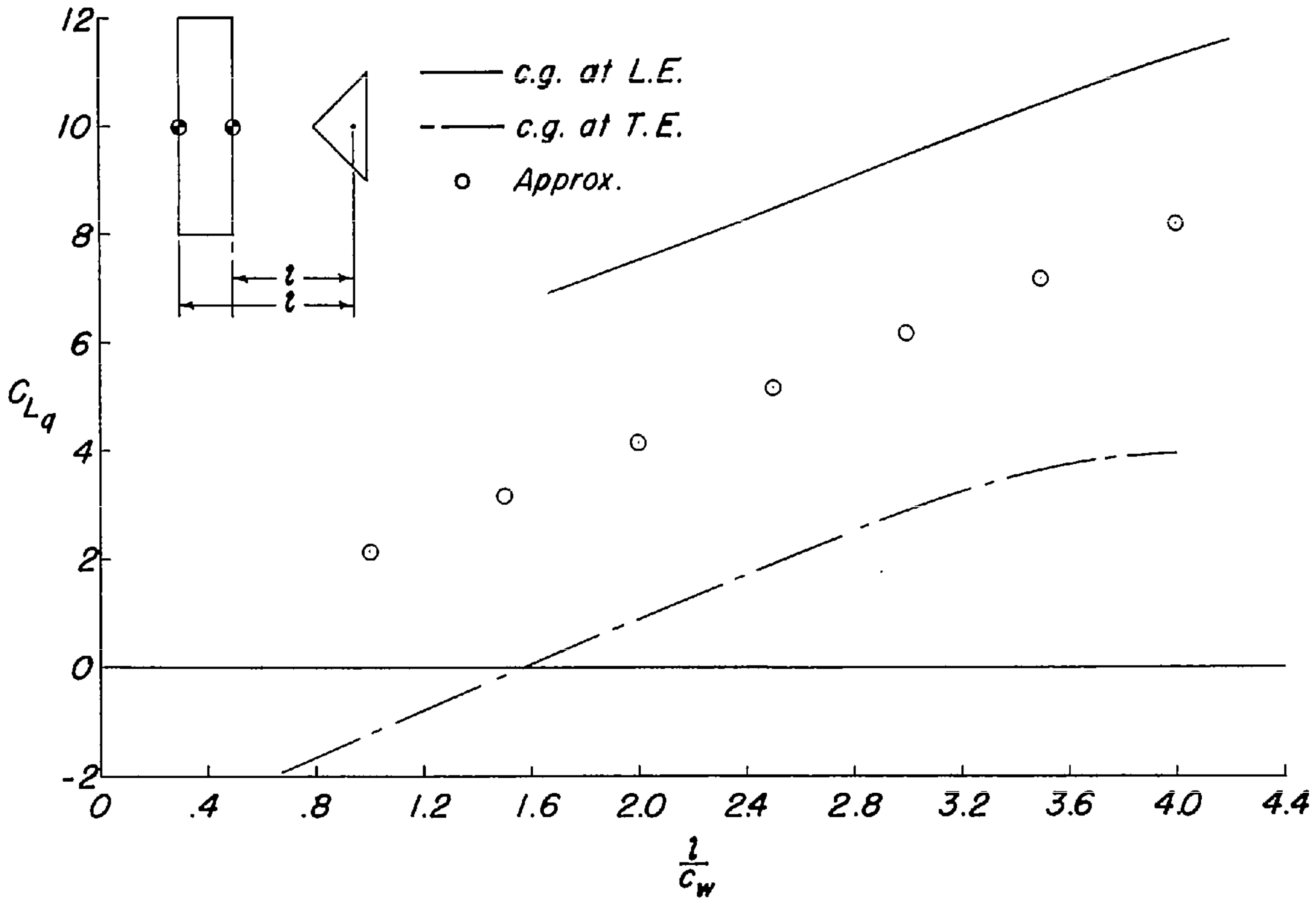

(b) Wing aspect ratio 4; $\frac{c_t}{c_w} = 1$.

Figure 51.- Concluded.

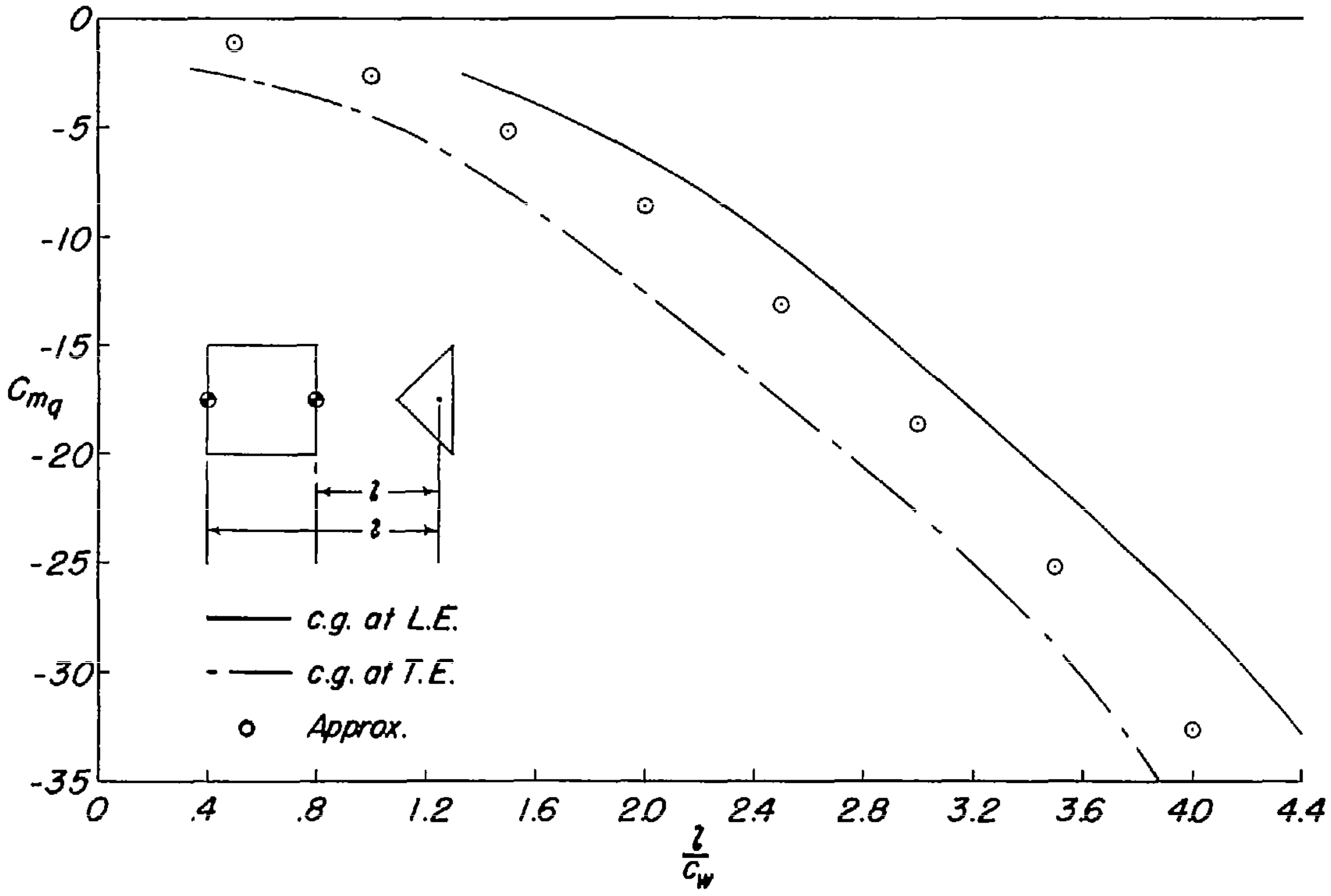

(a) Wing aspect ratio 1; $\frac{c_t}{c_w} = \frac{1}{2}$.

Figure 52.- Comparison of exact (linearized) and approximate (eq. (66)) values of C_{m_q} for two center-of-gravity locations for two rectangular-wing—triangular-tail combinations. M = 1.414.

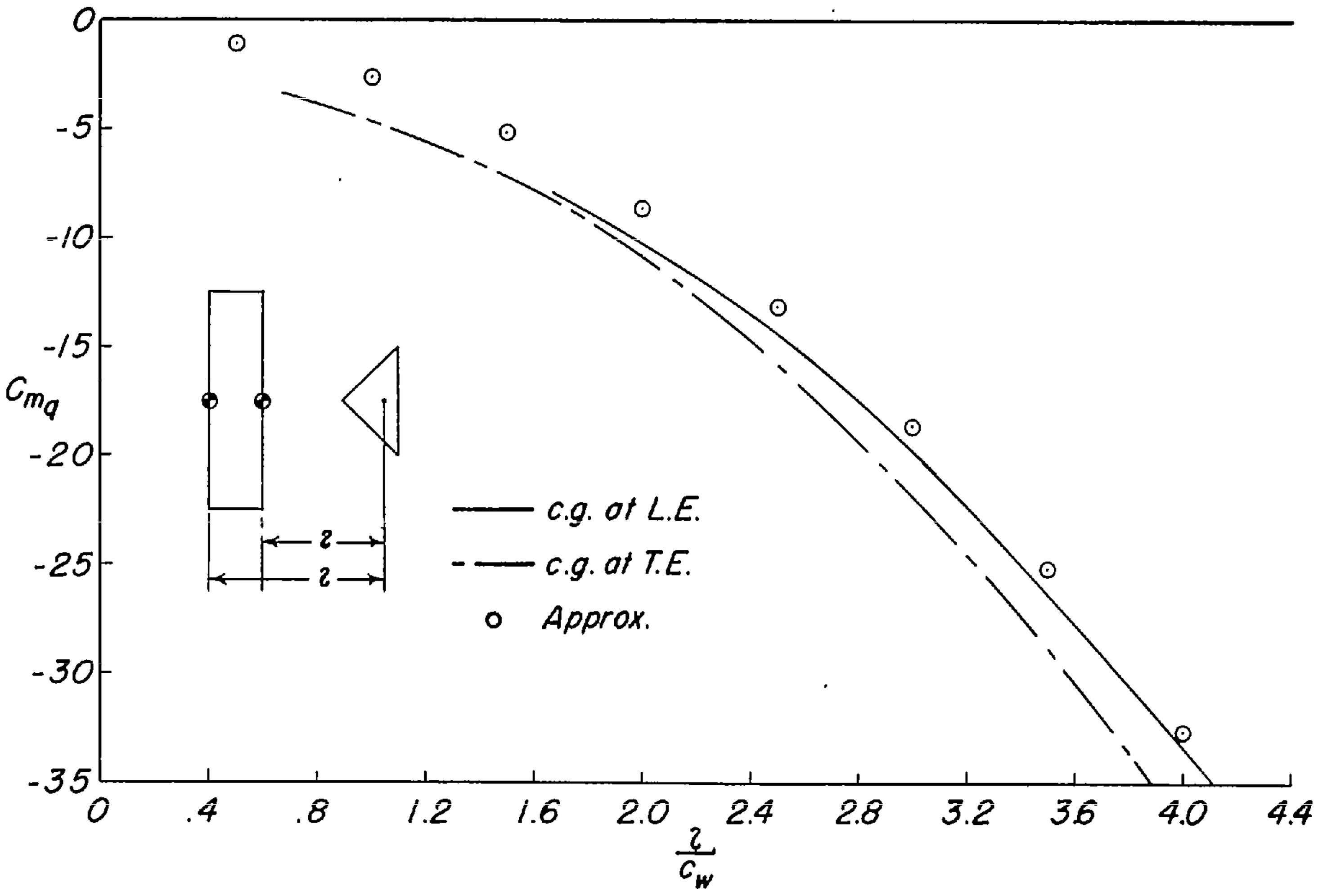

(b) Wing aspect ratio 4; $\frac{c_t}{c_w} = 1$.

Figure 52.- Concluded.

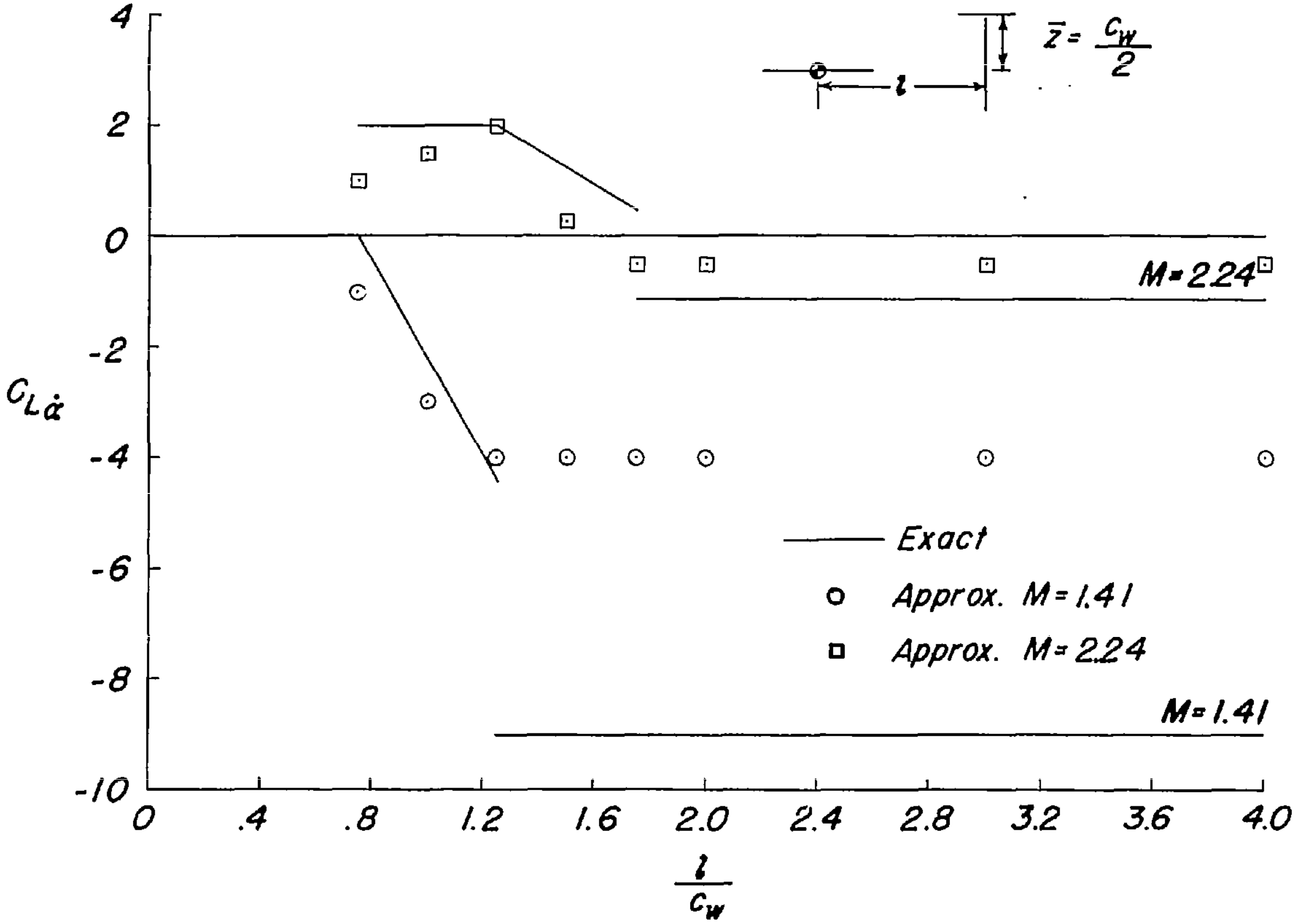

Figure 53.- Comparison of exact (linearized) and approximate (eq. (81)) values of $C_{L_{\dot{\alpha}}}$ for a two-dimensional wing-tail combination at two Mach numbers. $\bar{x} = c_t = \frac{c_w}{2}$.

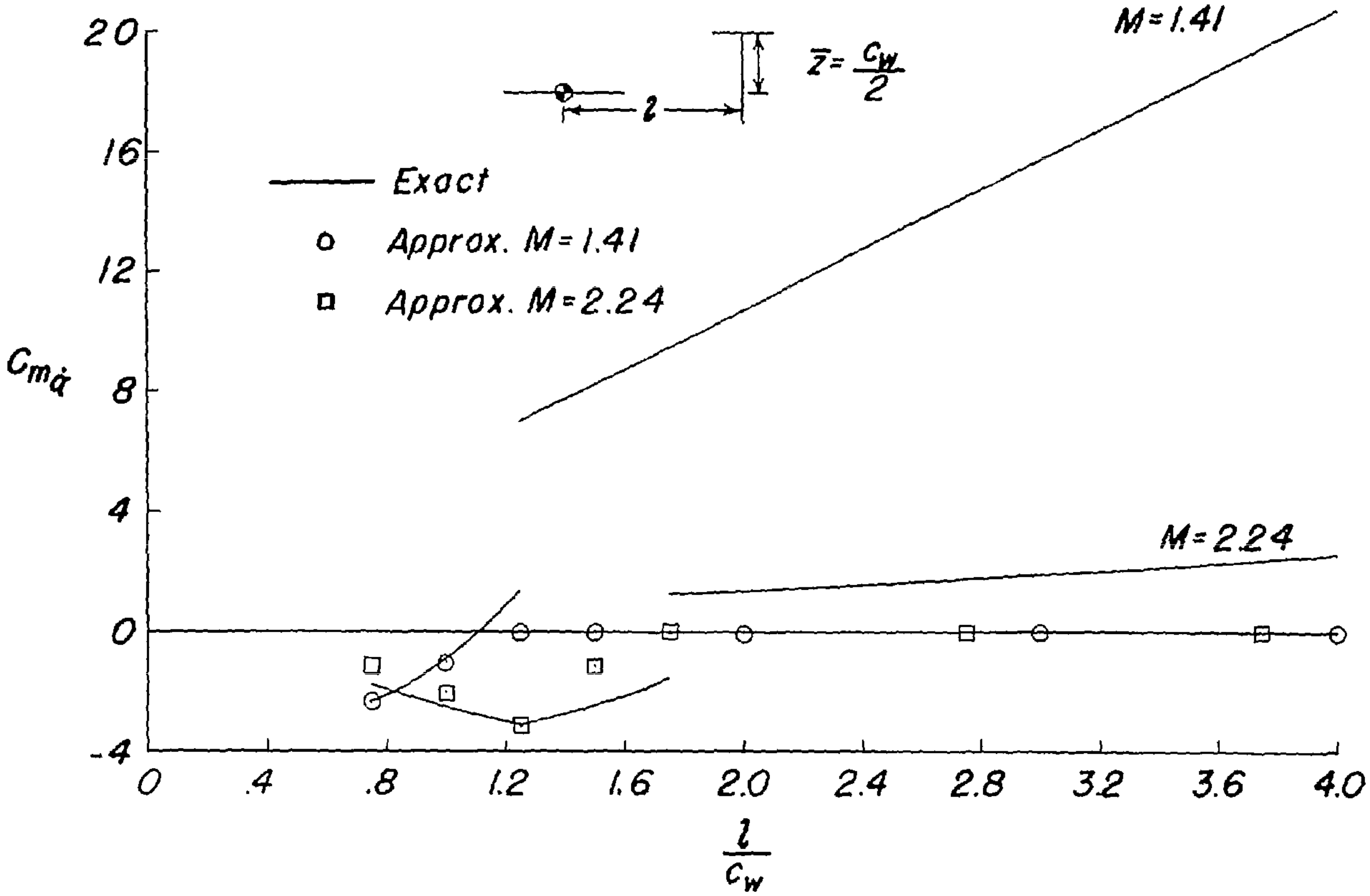

Figure 54.- Comparison of exact (linearized) and approximate (eq. (82)) values of $C_{m_{\dot{\alpha}}}$ for a two-dimensional wing-tail combination at two Mach numbers. $\bar{x} = c_t = \frac{c_w}{2}$.

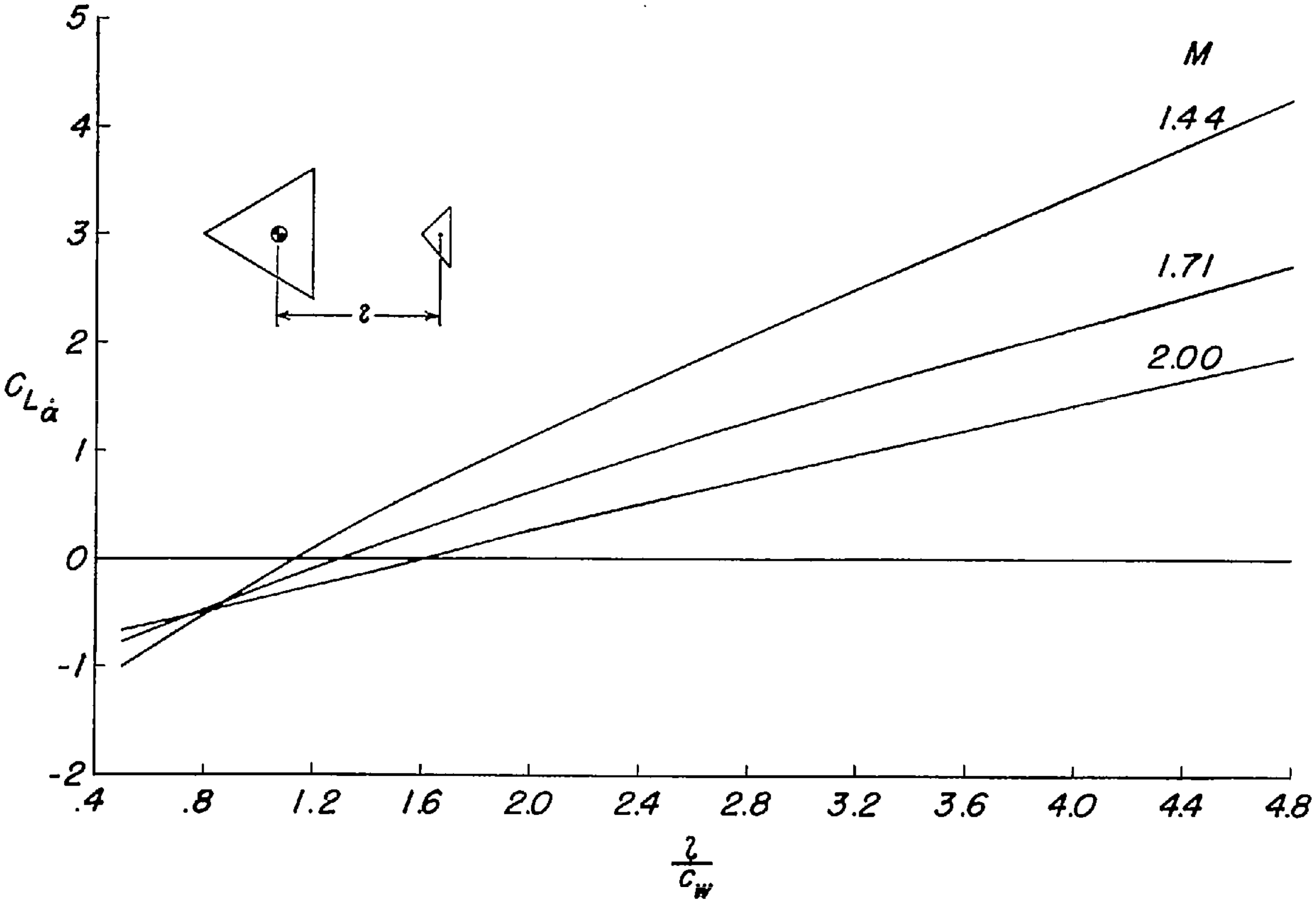

Figure 55.- Variation of $C_{L_{\dot{\alpha}}}$ with l/c_w for three Mach numbers for a triangular wing-tail combination.

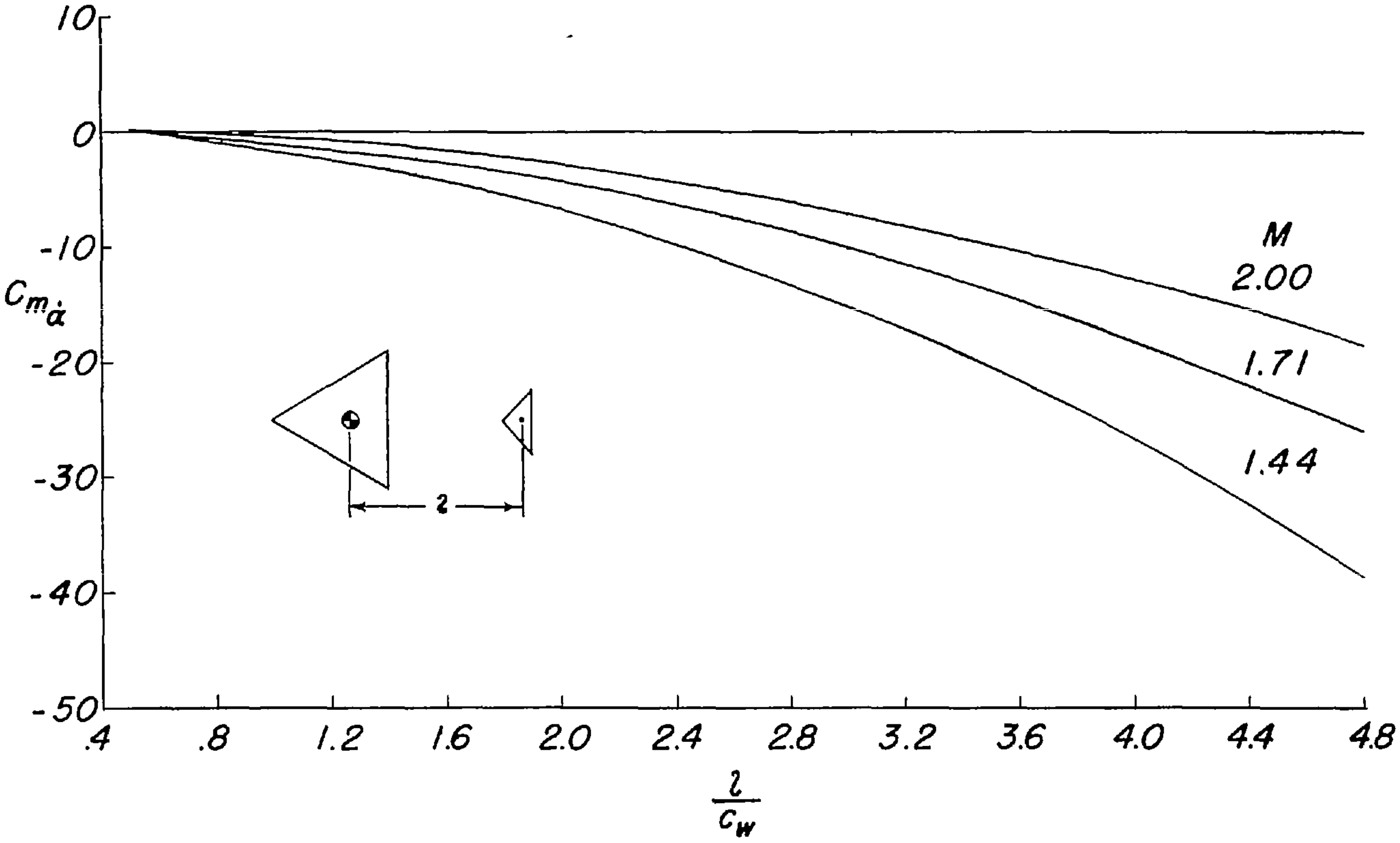

Figure 56.- Variation of $C_{m_{\dot{\alpha}}}$ with l/c_w for three Mach numbers for a triangular wing-tail combination.

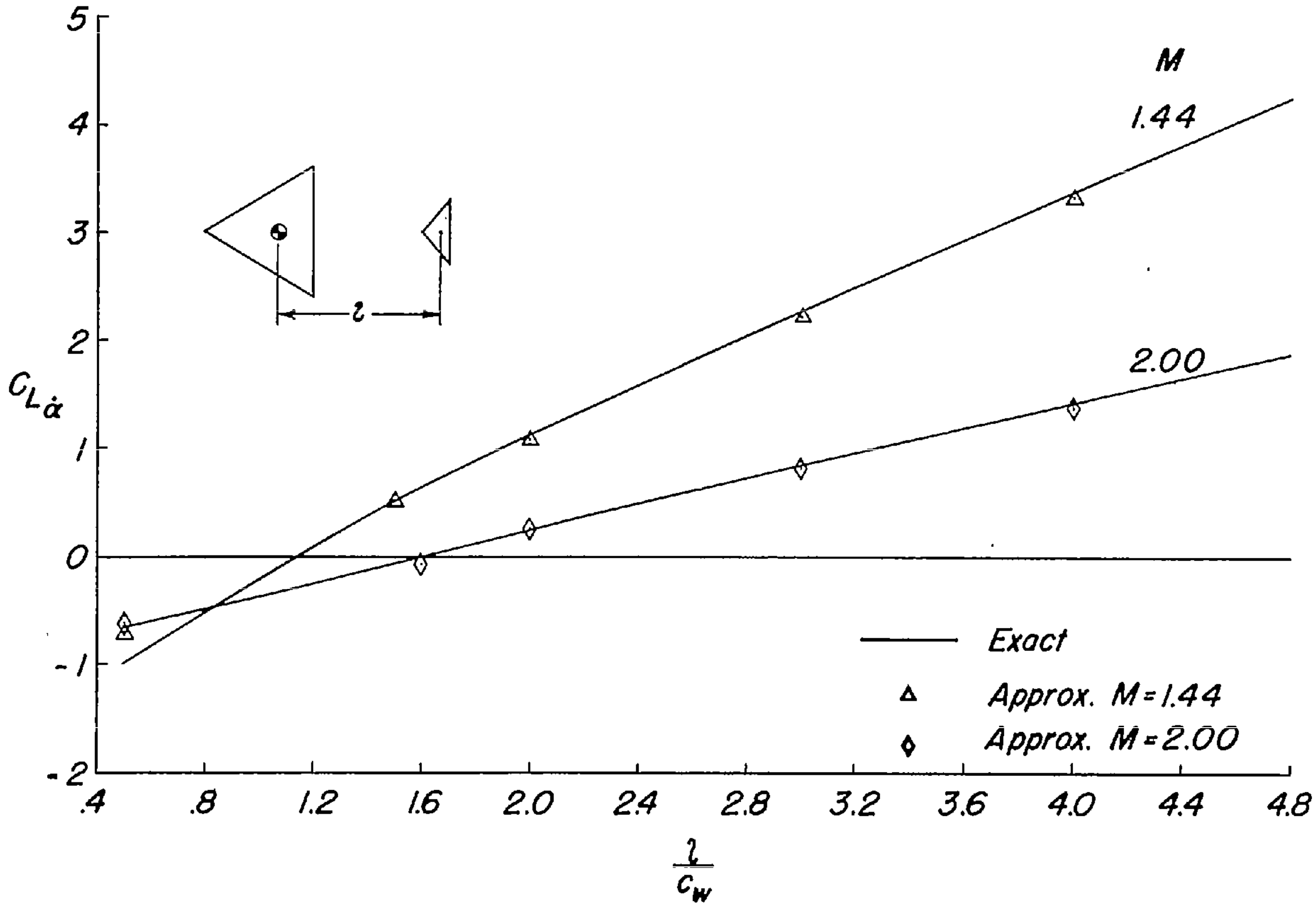

Figure 57.- Comparison of exact (linearized) and approximate (eq. (81)) values of $C_{L_{\dot{\alpha}}}$ for a triangular wing-tail combination at two Mach numbers.

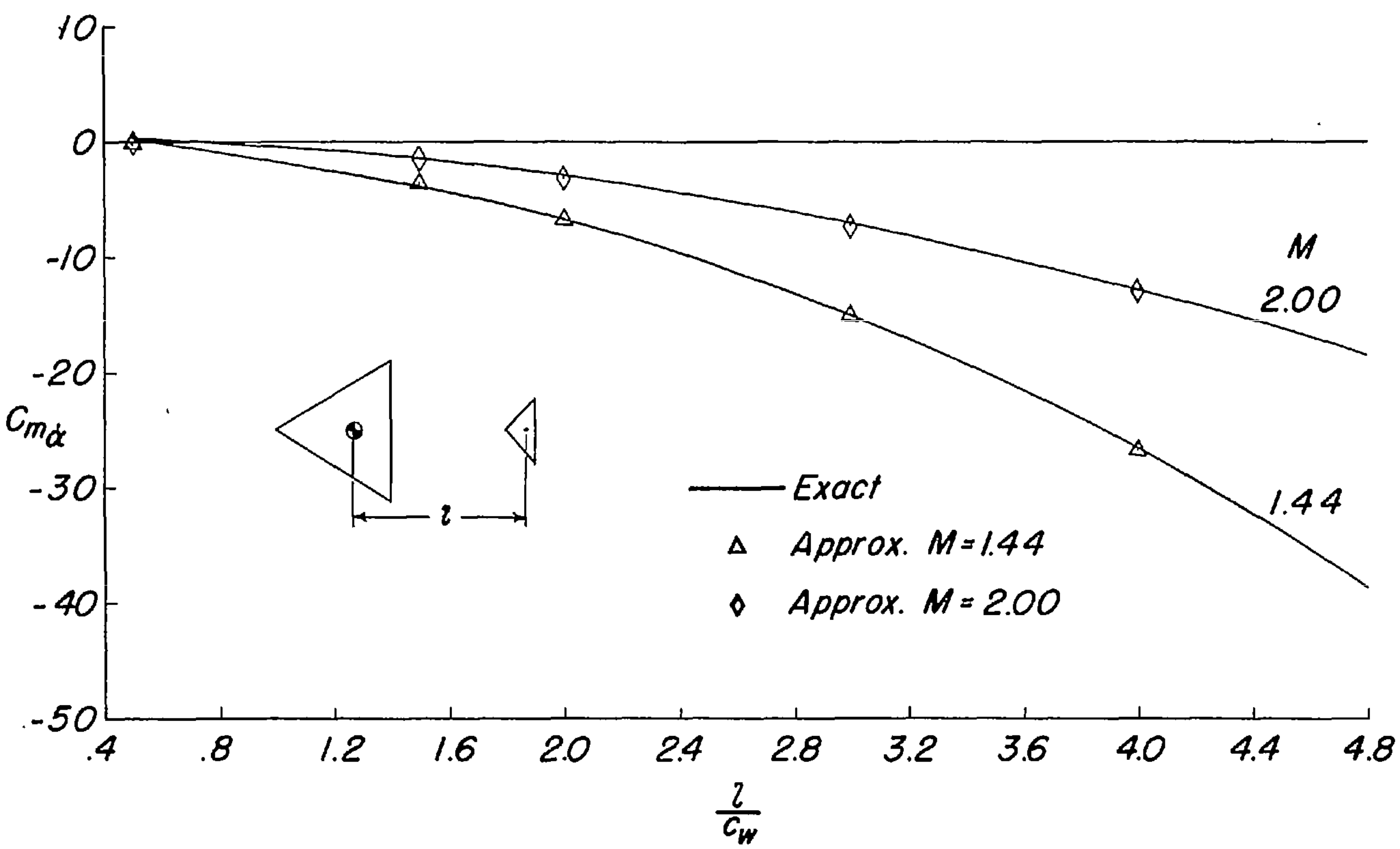

Figure 58.- Comparison of exact (linearized) and approximate (eq. (82)) values of $C_{m_{\dot\alpha}}$ for a triangular wing-tail combination at two Mach numbers.

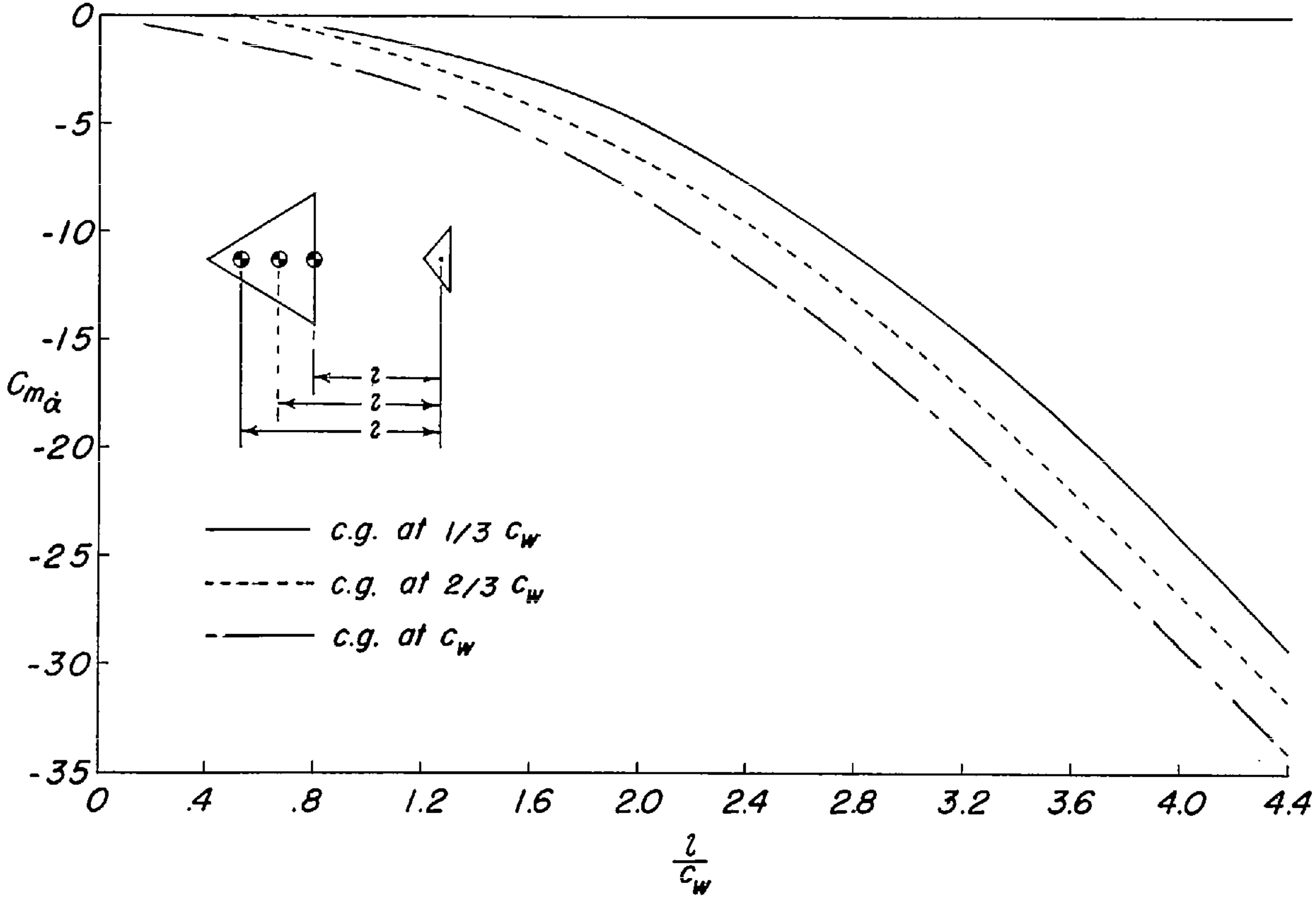

Figure 59.- Variation of $C_{m_{\dot{\alpha}}}$ with l/c_w for three center-of-gravity locations for a triangular wing-tail combination. M = 1.44.

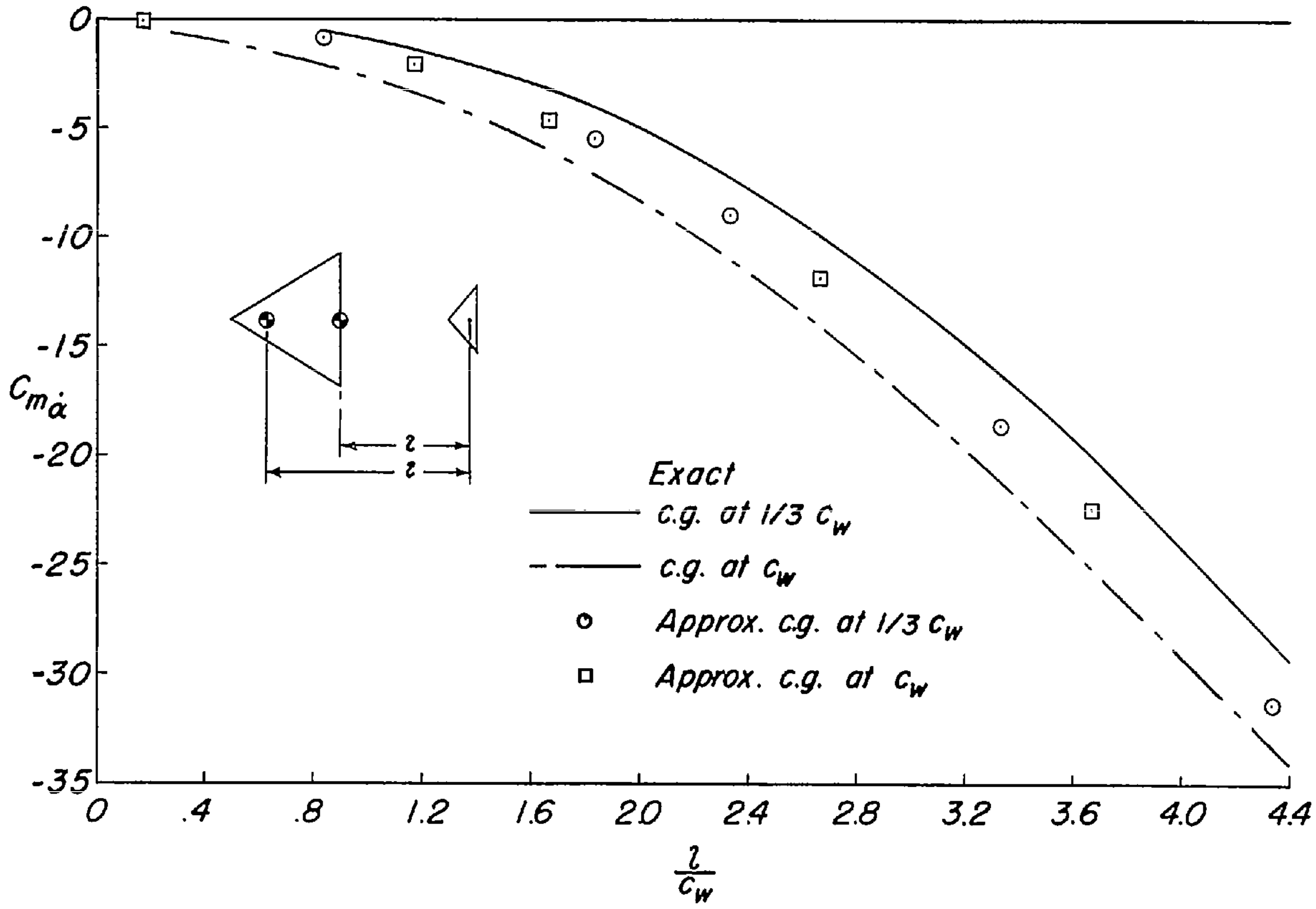

Figure 60.- Comparison between exact (linearized) and approximate (eq. (82)) values of $C_{m_{\dot{\alpha}}}$ for two center-of-gravity locations for a triangular wing-tail combination. M = 1.44.

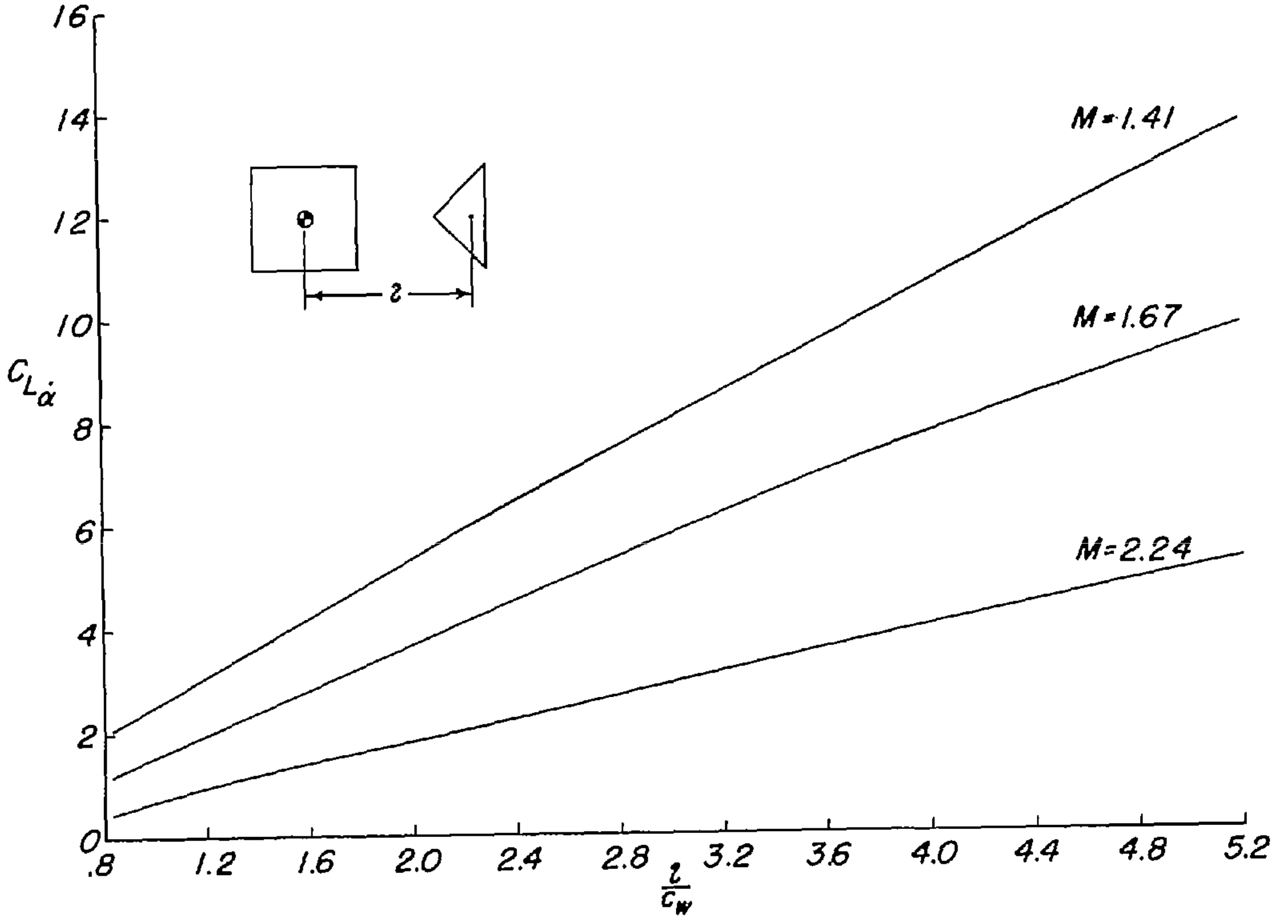

(a) Wing aspect ratio 1; $\frac{c_t}{c_w} = \frac{1}{2}$.

Figure 61.- Variation of $C_{L_{\dot{\alpha}}}$ with l/c_w for several rectangular-wing—triangular-tail combinations.

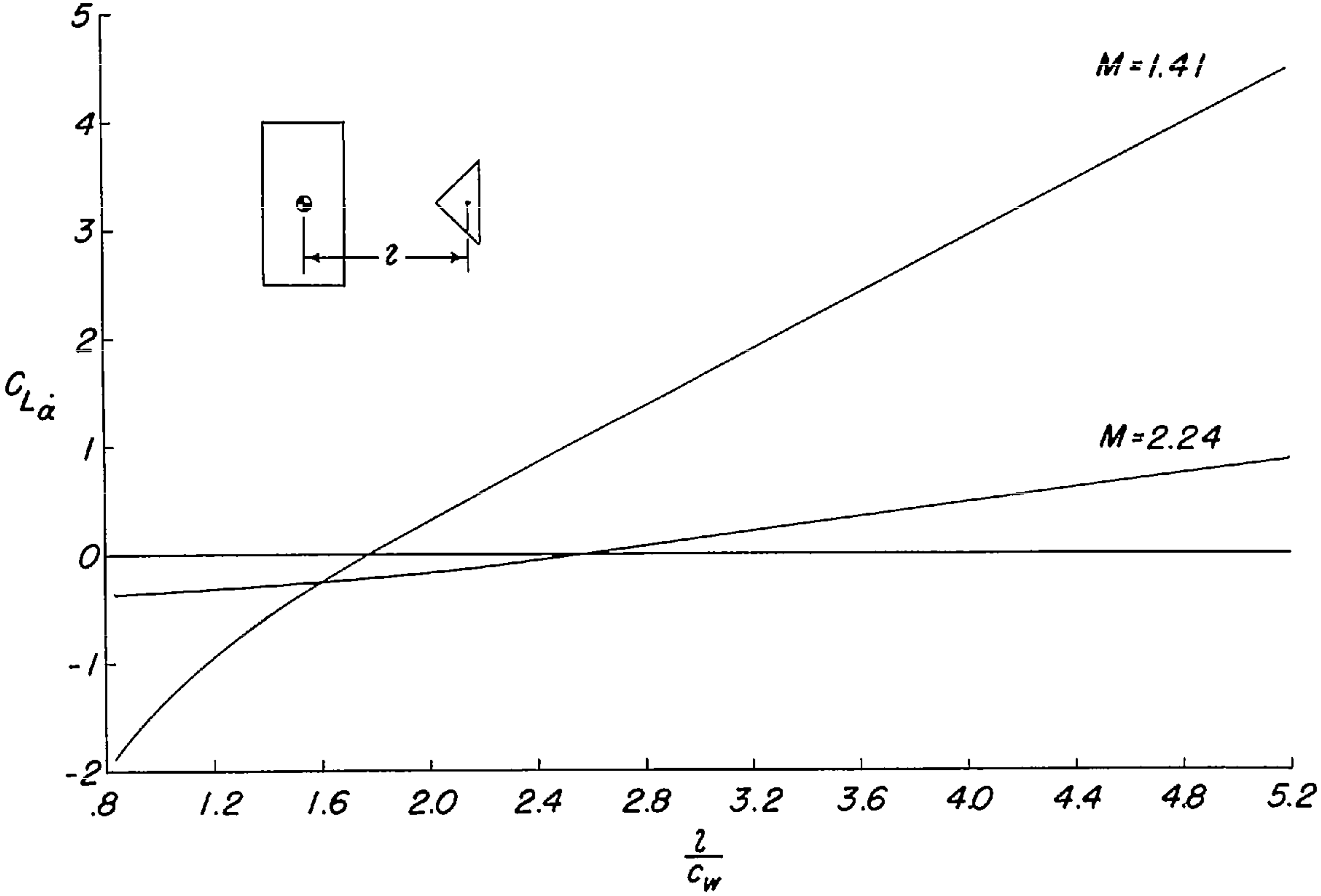

(b) Wing aspect ratio 2; $\frac{c_t}{c_w} = \frac{1}{2}$.

Figure 61.- Continued.

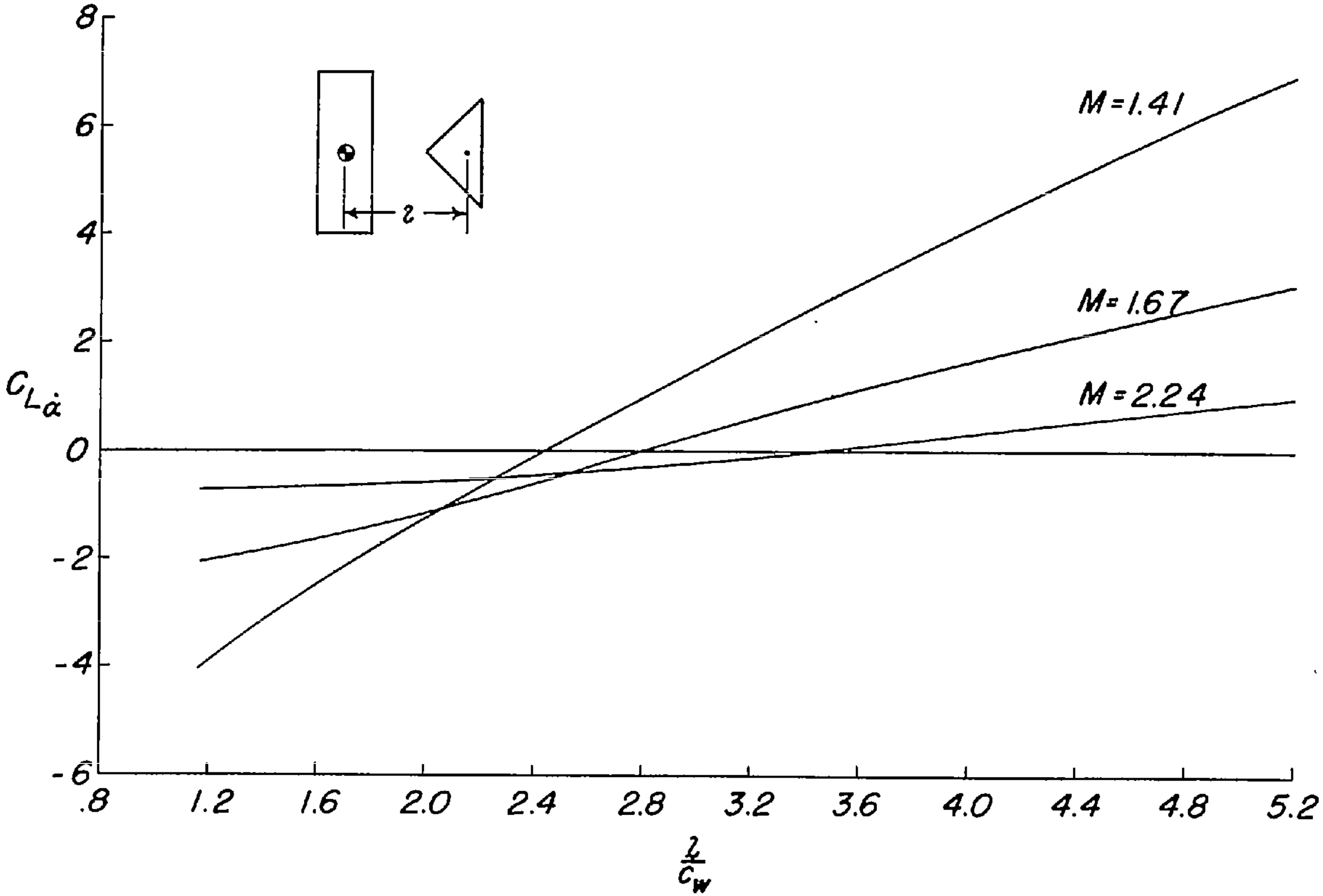

(c) Wing aspect ratio 3; $\frac{c_t}{c_w} = 1$.

Figure 61.- Continued.

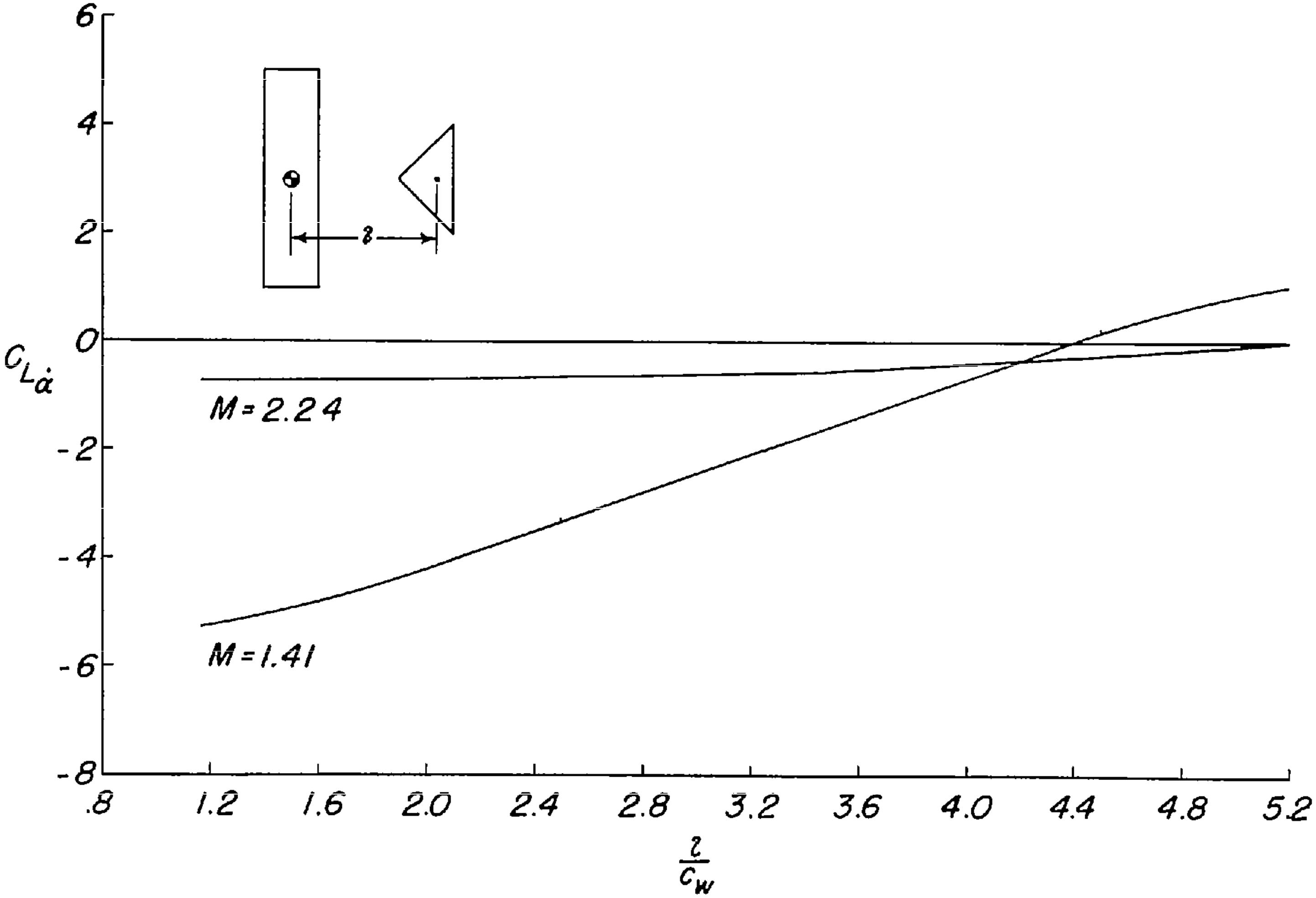

(d) Wing aspect ratio 4; $\frac{c_t}{c_w} = 1$.

Figure 61.- Concluded.

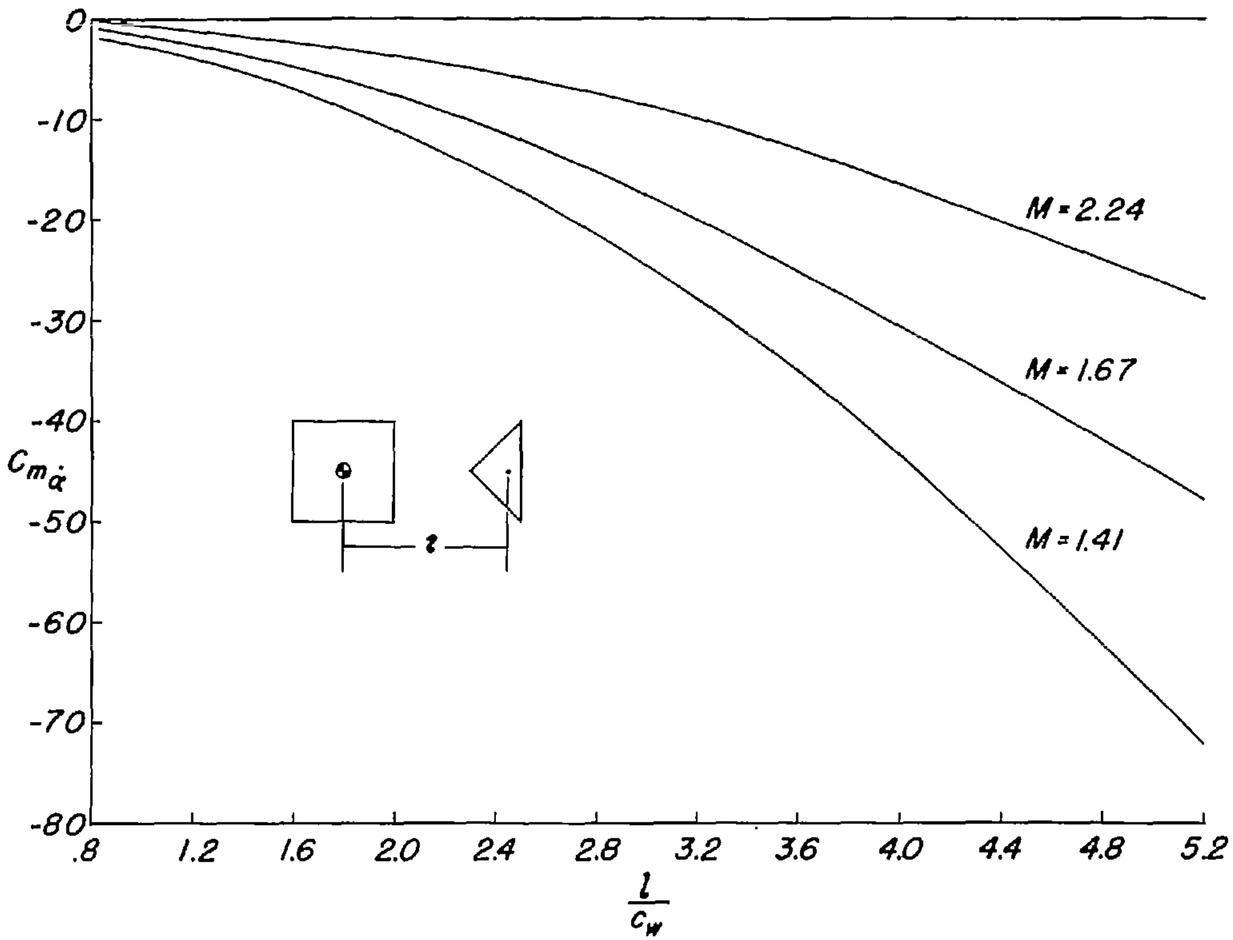

(a) Wing aspect ratio 1; $\frac{c_t}{c_w} = \frac{1}{2}$.

Figure 62.- Variation of $C_{m_{\dot{\alpha}}}$ with l/c_w for several rectangular-wing—triangular-tail combinations.

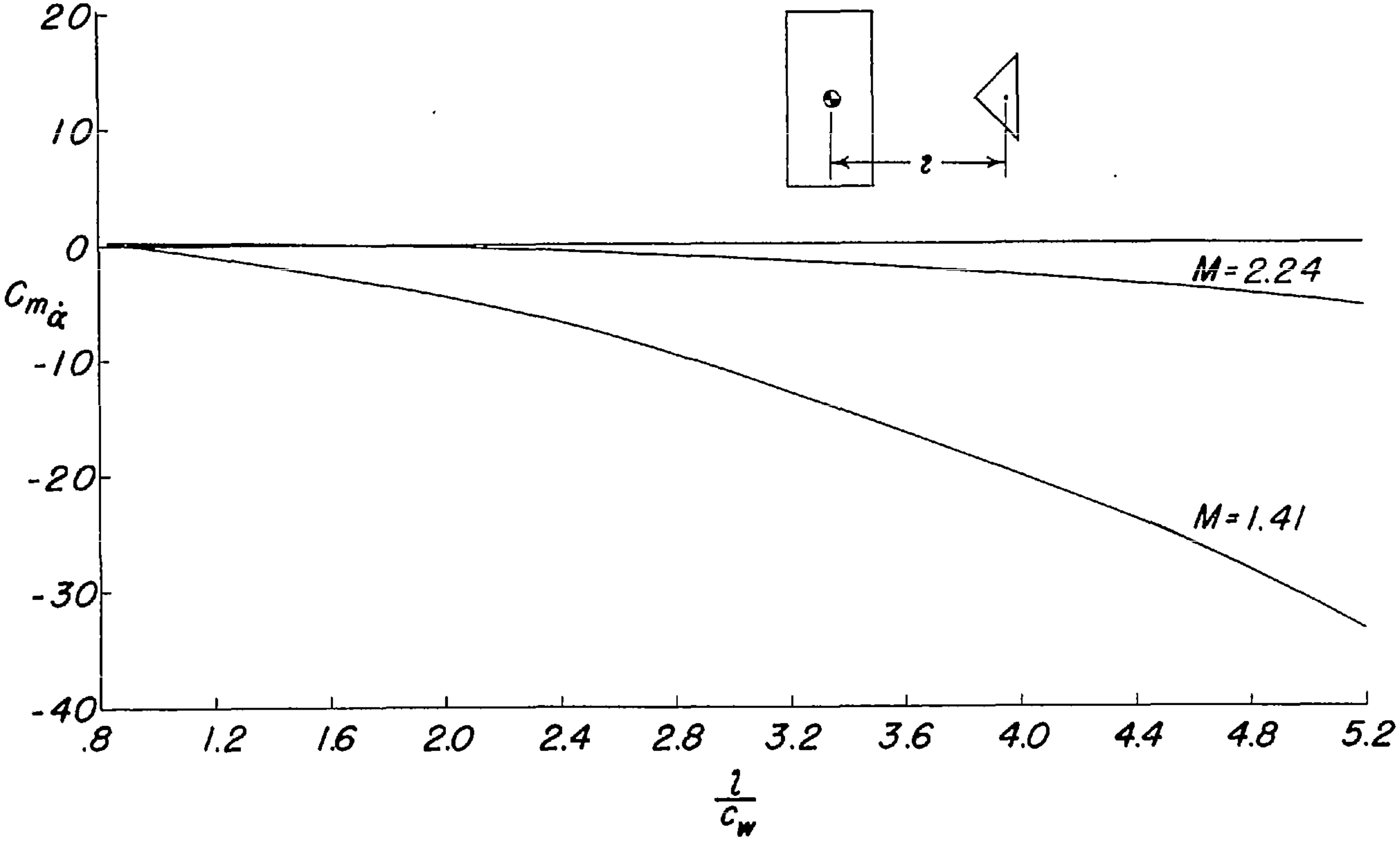

(b) Wing aspect ratio 2; $\frac{c_t}{c_w} = \frac{1}{2}$.

Figure 62.- Continued.

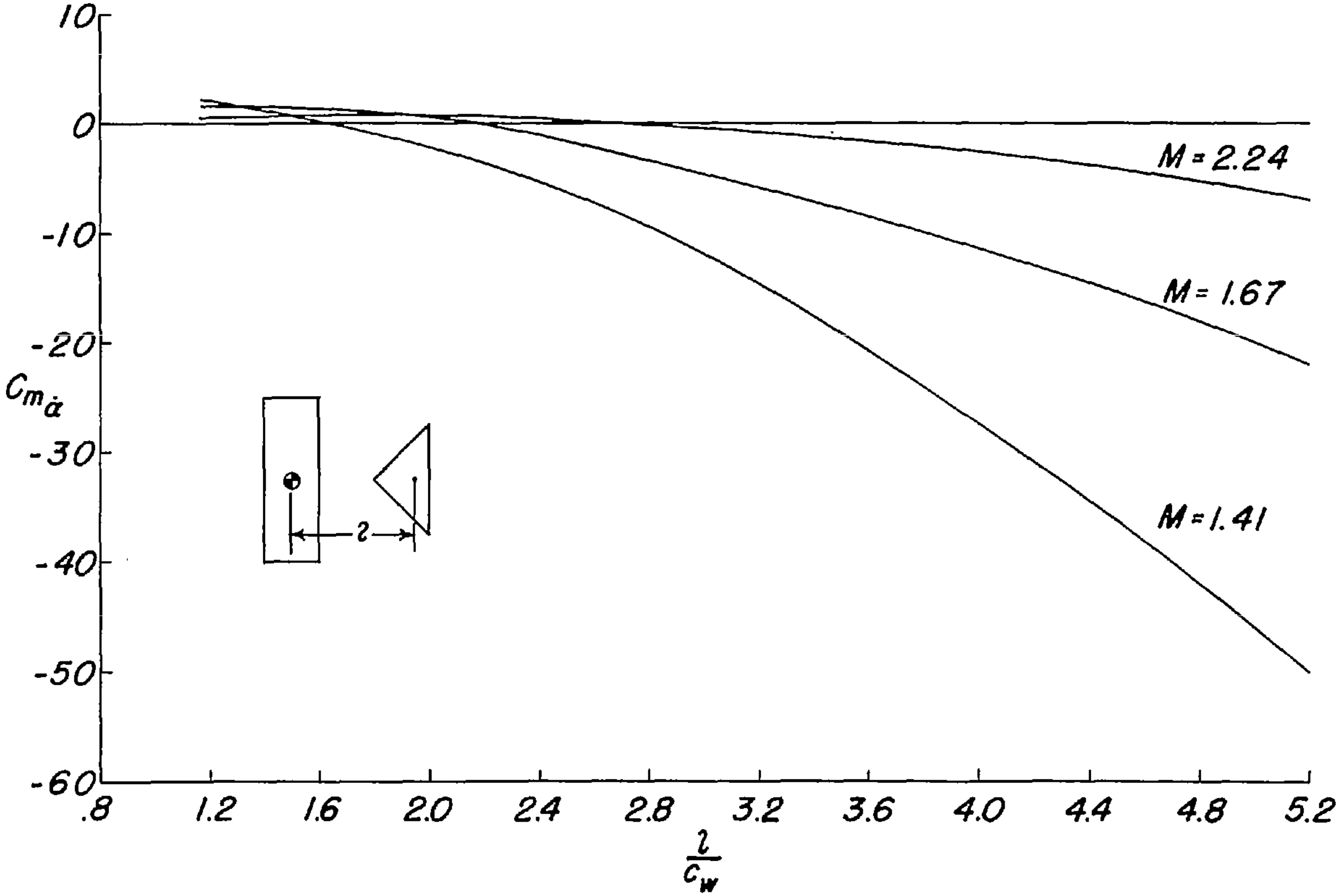

(c) Wing aspect ratio 3; $\frac{c_t}{c_w} = 1$.

Figure 62.- Continued.

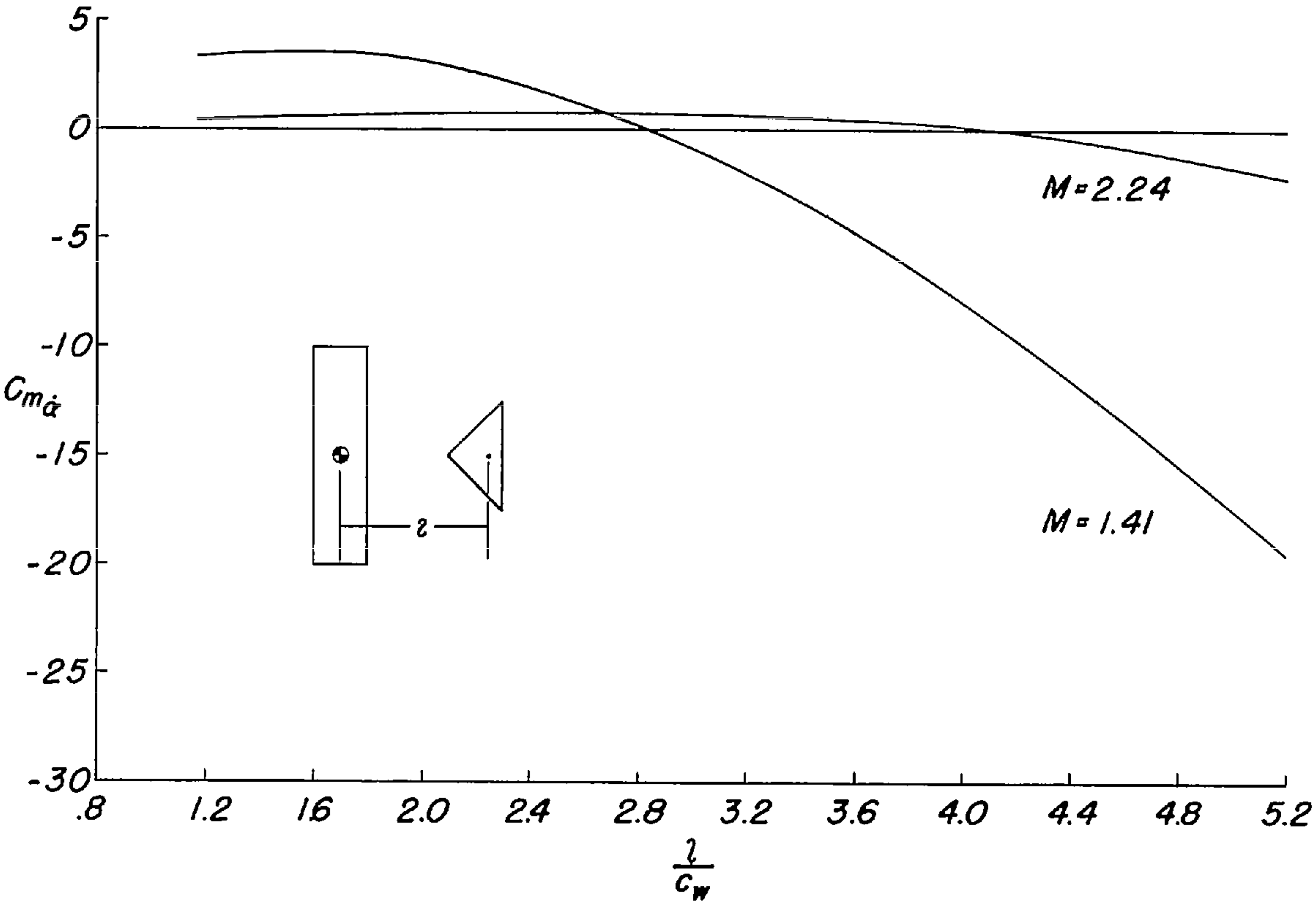

(d) Wing aspect ratio 4; $\frac{c_t}{c_w} = 1$.

Figure 62.- Concluded.

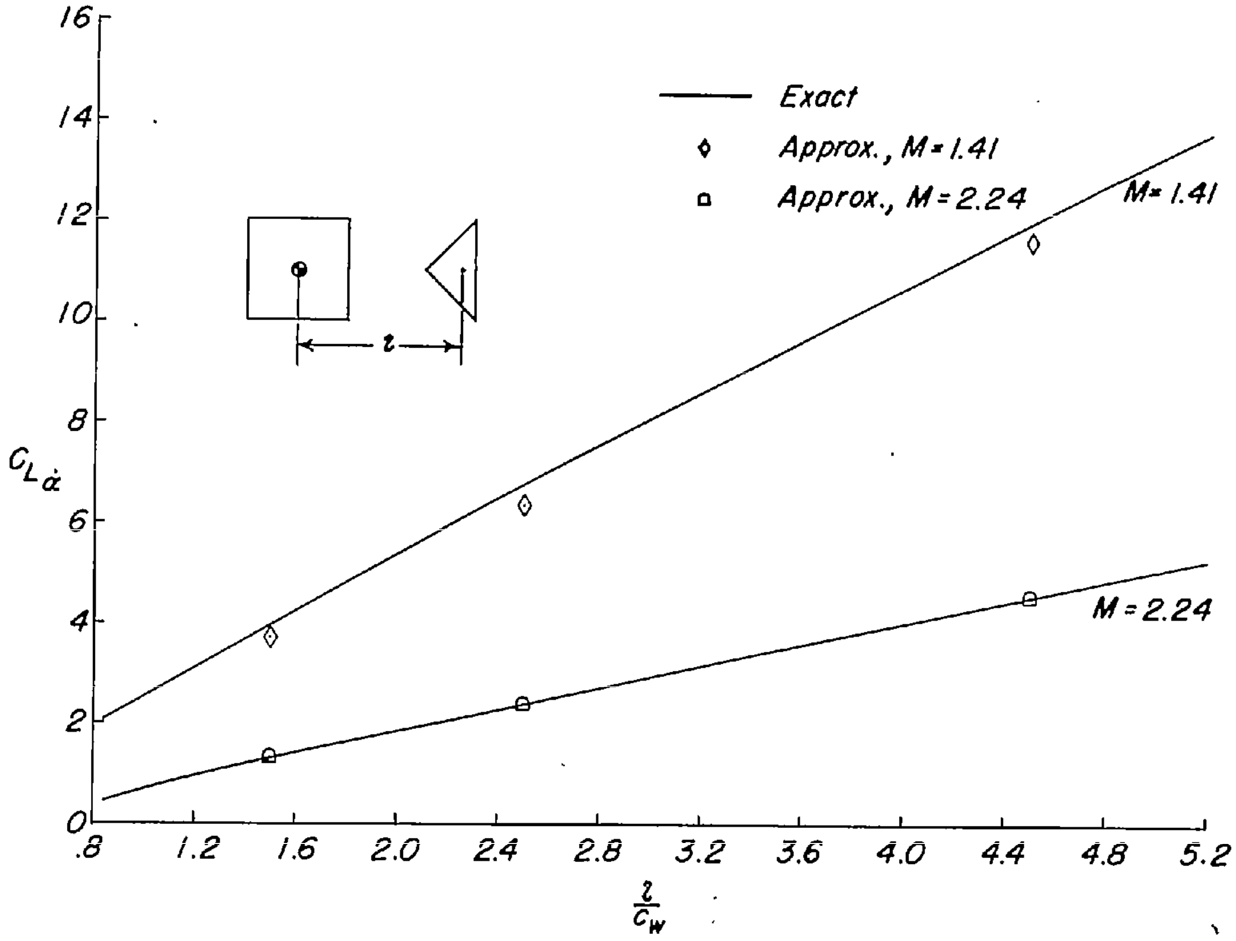

(a) Wing aspect ratio 1; $\frac{c_t}{c_w} = \frac{1}{2}$.

Figure 63.- Comparison between exact (linearized) and approximate (eq. (81)) values of $C_{L_{\dot{\alpha}}}$ for two rectangular-wing—triangular-tail combinations.

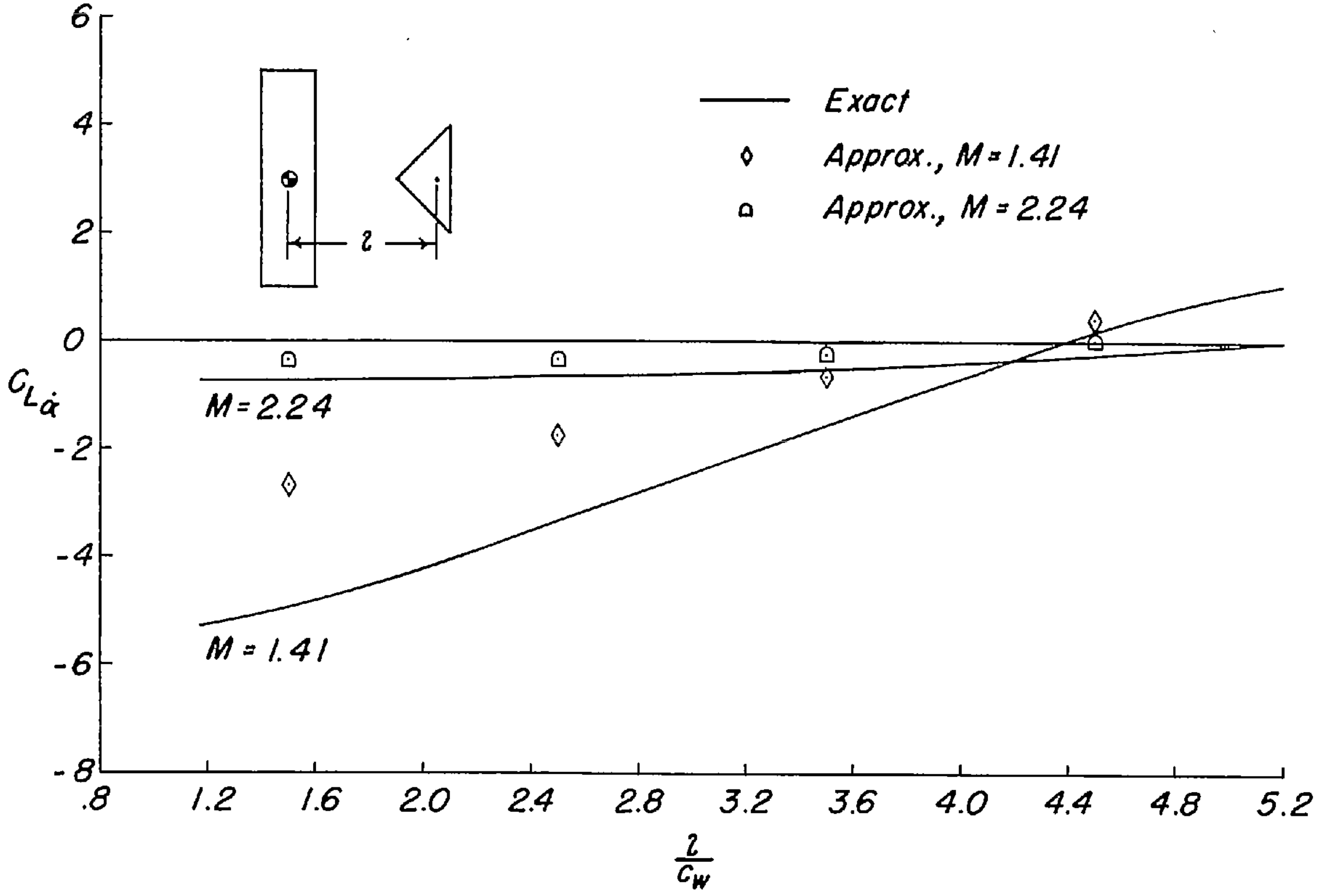

(b) Wing aspect ratio 4; $\frac{c_t}{c_w} = 1$.

Figure 63.- Concluded.

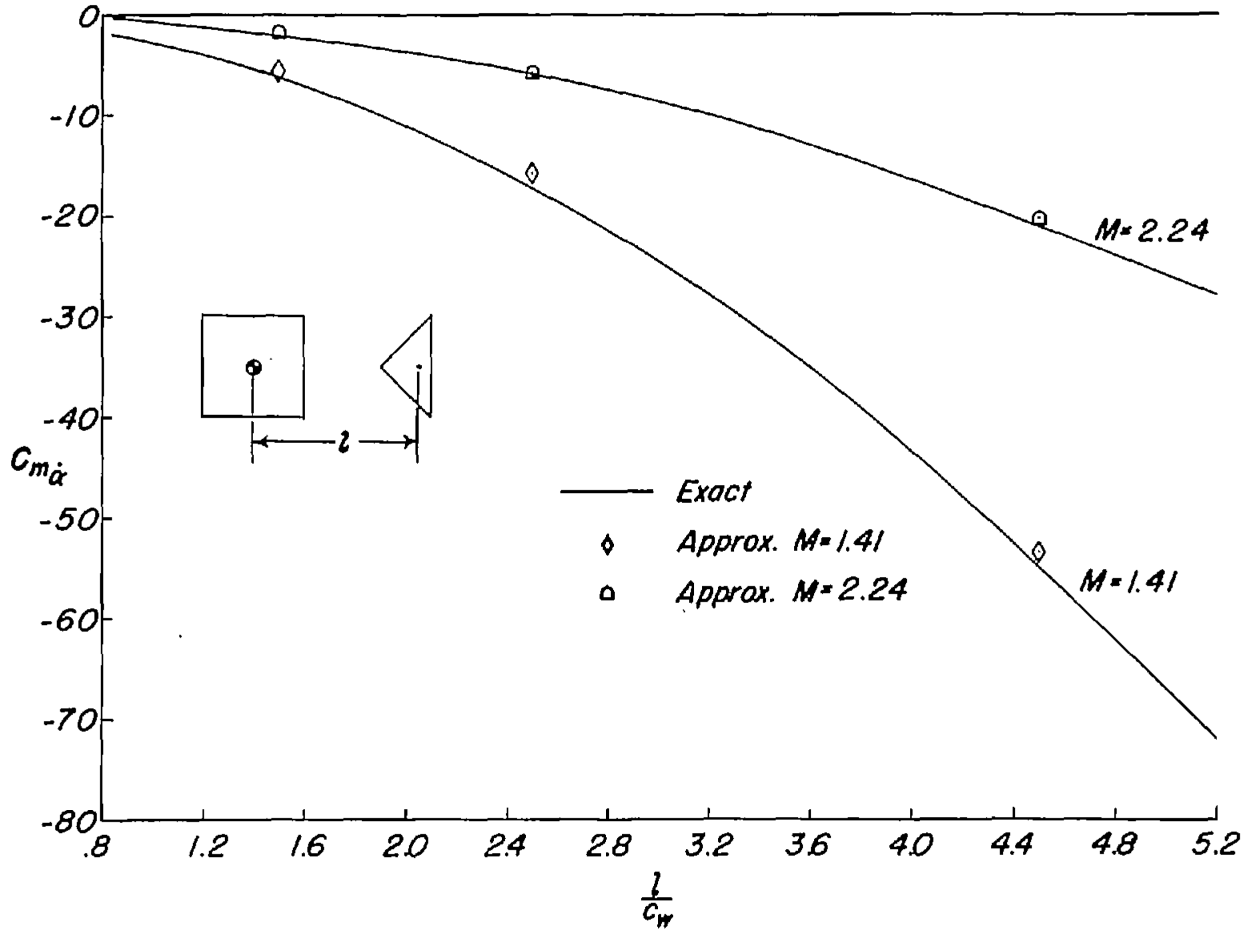

(a) Wing aspect ratio 1; $\frac{c_t}{c_w} = \frac{1}{2}$.

Figure 64.- Comparison between exact (linearized) and approximate (eq. (82)) values of $C_{m_{\dot{\alpha}}}$ for two rectangular-wing—triangular-tail combinations.

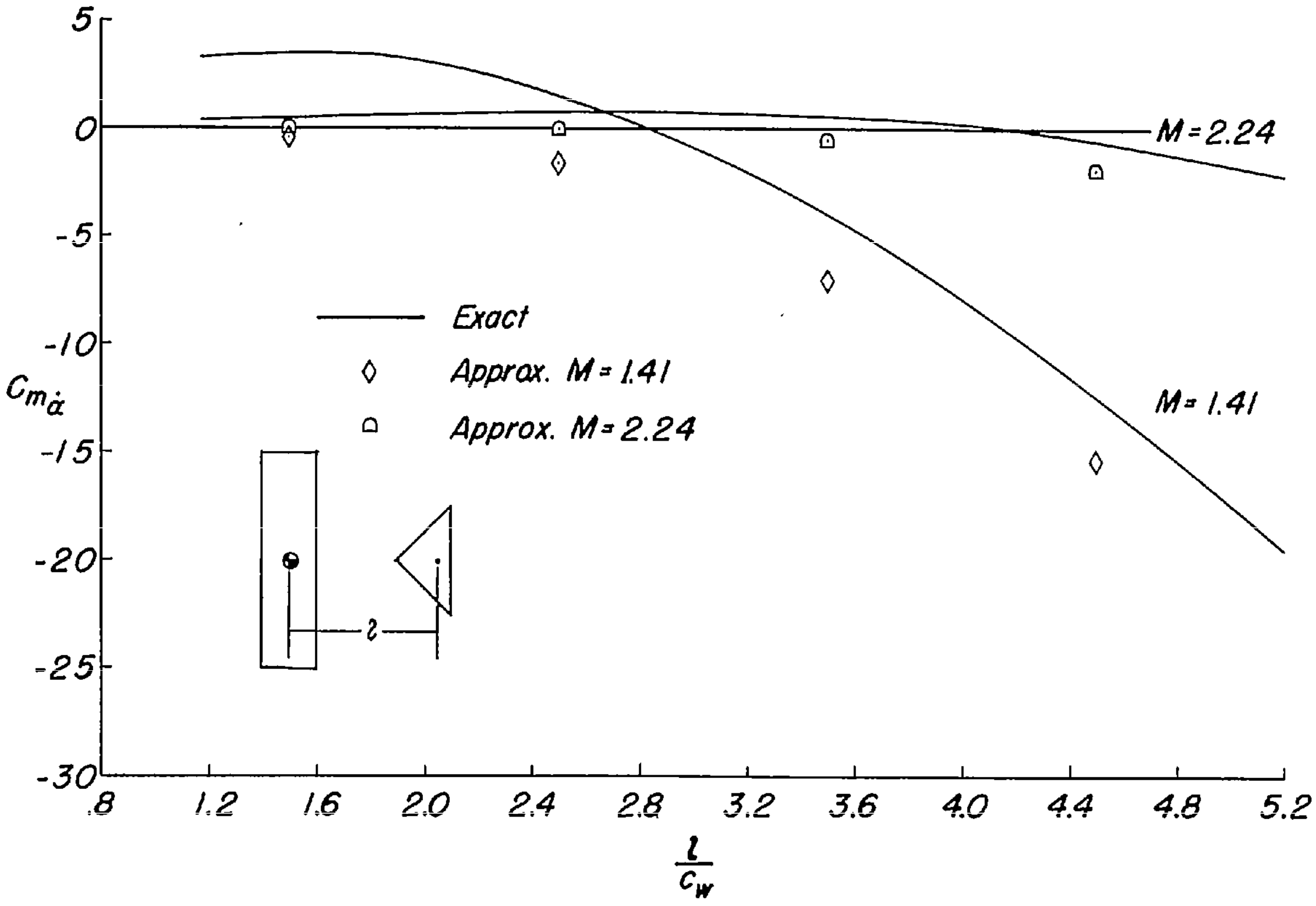

(b) Wing aspect ratio 4; $\frac{c_t}{c_w} = 1$.

Figure 64.- Concluded.

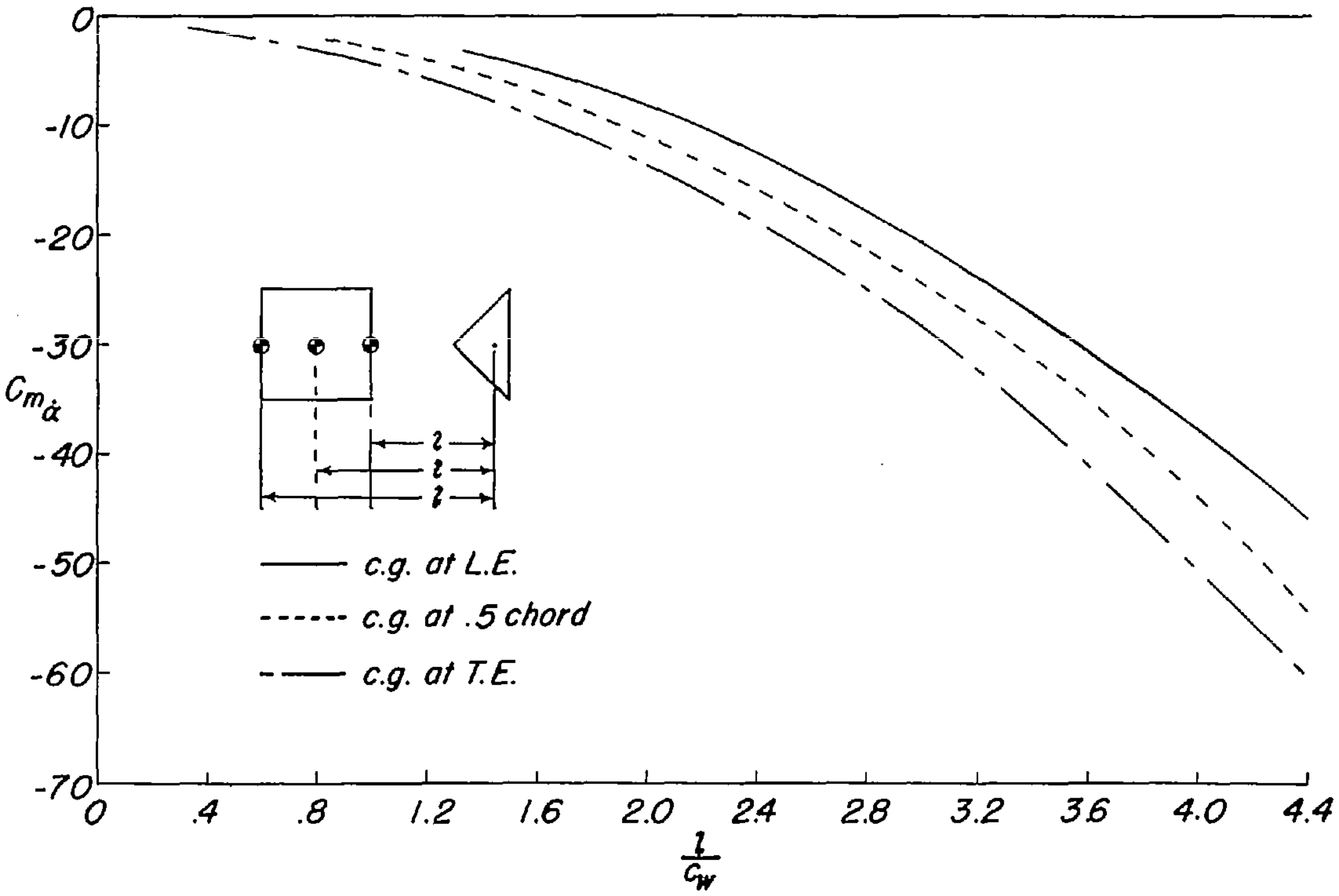

(a) Wing aspect ratio 1; $\frac{c_t}{c_w} = \frac{1}{2}$.

Figure 65.- Variation of $C_{m_{\dot{\alpha}}}$ with l/c_w for three center-of-gravity locations for two rectangular-wing—triangular-tail combinations. $M = 1.414$.

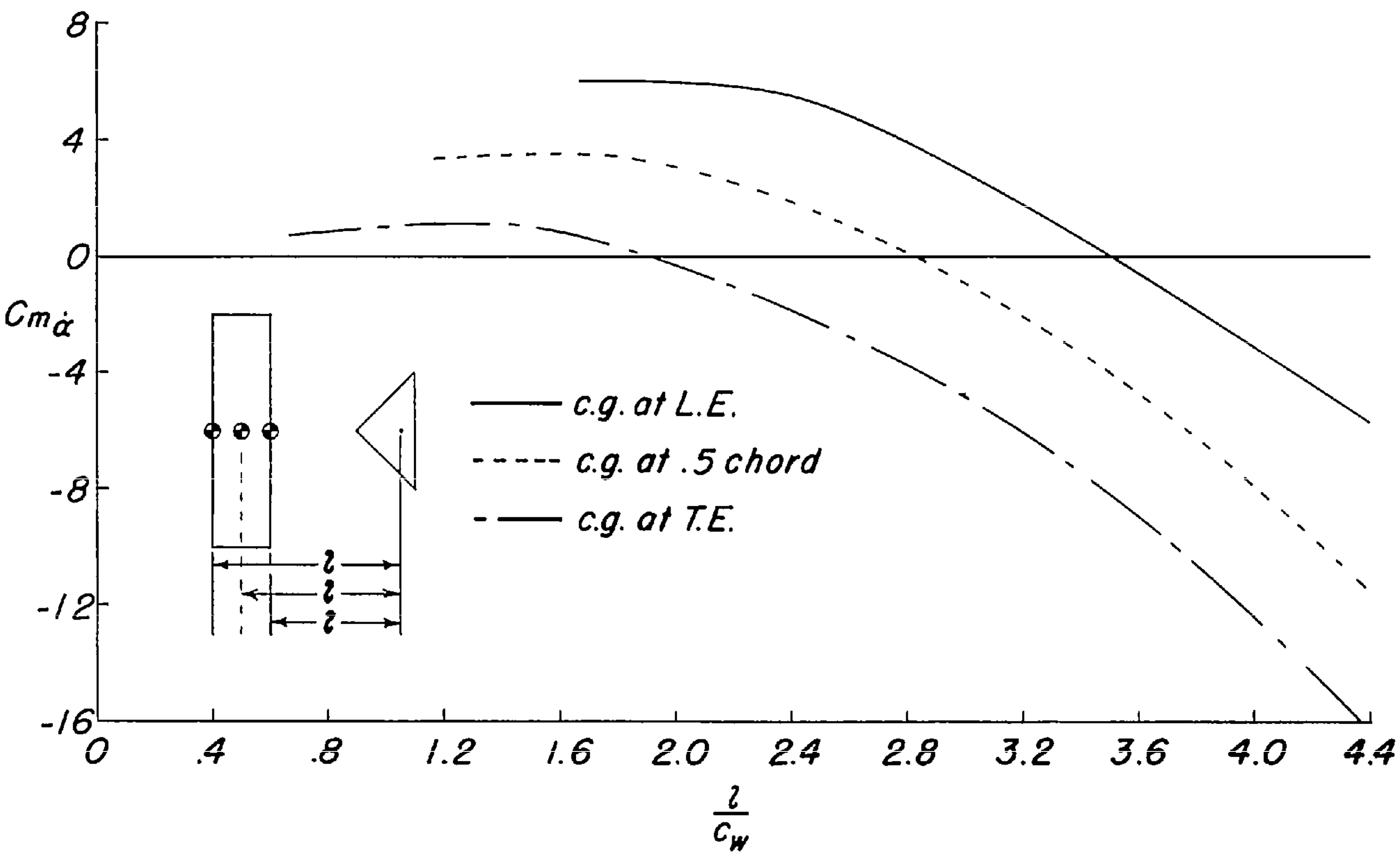

(b) Wing aspect ratio 4; $\frac{c_t}{c_w} = 1$.

Figure 65.- Concluded.

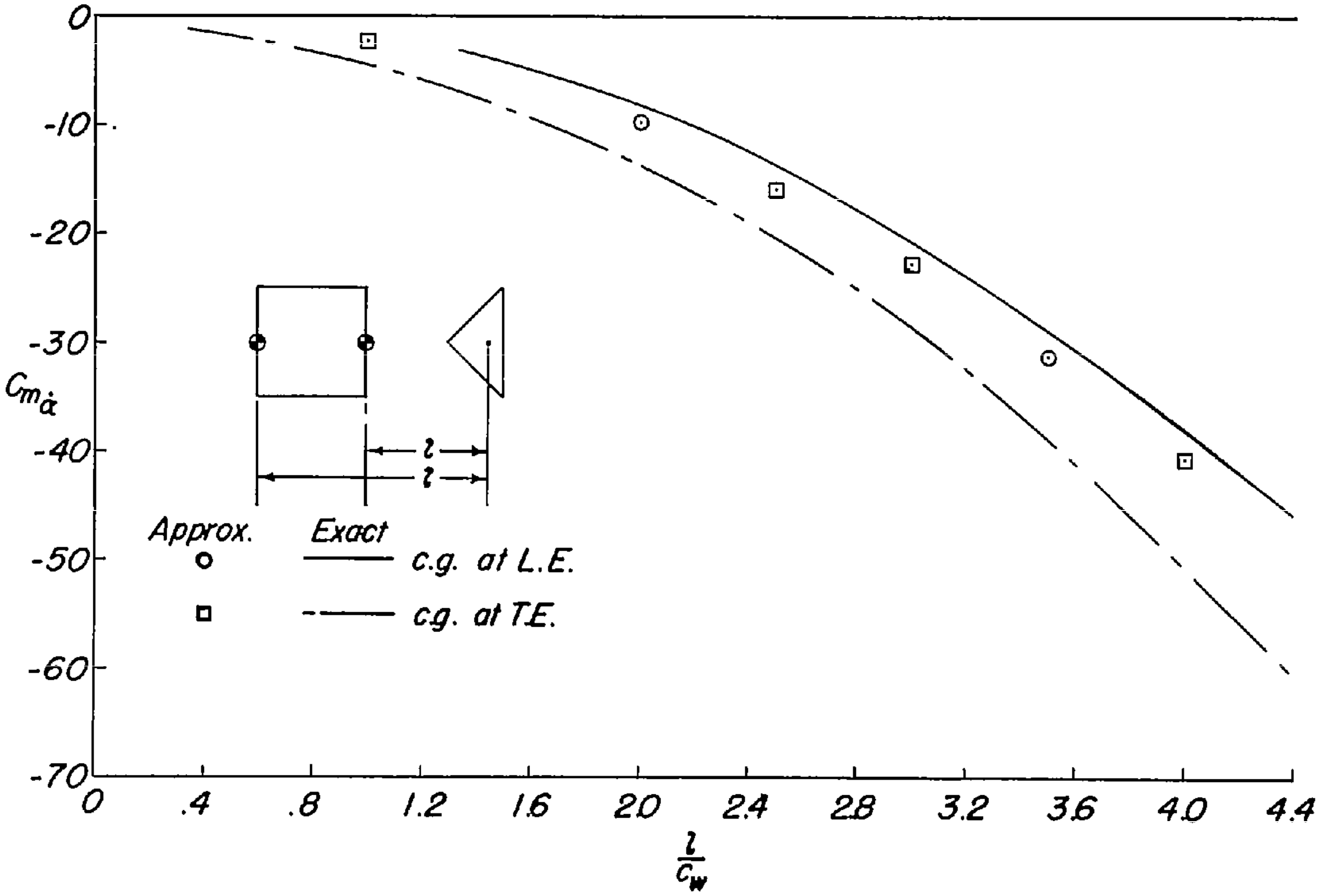

(a) Wing aspect ratio 1; $\frac{c_t}{c_w} = \frac{1}{2}$.

Figure 66.- Comparison between exact (linearized) and approximate (eq. (82)) values of $C_{m_{\dot{\alpha}}}$ for two center-of-gravity locations for two rectangular-wing—triangular-tail combinations. $M = 1.414$.

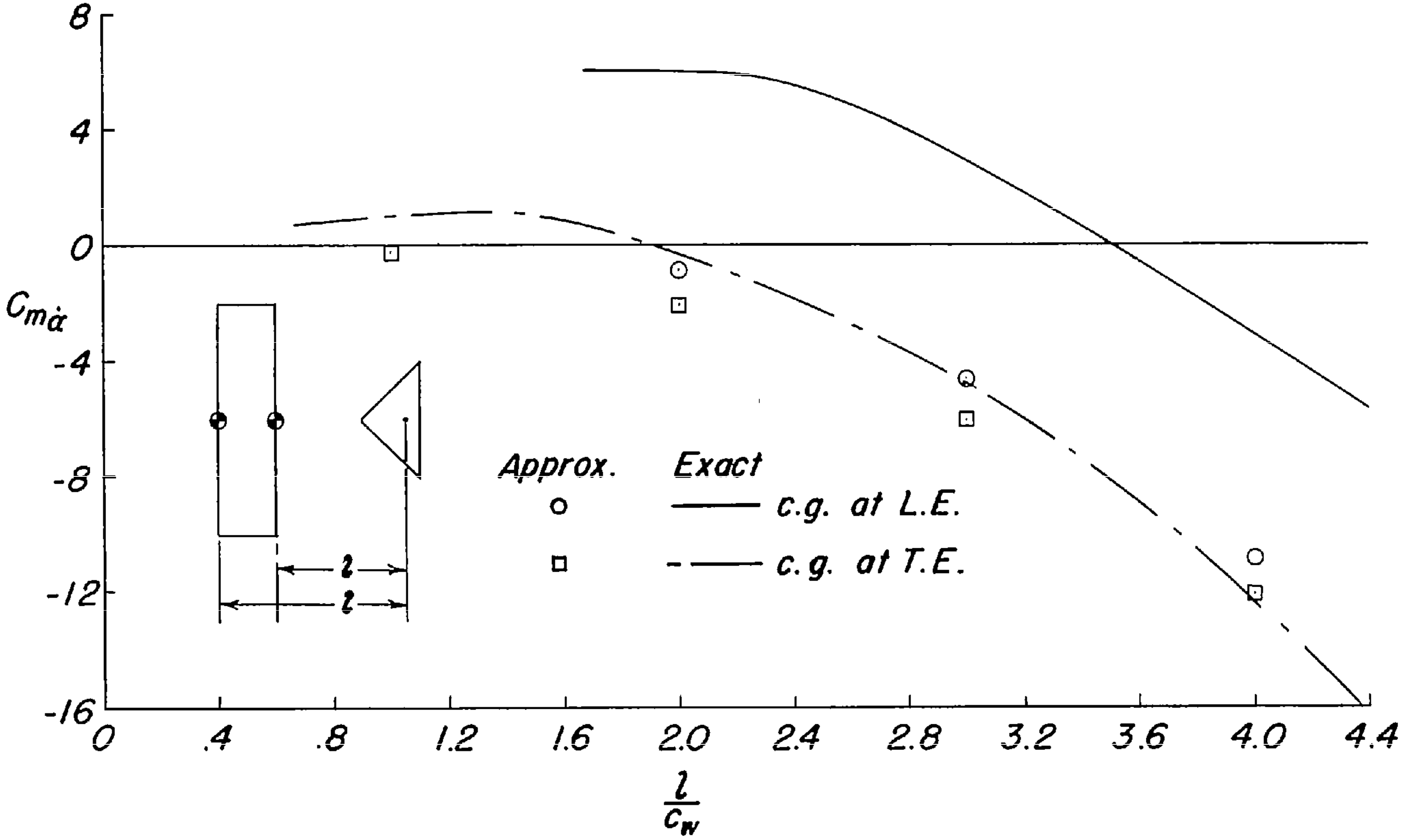

(b) Wing aspect ratio 4; $\frac{c_t}{c_w} = 1$.

Figure 66.- Concluded.

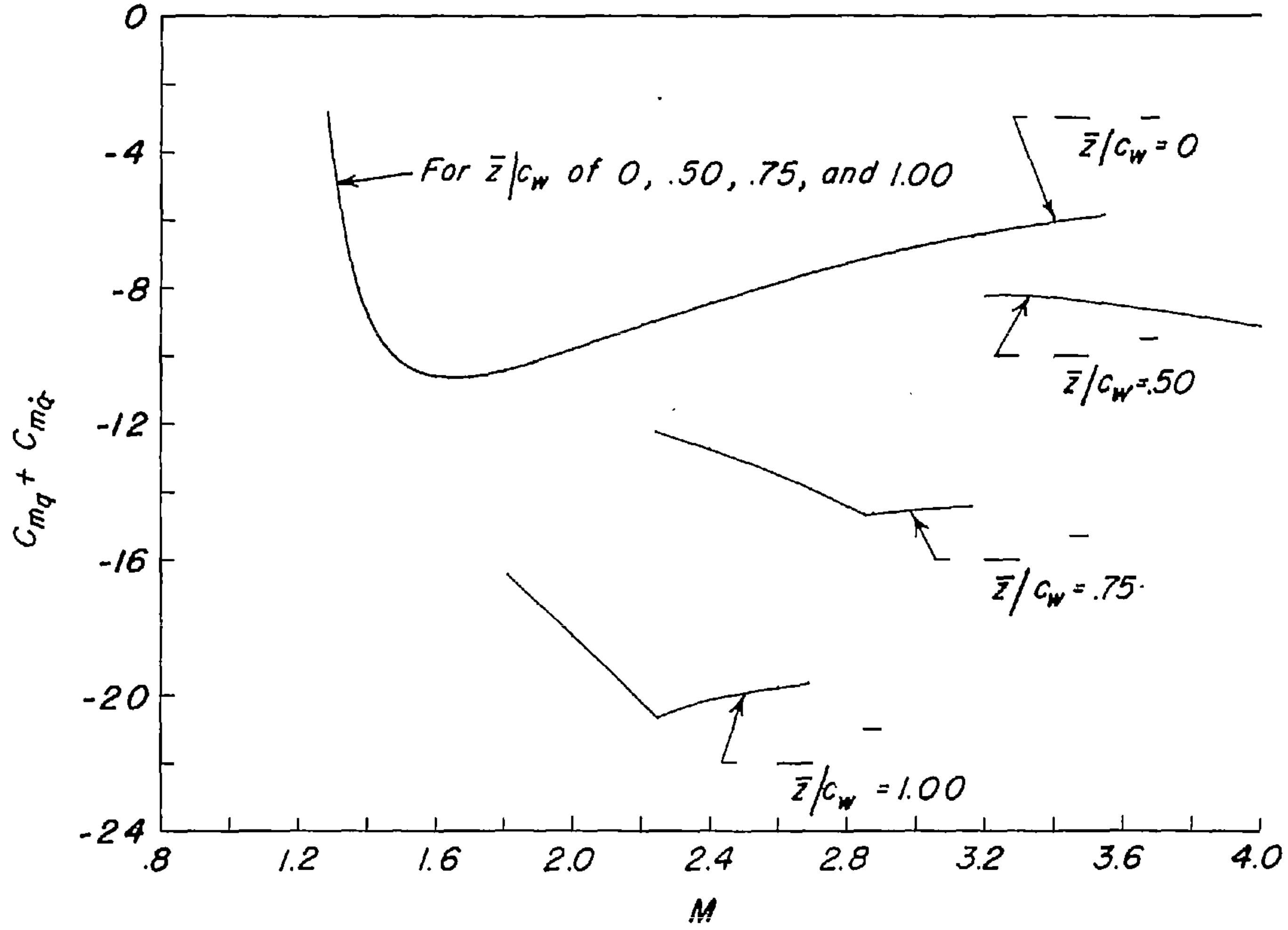

Figure 67.- Variation of $C_{m_q} + C_{m_{\dot{\alpha}}}$ with M for a two-dimensional wing-tail combination for various tail heights. $\frac{\bar{x}}{c_w} = \frac{c_t}{c_w} = \frac{1}{2}$; $\frac{l}{c_w} = 2.25$.

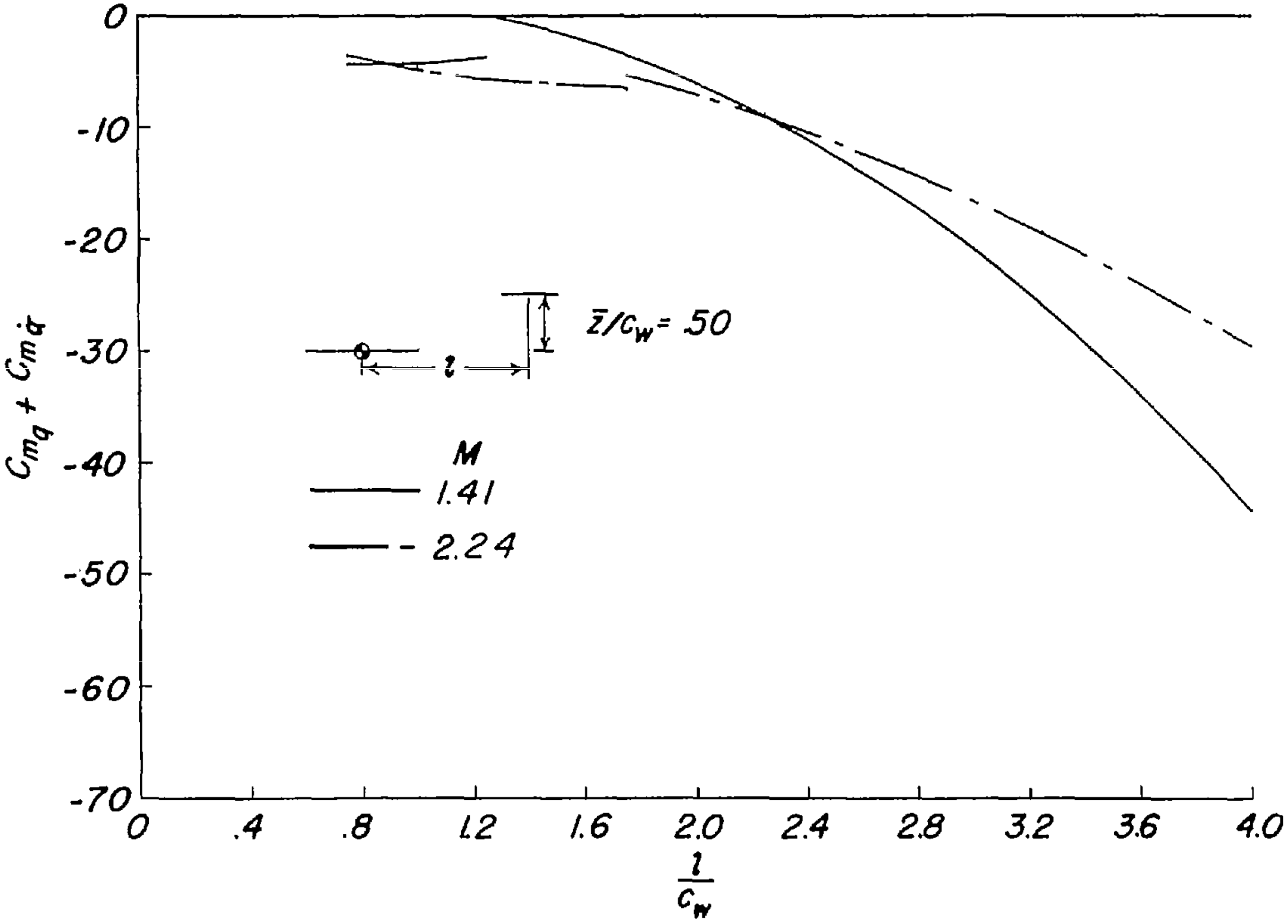

Figure 68.- Variation of $C_{m_q} + C_{m_{\dot\alpha}}$ with l/c_w for a two-dimensional wing-tail combination for two Mach numbers. $\frac{\bar{z}}{c_w} = \frac{\bar{x}}{c_w} = \frac{c_t}{c_w} = \frac{1}{2}$.

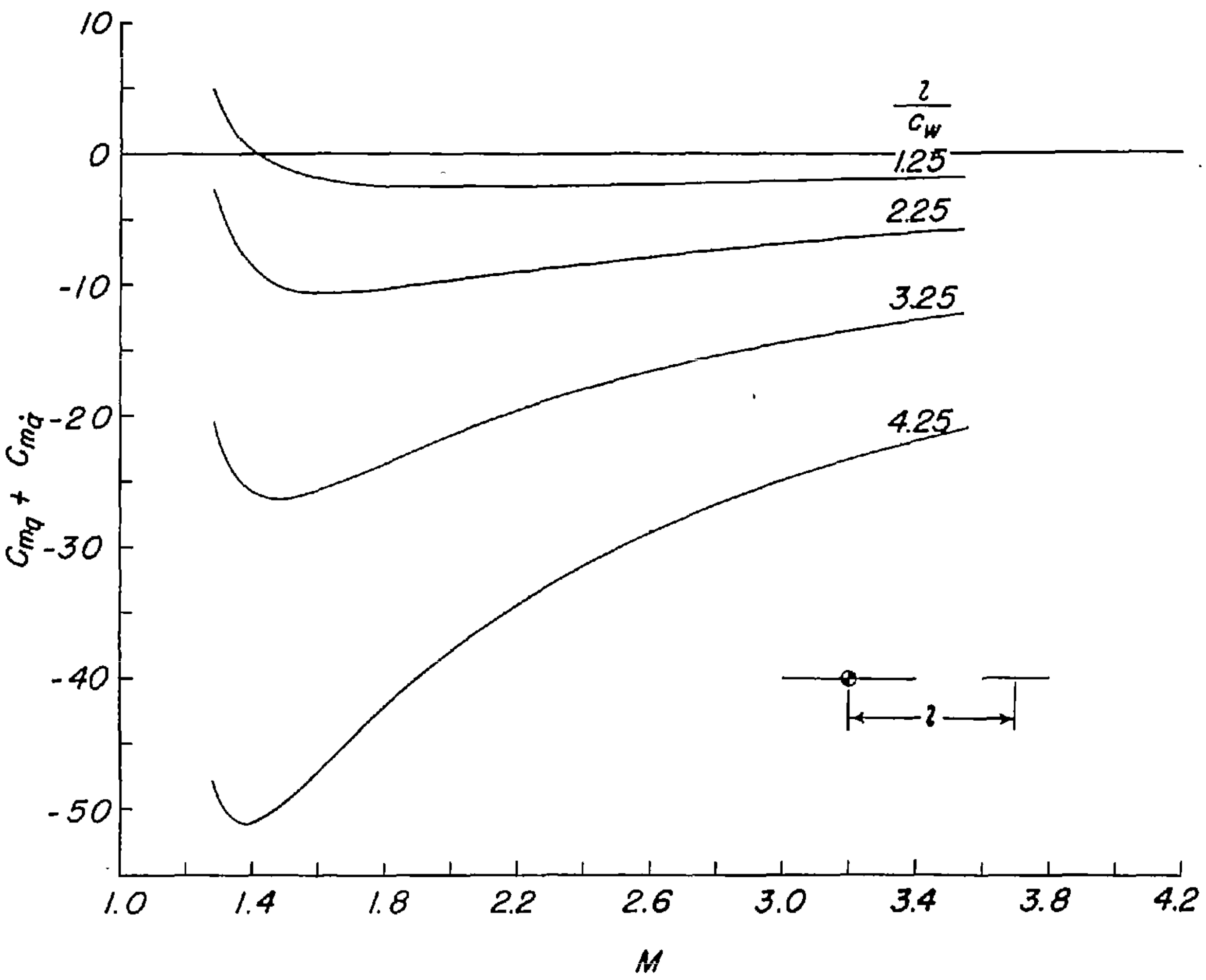

Figure 69.- Variation of $C_{m_q} + C_{m_{\dot{\alpha}}}$ with Mach number for a two-dimensional wing-tail combination for various values of $\frac{l}{c_w}$. $\frac{\bar{x}}{c_w} = \frac{c_t}{c_w} = \frac{1}{2}$; $\frac{\bar{z}}{c_w} = 0$.

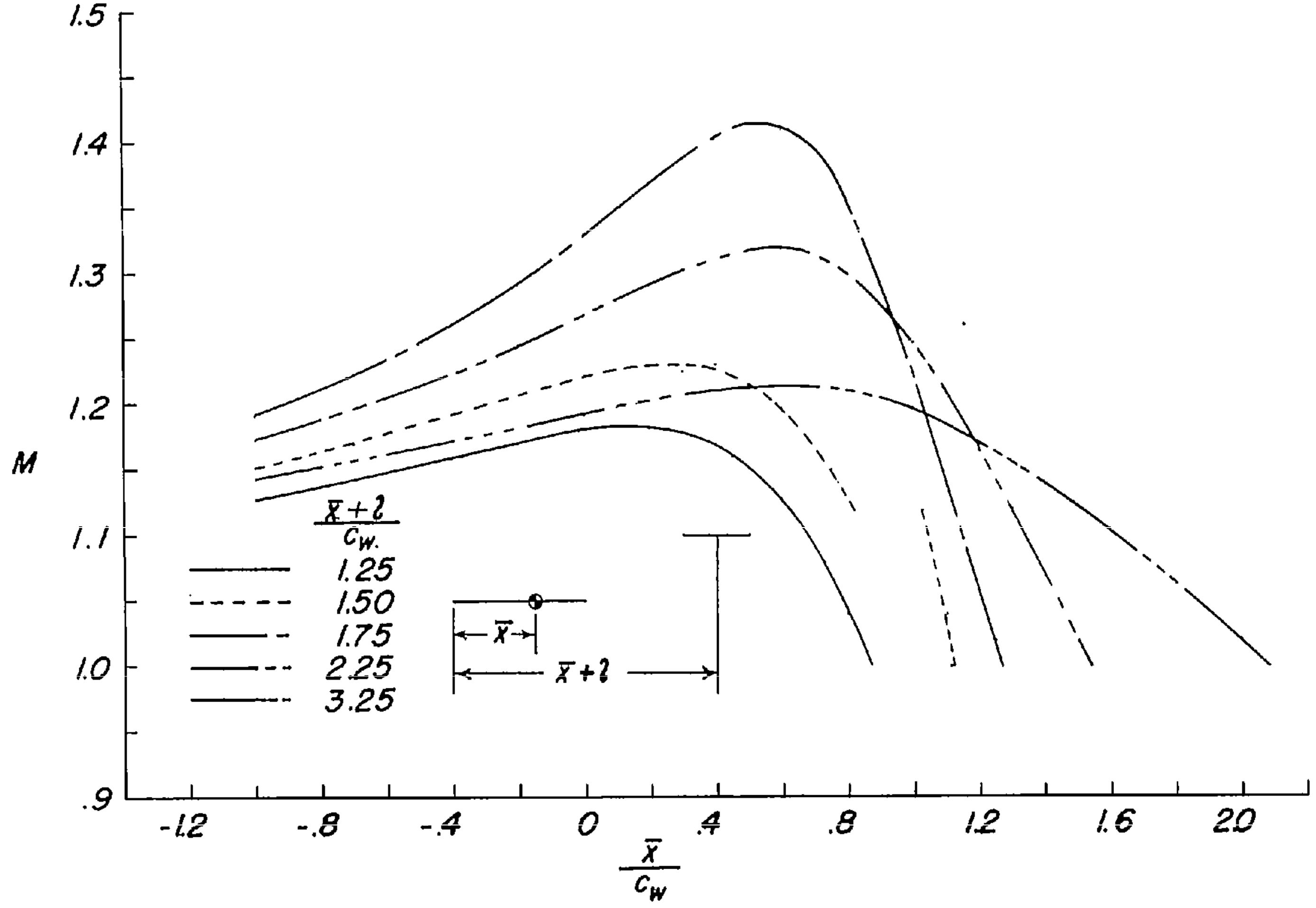

Figure 70.- Variation of Mach number M with center-of-gravity location $\bar{x}/c_w$ for which $C_{m_q} + C_{m_{\dot{\alpha}}} = 0$ for five two-dimensional wing-tail combinations. $\frac{\bar{z}}{c_w} = \frac{c_t}{c_w} = \frac{1}{2}$.

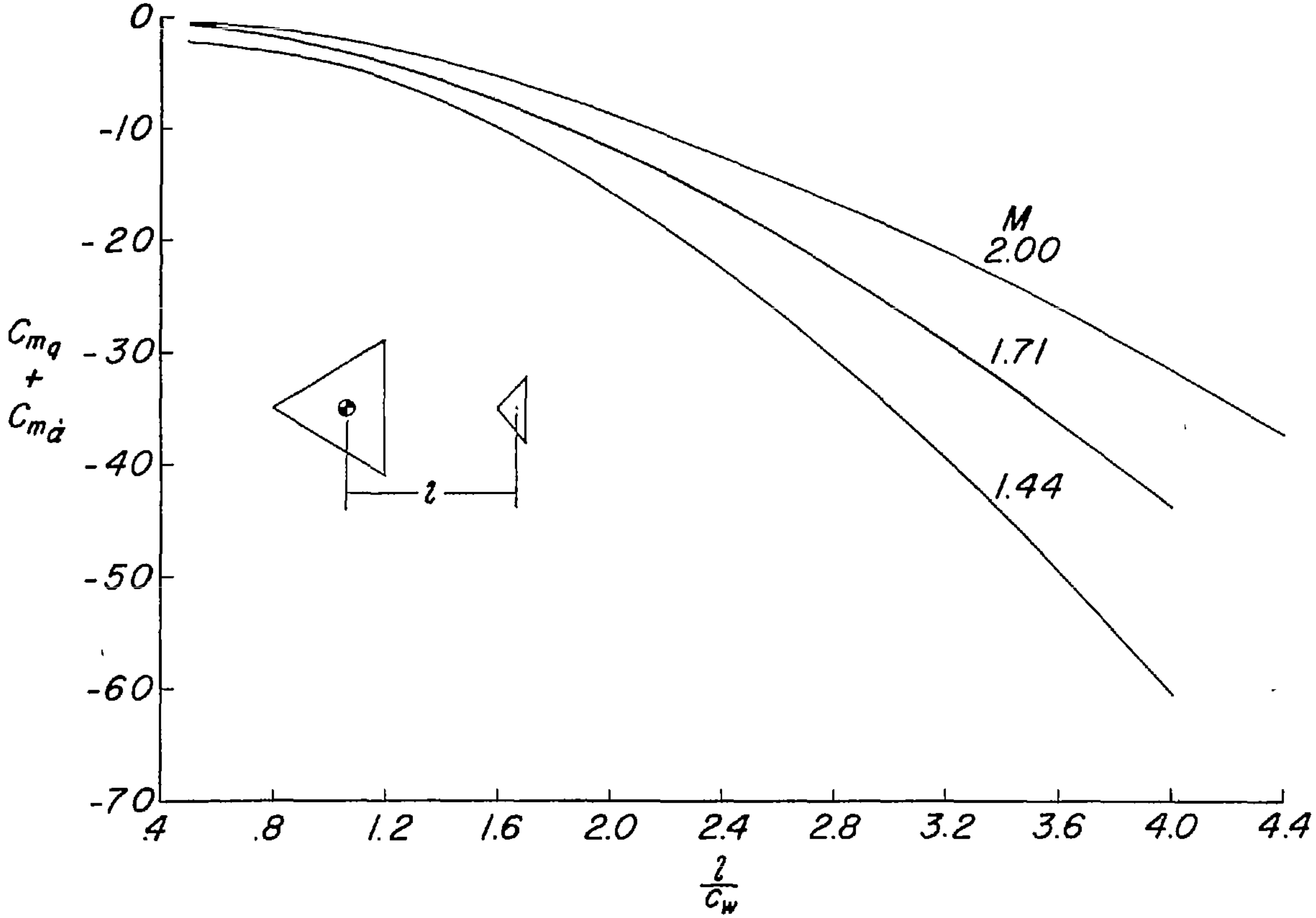

Figure 71.- Variation of $C_{m_q} + C_{m_{\dot{\alpha}}}$ with l/c_w for three Mach numbers for a triangular wing-tail combination.

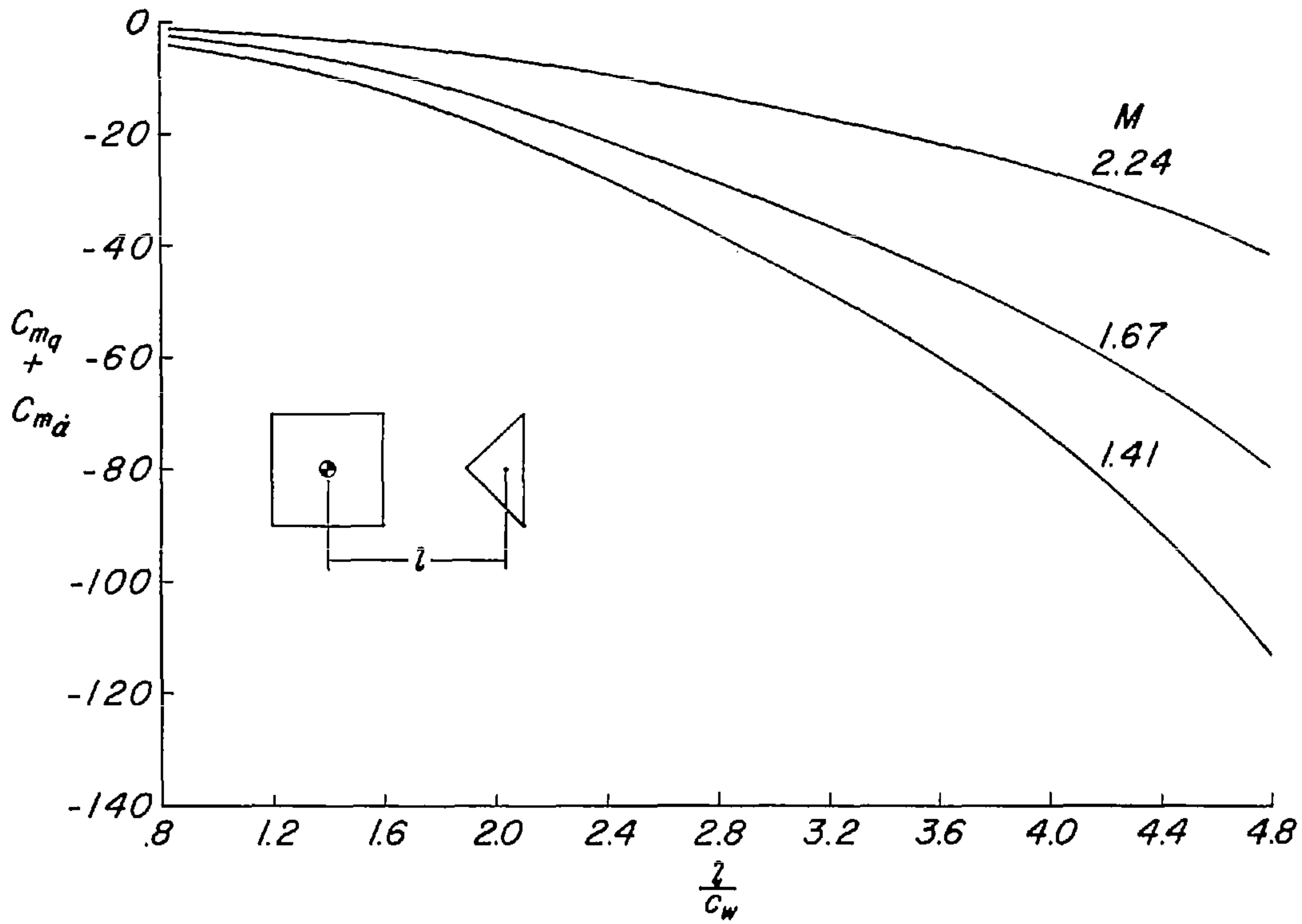

(a) Wing aspect ratio 1; $\frac{c_t}{c_w} = \frac{1}{2}$.

Figure 72.- Variation of $C_{m_q} + C_{m_{\dot{\alpha}}}$ with l/c_w for several rectangular-wing—triangular-tail combinations.

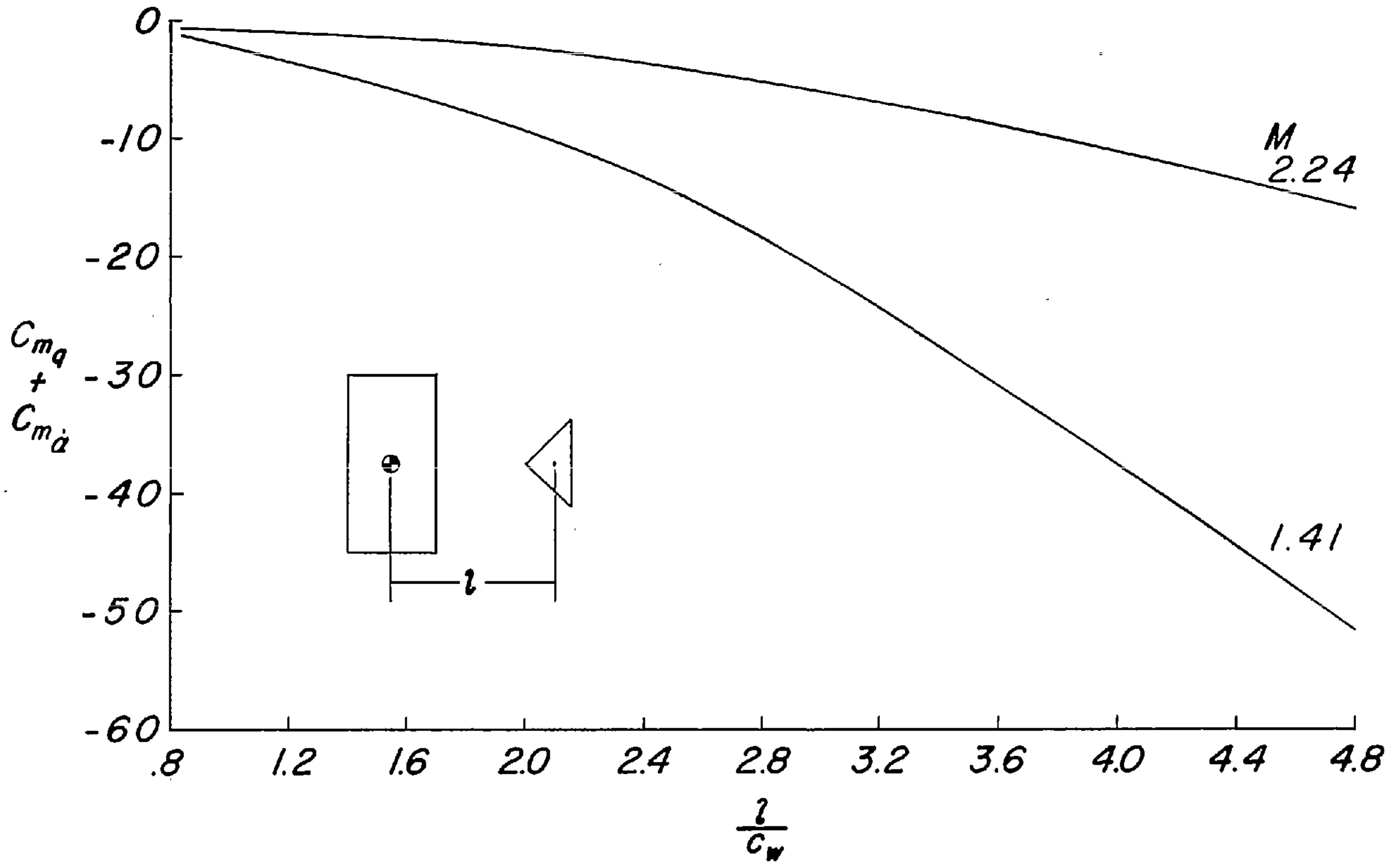

(b) Wing aspect ratio 2; $\frac{c_t}{c_w} = \frac{1}{2}$.

Figure 72.- Continued.

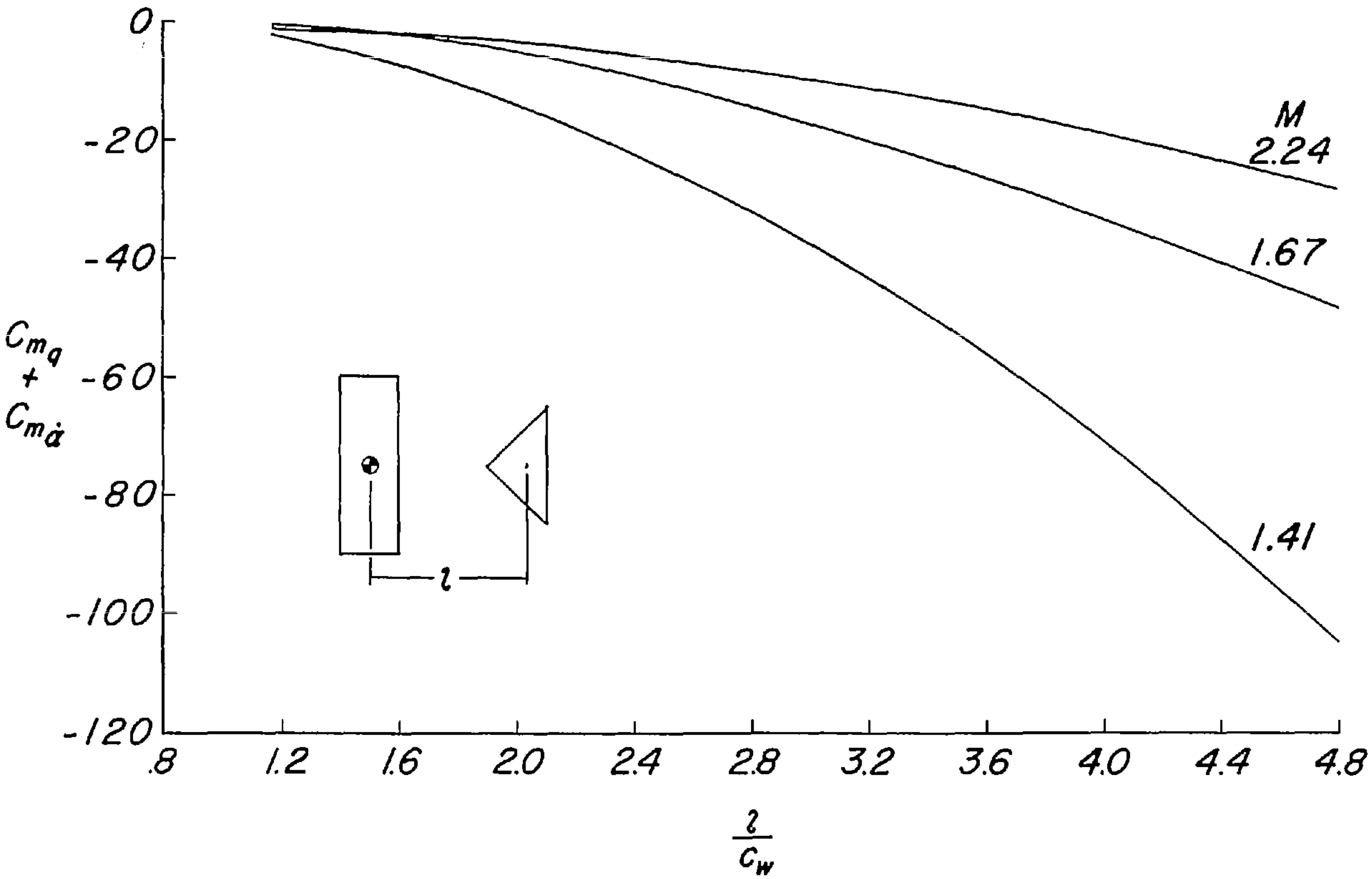

(c) Wing aspect ratio 3; $\frac{c_t}{c_w} = 1$.

Figure 72.- Continued.

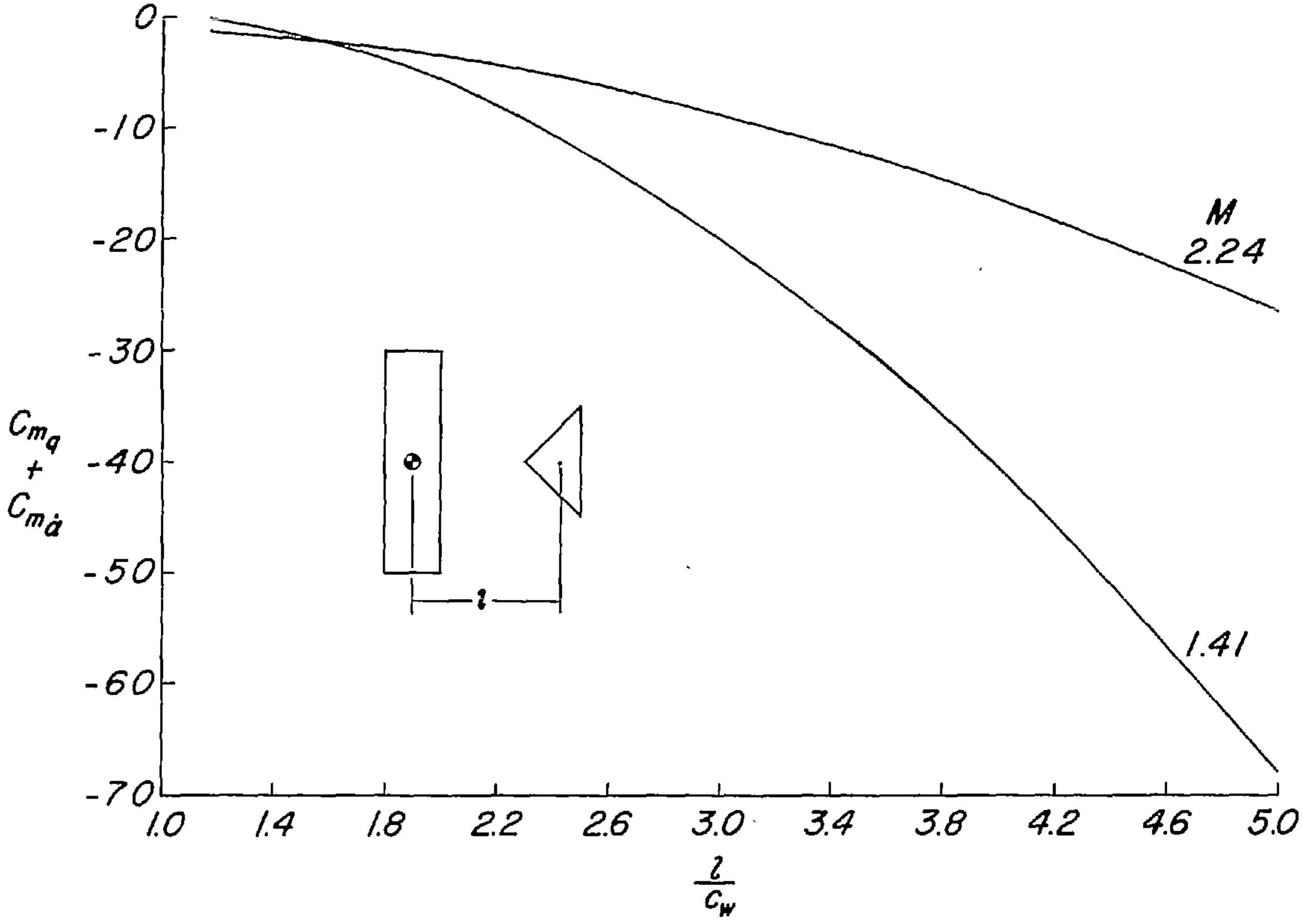

(d) Wing aspect ratio 4; $\frac{c_t}{c_w} = 1$.

Figure 72.- Concluded.

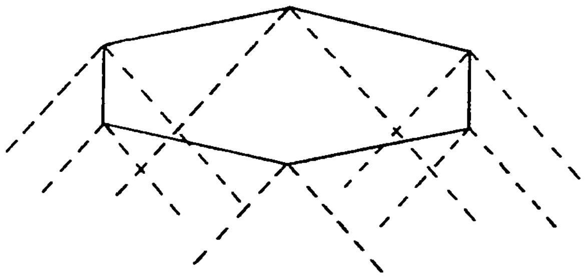

(a) Plan form with a supersonic trailing edge.

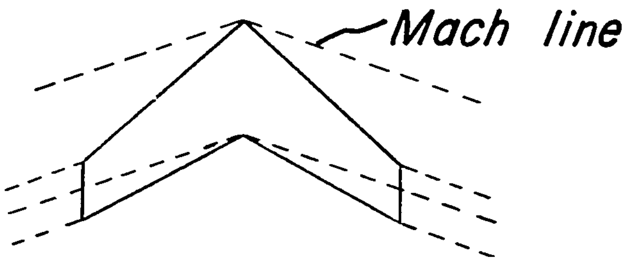

(b) Plan form with a subsonic trailing edge.

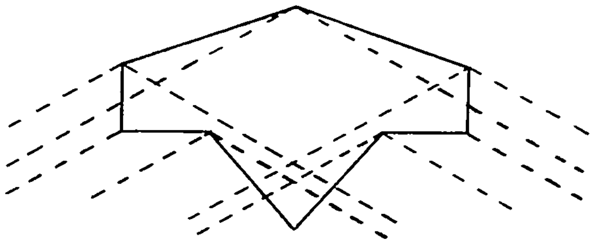

(c) Plan form with mixed supersonic and subsonic trailing edge.

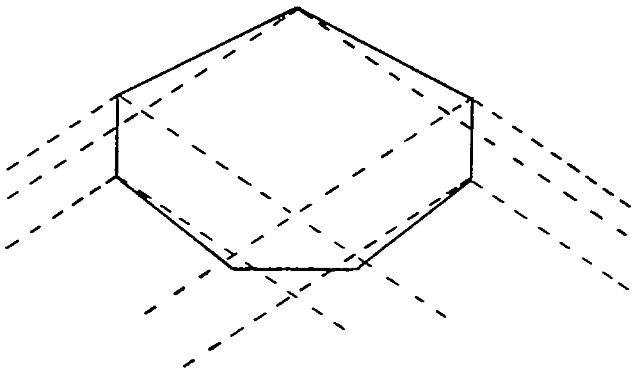

(d) Plan form with mixed supersonic and subsonic trailing edge.

Figure 73.- Plan forms with various types of trailing edges.

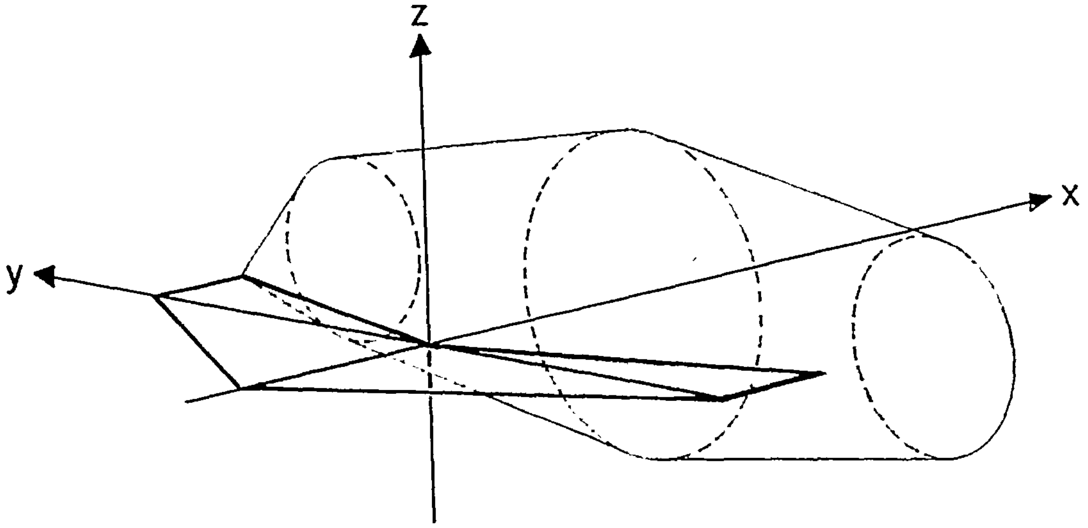

L-82070

Figure 74.- Plan form showing the Mach surface from a sweptback trailing edge.

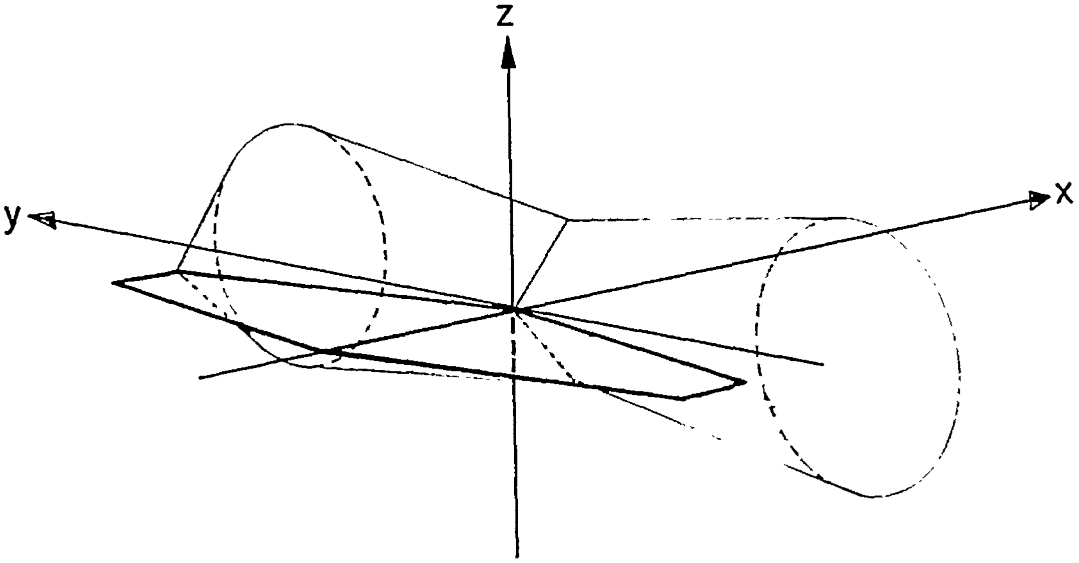

L-82071

Figure 75.- Plan form showing the Mach surface from a sweptforward trailing edge.

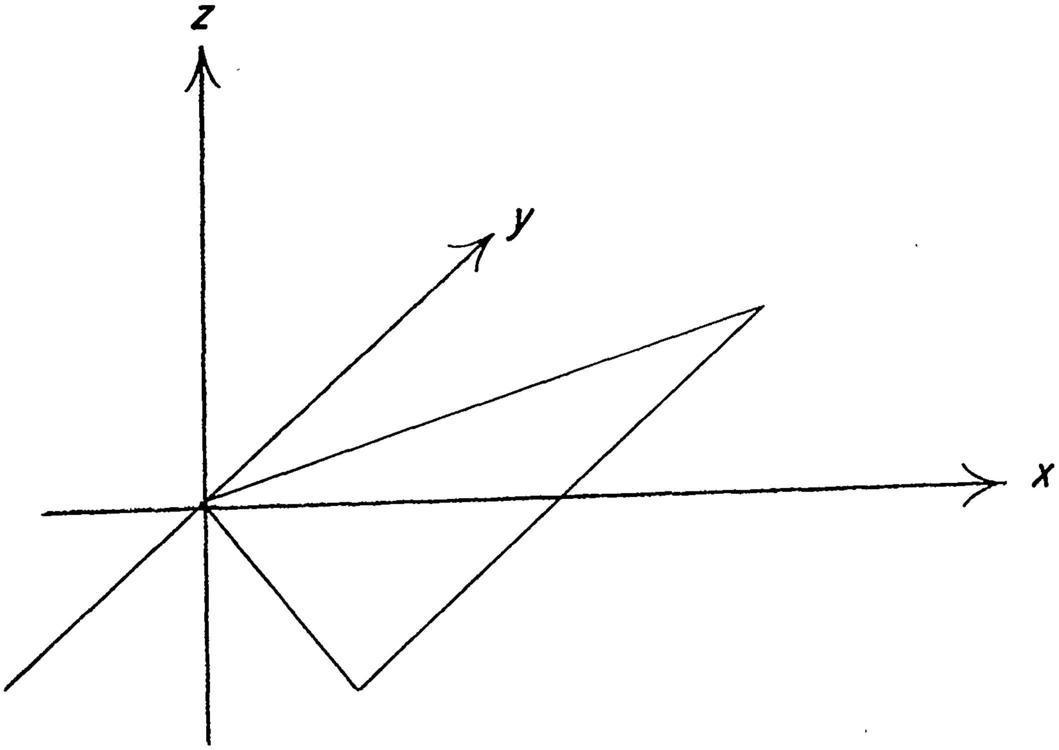

Figure 76.- Location of the coordinate axes associated with the triangular wing.

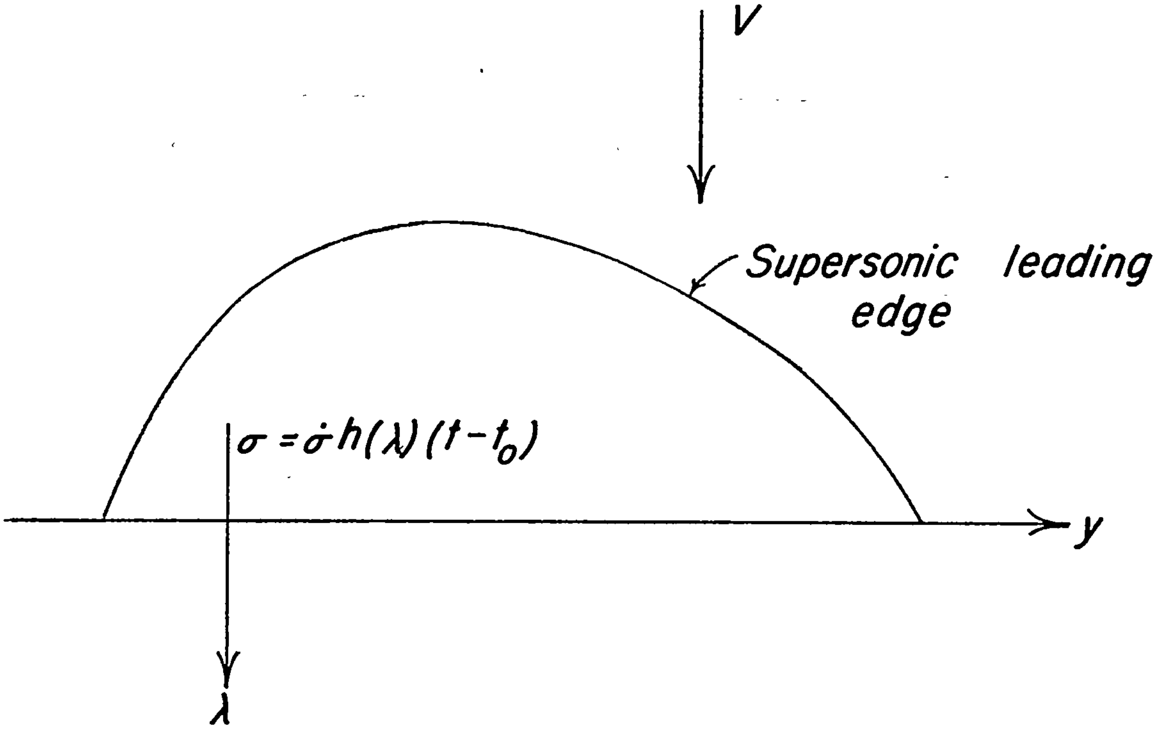

(a) Arbitrary angle-of-attack distribution over complete plan form.

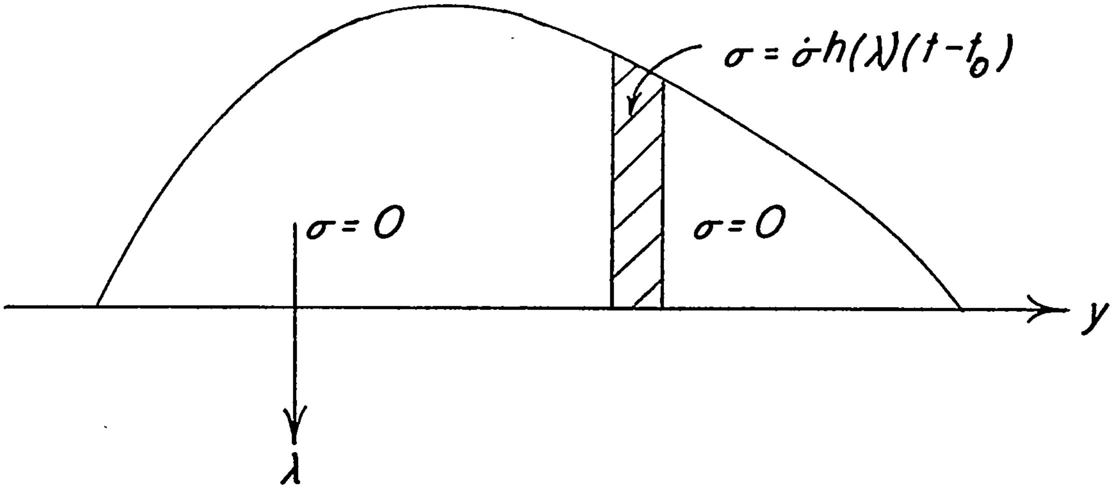

(b) Arbitrary angle-of-attack distribution confined to a strip.

Figure 77.- Airfoils with supersonic leading edges and trailing edges perpendicular to the free-stream direction.

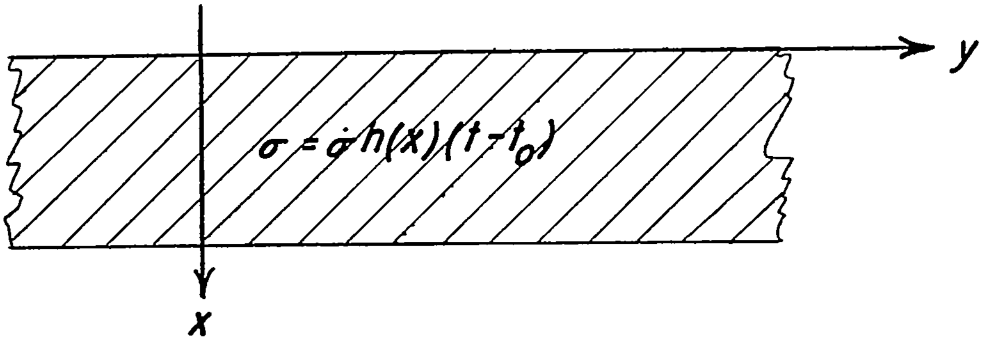

(a) Arbitrary angle-of-attack distribution.

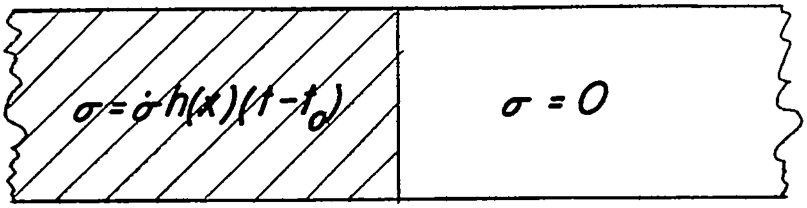

(b) Arbitrary angle-of-attack distribution confined to left side of airfoil.

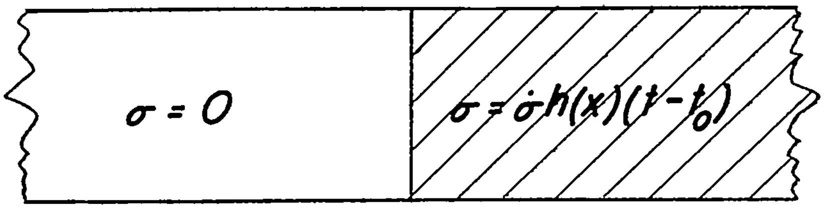

(c) Arbitrary angle-of-attack distribution confined to right side of airfoil.

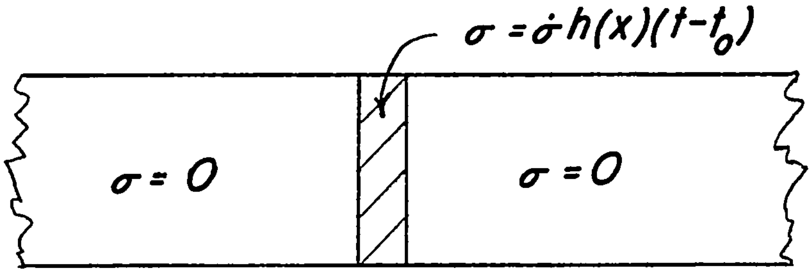

(d) Arbitrary angle-of-attack distribution confined to a strip.

Figure 78.- Infinite-aspect-ratio airfoils with arbitrary angle-of-attack distributions varying linearly with time.

NACA-Langley - 5-28-54 - 1000